Thermal Decomposition of Haloethanols and Ignition of JP-10

A thesis

Submitted for the degree of

Doctor of Philosophy

in the Faculty of Science

by

Harish Kumar Chakravarty

Department of Inorganic and Physical Chemistry

Indian Institute of Science

Bangalore - 560 012, India

August 2011

Dedicated to........

My Dear Parents

DECLARATION

*I hereby declare that the thesis entitled "**Thermal Decomposition of Haloethanols and Ignition of JP-10"** submitted for the degree of Doctor of Philosophy (Science) in the Faculty of Science is result of investigations carried out by me at the Department of Inorganic and Physical Chemistry, Indian Institute of Science, Bangalore, India, under the supervision of Prof. E. Arunan and Prof. K. P. J. Reddy. In keeping with the general practice of reporting scientific observations, due acknowledgements have been made wherever the work described in this thesis is based on the findings of other investigators. Any omission that might have occurred due to oversight or error is regretted.*

Date: ***Harish Kumar Chakravarty***

CERTIFICATE

*We hereby certify that the work presented in this thesis entitled "**Thermal Decomposition of Haloethanols and Ignition of JP-10**" is result of investigations performed by Harish Kumar Chakravarty at the Department of Inorganic and Physical Chemistry, Indian Institute of Science, Bangalore, India under our supervision and the same has not been submitted elsewhere for a degree. The work presented by him in this thesis is, to the best of our knowledge and belief, original except as acknowledged in the text.*

Professor E. Arunan   *Professor K. P. J. Reddy*

(Research Supervisor)   *(Co-Supervisor)*

Acknowledgements

*There are quite a lot of people who need to be acknowledged. Foremost among them is my adviser **Prof. E. Arunan** for introducing me to the field of shock tube chemistry and chemical kinetics. In addition to the guidance in the research, the constant suggestions to improve the personality as a well wisher are gratefully acknowledged. I thank him for giving an extremely great and unforgettable moral support.*

*I thank **Prof. K.P.J. Reddy** for his guidance and constant encouragement throughout my stay in the laboratory. I sincerely thank him for providing me the laboratory and for the liberty he has given me for demanding the facilities throughout. His guidance in making me to understand the physics behind the shock tube technique is gratefully acknowledged.*

I thank Chairmen (present and past) of both Inorganic and Physical Chemistry and Aerospace Engineering department for providing me the facilities to carry out my research work. I thank all the faculty members of the both the department for their encouragement and support. I take this opportunity to specially thank prof. S.Umapathy, who has always been encouraging.

My lab-mates Amit, Satish, Kulkarni, Mahapatra, Bhopathy, and Kiran are always helpful and appreciated. Summer fellows Shahul, Sandeep and Gaurav are highly acknowledged.

I would like to thank Prof. Robert goerges, Prof. Loudovick and Prof. Bertrand rowe for their support, encouragement and cooperation during my short term stay in the University of Rennes, France.

I take this opportunity to thank Dr. Vijayanand chandrashekharan for his support and cooperation during my stay in University of Rennes, France.

Contents

Chapter III   **Thermal Decomposition of 2-Chloroethanol**

Chapter V   Computational Calculation of Enthalpy of Formation of Haloethanols

Chapter VI   Shock tube Ignition Delay Studies of JP-10 and JP-10+Triethyl Amine

Chapter VII   Conclusions and Future Directions

Synopsis

In this thesis, the thermal decomposition investigation of haloethanols namely 2-chloroethanol and 2-bromoethanol are reported both experimental and theoretical. Computational calculation of enthalpy of formation haloethanols using isodesmic and atomization reactions has also been reported. Finally, the chemistry of JP-10 ignition has also been investigated using shock tube.

Chapter 1 gives a brief introduction to the experimental shock tube technique. Brief surveys of literature pertinent to haloethanols and JP-10 have also been discussed. The importance of thermal rate coefficient and detection techniques in shock tube chemistry is presented. Details of the theoretical methods used in the determination of thermal rate coefficients have been described at the end of the chapter.

In Chapter 2, I have discussed experimental methods used in carrying out this work. The details of the experimental shock tube set-up employed in this work have been elaborated in this chapter. Kinetic simulations performed to understand the mechanism of chemical transformation of haloethanols at high temperature have also been presented.

In chapter 3, thermal decomposition results obtained for 2-chloroethanol have been described. The kinetic data have been obtained in the temperature range of 930-1100 K behind the reflected shock wave in a shock tube. Analyses of pre and post shock mixture using FT-IR and gas chromatographic techniques are presented. Chemical kinetic simulation performed to simulate the product distribution is presented. The reduced kinetic model has also been presented which was obtained using the sensitivity analysis and was validated by comparison to the shock

tube measurements.   The details of the β-substitution effect have been shown. The kinetic parameters of the unimolecular elimination of HCl and H_2O have been presented both experimentally and theoretically. Theoretical results were obtained by transition state theory using quantum chemistry calculations HF, MP2 (FULL) and B3LYP/6-311++G** level of theory. The details of intrinsic reaction coordinate calculation and potential energy surface calculations have also been described. These experimental and theoretical results suggest that the rate of HCl elimination is faster than that of H_2O and HOCl elimination reaction.

In chapter 4, I have reported thermal decomposition results obtained for 2-bromoethanol. The kinetic data have been obtained in the temperature range of 910-1102 K behind the reflected shock wave in a shock tube. Analyses of pre and post shock mixture using FT-IR and gas chromatographic techniques are discussed. Chemical kinetic simulation performed to simulate the product distribution is presented. The details of the β-substitution effect are explained. Both experimental and theoretical kinetic parameters of the unimolecular elimination of HBr and H_2O have been presented. Theoretical results were obtained by transition state theory using quantum chemistry calculations at the HF, MP2 (FULL) and B3LYP/6-311++G** level of theory. The intrinsic reaction coordinate calculation and potential energy surface have been investigated in details. From this experimental and theoretical studies, it has been concluded that the rate of HBr elimination much faster than that of H_2O. However, the experiments show that the rate of HOBr elimination is faster than that of the H_2O.

In chapter 5, I have reported the computational calculation of enthalpy of formation of haloethanols. The enthalpy of formation of haloethanols of the general formula XC_2H_4OH were calculated by the HF, MP2, B3LYP, G2, G3, G2MP2, G3B3, G3MP2B3, CBS-Q, CBS-QB3 and CCSD/cc-pVDZ level of theories applying isodesmic and atomization reactions. Results

obtained using the Benson's group and bond additivity methods have also been described at 298.15 K and at 1 atm in the gaseous state.

In chapter 6, ignition delay measurement on neat jet propellent-10 (JP-10) and JP-10 + Triethyl amine (TEA) mixture have been reported. The JP-10 (Exo-tetrahydrodicyclopentadiene, $C_{10}H_{16}$) ignition delay times were measured behind a single pulse reflected shock wave in a shock tube. Experiments were performed over high temperature, high pressure, and three equivalence ratio and for different composition. It has been shown that the TEA can reduce the ignition delay of JP-10. A higher level quantum chemistry calculation has also been presented that were performed to obtain the bond dissociation energies of C-H bonds in JP-10.

Chapter7 is the concluding chapter where the main work done in this thesis is summarized and future direction is presented.

List of Tables

List of Figures

Chapter I

Introduction

I.1. Shock tube technique

Shock tube based research, over the last five decades, has revealed many potential research areas for scientific studies. However, the main focus of the shock tube research has been on application to aerodynamic and high temperature kinetic studies, though several interdisciplinary areas have also been investigated. The examples of interdisciplinary research involving shock waves includes medical applications of shock wave focusing; shock wave phenomena applied to geosciences and astrophysics; shock waves in condensed matter physics and material synthesis initiated using shock wave. Paul Vieille who operated the first shock tube in 1899 to investigate the gas explosions in mines could not have foreseen the potential of shock tube technique.[1]

Shock tube is being used as a high temperature wave reactor by kineticists around the world in order to estimate the thermal rate coefficient data under diffusion free conditions and with instantaneous heating of reactant. The temperature range under which the reaction could be studied can be extended far beyond that of the conventional flow reactor (1000K). The kinetic parameters of certain heterogeneous reaction systems have also been investigated successfully using shock tube technique. [1]

Shockwaves are basically non-linear waves that travel at supersonic speeds. Such disturbances occur in steady supersonic or transonic flows, during lightning strokes, earthquakes and explosions. Shock wave can be produced by the rapid movement of piston in a tube filled with gas. Any sudden release of energy will lead to the formation of shock waves within few μs as they are one of the efficient mechanisms of energy dissipation found in nature. Shock wave can also be produced by the dissipation of

mechanical, electrical, nuclear and chemical energy in a limited space. Shockwaves are defined as strong or weak based upon the instantaneous changes in flow properties like temperature and pressure that they bring about in the medium of propagation. Shock wave can be either weak wave formed during the bursting of a cracker or of enormous magnitude that produced from a nuclear explosion like the one that took place at Hiroshima, Japan during the Second World War. Shock wave can also be seen as a very thin and sharp wave front across which temperature, pressure, density, entropy and velocity of flow change abruptly. Because of the dissipative nature of shock waves they invariably require a medium both for generation as well as for propagation. Shock waves cannot travel in vacuum. Any molecule or a particle crossing the shock wave, whose width is about 2.5 Å, will acquire high temperature and undergoes compression, which depends on the strength of the shock wave. This width is very small compared to other characteristic lengths in fluid flow. [2, 3]

In simple words according to Lifshitz[4] "a shock wave is very sharp, thin front through which there exists a sudden change in all flow properties, such as pressure, temperature, density, velocity and entropy".

Shock waves can be easily generated in the laboratory using a shock tube. The shock tube is an ideal tool to determine the thermal rate constants. There are many unique features that make shock tube an important tool to obtain the thermal rate constant at high temperature for numerous reactions. Heating the test gas molecules under investigation to any desired high temperature homogeneously in very short span of time has been an important application of a shock tube in the field of chemistry. In addition to this, cooling

of the heated molecule can be achieved rapidly in about a millisecond timescale by the expansion wave travelling from other end inside the shock tube.

The sample under study can uniformly be heated rapidly at the desired temperature behind the reflected shock wave (This will be discussed in Chapter II in detail) without experiencing the ramp. Similarly, it also allows the sample to be cooled rapidly to room temperature by the expansion fan. The cooling rates commonly obtained are in the range of 0.5 to 5 K per μs. Hence, very well defined short reaction times can be achieved if the shock tube is being used for the study of kinetic reaction rates. The shock tube technique has negligible wall effects which makes it unique for the study of kinetics of the chemical reaction. This implies that only the test gas under study in the shock tube exposed to the reflected shock wave will be experiencing the temperature. However, the walls of the tube will remain at the room temperature. The two temperature zones (the test gas and the walls of the tube) will be at two different temperatures without being separated by any physical boundary. The concentration of the test gas molecules under study in the shock tube can be as low as in the range of parts per million levels. This avoids any secondary reactions in the thermal decomposition process, which will complicate the kinetic analysis. Also, the dwell time or reaction time in the shock tube is in the range of few hundreds of microseconds to a few milliseconds. With these special features, the pulse nature of the heating phenomenon in the shock tube can be used to study the thermal decomposition of the molecules of interest.

Shock tube techniques have received enormous attention as a chemical reactor for the past 5 to 6 decades.[1, 5-7] These features of the shock tube makes it a unique technique

as discussed above for investigation of thermal rate constants at elevated temperatures for numerous reactions.

I.2. Importance of thermal rate constants

For the modeling of combustion, incineration, detonation and for many other such phenomenons, the thermal rate constants are very much required. The molecule dissociates by a complex mechanism during its thermal decomposition. The compounds such as chlorofluorocarbons (CFCs) are one of the main causes of the ozone destruction in the stratosphere. These are non-biodegradable and are destroyed by incineration. Hence, kinetic modeling is essential in order to understand the complete mechanism of the incineration of these compounds. Kinetic modeling, in turn, needs reliable thermal rate constants.

It is well known that the experimental conditions define the rate constant of any elementary reaction. For example, unimolecular reactions have strong temperature dependence of rate constants as they usually have a high energy barrier. Hence, determination of the thermal rate constants of various channels in the thermal decomposition of haloethanols at high temperatures has been undertaken in the present investigation. The details of this research are presented in this thesis. Some other techniques which are available have been briefly discussed next.

I.3.Other methods of determining thermal rate constants

There are numerous techniques available for the measurement of thermal rate constants, which are either static cell or flow reactors, most of which are successful in measuring the thermal rate constants only up to some narrow temperature range. The static cell suffers from the defect of wall effects wherein the decomposition process might be catalyzed by collisions of the species to the wall[8-14]. Though, the wall effects are completely negligible in flow reactors, the temperature range of the study using this technique is very narrow. This technique is very widely used to study the unimolecular reactions[15-17], bimolecular reactions[18], and ion-molecule reactions[19].

Other spectroscopic techniques such as time resolved diode laser absorption technique[20-22] (TRDLA), infrared multiphoton dissociation[23-27] (IRMPD), flash photolysis [28-31], and infrared chemiluminescence[32,33] etc. can also be used to obtain the thermal rate parameters. Even though these techniques are highly sensitive, none of these methods give the thermal rate coefficients at elevated temperatures. Few of them can be coupled with the shock tube in order to obtain accurate thermal rate parameters.

I.4. Detection techniques in shock tube chemistry

The shock tube is a well established technique for determination of the thermal rate constants and it is fully understood by chemists. The drawbacks and difficulties in the shock tube method have been reviewed by Belford and Strehlow[34]. However, these drawbacks were eliminated to a large extent by the consistent efforts of Lifshittz, Bauer, Micheal, Tsang, Tschuikow-Roux and others. This technique has been used extensively for the study of the thermal decomposition of aliphatic[35-39] and aromatic[40-43]

hydrocarbons, heterocyclic[44-49] compounds, halogenated[50-54] compounds and compounds containing many other functional groups[55-59]. In this technique, equilibrated post-shock mixtures are analyzed by various detection techniques which include gas chromatograph (GC), GC with a mass spectrometer (GC-MS) and Fourier Transform Infrared (FTIR) spectrometer. The concentration profiles as a function of temperature have been used to obtain the kinetic parameters by modeling.

In addition, atomic resonance absorption spectroscopy (ARAS) is one of the widely used spectroscopic techniques in shock tube studies. This can be used as real-time diagnostic tool for getting the thermal rate constants. This technique is being used to obtain the kinetic parameters of the reaction like dissociation of molecular hydrogen[60] to atomic hydrogen, by following the absorption of hydrogen atom. However, this technique can be used only if the decomposition process involves atoms.

The important investigations carried out using ARAS technique include $O + N_2O \rightarrow O_2 + N_2$[61] (by following the absorbance of oxygen atom), $N_2O \rightarrow N_2 + O$[62,63] (by following the absorbance of oxygen atom), $D_2 + O \rightarrow OD + D$[64] (by following the absorbance of deuterium), $D_2 + Ar \rightarrow D + D + Ar$[65] (by following absorbance of Deuterium atom), $H + CH_4 \rightarrow H_2 + CH_3$[66], $SO_2 + M \rightarrow SO + O$[67], $HCN + Ar \rightarrow H + CN$[68], $C_2H_4 \rightarrow C_2H_3 + H$[69], and $CH_4 + Ar \rightarrow CH_3 + H + Ar$[70]. Michael et al. have extensively investigated the thermal decomposition of environmentally hazardous compounds mainly halogenated hydrocarbons using ARAS technique. These studies include the thermal decomposition of halogenated compounds[71-74], $CH_3Br + M \rightarrow CH_3 + Br + M$[75] and $CH_3I + M \rightarrow CH_3 + I + M$[76].

Another commonly used technique coupled to shock tube for kinetic studies which appears to offer the best combination of resolution and sensitivity for fast processes among the well-established methods is the laser schlieren (LS) technique. This technique is especially employed for those reactions which take place in very short times, typically about $10\mu s$. The method finds applications in finding vibrational relaxation times, incubation times and dissociation rate constants at elevated temperatures. Important investigations carried out using this technique include the measurement of the vibrational relaxation of H_2 (He, Ar, Ne, Ar, Kr as bath gases)[77,78], D_2 (Ar as bath gas)[79], D_2 (He, Kr as bath gas)[80], HD(HD as collision partner)[81], O_2 (O_2 as collision partner)[82], N_2 (N_2 as collision partner)[83], F_2 (F_2 and Ar as collision partner)[84], F_2 (He as collision partner)[85], HCl and DCl[86]. This technique has also been extensively used for the decomposition studies of CO_2[87], N_2O[88], SO_2[89], NF_3[90], CH_4[91] and Cyclobutane[92]. Though, this technique can be used only if the mechanism of thermal decomposition of the molecule under investigation has independently been well established.

Another commonly used technique coupled to shock tube is the emission spectroscopy for measurement of ignition delay at high temperature. These studies were done using online measurement of the CH emission near the end of the shock tube in our laboratory. Ignition delay studies on hydrocarbon fuels are suitable for developing chemical kinetic models that gives better insight in to the decomposition mechanisms. Recently, focus has been on measurements of individual species concentration time histories[93-96] that also improve the understanding of the details of reaction mechanisms. A shock tube has been used in combination with emission spectroscopy in our laboratory to

generate the ignition delay data on Jet Propellent-10 and the complete details of this have been presented in the chapter VI.

Some of the investigations carried out using this technique include the measurement of ignition delay of the C_3H_8-O_2-Ar system investigated behind reflected shock waves in the temperature range of 1350-1800 K and the pressure range of 0.75-1.57 bar[97]. The ignition delay time measurement in blends of CH_4/n-C_4H_{10}[98], C_2H_6 - O_2 mixture[99] and H_2-O_2-Ar[100] are some of the investigations that have also been reported in the past using this technique.

I.5. Why did we choose shock tube technique for the present investigation?

The characteristic features of shock tube technique have been discussed in Section I.1. The C-Cl bond scission was found to be the initiation step in thermal decomposition of 1, 2-dichloroethane using the static cell studies[101]. On the other hand, HCl elimination channel was found to be the major channel for its thermal decomposition using chemical activation studies[102-105]. However, these two observations are not in agreement with the fundamental aspects of microcanonical RRKM and transition state theory (TST) theory. In other words, these results suggest that, the outcome of reaction can be changed by the nature of the excitation. It is possible that the results obtained using the static cell experiments are affected by heterogeneous reactions. To resolve this anomaly, a single pulse shock tube technique was established in our laboratory in showing that thermal

decomposition of 1, 2-dichlorothane[106] takes place through 1, 2-HCl elimination and there was no difference between chemical and thermal activation.

I.6. Present investigations

I.6.A. Thermal decomposition of haloethanols

Recently, 2-fluoroethanol was suggested as a replacement for chlorofluorocarbons (CFC).[107] Hence, it is important to understand the physical and chemical properties of these molecules before putting them into commercial applications. Most often, the choice of disposing these chemicals is to incinerate them, and experimental data on the mechanism of thermal decomposition would be useful. Hence, both experimental and theoretical studies was performed on the pyrolysis of 2-fluoroethanol[108]. Objective of this investigation was to determine the kinetics of HF and H_2O elimination reactions and to propose the mechanism of thermal decomposition at high temperature and pressure. Another motive was to understand the β-substitution effect of the OH on the barrier to HF elimination and the effect of F on H_2O elimination barrier both experimentally and theoretically. With similar objective experimental and theoretical investigation on 2-chloroethanol and 2-bromoethanol were performed in this work.

I.6.A.1. Thermal decomposition of 2-chloroethanols

Our laboratory investigated the thermal decomposition of 2-fluoroethanol where the unimolecular elimination of HF and H_2O were found to be the major channel under our experimental condition in the temperature range 1000-1200K.[108] However, there is one report available on the thermal decomposition of CEOH describing only the HCl elimination channel in the temperature range 703- 769^0 K.[109] Will the pyrolysis of 2-chloroethaonl lead to the H_2O elimination at high temperatures? With this objective, thermal decomposition study of 2-chloroethanol was performed in our laboratory previously. However, it was not possible to resolve the two major products from the decomposition of CEOH namely acetaldehyde and vinyl chloride using Porapak-Q column in our previous analysis.[110] Hence, experiments on the thermal decomposition of 2-chloroethanol has been repeated using appropriate column in the temperature range of 930-1100 K behind the reflected shock wave in a shock tube.

A theoretical report available on this molecule mainly considers the structure and the vibrational frequencies of the ground state rotational isomers.[111] There is no theoretical report available so far for CEOH on H_2O and HCl elimination to the best of our knowledge. However, there are reports available in the literature that explains the kinetics of HCl and H_2O elimination from the ethyl chloride[112] and ethyl alcohol[113] respectively. Another motive for performing these experiments was to investigate the effect of β-chlorine substitution on the kinetics of H_2O elimination and effect of β-hydroxyl substitution on the kinetics of HCl elimination in the same molecule. These experiments were performed to understand the thermal stability of 2-chlorothanol, that has not been reported so far.

12

A chemical kinetic simulation has been performed to simulate the product distribution. This shows that the thermal decomposition of 2-chloroethanol molecule follows a complex mechanism. Ab initio, density functional theory (DFT) and transition state theory (TST) calculations have also been carried out to determine the kinetics of HCl and H_2O elimination reactions. These results were used to verify the experimental results. Experimental thermal decomposition results on kinetics of unimolecular elimination of HCl and H_2O from 2-chloroethanol have been discussed in detail in Chapter III. In addition to the above 2-chloroethanol, pyrolysis of ethyl chloride has been studied. This molecule has been used as an external standard to estimate the temperature behind reflected shock in this work.

I.6.A.2 Thermal decomposition of 2-bromoethanols

The studies of halogenated alcohols have attracted great attention realizing their importance in the atmospheric and combustion chemistry.[114] The first order gas phase kinetics of thermal decomposition of 1, 1- and 1, 2-Dibromoethanes in the static system at 415.5^{o}C was studied by the Maccoll et al. in 1971.[115] The reactions observed in each case was only HBr elimination leading to vinyl bromide. Here, the reported activation barrier for the unimolecular HBr elimination is 50.52kcal/mol which is higher than the that(48.4kcal/mol) of the HBr elimination from ethyl bromide.[112] However, the experimental activation energy for HCl elimination from 1,2-dichlorothane reported by Rajakumar et al. is 57.8kcal/mol at high temperature which is similar to HCl elimination from ethyl chloride.[106] These results show that the barrier for HBr elimination is lower as compared to that of the HCl elimination. Will the thermal decomposition of 2-

bromoethanol (BEOH) show unimolecular elimination of H_2O at higher temperatures? With this question in mind, shock tube studies on BEOH have been performed in our laboratory.

To the best of our knowledge the high temperature gas phase thermal reactions of the BEOH have never been investigated both experimentally and theoretically in the past. However, there have been reports available in the literature that deals with the kinetics of HBr and H_2O elimination from the ethyl bromide[112] and ethyl alcohol[113] respectively. Also, it will be interesting to study the effect of β-bromine atom on the barrier of H_2O elimination and at the same time the effect of β-hydroxyl group on the barrier of HBr elimination in the same molecule.

The chemical kinetic simulation was performed to propose the plausible reaction scheme for the thermal decomposition of the BEOH to account for the formation of different reaction products that was validated by comparison to experimental shock tube results. The sensitivity analysis has been performed with the aim of clarification of the importance of the different elementary reactions in scheme. This study has aimed mainly at experimental determination of the Arrhenius parameters for the two elementary unimolecular elimination reactions i.e. 1, 2-HBr and 1, 2-H_2O from BEOH. Ab initio, density functional theory (DFT) and transition state theory (TST) calculations have also been performed to estimate the kinetics of these elimination reactions. These calculations were done to verify the experimental results. These results would certainly lead to better understanding of pyrolysis mechanism of the BEOH. The detailed kinetic study, both

experimental and theoretical and thermal stability of 2-bromoethanol are discussed in Chapter IV.

I.6.B. Computational calculations of enthalpy of formation of haloethanols

The data on enthalpy of formation are useful for the determination of enthalpy of reaction of different gas phase unimolecular elimination reaction at high temperature in shock tube. In fact, these data were needed for the modeling of the thermal decomposition mechanism of the fluoroethanol, chloroethanol and bromoethanol at high temperature and were not available in literature. Recently, computational methods have been well established to estimate the enthalpies of formation of various molecules because the experimental measurements of thermodynamic properties are quite expensive and difficult to measure. Hence, computational methods HF, MP2, B3LYP, G2, G3, G2MP2, G3B3, G3MP2B3, CBS-Q, CBS-QB3 and CCSD/cc-pVDZ were employed to evaluate enthalpy of formation of haloethanols using atomization and isodesmic reactions. Benson's group and bond additivity methods were also employed to estimate the enthalpy of formation.[118] These results on thermo chemical data were used to evaluate polynomial thermodynamic coefficient which are needed for the modeling of thermal decomposition mechanism of haloethanols and have been discussed in detail in chapter V. These data can also be used for the determination of the kinetics of reaction. These calculated values of enthalpies of formation of haloethanols also give information about its structure and reactivity. However, after completion of this work, we found that there is one report available in literature on the experimental and theoretical calculation of

enthalpy of formation of haloethanols.[116] The standard molar enthalpies of formation of 2-chloro-, 2-bromo-, and 2-iodoethanol, at 298.15 K, were determined experimentally using rotating-bomb combustion calorimetry. However, enthalpies of formation of 2-fluoroethanol was not reported experimentally. They have investigated enthalpies of formation of 2-fluoroethanol at B3LYP/cc-pVTZ and CBS-QB3 level of theory using isodesmic and isogyric gas-phase reactions. Also, theoretical results on enthalpy of formation for 2-chloroethanol and 2-bromoethanol have not been reported. All our computations were performed using Gaussian-03 suite of program[117] for geometry optimization. The details are discussed in Chapter V.

I.6.C. Chemistry of Jet Propellent-10 (JP-10) Ignition

Exo-tetrahydrodicyclopentadiene ($C_{10}H_{16}$) is a single component energetic fuel (less variable) which is being used in scramjet engines because of its high volumetric density (owing to 39.6MJ/m^3 strained cyclic geometry) and higher stability. There has been recent increase in the need for ignition delay data for fuels used in supersonic combustion ramjet engines (volume limited combustion chamber).[93-96] Also, very little ignition time data available for JP-10 (Aviation Fuel) and combustion chemistry has not been very well-characterized. In fact, there are no reports available on ignition experiments of JP-10 with TEA as an additive to the best of our knowledge. Hence, these ignition data on JP-10 with and without additive would be useful for development of combustion models in future.

With these objectives, the JP-10 (Exo-tetrahydrodicyclopentadiene, $C_{10}H_{16}$) ignition delay times were measured behind a single pulse reflected shock wave in shock

tube. Experiments were performed over high temperature, high pressure, and three equivalence ratio and for different composition. Ignition delay was reduced by raising the temperature. Also, it was found that the delay was reduced significantly by addition of Triethyl amine. A higher level quantum chemistry calculation has also been performed to obtain the bond dissociation energies of C-H bonds in JP-10. The details are discussed in Chapter VI.

I.7.References

1. Bhaskaran, K.; Roth, P., Progress in Energy and Combustion Science; **2002**, 28, 151.

2. Gaydon, A.; Hurle, I.R. The shock tbe in high temperature chemical physics, Reinhold, New York. **1963**.

3. Jagadeesh, G. ; Resonance; **2008**, 13, 752.

4. Lifshitz, A. in Handbook of Shock Waves edited by Lifshitz, A.; Ben-Dor, G.; Igra, O.; Elperin, T. Academic Press, New York. **2001**, 3, ix.

5. Bauer, S.H. Annu. Rev. Phys. Chem. **1965**. 16. 245.

6. Tsang, W.; Lifshitz, A. Annu. Rev. Phys. Chem. **1990**. 41. 559.

7. Michael, J.V.; Lim, K.P. Annu. Rev. Phys. Chem. **1993**. 44. 429.

8. Perrin, D.; Martin, R. Int. J. Chem. Kinet. **2000**, 32, 340.

9. Bauge, J.C.; Battin-Leclerc, F.; Baronnet, F. Int. J. Chem. Kinet. **1998**, 30, 629.

10. Zils, R.; Martin, R.; Perrin, D.; Int. J. Chem. Kinet. **1998**, 30, 425.

11. Zils, R.; Martin, R.; Perrin, D.; Int. J. Chem. Kinet. **1998**, 30, 439.

12. Walker, K.L. ; Jardine, R.E. ; Ring, M.A. ; O'Neal, H.E. Zils, R.; Martin, R.; Perrin, D.; Int. J. Chem. Kinet. **1998**, 30, 69.

13. Huybrechts, G.; Eerdekens, K. Zils, R.; Martin, R.; Perrin, D.; Int. J. Chem. Kinet. **2001**, 33, 191.

14. Laws, P.A.; Hayley, B.D.; Anthony, L.M.; Roscoe, J.M. J. Phys. Chem. A **2001**, 105, 1830.

15. Winkler, I.C.; Stachnik, R.A.; Steinfeld, J.I.; Miller, S.M. J. Chem. Phys. **1986**, 85, 890.

16. Onsehuk, A.A.; Strunin, V.P.; Ushakova, M.A.; Panfilov, V.N. Int. J. Chem. Kinet. **1998**, 30, 99.

17. Alzueta, M.U.; Oliva, M.; Glarborg, P. Int. J. Chem. Kinet. **1998**, 30, 683.

18. Mcdaniel, A.H.; Allendorf, M.D. J. Phys. Chem. A. **1998**, 102, 7804.

19. Bierbaum, V.M.; Ellison, G.B.; Leone, S.R.; in Gas Phase Ion Chemistrey, edited by Bowers, M.T. Academic Press, New York. **1984**, 3, 1.

20. Laguna, G.A.; Baughcum, S.L. Chem. Phy. Lett. **1982**, 88, 568.

21. Wahner, A.; ZetZsch, C.; Berg. Bunsenges. Phy.Chem. **1985**, 89,323.

22. Balla, R.J.; Pasternack, J. Phys. Chem. **1987**, 91, 73.

23. Ashfold, M.N.R.; Hancock, G. in Ashmore, P.G.; Donovan, R.J.(Eds); Gas Kinetics and Energy transfer − Royal Society of Chemistry, London, **1980**, 4,73.

24. Danen, W.C.; Jang, J.; in Steinfeld, J.I (Ed), Laser-Induced Chemical Processes, Plenum, New York, **1981**,45.

25. Douglas, K.R. Chem. Soc. Rev. **1990**, 19, 407.

26. Hall, R.B.; Kaldor, A. J. Chem. Phys. **1979**, 70, 4072.

27. Puspa, K.K.; Kumar, A.; Vatsa, R.K.; Naik, P.D.; Rao, K.A.; Mittal, J.P.; Parthasarathy, V.; Sarkar, S.K. Chem. Phy. Lett. **1996**, 249, 167.

28. Porter, G. Proc. Roy. Soc. (London) **1950**, A200, 284.

29. Christie, M.I.; Norrish, R.G.W.; Porter, G. Proc. Roy. Soc. (London) **1952**, A216, 152.

30. Declemy, A.; Rulliere, C.; Rev. Sci. Instrum. **1986**, 57, 2733.

31. Porter, G.; Discuss. Faraday. Soc. **1962**, 33, 198.

32. Wodarczyk, F.J.; Moore, C.B. Chem. Phys. Lett. **1974**, 26, 284.

33. Arunan, E.; Setser, D.W. J. Phys. Chem. **1991**, 95, 4190.

34. Belford, R.L.; Strehlow, R.A.; Ann. Rev. Phys. Chem. **1969**, 20, 247.

35. Hidaka, Y.; Higashihara, T.; Ninomiya, N.; Oshita, H.; Kawano, H. J. Phys. Chem. **1993**, 97, 10977.

36. Hidaka, Y.; Nakamura, T. ; Tanaka, H. ; Inami, K. ; Kawano, H. Int. J. Chem. Kinet. **1990**, 22, 701.

37. Hidaka, Y.; Nakamura, T. ; Tanaka, H. ; Jinno, A.; Kawano, H.; Higashihara, T. Int. J. Chem. Kinet. **1992**, 24, 761.

38. Hidaka, Y.; Oki, T.; Kawano, H. Int. J. Chem. Kinet. **1989**, 21, 689.

39. Lifshitz, A.; Frenklach, M.; Burcat, A. J. Phys. Chem. **1976**, 80, 2437

40. Colket, M.B.III.; Seery, D.J.; Proc. 25th Int. Symp. on Combustion, **1994**, 883.

41. Laskin, A.; Lifshitz, A.; Proc. 26th Int. Symp. on Combustion, **1997**, 669.

42. Laskin, A.; Lifshitz, A.; Proc. 27th Int. Symp. on Combustion, **1999**, 313/

43. Lifshitz, A.; Cohen, Y.; Braun-Unkhoff, M.; Frank, P. 26th Int. Symp. on Combustion, **1997**, 659.

44. Laskin, A.; Lifshitz, A. J. Phys. Chem. **1997**, 101, 7787.

45. Lifshitz, A.; Bidani, M. J. Phys. Chem. **1989**, 93, 1139.

46. Lifshitz, A.; Bidani, M.; Bidani, S. J. Phys. Chem. **1986**, 90, 5373.

47. Lifshitz, A.; Bidani, M.; Bidani, S. J. Phys. Chem. **1986**, 90, 6011.

48. Lifshitz, A.; Tamburu, C.; Shashua, R. J. Phys. Chem. **1997**, 101, 1018.

49. Mackie, J.C.; Colket, M.B.III.; Nelson, P.F.; Esler, M. J. Phys. Chem. **1990**, 94, 4099.

50. Tsang, W. J. Phys. Chem. **1984**, 88, 2812.

51. Tsang, W. J. Phys. Chem. **1986**, 90, 414.

52. Tsang, W.; Lifshitz, A. Int. J. Chem. Kinet. **1998**, 30, 621.

53. Okada, K.; Tschikow-Roux, E.; Evans, P.J. J. Phys. Chem. **1980**, 84, 467.

54. Tschikow-Roux, E.; Quiring, W.J. J. Phys. Chem. **1971**, 75, 295.

55. Barnard, J.A.; Cocks, A.T.; Parrot, T.K. J. Chem. Soc. Faraday. Trans. **1976**, 72, 456.

56. Gutman, D.; Braun, W.; Tsang, W. J. Chem. Phys. **1977**, 67, 4291.

57. Lifshitz, A.; Tamburu, C.; Int. J. Chem. Kinet. **1998**. 30. 341.

58. Rickborn, S.E.; Ring, M.A.; O'Neal, H.E. Int. J. Chem. Kinet. **1984**. 16. 1371.

59. Tsang, W. Int. J. Chem. Kinet. **1984**. 16. 1543.

60. Myerson, A.L.; Watt, W.S. J. Chem. Phys. **1968**, 49, 425.

61. Monat, J.P.; Hanson, R.K. ; Kruger, C.H. ; Comb. Science Techn. **1977**, 16,21.

62. Olschewski, H.A.; Troe, J.; Wagner, H.G. Berg. Bunsenges. Phy.Chem. **1966**, 70, 450.

63. Roth, P.; Just, Th. Berg. Bunsenges. Phy.Chem. **1977**, 81, 572.

64. Sulzmann, K.G.P. ; Kline, J.M. ; Penner, S.S. Proc. 12th Int. Symp. Shock Tubes and waves edited by Lifshitz, A.; Rom, J. The Magnes Pres, The Hebrew University of Jerusalem, **1980**, 465.

65. Appe, D.; Appleton, J.P. 15th international symposium on combustion, Combustion Institute, Pittsburgh, **1975**, 701.

66. Roth, P.; Just, Th. Berg. Bunsenges. Phy.Chem. **1975**, 79, 682.

67. Dove, J.E.; Nip, W.S.; Teitelbaum, H. 15th International Symposium on Combustion, Combustion Institute, Pittsburgh, **1975**, 903.

68. Olschewski, H.A.; Troe, J.; Wagner, H.G. Z. Phys. Chem. N.F. **1965**, 44, 173.

69. Just, Th.; Roth, P.; Damm, R. 16th International Symposium on Combustion, Combustion Institute, Pittsburgh, **1977**, 961.

70. Roth, P.; Just, Th. Berg. Bunsenges. Phy.Chem. **1976**, 80, 171.

71. Kumaran, S.S. ; Su, M.-C. ; Lin, K.P. ; Michael, J.V. J. Phys. Chem. **1996**, 100, 7533.

72. Kumaran, S.S. ; Su, M.-C. ; Lin, K.P. ; Michael, J.V. Chem. Phys. Lett. **1995**, 59, 243.

73. Kumaran, S.S. ; Su, M.-C. ; Lin, K.P. ; Michael, J.V. Wagner, A.F. ; Dixon, D.A. ; Kiefer, J.H. ; Difelice, J. J. Phys. Chem. **1996**, 100, 15827.

74. Michael, J.V. ; Kumaran, S.S. Combust. Sci. Tech.; **1998**, 31, 134.

75. Hranisavljevic, J.; Carrol, J.J.; Su, M.-C.; Michael, J.V. Int. J. Chem. Kinet. **1998**, 30, 859.

76. Kumaran, S.S. ; Su, M.-C. ; Michael, J.V. Int. J. Chem. Kinet. **1997,** 29, 535.

77. Dove, J.E.; Jones, D.G.; Tellelbaum, H.; 14th International Symposium on Combustion, Combustion Institute, Pittsburgh, **1973**, 177.

78. Dove, J.E.; Tellelbaum, H. Chem. Phys. **1974**, 6, 431.

79. Kiefer, J.H.; Lutz, R.W. J. Chem. Phys. **1966**, 44, 658.

80. Bird, P.F.; Breshears, W.D. Chem. Phys. Lett. **1972**, 13, 529.

81. Simpson, C.J.S.M.; Price, I.J.; Crowther, M.E. Chem. Phys. Lett. **1975**, 34, 181.

82. Bander, J.A.; Sanzone, G.; Rev. Sci. Instrum. **1974**, 45, 949.

83. Breshears, W.D.; Bird, P.F. J. Chem. Phys. **1968**, 48, 4768.

84. Diebold, G.J.; Santoro, R.J.; Goldsmith, G.J. J. Chem. Phys. **1974**, 60, 4170.

85. Diebold, G.J.; Santoro, R.J.; Goldsmith, G.J. J. Chem. Phys. **1975**, 62, 296.

86. Breshears, W.D.; Bird, P.F. J. Chem. Phys. **1969**, 50, 333.

87. Kiefer, J.H. J. Chem. Phys. **1974**, 61, 244.

88. Dove, J.E.; Nip, W.S.; Tellelbaum, H.; 15th International Symposium on Combustion, Combustion Institute, Pittsburgh, **1974**, 903.

89. Kiefer, J.H. J. Chem. Phys. **1975**, 62, 1354.

90. Breshears, W.D.; Bird, P.F. J. Chem. Phys. **1978**, 68, 2996.

91. Gardiner Jr., W.C.; Owen, J.H.; Clark, T.C.; Dove, J.E.; Bauer, S.H.; Miller, J.A.; McLean, W.J. 15th International Symposium on Combustion, Combustion Institute, Pittsburgh, **1974**, 857.

92. Lewis, D.K.; Feinstein, S.A.; Jeffers, P.M. J. Phys. Chem. **1977**, 81, 1883.

93. Davidson, D. F.; D.C.; Horning, J.T. Herbon; R.K. Hanson; Proc. Combust.Inst. **2000,** 28, 1687.

94. Davidson, D. F.; D.C. Horning; R.K. Hanson; AIAA; **1999**, 99, 2216.

95. Colket, M. B.; L.J. Spaddaccini; J. Propulsion and Power; **2001**, 17, 315.

96. Olchansky, E.; A. Burcat: 21st International Symposium on Shock Waves; **2001,** 5962.

97. Kim, K.; Shin, K. S.; Bull. Korean Chem. Soc. **2001**, *22*, 303.

98. Healy, D.; Kopp, M. M.; Polley, N. L.; Petersen, E. L.; Bourque, G.; Curran, H. J. Energy & Fuels; **2010**, *24*, 1617.

99. M. Nagaboopathy, G. Hegde, K. P. J. Reddy, V. Chandrasekhar, D. S. S. Hembram, D. Bilehal,E.Arunan.;Proceedings of the 26th International Symposium on Shockwaves, Ed.: K. Hannerman, **2007.**

100.   Pang, G.; Davidson, D.; Hanson, R. Proceedings of the Combustion Institute, **2009**, *32*, 181.

101.   Barton, D.H.R.; Howlett, K.E.; J. Chem. Soc. **1949**, 155 and 165.

102.   Hassler, J. C.; Setser, D. W.; Johnson, R. L.; J. Chem. Phys. **1966**, 45, 3231;

103.   Hassler, J. C.; Setser, D. W.; J. Chem. Phys. **1966**, 45, 3246.

104.   Dees, K.; Setser, D. W.; J. Chem. Phys. **1968**, 49, 1193.

105.   Roussel, P. B.; Lightfoot, P. D.; Carlap, F.; Catoire, V.; Lesclaux, R.; Forst, W.; J. Chem. Soc. Faraday Trans. **1991**, 87, 2367.

106.   Rajakumar, B.; Reddy, K. P. J.; Arunan, E. *J. Phys. Chem. A* **2002**, *106*, 8366.

107.   Kelly, T.; Manning, M.; Bonard, A.; Wenger, J.; Treacy, J.; Sidebottom, H. Transport and Chemical Transformation in the Troposphere, Proceedings of EUROTRAC Symposium, 6th, Garmisch-Partenkirchen, Germany, **2000**, 410-413.

108.   Rajakumar, B.; Reddy, K. P. J.; Arunan, E. *J. Phys. Chem. A* **2003**,*107*, 9782.

109.   Skingle, D. C.; Stimson, V. R. Aust. J. Chem. **1976**, 29, 609.

110.   Proceedings of the 24th International symposium on shock waves, **2004**, 1, 621.

111.   Buemi, G. *J. Chem. Soc. Faraday Trans*. **1994**, *90*, 1211.

112.   Mcgrath, M. P.; Rowland, F. S.; *J. Phys. Chem. A,* **2002**,106, 8191.

113.   Park, J.; Zhu, R. S.; Lin, M. C.; *J. Chem. Phys.* **2002**, 117, 3224.

114.   Indulkar,Y.N.; Upadhayaya,H.P.; Kumar,A.; Waghmode,S,B.; Naik,P.D. *J. Phys. Chem. A* **2009**, 113, 8462.

115.   Good,P.T.; Maccoll, A. *J. Chem. Soc. (B),* **1971,** 268.

116.   Bernardes, C. E. S.; Minas, M. E.; Amaral, M. P. F.; Ferreira, A. I. M. C. L.; Ribeiro, M. A. V.; Cabral, B.; J. Phys. Chem. A; **2007**, 111, 1713.

117.   Frisch, M. J.; Trucks, G. W.; Schlegel, H. B.; Scuseria, G. E.; Robb, M. A.; Montgomery, J. R. C. J. A.; Vreven, T.; Kudin, K. N.; Burant, J. C.; Millam, J. M.; Iyengar, S. S.; Tomasi, J.; Barone, V.; Mennucci, B.; Cossi, M.; Scalmani, G.; Rega, N.; Petersson, G. A.; Nakatsuji, H.; Ehara, M. H. M.; Toyota, K.; Fukuda, R.; Hasegawa, J.; Ishida, M.; Nakajima, T.; Honda, Y.; Kitao, O.; Nakai, H.; Klene, M.; Li, X.; Knox, J. E.; Hratchian, H. P.; Cross, J. B.; Adamo, C.; Jaramillo, J.; Gomperts, R.; Stratmann, R. E.; Yazyev, O.; Austin, A. J.; Cammi, R.; Pomelli, C.; Ochterski, J. W.; Ayala, P. Y.; Morokuma, K.; Voth, G. A.; Salvador, P.; Dannenberg, J. J.; Zakrzewski, V.

G.; Dapprich, S.; Daniels, A. D.; Strain, M. C.; Farkas, O.; Malick, D. K.; Rabuck, A. D.; Raghavachari, K.; Foresman, J. B.; Ortiz, J. V.; Cui, Q.; Baboul, A. G.; Clifford, S.; Cioslowski, J.; Stefanov, B. B.; Liu, G.; Liashenko, A.; Piskorz, P.; Komaromi, I.; Martin, R. L.; Fox, D. J.; Keith, T.; Al-Laham, M. A.; Peng, C. Y.; Nanayakkara, A.; Challacombe, M.; Gill, P. M. W.; Johnson, B.; Chen, W.; Wong, M. W.; Gonzalez, C.; Pople, J. A. *Gaussian 03*, Revision A.1; Gaussian, Inc.: Pittsburgh, PA**, 2003.**

118.   Benson S. W.; Thermo chemical kinetics, 2nd ed.; John Wiley & Sons, New York, **1976.**

Chapter II

Experimental and Theoretical Methods

II.1. Uniqueness of the Shock Tube

Shock tube is an excellent tool to obtain thermal rate constants k (T) at high temperature as explained earlier in the chapter I. Shock tubes are a unique chemical reactor or vessel using which temperature gradients exceeding million degrees Kelvin per second can be achieved. The unique feature of this technique is that the sample will uniformly be heated to the desired temperatures without experiencing the ramp strictly under homogeneous conditions when it is exposed to the shock wave. Similarly, the heated test gas will be cooled to room temperature in ms time by expansion wave traveling from other end of the tube. The cooling rates observed were in the range of 0.5 to 5 K/μs. Heating of the sample behind reflected shock wave and cooling by the expansion wave in this manner is defined as single pulse operation. When the test gas in the shock tube is exposed to the reflected shock, only the test gas will be experiencing the temperature but the walls of the tube will be at the room temperature. The two zones (the test gas and the walls of the tube) are kept at two different temperatures but they are separated by no physical boundary. Very low concentration of the sample in ppm level is required for the investigation of any molecule using this technique. In the decomposition process, this avoids any secondary reactions, which will complicate the kinetic analysis. The dwell time or reaction time is generally in the range of few hundreds of μs to 2 ms. These characteristic features makes the single pulse nature of the shock tube unique for investigation of the pyrolysis of any molecule having enough vapour pressure.

II.2.The Shock Tube

Shock tube is a long cylindrical tube of uniform internal diameter and it consists of two portions, driver and driven section. These two sections are separated by a thin metallic diaphragm[1]. The shorter high pressure side is referred to as the driver section and the low-pressure longer side is referred to as the driven section. Shock wave is generated by the sudden bursting of the diaphragm by increasing the pressure in the driver section. This leads to the formation of primary shock that travels in driven section with a velocity of 2 to 3 times the velocity of the sound in the medium ahead of it. This primary shock increases the temperature and pressure of test gas to T_2 and P_2 in the driven section. The primary shock reflected from end flange of the driven section will further rise the temperature and pressure by traveling back into the previously heated test gas. The temperature achieved behind the reflected shock wave is defined as reflected shock temperature and is denoted as T_5. The idealized picture of the formation of shock wave has been explained in detail in the section II.4.

The shock tube facility used for the chemical kinetic studies in the present investigation is completely homemade. This facility is very similar to those used for this purpose anywhere around the world. The shock tube facility used in present investigation was developed earlier for the chemical kinetic studies in our laboratory. Commercial aluminum rod of 101.6 mm diameter was used for fabrication of this shock tube. This tube was segmented in to two sections of equal length 609.6 mm each. Each segment was bored to 50.8 mm internal diameter and its internal surface was smoothened to micron level. Male and female threading of the same size was made on two ends of each

segment. This thread size was 10 per inch. For the perfect sitting of the "O" ring on the projection of the male threaded side, smooth groove of the size 71.25mm x 62.30mm was turned. High quality silicon rubber "O" rings were used in the present work. . The schematic view of one of the segment has been depicted in the Figure II.1. These segments are connected with the help of the threads and an "O" rings in between till the required length was achieved. Similar segments were used for both driver and driven section. Each section length can be altered by attaching or detaching the segments. In fact, during the course of this work, a dump tank of diameter 100mm having a length of 1661mm has been added near to the diaphragm in the driven section at an angle of 45^0 to this shock tube facility. However, many laboratories do not use dump tank. Main purpose of adding a dump tank was to quench the multiple reflections which can lead to shock waves of smaller intensity.

In case of 2-chloroethanol and 2-bromoethanol experiments, the driven and driver section length was 2540 and 1850 mm respectively. The driver and driven sections are fixed with an adapter. Two metal flanges are fixed to the two ends, one joined at the start of the driven section and another one is connected to the end of the driver section. These mounting were done in such a way that the "O" rings on their faces face each other. The aluminum metal diaphragm can be placed in between these two flanges and can be closed with the help of the bolts provided round the circumference. An aluminum flange with an "O" ring seal was used to close the other ends of the driver and driven section. However, driven section flange has a hole of 6.36 mm diameter at its center for loading the test gas and for withdrawing it after the experiment is over for further qualitative and quantitative analysis. At this hole a four-way connecter with 6.36 mm ball valves (Swagelok) was

connected for the purpose of loading and collecting the sample. A hole of 9.525 mm diameter was created on the body of the shock tube which is at 900 mm from the diaphragm station at the center of the driver section. At this hole a four-way connector with 6.35 mm diameter ball valves (Swagelok) was connected for evacuating the driver section. Similarly, another four-way connector with ball valves (Swagelok) was joined in the driven section at 100 mm from the diaphragm station for the purpose of evacuation of the driven section.

Two piezoelectric pressure transducers were mounted in the driven section separated by 304 mm for the measurement of the velocity of shock. These pressure transducers were mounted on the tube in such a way that it is in flush with the inner surface of the shock tube. A third piezoelectric pressure transducer (Kistler model: 601 A) which is in flush with the inner surface of the shock tube was mounted at 25 mm from the end flange of the driven section. This transducer was used for recoding the arrival of primary and reflected shocks. A universal counter (Agilent 53131A, 225MHz), connected to the two piezoelectric pressure transducers, was used to record the time taken by the shock wave to travel the fixed distance between two stations. This counter was started by first transducer and the stopped by the second transducer. A digital storage oscilloscope (Tektronix, TDS-2014B/100MHz/1GS/s) connected to the piezoelectric pressure transducer was used for recording the pressure jumps across the shock front. The oscilloscope was triggered obtaining the output from one of the piezoelectric pressure transducer. Hence, the shock velocity measured using the universal counter can easily be cross-checked with that measured using the oscilloscope independently. The schematic

diagram of the shock tube can be seen in the Figure II.2. The experimental and theoretical

P_2 and P_5 values were compared for calibration of the shock tube.
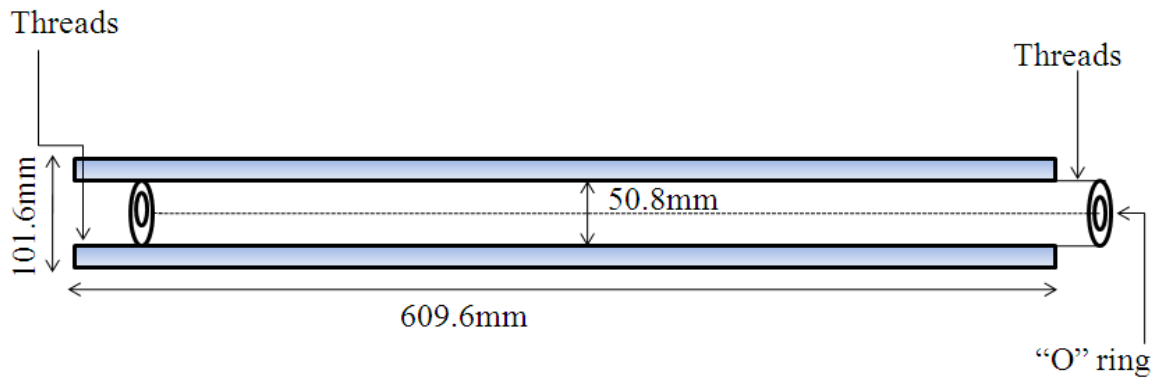
Figure II.1. Schematic diagram of each segment of the shock tube.
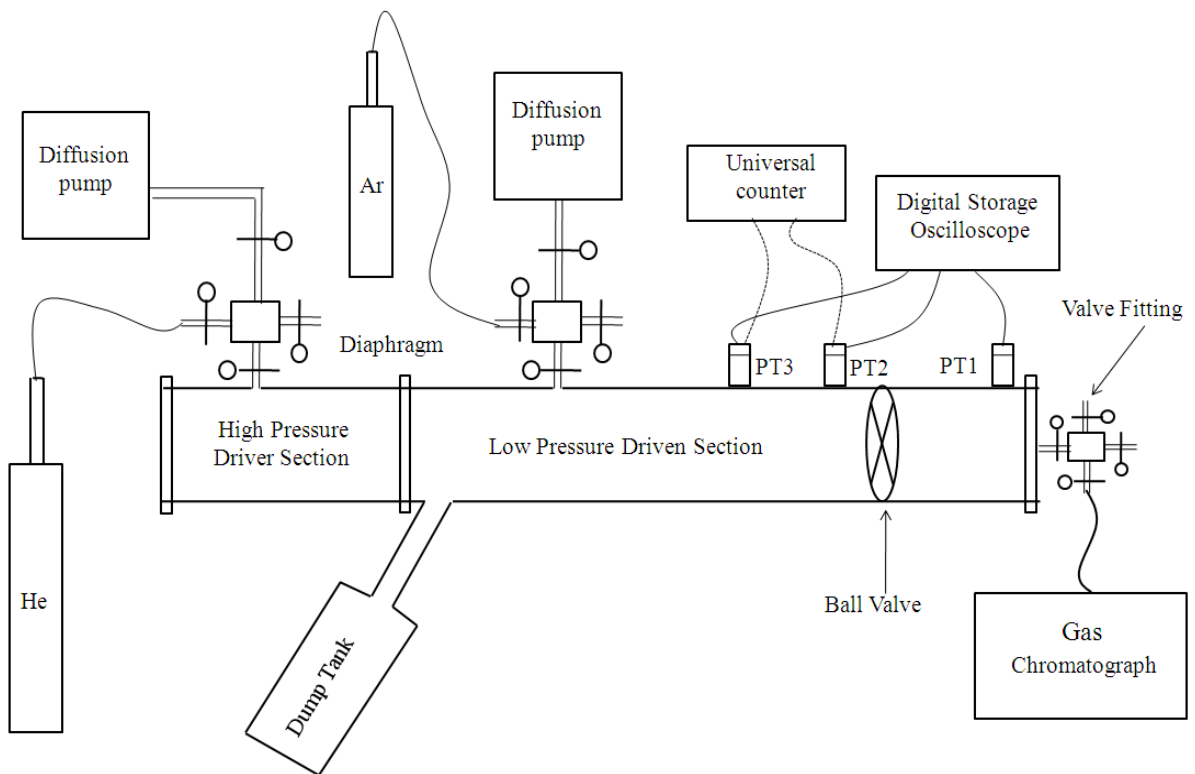
Figure II.2. Schematic diagram of the shock tube facility used for pyrolysis experiments

(PT – Piezoelectric pressure transducer).

The shock tube facility developed for the ignition delay experiments on jet propellent-10 experiments has been shown in Figure II.3. The shock tube is of 39 mm diameter, having driver section of 1970mm length and driven section of 4202mm separated by an aluminium diaphragm. Four high-speed PCB pressure transducers are mounted on the driven section side of the shock tube to measure the shock velocity.
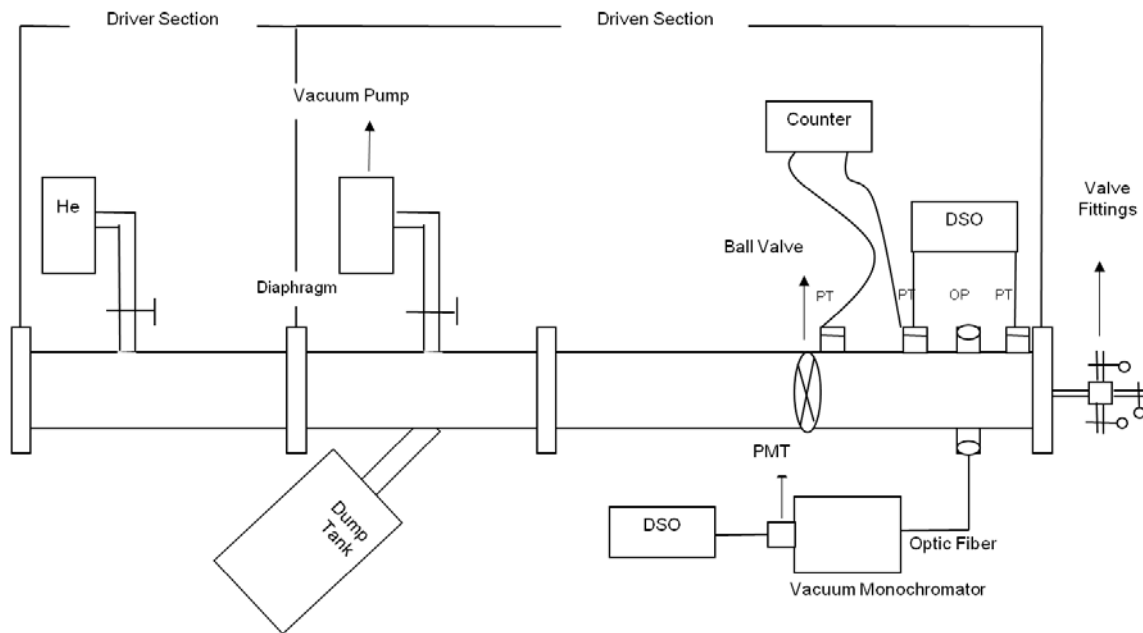
Figure II.3. Schematic diagram of the shock tube facility with emission spectroscopy used for combustion experiments on JP-10. OP, Optical ports; DSO, Digital storage oscilloscope (Tektronix, TDS 210); PMT, Photo-multiplier tube; PT, Pressure transducers (PCB model 113A24); Counter, HP 5314A universal counter.

One of the transducer is placed very close to the end of the driven section near the end flange to measure accurate ignition delay after the reflected shock has passed. Two optical ports close to the end of driven section (in the test section) facilitate the real time observation of absorption and emission spectra following ignition. One of the optical

ports is interfaced to a vacuum monochromator (Acton VM 502) through optical fiber bundles. The monochromator has an inbuilt photo-multiplier tube (DA-780-VUV). The monochromator covers a wavelength range of 30 nm to 600 nm and PMT has a range of 200 nm to 600 nm. The monochromator was fixed at 431.5 nm to record CH emission signal following ignition of any fuel. A pressure transducer was fixed in the other optical port to measure pressure and CH emission at the point simultaneously. A typical experimental signal for ignition experiment is shown in Figure II.5. The figure shows the CH emission signal as well as pressure signals obtained from the pressure transducer mounted near the end flange.

II.3. Operation of the shock tube

As already mentioned in the previous section, an aluminum diaphragm kept at the diaphragm station was used to separate the driver and the driven sections. The aluminum diaphragm which is a circular aluminum metal sheet of desired thickness was scored to generally $1/3^{rd}$ of the thickness of the sheet. The diameter of the scored part of the diaphragm is equal to the internal diameter of the shock tube i.e. 50.8 mm. To obtain different reflected temperatures behind shock, aluminum sheets of different thickness were used in the experiments. Before the evacuation, the shock tube was closed with a diaphragm in between the driver and driven section. Then, both the sections were evacuated using a 6" diffusion pump (Hind Hivac-VS6) up to 10^{-6} torr. The evacuated driven section is then loaded with the test sample to a pre-determined pressure through the four way set up at the end flange. The sample is made independently in a 12 L pyrex bulb by mixing the reagent with argon. The UHP grade argon gas was used for further

diluting the sample till the required pressure P_1 is reached (the choice of which is crucial in our experiments and is usually maintained in between 400-600 torr). The diluted mixture in the driven section is allowed to mix thoroughly for about 2 hr. Now, the UHP grade helium was filled rapidly in the driver section till the breakdown pressure of the aluminum diaphragm. Instantaneously bursting of the aluminum diaphragm at a particular pressure in the driver section results in the formation of shock wave which travels with the velocity of 2 to 3 times to that of the sound wave in the medium ahead of it. The ratio of the shock wave velocity to the sound velocity in the medium ahead is defined as the Mach number, and is designated as M_s. The test gas molecules will be heated to temperature T_2 after the primary shock front crosses these molecules. When the primary shock wave crosses the first piezoelectric transducer P1 the resistance of the piezoelectric surface changes resulting in the change of output of voltage, which is further amplified and fed into the universal counter. This primary shock triggers the counter on. Based on the same principle, the second piezoelectric transducer P2 mounted at 30.4 cm from the first transducer will trigger off the counter. Using this distance between the transducer and time, the velocity and hence, the Mach number of the shock wave (Ms) can be estimated. These piezoelectric transducers are placed at a distance where, the shock wave is completely formed before the first transducer and is traveling uniformly. This is confirmed by measuring the time travel between second and third pressure transducer. The primary shock wave travels and gets reflected at the end flange. The reflected shock wave will be traveling in the driven section back, where the test gas is heated previously by the primary shock wave. When this reflected shock travels through the test gas molecules, they will further be heated to reflected shock temperature

T_5. Similarly, there will be pressure jumps across the primary and the reflected shock wave fronts and are denoted as P_2 and P_5 respectively. The digital storage oscilloscope was used for recording these pressure jumps across the primary and reflected shock fronts. A third pressure transducer mounted on the driven section on the shock tube at 25mm from the end flange was used for this purpose. A typical pressure trace has been displayed in Figure II.4. The pressure jumps are recorded as voltage against time. The oscilloscope is triggered externally by using the output of one of the pressure transducer. This way the velocity of the shock wave between the first pressure transducer which is used to trigger the scope externally and the second pressure transducer can be determined and always compared with that measured by using the second and third transducer which is mounted at 25mm from the end flange in the driven section. These two velocities were found to be in very good agreement. This shows that the shock wave is formed fully and the velocity is constant in the test region. The reflected shock wave travels further down the driven section, until the expansion fan arrives and quenches it.

Details of growth of shock wave[2], selection of gases[2], effect of initial pressure on the experimental conditions[3], calibration of shock tube[3], and importance of dump tank have been described previously elsewhere[4-6].
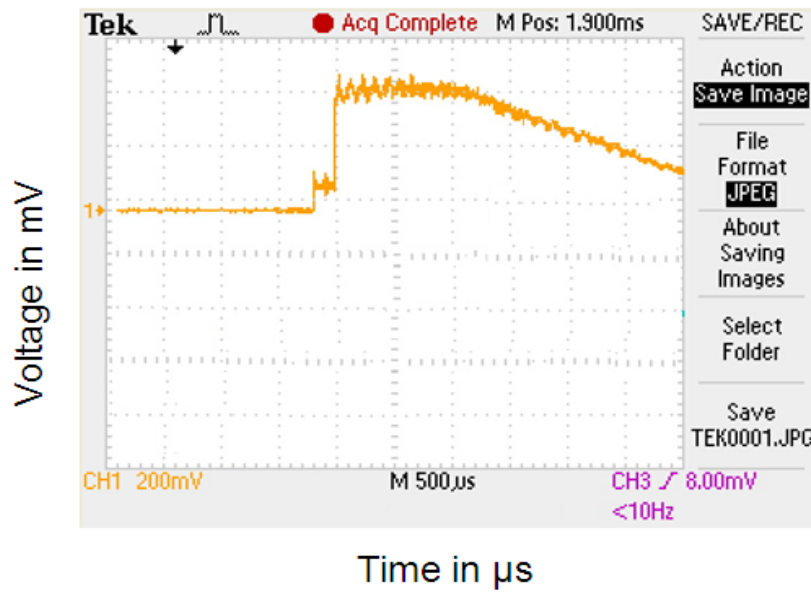
Figure II.4. A typical pressure trace recorded in by the oscilloscope showing the arrival of the primary and the reflected shock wave.
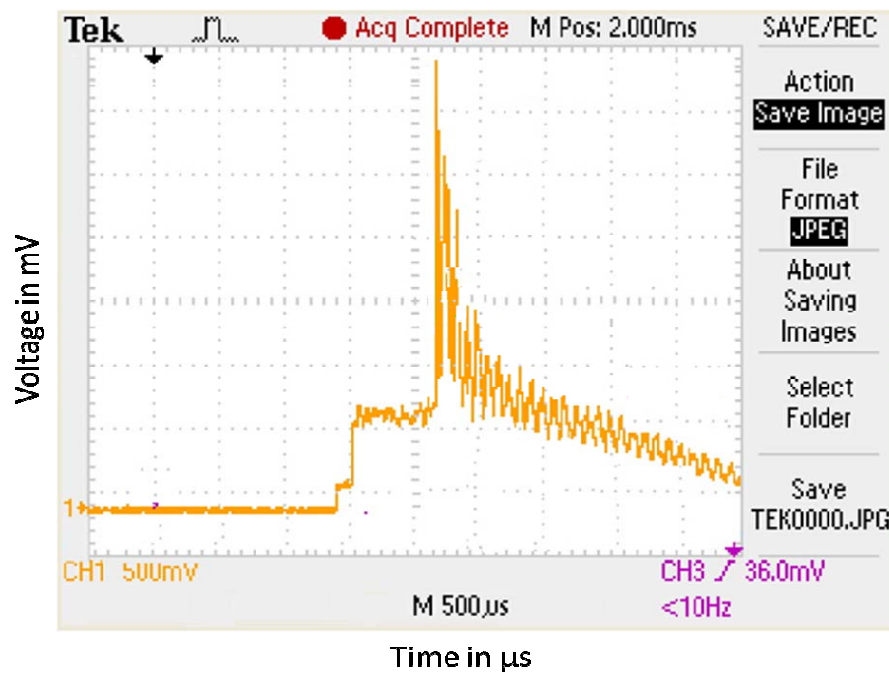
Figure II.5. A typical signal obtained in the digital oscilloscope showing pressure rise for ignition experiments.

II.4. Reflected shock temperature

The conventional Rankine–Hugoniot relations for the normal shock waves were employed for the theoretical calculation of the temperature behind the primary shock (T_{21}) and the reflected shock wave (T_{51}).

$$T_{21} = \frac{\left(\gamma M_s^2 - \dfrac{\gamma - 1}{2}\right)\left(\dfrac{\gamma - 1}{2} M_s^2 + 1\right)}{\left(\dfrac{\gamma + 1}{2}\right)^2 M_s^2} \qquad (1)$$

$$T_{51} = \frac{\left\{2(\gamma - 1)M_s^2 + (3 - \gamma)\right\}\left\{(3\gamma - 1)M_s^2 - 2(\gamma - 1)\right\}}{(\gamma + 1)^2 M_s^2} \qquad (2)$$

However the properties of the reflected shock determined using these ideal shock relations are not accurate due to several reasons including boundary layer problems, real gas effects, exo/endothermicity of the chemical reactions, etc. Consequently the temperature experienced by the test gas in the reaction zone differs from what estimated using above relations.

Comparison of the four different methods of evaluating the T_5 has been reported by Tschuikow-Roux et al.[7] First the most commonly employed method where all the shock properties were estimated from measured incident shock velocity using normal shock relationships given above in equation 2. Whereas in the second method, the measured reflected shock velocities were employed for determination of T_5. In the third method, both the measured incident and reflected shock velocities are employed and at the same time, the boundary condition of zero particle velocity behind the reflected shock

was taken into account. The forth one too considers both the measured incident and reflected shock velocities. However it does not invoke any assumption on the particle velocity behind the reflected shock. Of the four above mentioned methods, the fourth one only shows closer agreement to the true temperatures (obtained by internal standard method which is explained below). However, the first and third methods give temperatures higher than the true values while the second one gives lower temperature. The relations resulting from the fourth method are given below.

$$M_s = \left[\beta_1 \left(1 + \alpha_1 P_{21}\right)\right]^{\frac{1}{2}}$$

(3)

$$T_{21} = \left[\frac{P_{21}\left(\alpha_1 + P_{21}\right)}{1 + \alpha_1 P_{21}}\right]^{\frac{1}{2}}$$

(4)

$$M_r = \left[\beta_1 (1 + \alpha_1 P_{52}\right]^{\frac{1}{2}}$$

(5)

$$T_{52} = \frac{P_{52}\left(\alpha_1 + P_{52}\right)}{\left(1 + \alpha_1 + P_{52}\right)}$$

(6)

Here $\alpha_1 = (\gamma_1 + 1)/(\gamma_1 - 1)$ and $\beta_1 = (\gamma_1 - 1)/2\gamma_1$. M_s and M_r designate the primary and reflected shock Mach numbers respectively.

An accurate and convenient technique generally referred to as *"internal standard"* method has been developed by chemists for estimating the reflected shock temperature T_5. This method involves subjecting a molecule, the kinetic parameters of which are known, to shock wave along with the molecule of interest i.e. test sample. Then, the rate

constant(k) for the decomposition of the internal standard was obtained by measuring the

concentration of the unreacted internal standard (A_t) and one of the products formed from

it (internal standard) based on the relation given below.

$$A_t = A_0 \exp(-kt) \tag{7}$$

Here A_0 is the initial concentration of the internal standard, k is the rate constant

and t is the reaction time. Finally, using this rate constant (k), the temperature at which

the reaction is performed can be accurately estimated using the relation.

$$\ln(k) = \frac{1}{2.303\ t} \times \exp\left[\frac{-E_a}{RT}\right] \tag{8}$$

Where R is the universal gas constant and E_a is the activation energy for the process.

Now, the reaction temperature being known, it becomes easier to study the kinetics of the

test sample, more accurately, that has decomposed along with the internal standard.

However this method suffers from some limitations for it to be generally applicable. The

first limitation arises from the fact that it cannot be employed for those systems where the

product formed by the decomposition of the internal standard is same or one of the

products for decomposition of the test sample. Secondly, either the internal standard or

any of its products should not react either with the compound under investigation or any

of its products.

The external standard method of obtaining the temperature behind the reflected

shock waves has been reported by group[8] at University of Illinois at Chicago. Where,

ethyl chloride, whose thermal decomposition kinetics is very well established, has been

selected as the compound for the external standard method. The thermal decomposition

of ethyl chloride gives rise to ethylene by unimolecular elimination of HCl. This reaction was investigated by Tschuikow-Roux[10] and Tsang[9] in the shock tube. Temperature range of 960-1100 K was covered in the Tschuikow-Roux's work and the reported rate constant was $10^{13.8\pm0.2}$exp [-57.8±1.0/RT] s^{-1}. A rate constant of $10^{13.2\pm0.1}$exp[-56.5±0.5/RT] s^{-1} has been reported by Tsang in the temperature range of 800-1000 K. In fact, the temperature range of 900-1100 K was used for most of our investigations on haloethanols. The temperature range reported by Tschikow-Roux is very close to our work. Moreover, as we mentioned earlier that the pre-exponential factor reported by Tsang might be low[11-12]. Hence, the rate constant reported by Tsuchikow-Roux was used as the standard in our investigation. For this purpose, thermal decomposition study of ethyl chloride was performed in the temperature range of 950 to 1130 K independently. The reaction temperatures, at which the reaction takes place, were estimated using the known rate constant[10] as discussed above. These temperatures are plotted against the reflected shock temperatures evaluated using the fourth method that is suggested by Tschuikow-Roux, as shown in Figure II.6. To determine T_5 for all the experiments, least squares fitting of this data were performed. In this way the actual reaction temperature has been determined for all the experiments. The temperature behind reflected shock waves, T_5, determined using three different methods has been shown in the Table II.1. These data have been taken from Ph. D. thesis of Dr. Rajakumar.[3]
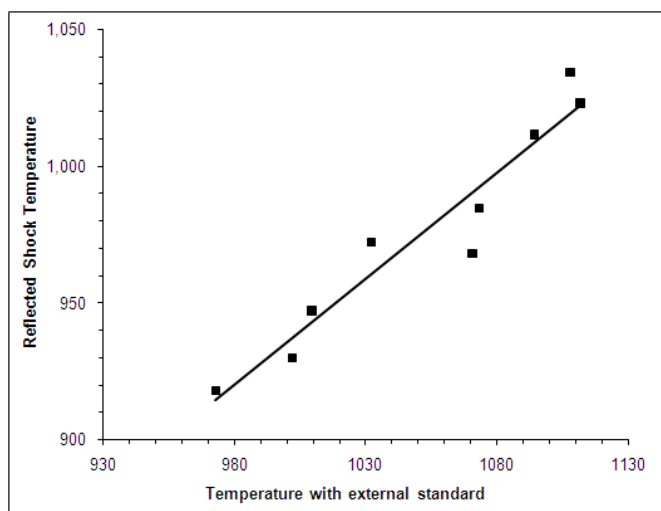
Figure II.6. The plot of T_5 obtained from external standard against T_5 obtained with reflected shock Mach number.

Table II.1. The temperature behind reflected shock wave (T_5) determined using three different methods.

No.	$T_5 (M_s)^a$	$T_5 (M_r)^b$	$T_5 (Kinetic)^c$
1	1068	1000	991
2	1094	1035	1024
3	1146	1056	1031
4	1153	1087	1060
5	1157	1082	1061
6	1236	1138	1104
7	1236	1138	1107
8	1261	1172	1125
9	1325	1232	1171
10	1384	1278	1210

a. Calculated from the measured incident shock velocity and ideal shock relations.

b. Calculated from the measured incident and reflected shock velocity without any assumptions about the particle velocity in the reflected zone. See reference 7 for details.

c. Determined using the kinetic parameters for $CH_3CH_2Cl \rightarrow C_2H_4 + HCl$ reaction from

reference 10.

II.5. Analysis

The proper analysis of the post shock mixtures determines the accuracy of the experimental results. Hence, the concentrations of all the species involved in the reaction has to be measured accurately in order to obtain reliable kinetic parameters other than the accurate measurement of the reaction time and temperature,. Here, in our experiments all the reactant and product molecules involved exist in gaseous phase. Gas Chromatography (GC) is the best quantitative technique for the analysis gas phase samples. Qualitative analysis of the samples can be performed using infrared spectroscopic technique. In our analysis, we have used both of these techniques. These two techniques of qualitative and quantitative analysis have been discussed in detail in the following sections.

II.5.A. Gas Chromatography

The word chromatography was first coined in 1906 by Tswett[13] to describe his technique for separating the components of pigments by introducing the mixture on to the top of solid adsorbent and allowing solvent to percolate down the column. He found that the different components were carried down the column at different rates, and thus became separated, to form discrete colored bands. The term chromatography is used to describe any technique where a separation of the components of a mixture is achieved by their distribution between a fluid mobile and a stationary phase. If the mobile phase is a gas and the stationary phase is liquid adsorbed on a solid support, the technique is referred to as gas-liquid or simply gas chromatography. The principle of gas

chromatography is based on selective adsorption of different compounds in a mixture of compounds as they are carried by the mobile phase (gas) through a column packed with finely ground adsorbent materials. As the compounds move through the column, by a process involving successive adsorptions and desorptions, those adsorbed least strongly will move most rapidly, hence the separation of compounds in the mixture are based on the degree of adsorption. As the degree of adsorption and desorption depends on the temperature, for better separation it is essential to keep the column at an optimum temperature. Sometimes the oven in which the column is kept can be programmed for better separation of the compounds. The basic structure and operation of a gas chromatograph is described below.

The schematic diagram of the gas chromatograph set up is shown in the Figure II.7. It contains an injector port with a rubber septum (to avoid any leakage), an oven in which the column is fixed as a coil and a detector. Both injector port and the detector are attached to the oven. One end of the column is connected to the injector port and the other end of the column is connected to the detector. All the injector port, oven and the detector can be maintained at different temperatures independently. Usually the injector port is kept at a temperature above the boiling point of all the compounds in the mixture to be analyzed. The oven is either kept at a constant temperature or it is programmed depending on the situation (this will be discussed in individual cases separately in case of each compound). The detector used for our experiments is a Flame Ionization Detector (FID).

In the FID, there are two electrodes, which are maintained at a constant potential difference (about 300V). In between the electrodes oxygen and hydrogen are lit to give

the flame. When the compound is eluted out of the column, it will be ionized in the flame between the electrodes. The ions will be captured by the electrodes, whereby there will be a sudden change in the potential difference between the electrodes because of the additional current due to the ions. The magnitude of the potential difference between the electrodes because of the ions depends on the concentration of the compound that is eluted. The data is collected in to a PC for further analysis. The FID is kept at 498K constantly, to avoid any condensation of water or compounds.

In general, a known amount of the sample is to be injected directly in to the injection port with a micro syringe (in case of gases a gas tight micro syringe is used), which will be converted in to the vapour at its boiling point and will be carried away in to the column in the oven along with the carrier gas. The sample will be separated in to its components according to their individual adsorption coefficients. The separated compounds reach the detector, where they are detected as described earlier. But in our
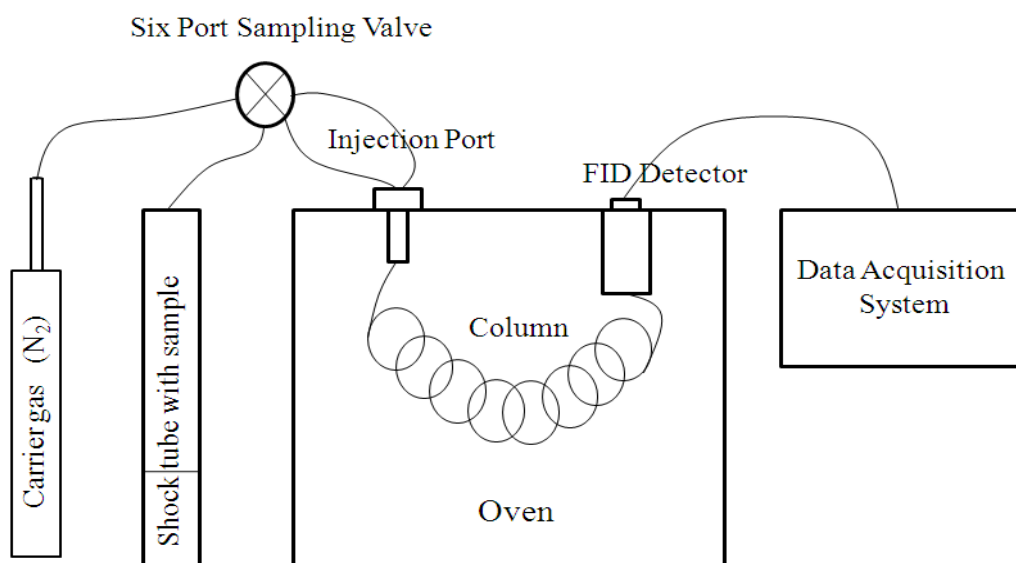
Figure II.7. Schematic diagram of the analysis set up with GC

case, the sample is a mixture of gases. For quantitative measurements (which is very much essential for kinetics), rather than using a gas tight syringe, a constant amount of (25 μl) the post shocked mixture is injected using an online gas sampling valve, which is in between the sample reservoir and the injection port. It is a six port valve, out of which two ports are connected to a standard loop of 25 μl, two are for the inlet and outlet of the carrier gas and the other two ports are connected to the sample input and outlet. When the valve is in closed condition, the loop can be filled with the sample while the carrier continues to flow in to the column. When the valve is set to be in the injection mode, the loop will be connected to the inlet port along with the carrier while the sample flow from the sample reservoir will be left in to the outlet. This can be seen in the Figure II.7. In the present work HP 6890^{plus} gas chromatograph is used.

The products in the post shock mixture are identified by injecting the original compound in the same operating conditions of the GC and comparing its retention times.

II.5.B. Column

The compound (both reactants and products) involved in the present work are mainly organic compounds namely halogenated alcohols, halogenated hydrocarbons and lower hydrocarbons. Porapak Q column is best for the investigation of aliphatic hydrocarbons, aromatic hydrocarbons, ketones, esters, aldehydes, alcohols and halogenated derivatives among many porapak columns such as N, P, Q , S, T, R, PS and QS which are very good columns for the separation of lower hydrocarbons from C1 to C10. Packed "porapak Q" column found to have clearly distinguishable retention times for most of the compounds under investigation in the present study. As we know that the

adsorption and desorption depends on the temperature and hence compounds in the mixture whose retention times are very close to each other was separated by changing the temperature of the oven. In the present investigation we have used porapak Q column for the study of pre and post shock mixture of thermal decomposition of 2-bromoethanol. This is 2 meters long stainless steel column which is packed with divinylbenzene on ethylvinylbenzene (mess size 80/100) having a surface area of 500-600 m^2/g. This column can be used up to 230^0C. However, the quantitative analyses of thermal decomposition products of 2-chloroethanol was carried out using the selective porapak S and T column. This column was used specifically for the separation of acetaldehyde and vinyl chloride which was not possible using porapak Q column. This is a selective 1.8m • 1/8" GC column which consists of a mixture of porapack S and T (80: 20 parts by weight) where the two stationary phases have the different polarities.[14] For this column none of the other substances have the same retention time as vinyl chloride. Hence, this column was used for quantitative analysis of the reaction products with HP-6890 gas chromatograph. This column can also be used up to 230^0C.

II.5.C. Calibration of GC

The sensitivity of any detector is, in general, different for different compound. Therefore, in present work, determination of sensitivity factor was carried out for all the compounds towards the flame ionization detector (FID). The calibration of all the compounds was performed in the dynamic range of flame ionization detector i. e. 10^7. For this purpose, all the samples for the calibration were prepared in our laboratory. Each compound was calibrated by loading it up to 4 torr in to a highly evacuated chamber

manometrically. This sample was diluted further with argon up to 2 atm. Before the analysis of experimental sample, the GC was purged completely with argon and it was confirmed that there was no signal/peak from any reactant or product from the previous experiment. Then, it was injected in to GC through the six port valve after proper equilibration and analyzed. To confirm the reproducibility, this procedure was repeated 3-4 times at each concentration. The sample concentration was then reduced to half by diluting it with argon after each analysis. This process of reducing the concentration was continued till the concentration of the species comes below the sensitivity of the detector. The mole fractions of the species taken were plotted against the areas under the peaks which correspond to the concentrations. The sensitivity of the flame ionization detector towards the compound was given by the slope of the best fit of the data through the origin (where the area is zero at zero concentration). The concentration of the unknown compound can be determined by knowing the area of this compound using the sensitivity factor. The calibration of all the compounds involved in our work was performed using this procedure before[3] except vinyl bromide and 2-bromoethanol for which the calibration plots have been shown in Figures II.8-9. Table II.2 contains the sensitivity factors of all the compounds.
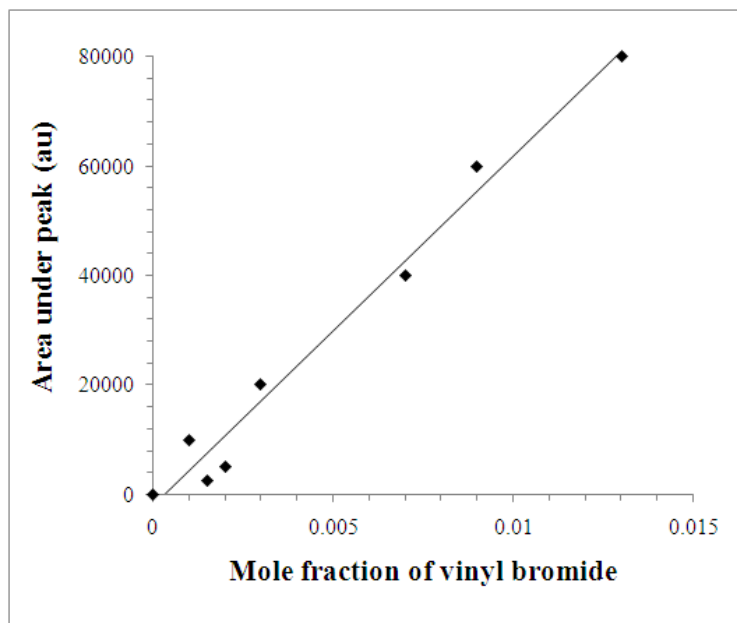
Figure II.8. Calibration plot of vinyl bromide
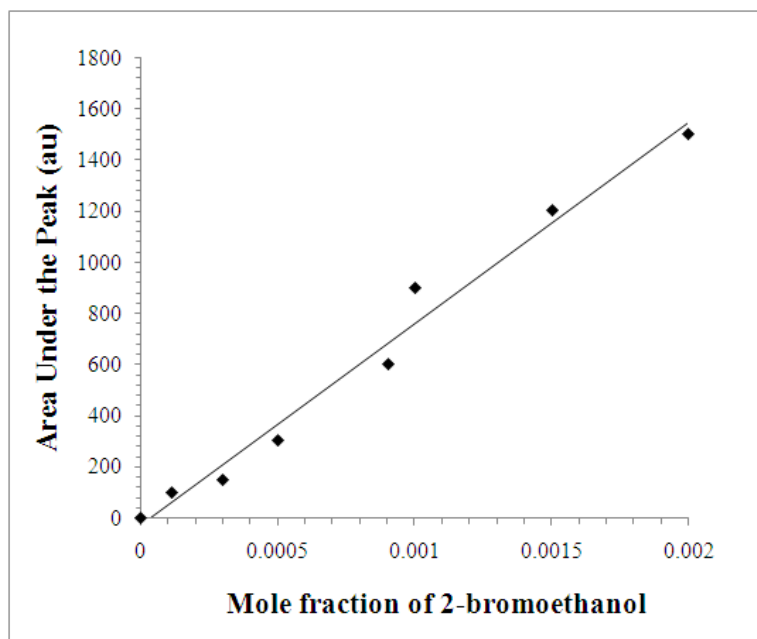
Figure II.9. Calibration plot of 2-bromoethanol

Table II.2. Sensitivity factors of Flame Ionization detector (FID) towards each compound.

Compound	Sensitivity factor (pA^2)
Methane	4.49342×10^6
Ethane	6.48276×10^6
Ethylene	4.55206×10^6
Propylene	1.29305×10^7
Acetylene	9.93781×10^6
Vinyl bromide	5.53573×10^6
Vinyl chloride	6.79096×10^6
Ethyl chloride	4.12210×10^6
2-bromoethanol	7.85842×10^4
2-chloroethanol	8.45681×10^5
Acetaldehyde	2.97609×10^6

II.5.D. FTIR

FTIR spectrometer was used for qualitative analysis of the post shock samples. A sample cell, which is a Pyrex glass tube (2.5" diameter & 25 cm length) closed at two ends with antireflection coated ZnSe windows using epoxy resin was designed to serve this purpose. High vacuum Teflon stop cocks have been connected at the center of the cell. The IR sample cell was connected at the end flange of the driven section using the four way attachment. Then, a rotary pump was used for evacuating it up to 10^{-3} mbar. The post shock mixture was filled in to the sample cell up to one atmosphere manometrically. Analysis of the sample was performed using Fourier Transform Infrared Spectrometer (Thermo Nicolet FTIR).

II.6. Sample preparation

Triple distillation of all the commercially available high purity liquid compounds was carried out before use and analyzed in GC for purity. However, the gas phase samples were used directly after checking their purity in GC. Besides this, freeze-pump-thaw procedure was also performed several times for degassing and further purification of the samples. The sample was prepared by loading a 1% mixture of the compound of interest in argon in to a previously evacuated 10 *l* pyrex glass bulb manometrically. The sample was allowed to mix thoroughly for a day or two. The purity of the sample was tested frequently using gas chromatograph.

II.7. General experimental procedure

The experimental procedure suggested by Tsang was followed for carrying out the single pulse shock tube experiments[8]. Both the driver and driven section of the shock tube was evacuated using a 6" diffusion pump to 10^{-6} torr during which the ball valve was kept opened. The ball valve was closed after the evacuation. The sample loaded in the sample chamber was diluted with argon manometrically until a desired pressure P_1, is reached. To avoid back diffusion of the sample, the argon chamber is filled only with argon was kept a slightly higher pressure (30 torr) as compared to the sample chamber. The ball valve was opened just before the experiment, and the helium was used to pressurize the driver section until the aluminum diaphragm bursted. The ball valve is closed immediately after the experiment to avoid the mixing of the sample with helium. Analysis of the post shock mixture was performed using the gas chromatograph and IR

spectrometer as explained before. The complete analyses have been described in each individual case in the corresponding chapters.

Materials and chemicals

Gases: Helium (99.999%), Argon (99.999%), Hydrogen (99.99%), Nitrogen (99.99%), Oxygen (99.99%). These gases are supplied by Bhoruka Industrial Gases, India.

Chemicals: Vinyl chloride (Fluka-99.5%) Vinyl bromide (Sigma Aldrich-98%), Acetylene (Bhoruka-99.96%), Ethyl chloride (Fluka-98%), Methane (Bhoruka-99.99%), Ethane (Bhoruka-99.5%), Ethylene (Bhoruka-99.91%), Propylene (Bhoruka-), 2-Bromoethanol (Fluka-95%), 2-chloroethanol (Loba-cheme Indoaustranal.Co, India-99%), acetaldehyde (Merck).

Equipment: Digital storage oscilloscope (Tektronix-TDS 210), Piezoelectric pressure transducer (Kistler-601A), Universal counter (HP-5314A), Diffusion pump 6" (Hind Hivac, India-VS6), Digital high pressure gauge (Instrument research associates, India-PRM 300M), Gas chromatograph (HP-6890[plus]), FTIR Nexus-870 spectrometer (Thermonicolet, US). Needle and ball valves (Swagelok).

II.8. Ab initio, DFT and TST calculations on haloethanols

Ab initio and density functional theory (DFT)[15-17] methods which are commonly being used in electronic structure theory have been employed for calculations reported in this thesis. The Hartree-Fock (HF) method is preferred as a useful starting point for all optimizations. This method neglects the electron correlation and it assumes that the each

electron sees all of the others as an average field. This will result in the inaccurate wave function. Therefore, the results obtained using this method is not reliable.

Both Møller-Plesset perturbation theory (MP2-FULL) and DFT methods include electron correlation. The MP2 (FULL) method explicitly considers the inner electrons also in determining the correlation energy. The electron correlation was taken into account considering perturbation theory. Here 2 is the order at which the perturbation theory is truncated. In the case of DFT method, many-body electronic wave function (function of 3N variables) is replaced by electron density (function of 3 variables) which is a simple quantity to deal with both practically and conceptually. The DFT calculations were performed with B3LYP correlation hybrid functional. The acronym B3LYP stands for Becke 3-parameter-Lee-Yang-Parr. Another quantum mechanical method which was employed for the geometry optimization and frequency calculations for haloethanols and haloethanes is CCSD (an ab initio method).

Considering the size of the molecules, the numbers of different systems studied and based on the computational resources available MP2 and DFT methods were preferred for these calculations. DFT methods appear to give reliable results at reasonable computational cost. The basis sets employed were reasonably large 6-31G**, 6-31+G** and 6-311++G**. However, with CCSD method, the basis set that we have used was cc-pVDZ. These calculations have been done to get optimized geometries, frequencies, molecular energies and moment of inertia.

Both geometry optimization and frequency calculation were carried out at different levels of theory with different basis sets starting from 6-31G** up to 6-311++G**. Geometry optimization, a theoretical procedure for obtaining the position of

nucleus of a given molecule at a minimum of the potential energy surface, was carried out to obtain the molecular structural parameters. Frequency calculations were performed to confirm whether the optimization gives minimum or not. For the optimized ground state conformers of haloethanols, all the minima had only positive Eigen values in the Hessian. However, transition state (saddle point) was confirmed by one negative Eigen value in the Hessian. The vibrational motion corresponding to imaginary frequency was confirmed to be the reaction coordinate for going from transition state to reactant as well as product. Intrinsic reaction coordinate (IRC) calculation was also performed for the verification of transition state. A relaxed potential energy surface (PES) scanning has also been done using the optimized geometry of haloethanols at HF, MP2 and B3LYP level of theory with different basis set. These calculations were carried out to assign their global minima and also to identify the number of conformers for internal rotation about C-C and C-O bonds. All these calculations have been performed using Gaussian 03 suite of program.[18]

Results of the ab initio and DFT calculations which were used to find out the ground state and transition state structures were employed in the transition state theory (TST) calculation to determine the kinetics of different unimolecular elimination pathways.

These calculations have been performed on 2-chloroethanol to find the TS for HCl and H_2O elimination channels. To obtain the Arrhenius parameters following transition–state theory expression was used for the both HCl and H_2O elimination channels from CEOH.

$$k(T) = l \, \frac{k_B T}{h} \frac{Q_{\neq}}{Q_R} \exp\left[\frac{-E_0}{RT} \right] \tag{2}$$

Here l is the reaction path degeneracy, k_B is the Boltzmann constant, $Q_{\#}$ and Q_R are partition functions for the TS and reactant, respectively, and E_0 is the zero-point barrier for the reaction. The E_a and A were then estimated using the thermodynamic formulation of TST. The rate constant for a unimolecular reaction is given by

$$k = le \, \frac{k_B T}{h} \exp\left[\frac{\Delta S^{\neq}}{R} \right] \exp\left[\frac{-E_a}{RT} \right] \tag{3}$$

Here, $\Delta S^{\#}$ is the entropy of activation calculated using the partition functions of reactant and the TS.

Higher level CBS-QB3 and G3B3 calculations have also been performed on 2-chloroethanol for the same purpose. These Arrhenius parameters have been compared with the experimental results. These calculations have been done to understand the effect of Cl substitution on H_2O elimination and OH substitution on HCl elimination in the same molecule. The TS for HOCl elimination have also been optimized successfully and kinetic parameters have been evaluated.

To understand the effect of β-Cl and OH substitution on HCl and H_2O elimination from ethyl chloride and ethyl alcohol respectively, kinetic data was taken from literature[19-20]. The variation in the molecular structural parameters such as bond length

and bond angles on going from reactant to transition state has also been discussed in detail in chapter III.

Similar calculations have been done on 2-bromoethanol to find the TS for HBr and H_2O elimination channels and to obtain the Arrhenius parameters for both the channels. Higher level CBS-QB3 level calculations were also done for H_2O elimination pathway. The TS for HOBr elimination have been optimized successfully at all levels and kinetic parameters have been evaluated using TST calculations. It is discussed in detail in Chapter IV.

Also, to understand the effect of OH substitution on HBr elimination from ethyl bromide, calculations have been performed on ethyl bromide independently. The trends of the barriers from ethanol to BEOH through CEOH have been described in chapter IV. In a similar fashion, calculations have been performed on fluorobromoethane, bromochloroethane and 1, 2-dibromoethane to understand the effect of β-fluorine, chlorine and bromine substitution on HBr elimination and the results are compared with the experimental rate parameters in our work. The changes in the structural parameters related to the corresponding reaction coordinate have also been discussed in detail in chapter IV.

For TST calculations all the normal modes of vibrations were treated as harmonic oscillators except for the two low frequency torsional modes present in the haloethanols. The rotational degrees of freedom are treated as rigid rotors. For the two torsional modes, harmonic oscillator, hindered rotor and free rotor models are used to evaluate the corresponding partition function to understand its effects on pre-exponential factors and

57

in turn, on kinetics of unimolecular HX, H_2O and HOX elimination reaction and the results have been discussed. Hindered rotor partition function calculations have been carried out following Truhlar and co-workers methodology[21] as given below.

We know that the all thermodynamic quantities may be calculated from the canonical partition function Q. Here, we will consider a method described by Truhlar in order to determine the free and hindered rotor partition function for the low frequency torsional modes about C-C and C-O bonds in complex molecules having non-symmetric multiple minima along the internal rotation coordinate.

First we will consider the limit where $k_BT \geq W_j$ all j. Then a free rotor approximation is valid, and the partition function is given by the standard classical result.

$$Q^{FR} = \frac{(2\pi I k_B T)^{1/2}}{\hbar\sigma} \quad (9) \qquad I_{eff} = \frac{I_1 I_2}{I_1 + I_2} \quad (10)$$

Here k is Boltzmann's constant, h is Planck's constant, T is temperature, I_{eff} is the effective moment of inertia and Q is the partition function and σ is the effective symmetry number. FR is the abbreviation used for free rotor. This expression has been used for evaluating the free rotor partition function about the C-C and C-O bonds in 2-chloroethanol.

Next consider the regime when $k_BT \leq \hbar\omega_j$ all j. Then the partition function may be written as a sum of harmonic oscillator partition functions for the distinct minima:

$$Q^{HO} = \sum_{j=1}^{P} \frac{e^{-(U_j + \hbar\omega_j/2)/k_BT}}{1 - e^{-\hbar\omega_j/k_BT}} \quad (11)$$

ω is harmonic frequency of the lowest internal rotation mode, P is no. of non-equivalent minima, U is the energy difference between the conformations. HO is the abbreviation used for harmonic oscillator.

A third important regime is $\hbar\omega_j \leq k_B T \leq W_j$ for all j. The partition function for this intermediate (Q^I) case is given by the high temperature limit of the following equation

$$Q^I = \frac{k_B T}{\hbar} \times \sum_{j=1}^{P} \frac{e^{-U_j/k_B T}}{\omega_j} \qquad (12)$$

After evaluating the partition function in three different regimes, an interpolatory function has been evaluated that is reasonably accurate in the limits but smooth between them. That yields:

$$Q^{HR} = Q^{HO} \tanh\left(\frac{Q^{FR}}{Q^I}\right) \qquad (13)$$

Here, Q^{HR} indicates the hindered rotor partition function. This equation is a convenient ansatz, not an exact result. This method of evaluation of hindered rotor partition function is described as the full approximation. These calculations for Q^{FR} and Q^{HR} have been performed for the low frequency torsional modes about C-C and C-O bonds in 2-chloroethanol at HF, MP2 (FULL) and DFT level of theory using 6-311++G** basis set. Then, these results have been employed in TST calculations to obtain the k (T) in the temperature range of investigation theoretically. The results obtained using the combination of quantum chemistry and TST calculations with different models have been explained in detail in chapters III and IV.

We have also employed computational methods like HF, MP2, B3LYP, G2, G3, G2MP2, G3B3, G3MP2B3, CBS-Q, CBS-QB3 and CCSD/cc-pVDZ to estimate enthalpy of formation of haloethanols using atomization and isodesmic reactions. Details of which have been described in chapter V.

These quantum chemistry calculations have also been employed to estimate the energies of different C-H bonds present in the Jet Propellent-10 (JP-10) at B3LYP level with 6-311++G** basis set. Six transition states were also optimized successfully to determine the activation energies for the abstraction of six unique hydrogen atoms from JP-10 at B3LYP/6-311++G** level of theory. Similar calculations have been performed on the Triethylamine (TEA) as well to determine its C-C, C-N and C-H bond energies for comparison with that of the JP-10. The C-H bond breaking energy of C_2H_5 radical was also estimated at similar level. Chapter VI contains the complete details of these calculations.

The chemical kinetic modeling of the thermal decomposition mechanism of both 2-chloroethanol and 2-bromoethanol which is discussed in next chapter at high temperature was performed using a chemical kinetics simulator (CKS-1.01) program which is a scientific software tool developed by chemists at IBM's Almaden Research Center . The CKS program has rigorously accurate stochastic algorithm to propagate a reaction for the accurate simulation of chemical reactions.[22]

II.9. References

1. Bauer, S.H. *Science*, **1963**,141, 3584.

2. Gaydon, A.; Hurle, I.R. *The shock tube in high temperature chemical physics*, Reinhold, New York. **1963.**

3. Rajakumar, B.; Ph. D. Thesis on Thermal decomposition of haloethanes and haloethanols: single pulse shock tube and ab initio studies. Chapter 2, **2002.**

4. Glick, H.S.; Klein, J.J.; Squire, W. *J. Chem. Phys*. **1957**, 27, 850.

5. Lifshitz, A.; Bauer, S.H.; Resler, E. L. Jr. *J. Chem. Phys*. **1963**, 38, 2056.

6. Ben-Dor, G.; Igra, O. ; Elperin, T.; Lifshitz.A. (Eds.) *Handbook of shock waves*, Academic Press, 2000.

7. a. Tschuikow-Roux, E.; Simmie, J. M.; Quiring, W. J.; *Astonamica Acta* **1970**, *15*, 511; b) Tschuikow-Roux, E; *Phys. Fluids.* **1965**, *8*, 821.

8. Tranter, R. S.; Sivaramakrishnan, R.; Srinivasan, N.; Brezinsky, K.; *Int. J. Chem. Kinet.* **2001**, *33*, 722.

9. Tsang, W.; *J. Chem. Phys.* **1964**, 41, 2487.

10. Evans, P. J.; Ichimura, T.; Tschuikow-Roux, E.; *Int. J. Chem. Kinet.* **1978**, *10*, 855.

11. a) Hassler, J. C.; Setser, D. W.; Johnson, R. L.; *J. Chem. Phys.* **1966**, *45*, 3231; b)Hassler, J. C.; Setser, D. W.; *J. Chem. Phys.* **1966**, *45*, 3246.

12. Dees, K.; Setser, D. W.; *J. Chem. Phys.* **1968**, *49*, 1193.

13. Tswett, M. *Ber. Deut. Botan. Ges*. **1906**, 24, 316.

14. Krockenberger, D.; Lorkowski, H.; Rohrschneider, L.; Chromatographia, **1979**, 12, 787.

15. Szabo, Ostuland, N. S.; " Modern Quantum Chemistry: Introduction to Advanced Electronic Structure Theory", Dover publications Inc., Mineola, **1996.**

16. Jensen, F.;" Introduction to Computational Chemistry" , John Wiley & Sons, New York, **1999.**

17. Foresmen, J. B.; Frisch, A. E.;" Exploring Chemistry with Electronic Structure Method" , Gaussian Inc, Pittsburgh, **1996.**

18. Frisch, M. J.; Trucks, G. W.; Schlegel, H. B.; Scuseria, G. E.; Robb, M. A.; Montgomery, J. R. C. J. A.; Vreven, T.; Kudin, K. N.; Burant, J. C.; Millam, J. M.; Iyengar, S. S.; Tomasi, J.; Barone, V.; Mennucci, B.; Cossi, M.; Scalmani, G.; Rega, N.; Petersson, G. A.; Nakatsuji, H.; Ehara, M. H. M.; Toyota, K.; Fukuda, R.; Hasegawa, J.; Ishida, M.; Nakajima, T.; Honda, Y.; Kitao, O.; Nakai, H.; Klene, M.; Li, X.; Knox, J. E.; Hratchian, H. P.; Cross, J. B.; Adamo, C.; Jaramillo, J.; Gomperts, R.; Stratmann, R. E.; Yazyev, O.; Austin, A. J.; Cammi, R.; Pomelli, C.; Ochterski, J. W.; Ayala, P. Y.; Morokuma, K.; Voth, G. A.; Salvador, P.; Dannenberg, J. J.; Zakrzewski, V. G.; Dapprich, S.; Daniels, A. D.; Strain, M. C.; Farkas, O.; Malick, D. K.; Rabuck, A. D.; Raghavachari, K.; Foresman, J. B.; Ortiz, J. V.; Cui, Q.; Baboul, A. G.; Clifford, S.; Cioslowski, J.; Stefanov, B. B.; Liu, G.; Liashenko, A.; Piskorz, P.; Komaromi, I.; Martin, R. L.; Fox, D. J.; Keith, T.; Al-Laham, M. A.; Peng, C. Y.; Nanayakkara, A.; Challacombe, M.; Gill, P. M. W.; Johnson, B.; Chen, W.; Wong, M. W.; Gonzalez, C.; Pople, J. A. *Gaussian 03*, Revision A.1; Gaussian, Inc.: Pittsburgh, PA, 2003.

19. Indulkar, Y.N.; Upadhayaya, H.P.; Kumar, A.; Waghmode, S,B.; Naik, P.D.; *J. Phys. Chem. A*, **2009**, 113, 8462.

20. Good,P.T.; Maccoll, A. *J. Chem. Soc. (B),* **1971,** 268.

21. Chuang, Y.Y.; Truhlar, D. G.; *J. Chem. Phys.* **2000**, 112, 1221.

22. A chemical kinetics simulator (CKS-1.01) program, IBM's Almaden Research Center.

Chapter III

Thermal Decomposition of 2-Chloroethanol

III.1. Abstract

A single pulse shock tube was used to investigate the kinetics of thermal decomposition of 2-chloroethanol (CEOH) diluted homogeneously in high purity argon behind the reflected shock wave over the temperature range 930-1100K and the pressure varied between 13-18 atm. Pre and post shock mixtures were analyzed using FT-IR and gas chromatographic techniques revealing the presence of six reaction products. The products observed in order of increasing abundance were CH_2CHCl, C_2H_6, C_2H_4, CH_4 and CH_3CHO. The formation of CO was observed qualitatively using FT-IR in our analysis. Experimentally determined gas phase first order rate coefficients for major HCl and H_2O, elimination channels are $10^{14.37\pm0.35}$ exp $[-(57.80\pm1.64)/(RT)]$ s^{-1} and $10^{14.95\pm0.33}$ exp $[-(67.95\pm1.50)/(RT)]$ s^{-1} respectively. The first order overall decomposition rate constant is given by $10^{14.61\pm0.34}$ exp $[-(58.70\pm1.55)/(RT)]$ s^{-1}. The E_a have been reported in kcal/mol. Similar to 2-fluoroethanol case, formation of CH_4 and C_2H_6 was explained by the decomposition of vibrationally excited acetaldehyde formed by HCl elimination. The possibility of the direct HOCl elimination along with C-Cl bond fission channel has been considered to account for the formation of C_2H_4. Perhaps, the chloroethanol dissociation by the roaming pathway can account for observed higher concentration of C_2H_4. The kinetics of decomposition of CEOH was simulated using a model containing 45 elementary reactions and 28 species at 10K intervals to understand the mechanism of chemical transformation. This mechanism was validated by comparison to the shock tube measurements. This scheme was later reduced to 21 reactions and 23 species using

sensitivity analysis. This chapter also deals with the Ab initio (Hartree-Fock [HF] and Mφller-Plesset perturbation theory [MP2]) and density functional theory [DFT] computations that have been conducted considering harmonic oscillator, hindered and free rotor models (for low frequency C-C and C-O bond torsional mode) to obtain the activation barrier and preexponential factor for unimolecular four centered concerted HCl, H_2O and HOCl elimination pathways using transition state theory calculations. DFT hindered rotor results, reducing preexponential factor by an order of magnitude, are in good agreement for rate coefficient (k) with experimental results for HCl elimination. Present study has revealed both experimentally and theoretically that the fluorine substitution leads to an increase in E_a, however, Cl and OH substitution do not. The higher level G3B3 and CBS-QB3 calculations also underestimate the experimental rate coefficient for HCl and H_2O elimination reactions.

III.2. Introduction

CEOH has a lot of medicinal[1] and bio-chemical [2-4] importance because of its toxic nature. Pace et al.[5] have reported the degradation mechanism of CEOH by studying the oxidation of CEOH with H_2O_2 under UV irradiation. They have observed acetic, glycolic and formic acids and acetaldehyde as the reaction products. However, there has not been much effort in the thermal decomposition studies of the CEOH.

Thermal decomposition of ethanol has been reported extensively. It is suggested as an additive to the gasoline, used as fuel. It decomposes at higher temperatures through C-C bond scission[6-10] and through unimolecular elimination of H_2O.[11-15] Recently Lin et

al.[16] has investigated the unimolecular decomposition of ethanol at G2M (RCC2) level of theory and their results suggest that the mechanism of the decomposition depends strongly on pressure and temperature. They addressed the need for reliable high temperature experimental data.

Halogen substitution on ethanol introduces the possibility of another channel, namely HX elimination. The substitution effects on the activation barrier of HX elimination from haloethanes have been reported extensively by both experimental[16-27] and theoretical researchers.[28-29]   Whereas, the effect of OH substitution on HX elimination has not been addressed so far other than the work reported by Skingle et al.[30] Recently, 2-fluoroethanol has been suggested as a potential replacement for chlorofluorocarbons.[31] It will be interesting to study the effect of β-halogen atom on the barrier of H_2O elimination and at the same time the effect of β-hydroxyl group on the barrier of HX elimination in the same molecule.

Recently, 2-fluoroethanol has been suggested as a replacement for the chlorofluorocarbons (CFC) and its thermal decomposition has been described in our previous publication.[33] There is only one report available on the thermal decomposition of CEOH describing only the HCl elimination in the temperature range 703- 769^0 K.[30] Naturally, it is of interest to understand the effect of chlorine substitution at β-carbon, on thermal decomposition mechanism of CEOH.

A theoretical report available on this molecule mainly considers the structure and the vibrational frequencies of the ground state rotational isomers.[32] There is no theoretical report available so far on reactions of CEOH. Our laboratory investigated the thermal

decomposition of 2-fluoroethanol where the unimolecular elimination of HF and H_2O were found to be the major channel under our experimental condition in the temperature range 1000-1200K.[33] Will the thermal decomposition of CEOH show unimolecular elimination of water at higher temperatures? With this question in mind, shock tube studies on CEOH were carried out earlier. However, it was not possible to resolve the two major products from the decomposition of CEOH namely acetaldehyde and vinyl chloride using Porapak-Q column in our previous analysis.[34] In the current series of experiments a porapak column consisting of porapak-S and porapak-T (80: 20 parts by weight) was used to resolve the two products. [35]

The present work is the second part of the series of the ongoing investigations on the thermal decomposition of haloethanols at high temperature. Here, we focus on the high-temperature pyrolysis of CEOH behind reflected shock waves performed over the temperature range 930–1100 K and pressures varied between 13 and 18 atm. Ab initio (HF and MP2) and DFT calculations have been employed to obtain moment of inertia and vibrational frequency. Transition State Theory (TST) calculations have been carried out considering harmonic oscillator, hindered and free rotor models to obtain the Arrhenius parameters for the HCl, H_2O and HOCl elimination pathways. The kinetic differences and similarities of thermal reactions involving the HCl and H_2O reaction channels from CEOH have been compared with that from the ethyl alcohol, ethyl chloride, chlorofluoroethane and fluoroethanol.

In this chapter we report the chemical kinetic simulation as well performed to propose the plausible reaction scheme for the thermal decomposition of the CEOH to

account for the formation of different reaction products. These modeling results were validated by comparison to shock tube experimental results. The sensitivity analysis has also been performed with the aim of clarification of the importance of the different elementary reactions in the scheme. These results would certainly be useful in the understanding of thermal decomposition mechanism of the CEOH both theoretically and experimentally.

III.3. Experimental Section

III.3.A. Experimental Details

The shock tube facility and its mode of operation used in this study were described in detail in chapter II and previous publications [36, 37] and only a brief description is given here. Both the driver and driven section were routinely pumped down to 10^{-5} mbar before each experiment using the diffusion pump backed up by the rotary pump. All experiments were performed in shock tube behind reflected shock waves with argon as the bath gas. Reaction mixture used contains 0.5% mixture of CEOH in Ar. The final concentration of CEOH used in experiments was in range of 400-500 ppm. The initial pressure (P_1) used was in the range of 750 to 600 torr. The shock waves were generated by pressure bursting of the aluminum diaphragm of different grooves with helium as the driver gas to obtain the different temperature in the range 930-1100K. Experimental pressure trace was used to measure the reaction dwell time which was typically in the range of 1120-1305 microseconds. The observed cooling rates were found to be about 5×10^5 K/s. The HCl elimination from ethyl chloride was used as an external

standard reaction to estimate the reflected shock temperature under similar conditions. Since, the thermal decomposition of ethyl chloride forming C_2H_4 and HCl is a first order process with the rate constant of $k = 10^{13.83}$ exp $(-57.83 \times 10^3/RT)$ s^{-1}. All shock properties have been estimated from measured incident shock velocity using normal shock relationships determined considering the three conservation equations and ideal gas equation of state. The pressure P_5, behind the reflected wave was calculated using ideal shock relations, was between 13 and 18 atm in all runs. The sample section of the shock tube was connected to the gas chromatograph, and 0.5mL of the mixture was injected through an online sampling valve. The quantitative analyses of all products including separation of acetaldehyde from vinyl chloride was carried out using the selective 1.8m • 1/8" GC column which consists of a mixture of porapack S and T (80: 20 parts by weight) where the two stationary phases has different polarities.[38] For this column none of the other substances have the same retention time as vinyl chloride. Therefore, this column was used for quantitative analysis of the reaction products with HP-6890 gas chromatograph. Products were identified by comparing the retention times of the known pure authentic samples with those of unknown. The gas chromatographic analysis was carried out at a constant oven temperature of 100^0C with flame ionization detector (FID) at 150^0C. The inlet temperature was maintained at 110^0C in all the runs. Nitrogen was used as a carrier gas and its flow rate was maintained at 23ml m^{-1} in all runs. The FT-IR Spectra of post shocked mixture confirming the presence of all reaction products were recorded for qualitative analyses using the Thermo Nicolet-870 model.

III.3.B. Materials and Analysis

CEOH received from Loba Chemie Pvt. Ltd. specified to be 99.5% pure was used for sampling. Before making the sample freeze-pump-thaw method was used many times for degassing and further purification. Gas chromatographic analyses of the post shock gas mixture was carried out using the HP 6890 gas chromatograph with FID. FT-IR spectra of the compounds were recorded using Thermonicolet (Nexus 870) spectrometer for qualitative analysis. The Porapack S-T column used for separation of acetaldehyde and vinyl chloride was manufactured by the Chromatopak Analytical Instrumentation Pvt. Ltd, Mumbai, India. The FID sensitivity was evaluated for each of the compound with standard samples in order to determine the concentrations of all the species involved. These samples were bought from different sources. We bought acetaldehyde from Merck chemicals. Ethyl chloride and vinyl chloride was from the Fluka. Methane and Ethane were supplied by the Bhoruka Gas Agency. Ethene was bought from Hydrogas. The gases used in gas chromatogram analysis are from Bhoruka Gases, India. These gases are argon, helium, oxygen, and hydrogen. All these gases are of high purity (UHP grade 99.999%).

III.3.C. Theoretical Details

The optimization of both equilibrium ground state and transition state(TS) structures for H_2O and HCl elimination reaction from CEOH were carried out at HF, MP2 (FULL) and DFT(B3LYP) levels of theory with the standard 6-31G*, 6-31G**, and

6-311++G** basis sets. Transition states are characterized by one imaginary frequency corresponding to the reaction coordinate. These calculations were performed for evaluating the pre-exponential factor and activation energy for H_2O and HCl reactions using conventional transition-state theory (TST). These theoretically determined rate coefficients were then used for comparison with experimentally calculated rate coefficient of elimination reactions under consideration. In these calculations the zero point energies and vibrational frequencies were used without the scaling. The TS for HOCl elimination was also optimized successfully at MP2/6-311++g** level. But previous efforts[33] for optimizing the TS for HOF elimination from 2-fluoroethanol was not successful at any level in order to determine the activation energy for comparison with the HOCl elimination from CEOH. Optimizations of the all five conformer have been carried out to find out the minima and will be discussed in detail next. The calculations of enthalpy of formation of CEOH performed to estimate the internal energy of the products have been discussed in detail in chapter V. The C-C, C-X, C-H, and H-X (O/Cl) bond distances and percent changes calculated for the transition states for HCl and H_2O elimination reactions from CEOH have been discussed. Intrinsic reaction coordinate calculations have been performed for the verification of three transitions states leading to different products.

III.4. Experimental results and discussions

Thirty-three experiments have been performed with CEOH in argon between 930 and 1100 K. The total pressures behind the reflected shocks were varied between 13 and 18 atm. The post-shock mixtures were quantitatively analyzed with gas chromatograph.

The vinyl chloride and acetaldehyde separated using this column was found to be the major product in the post-shock mixture of CEOH. The other observed products were CH_4, C_2H_4, and C_2H_6. A typical gas chromatogram of the reaction mixture at the 1100K is shown in Figure III.1.
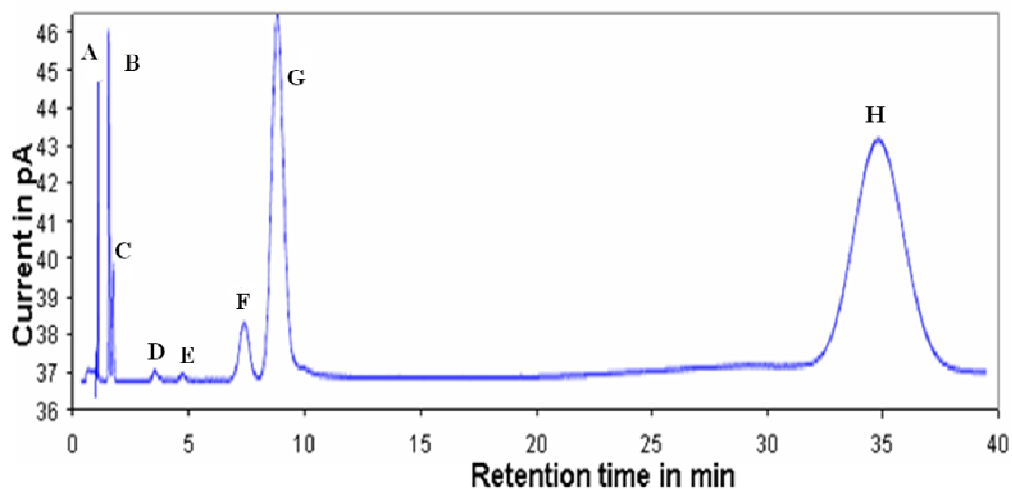
Figure III.1. Gas chromatogram of a post shock mixture of 2-chloroethanol in argon heated to 1100 K obtained on a 2-m Porapak S-T column using FID: (A) Methane; (B) Ethene; (C) Ethane; (D) Acetylene; (E) Butane; (F) Vinyl chloride; (G) Acetaldehyde; (H) 2-Chloroethanol.

The FT-IR spectrum of the post–shocked mixture obtained from thermal decomposition of CEOH was recorded at 1100K for qualitative analysis. Table III.1 contains the information about the distribution of all the reaction products and the experimental conditions i. e. P_5, T_5 and dwell time. The notation P_5 and T_5 implies the pressure and temperature behind the reflected shock wave respectively.

Table III.1. Summary of the experimental conditions and distribution of the reaction products for the thermal decomposition of 2-chloroethanol

S. No.	P_5(atm)	Dwell Time (μs)	T_5 (K)	$[CH_4]_t/[CEOH]_0$	$[C_2H_4]_t/[CEOH]_0$	$[C_2H_6]_t/[CEOH]_0$	$[CH_2CHCl]_t/[CEOH]_0$	$[CH_3CHO]_t/[CEOH]_0$	$[CEOH]_t/[CEOH]_0$	$k(s^{-1})$
1	13.6	1240	933	0.000040	0.000413	0.000023	0.000107	0.008997	0.990640	7.6
2	13.5	1220	936	0.000118	0.000614	0.000035	0.000146	0.007102	0.991985	6.6
3	13.1	1210	941	0.000291	0.000365	0.000091	0.000218	0.010452	0.988583	9.5
4	13.5	1224	944	0.000141	0.001056	0.000105	0.000167	0.008120	0.990412	7.9
5	13.9	1220	952	0.000112	0.001194	0.000435	0.000280	0.013621	0.984359	12.9
6	13.3	1120	953	0.000296	0.000713	0.000233	0.000361	0.010181	0.988215	10.6
7	13.4	1220	960	0.000133	0.001306	0.000371	0.000269	0.012474	0.985447	12.0
8	14.3	1225	964	0.000889	0.001152	0.000103	0.000398	0.017205	0.980254	16.3
9	12.3	1220	966	0.001194	0.002443	0.000356	0.000521	0.031078	0.964408	29.7
10	13.9	1270	984	0.001478	0.003941	0.000831	0.000827	0.037461	0.955461	35.9
11	14.2	1220	985	0.001172	0.004659	0.000527	0.000972	0.055906	0.936765	53.5
12	14.4	1120	990	0.001335	0.003195	0.000929	0.000825	0.071124	0.922592	71.9
13	14.5	1220	991	0.001672	0.007709	0.001256	0.001035	0.061803	0.926524	62.6
14	16.1	1250	1000	0.004421	0.006104	0.001740	0.001321	0.081151	0.905263	79.6
15	14.5	1220	1005	0.003211	0.004166	0.001159	0.001584	0.058404	0.931044	58.6
16	14.8	1220	1011	0.007045	0.008733	0.003207	0.002248	0.081252	0.897515	88.6
17	13.6	1140	1015	0.008690	0.007566	0.006497	0.002211	0.091095	0.883941	108.2
18	14.2	1220	1019	0.005823	0.010748	0.005116	0.002468	0.114197	0.861648	122.1
19	15.2	1120	1027	0.009771	0.013146	0.006715	0.004333	0.137621	0.828413	168.1
20	16.3	1320	1029	0.005719	0.011912	0.004216	0.002948	0.115551	0.859653	114.6
21	16.0	1220	1033	0.006528	0.014229	0.007352	0.004162	0.142046	0.825682	157.0
22	15.0	1260	1038	0.011865	0.012550	0.009726	0.004792	0.152020	0.809046	168.2
23	15.5	1220	1041	0.013934	0.015696	0.011210	0.004627	0.177723	0.776810	207.0
24	15.6	1220	1042	0.022199	0.020786	0.009115	0.008585	0.162862	0.776452	207.4
25	17.5	1290	1051	0.031477	0.019612	0.016062	0.007211	0.183014	0.742624	230.7
26	15.0	1220	1054	0.013967	0.021256	0.011236	0.010717	0.223994	0.718829	270.6
27	16.0	1221	1059	0.015486	0.024158	0.019050	0.008300	0.192530	0.740476	246.3
28	16.4	1220	1062	0.040426	0.033701	0.023587	0.007847	0.213488	0.680950	315.0
29	16.6	1250	1069	0.034893	0.040312	0.031230	0.011512	0.233997	0.648057	347.0
30	15.3	1220	1077	0.060125	0.054312	0.028313	0.012523	0.254137	0.590590	431.7
31	16.6	1220	1078	0.085393	0.045024	0.044561	0.016191	0.294031	0.514800	544.2
32	16.8	1305	1092	0.104012	0.060497	0.054607	0.014761	0.324200	0.441922	625.8
33	17.7	1265	1100	0.120124	0.078302	0.070236	0.019149	0.348351	0.363839	799.2

The concentrations of ethane, ethene, and methane have also been found to be larger than that of vinyl chloride in our temperature range of investigation. It was noticed that ethane and ethene appear in almost equal concentrations and the concentrations of these two species were found to be half to that of methane. The concentrations of all the species were found to be increasing with rise in temperature. It is clear from the Table III.1 that the concentrations of methane, ethane, ethene, and vinyl chloride are very low till 966K. In the case of 2-fluoroethanol the ethene and ethane were found to be started forming above 1050 and 1100 K respectively. However, vinyl fluoride was observed only above 1013 K.[36] Almost 65 percent of the CEOH is consumed within the temperature range and reaction times of our experiments. However, consumption was found to be less than 28% in case of 2-fluoroethanol in the temperature range of 1000-1200K. The formation of CO was observed qualitatively under our experimental condition that is produced by the decomposition of the formyl radicals. Carbon monoxide and hydrogen were not observed quantitatively in our analysis as it needs thermal conductivity detector. However, CO was qualitatively identified in the post-shock mixture using FT-IR spectroscopy in our analysis. In fact the production of H_2 has also been predicted in our numerical simulations and it is around 3%.

The rate constant for the overall decomposition of CEOH in the gas phase was calculated using the expression for the first order rate constant. The expression for which is given below.

$$k_{total} = -\frac{1}{t} \ln \frac{[C_2H_4ClOH]_t}{[C_2H_4ClOH]_0} \qquad (1)$$

Here $[C_2H_4ClOH]_t$ and $[C_2H_4ClOH]_0$ represents the final and initial concentration of the CEOH respectively. The rate parameters A and E_a were evaluated from the intercept and the slope of Arrhenius plot respectively. The linear plot of lnk against the 1/T implies that the overall thermal decomposition of CEOH is of the first order. The value of the rate coefficient for overall decomposition of CEOH was found to be $10^{14.61\pm34}$exp $[-(58.70\pm1.55)/(RT)]$ s^{-1}.The E_a is expressed in terms of kcal/mol. The rate coefficient for the total decomposition was found to be 8.04×10^2 s^{-1} at 1100K using our experimental result. Figure III.2 shows the Arrhenius Plot for the overall thermal decomposition of the CEOH in temperature range of investigation.
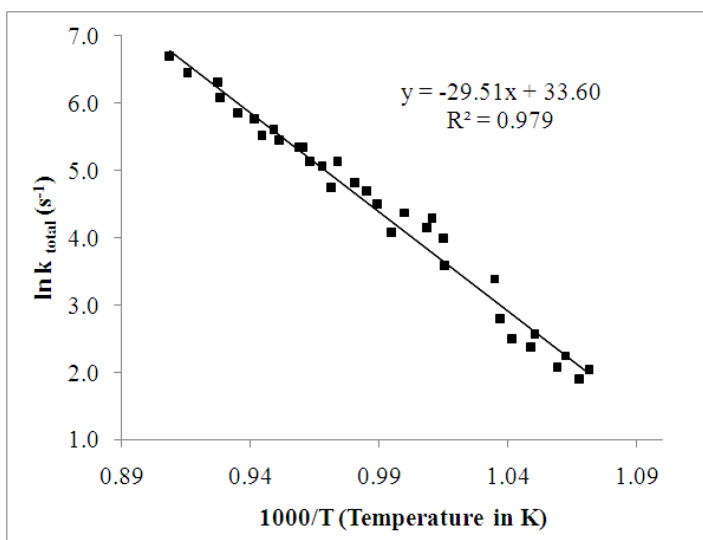
Figure III.2. Arrhenius Plot for the first order overall thermal decomposition of the 2-chloroethanol.

The Arrhenius plot for the unimolecular elimination of H_2O and HCl elimination from CEOH have been shown in the Figure III.3 and III.4.
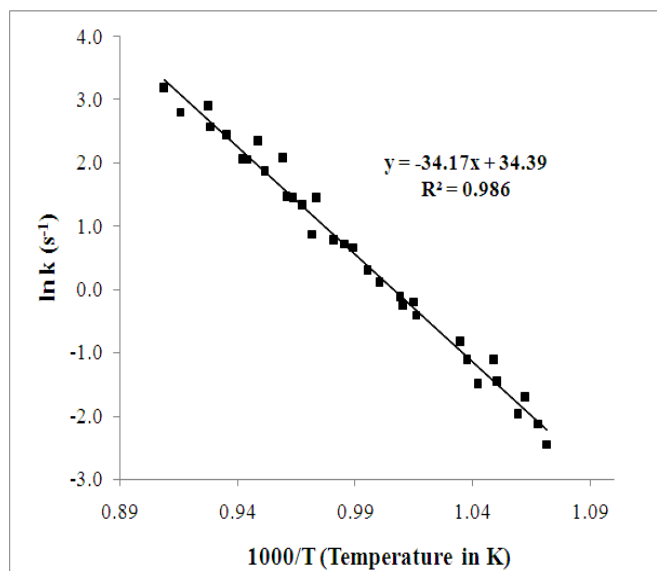
Figure III.3. Arrhenius Plot for the unimolecular elimination of the H_2O from 2-chloroethanol.
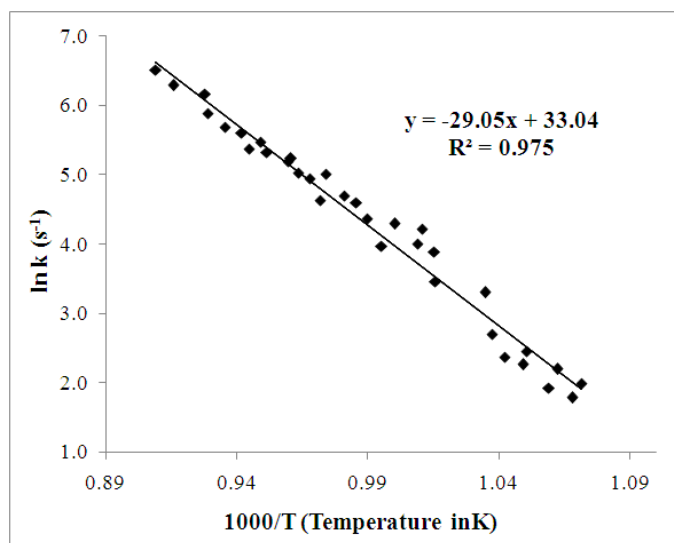
Figure III.4. Arrhenius Plot for the unimolecular elimination of the HCl from 2-chloroethanol.

However, the rate coefficient for both HCl and H_2O elimination reactions determined experimentally has been refined marginally using chemical kinetic simulation. The rate coefficient for the unimolecular elimination of HCl and H_2O was

found to be 7.62×10^{-3} and 3.69×10^{-5} s^{-1} respectively at 769 K using our experimental result. This could be the reason that Skingle et al. have not been able to observe the water elimination in their temperature range of 703-769 K because the ratio of k_{HCl}/k_{H2O} at 769 K was found to be very high, 2.07×10^2 determined using our experimental results.

The experimental results were described using the reaction scheme which contains unimolecular elimination reactions, thermal decompositions of radical intermediates, bimolecular transfer reactions, abstractions and recombination reactions. The reaction scheme containing 45 elementary reactions and 28 species was composed to explain the distribution of reaction products for the decomposition of CEOH and it is given in the Table III.2. The reaction scheme used in modeling of thermal decomposition mechanism of CEOH is essentially similar to that employed to model the kinetics of decomposition of 2-fluoroethanol. However, the differences have been discussed in detail next. The entire rate coefficients used in our mechanism are at high temperatures and pressures. The simulation was done within the experimentally determined reaction times i.e. 1.3ms. The references of all the reaction used in the mechanism are given in the Table III.2. The chemical kinetic mechanism includes experimentally determined expression for rate constant of the H_2O and HCl elimination reaction. The rate coefficient for HOCl elimination was derived from fitting to the complex mechanism in the simulation. The rate coefficients of all other reactions except 5 and 7 were taken from literature and NIST chemical kinetic database for simulating the profiles of products. The rate constants listed in the Table III.2 have been reported as either k = A exp (-E_0/RT) or k = A T^n exp (-E_0/RT). The units are expressed in terms of kcal, mol^{-1}, cm^3, and K. Later, sensitivity

analysis was used to find the effect of different chemical reactions in kinetic mechanism on the distribution of various reaction products. It was found that there are 24 reactions among 45 reactions which do not affect appreciably the distribution of any of the chemical species. It was verified by performing the simulations with the reduced kinetic mechanism containing 21 elementary reactions and 23 species that reproduces the experimental concentrations similar to the complete kinetic model within ±2% variations in concentrations of minor products. This is because of the very low concentrations of the C_2H_5 and C_2H_3 radicals involved in these chemical reactions. Hence, these chemical reactions were excluded from the kinetic scheme. Among the 21 reactions used in the reduced scheme to reproduce the experimental concentrations have 12 unimolecular and 9 bimolecular reactions.

Table III.2. Reaction scheme proposed for the thermal decomposition of 2-chloroethanol[a]

Reaction No.	Reactions	A	n	E_a	k (1100K)	Reference
R1	$ClC_2H_4OH \rightarrow CH_3CHO + HCl$	1.92×10^{14}	0.00	57.46	6.69×10^2	Present study
R2	$ClC_2H_4OH \rightarrow CH_2CHCl + H_2O$	7.00×10^{14}	0.00	67.81	2.11×10^1	Present study
R3	$CH_2CHCl \rightarrow C_2H_2 + HCl$	1.00×10^{14}	0.00	69.35	1.48	37
R4	$ClC_2H_4OH \rightarrow C_2H_4 + HOCl$	5.46×10^{17}	0.00	81.50	3.06×10^1	Present study [b]
R5	$ClC_2H_4OH \rightarrow Cl + C_2H_4OH$	5.50×10^{16}	0.00	75.89	4.05×10^1	Present study
R6	$C_2H_4OH \rightarrow C_2H_4 + OH$	6.19×10^{11}	0.00	23.65	1.19×10^7	38
R7	$ClC_2H_4OH \rightarrow OH + C_2H_4Cl$	8.0×10^{17}	0.00	84.84	3.68	Present study
R8	$C_2H_4Cl \rightarrow C_2H_4 + Cl$	3.90×10^{13}	0.00	21.66	1.87×10^9	39
R9	$2C_2H_4 \rightarrow C_2H_5 + C_2H_3$	4.82×10^{14}	0.00	71.54	2.62	40
R10	$CH_3CHO \rightarrow CH_3 + HCO$	3.60×10^{13}	0.00	55.00	3.88×10^2	41
R11	$CHO \rightarrow CO + H$	3.60×10^{13}	0.00	15.34	3.14×10^{10}	42
R12	$2CH_3 \rightarrow C_2H_6$	3.30×10^{13}	0.00	0.00	3.30×10^{13}	41
R13	$CH_3CHO \rightarrow CH_4 + CO$	1.21×10^{13}	0.00	53.0	3.27×10^2	41
R14	$CH_3CHO + C_2H_5 \rightarrow C_2H_6 + CH_3CO$	2.25	3.65	9.14	4.27×10^9	43
R15	$CH_3CO \rightarrow CO + CH_3$	8.73×10^{42}	-8.62	22.45	1.77×10^{12}	40
R16	$CH_3 + CHO \rightarrow CH_4 + CO$	2.00×10^{14}	0.00	0.00	2.00×10^{14}	40

R17	$2CH_3 \rightarrow H + C_2H_5$	2.40×10^{13}	0.00	12.88	6.49×10^{10}	44
R18	$CH_3 + OH \rightarrow CH_3OH$	6.02×10^{13}	0.00	0.00	6.02×10^{13}	45
R19	$C_2H_5 \rightarrow C_2H_4 + H$	4.00×10^{14}	0.00	40.50	3.36×10^{6}	46
R20	$C_2H_5 + CH_3 \rightarrow C_2H_4 + CH_4$	9.80×10^{12}	-0.50	0.00	2.95×10^{11}	43
R21	$2C_2H_5 \rightarrow C_2H_4 + C_2H_6$	1.39×10^{12}	0.00	0.00	1.39×10^{12}	40
R22	$2C_2H_5 \rightarrow C_4H_{10}$	1.08×10^{13}	0.00	0.00	1.08×10^{13}	40
R23	$C_2H_5 + H \rightarrow C_2H_6$	4.80×10^{12}	0.00	0.00	4.80×10^{12}	43
R24	$C_2H_5 + OH \rightarrow C_2H_5OH$	7.71×10^{13}	0.00	0.00	7.71×10^{13}	47
R25	$C_2H_5 + CHO \rightarrow C_2H_6 + CO$	1.20×10^{14}	0.00	0.00	1.20×10^{14}	43
R26	$C_2H_5 + CH_4 \rightarrow CH_3 + C_2H_6$	1.50×10^{6}	4.14	6.32	3.21×10^{17}	48
R27	$C_2H_5 + H \rightarrow 2CH_3$	3.60×10^{13}	0.00	0.00	3.60×10^{13}	49
R28	$C_2H_4 + C_2H_5 \rightarrow C_2H_6 + C_2H_3$	6.32×10^{2}	3.13	18.01	5.36×10^{8}	43
R29	$C_2H_5 + H_2 \rightarrow C_2H_6 + H$	1.41×10^{12}	0.00	13.10	3.44×10^{9}	37
R30	$C_2H_4 \rightarrow C_2H_3 + H$	2.00×10^{16}	0.00	110.00	2.33×10^{-6}	50
R31	$C_2H_4 + H \rightarrow C_2H_3 + H_2$	5.00×10^{15}	0.00	23.00	1.30×10^{11}	51
R32	$C_2H_4 + H_2 \rightarrow C_2H_5 + H$	1.02×10^{13}	0.00	68.16	2.61×10^{-1}	40
R33	$C_2H_4 + CO \rightarrow C_2H_3 + HCO$	1.51×10^{14}	0.00	90.62	1.29×10^{-4}	40
R34	$C_2H_3 + H \rightarrow C_2H_4$	1.50×10^{13}	0.00	98.20	3.94×10^{-7}	51
R35	$C_2H_3 + CHO \rightarrow C_2H_4 + CO$	9.05×10^{13}	0.00	0.00	9.05×10^{13}	40
R36	$C_2H_3 + C_2H_5 \rightarrow 2C_2H_4$	6.46	0.00	0.00	6.46	52
R37	$C_2H_6 + H \rightarrow CH_4 + CH_3$	5.40×10^{1}	0.00	11.63	2.59×10^{2}	53
R38	$C_2H_6 \rightarrow 2CH_3$	1.88×10^{50}	-9.72	102.00	2.36	54
R39	$CH_3OH \rightarrow CH_3 + OH$	1.90×10^{16}	0.00	91.81	9.37×10^{-3}	55
R40	$C_2H_5OH \rightarrow C_2H_5 + OH$	6.88×10^{39}	-19.70	114.00	1.55×10^{-43}	56
R41	$2Cl \rightarrow Cl_2$	2.23×10^{14}	0.00	-1.80	5.10×10^{14}	57
R42	$OH + Cl_2 \rightarrow HOCl + Cl$	4.73×10^{11}	1.40	1.48	4.34×10^{15}	58
R43	$O + HCl \rightarrow OH + Cl$	9.98×10^{10}	2.11	4.02	4.12×10^{16}	59
R44	$OH + Cl \rightarrow HCl + O$	5.90×10^{12}	0.00	5.68	4.35×10^{11}	57
R45	$2O \rightarrow O_2$	1.89×10^{13}	0.00	-1.79	4.30×10^{13}	40

[a]The rate constants ($k = A\, T^n \exp\,(-E_0/RT)$) are listed in the units of kcal, mol^{-1}, cm^3, and K. [b]The rate constant for HOCl elimination has high energy barrier theoretically, however, rate constant, 5.46×10^{17} exp [-(81.50)/(RT)] s^{-1}, was derived to best fit our data.

III.4.A. Major Channels

III.4.A.1. HCl and H$_2$O elimination

       The unimolecular elimination reactions of HCl and H$_2$O were found to be the major channels that account for the formation of acetaldehyde and vinyl chloride from CEOH respectively in our temperature range of investigation. It has been found by our quantum chemical computations as well as by experimental results that elimination of H$_2$O is slower than that of HCl. Experimentally determined rate coefficients of these two reaction channels were used in the modeling to explain their distribution. The concentration of vinyl bromide is almost 17 times smaller than that of the acetaldehyde. This is attributed to the difference in A & E$_a$ values of these two reactions.

$$Cl\text{-}CH_2CH_2\text{-}OH \rightarrow CH_2\text{=}CH\text{-}OH + HCl \hspace{3cm} (R1)$$

$$Cl\text{-}CH_2CH_2\text{-}OH \rightarrow CH_2\text{=}CH\text{-}Cl + H_2O \hspace{3cm} (R2)$$

  It was found that the reactions which were considered to account for the formation of the methane, ethane and ethene have no effect on concentration profile of acetaldehyde and vinyl chloride. The rate coefficients of these two reactions have been refined marginally in simulation to best fit our data. The rate coefficients of HCl and H$_2$O elimination reactions have been marginally modified as shown in the reaction scheme in Table III.2. The distributions in terms of logarithmic normalized concentrations of all the reaction products as a function of temperature have been shown in the Figure III.5.
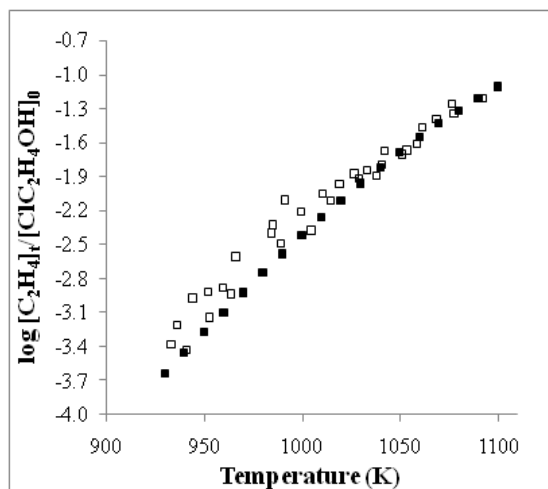
(a)
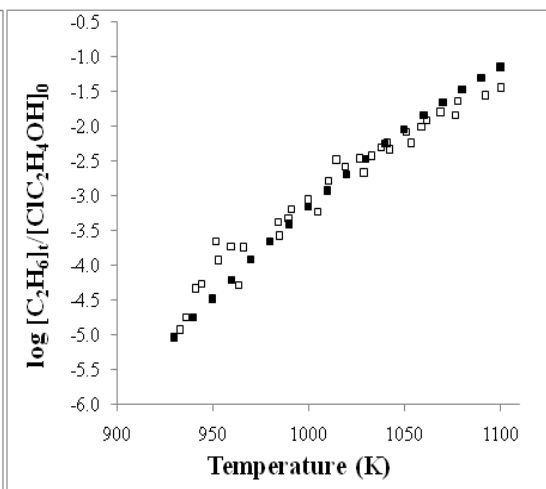
(b)
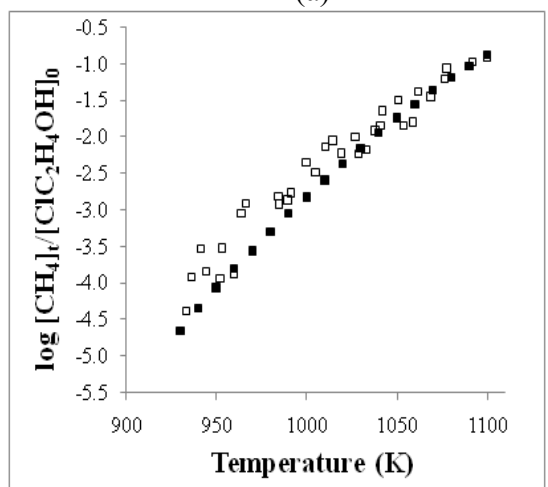
(c)
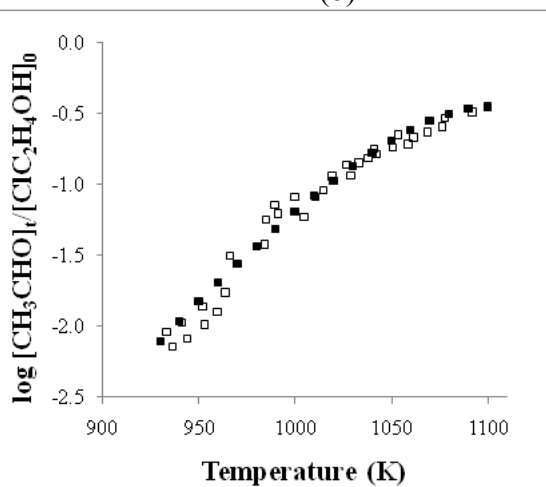
(d)
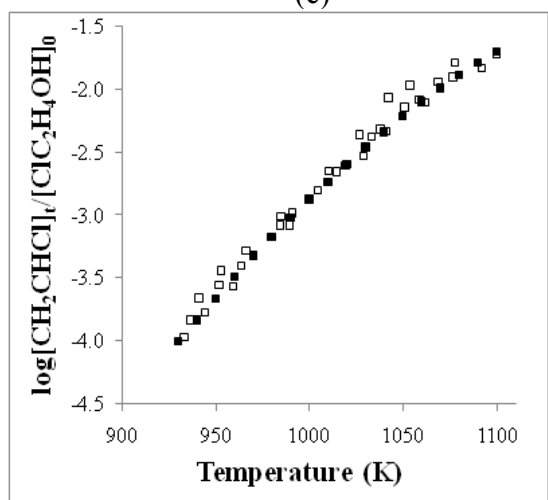
(e)
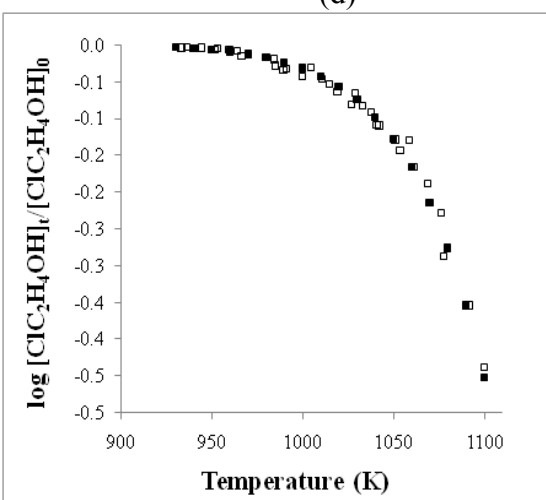
(f)

Figure III.5. Comparison of the experimental and simulated concentrations of five reaction products (a) C_2H_4 (b) C_2H_6 (c) CH_4 (d) CH_3CHO and (e) CH_2CHCl and reactant (f) ClC_2H_4OH plotted as a function of temperature for the thermal decomposition of 2-chloroethanol. The open squares are the experimental concentrations and filled solid squares are the model predicted values carried out at 10K intervals in the temperature range of 930 to 1100K.

III.4.B. Minor Channels

III.4.B.1.Methane

A previous experimental study reveals that the thermal decomposition of CH_3CHO produces CH_3 and CHO by C-C bond fission.[60,61] Theoretical analyses indicates entropically favored pathway of C-C bond scission over the molecular elimination of leading to CH_4 and CO by tight transition state with the transition state theory calculations predicts negligible contributions from this channel at high temperature.[62,63]

Recently, in case of HCHO, it has been shown that H-atoms produced by C-H bond fission can roam around HCO species at long range and later abstracts H-atom producing H_2 and CO.[64] However, recent experimental and theoretical studies of acetaldehyde photodissociation suggest that the formation of methane can take place by new pathway described as roaming radical mechanism where CH_3 formed by C-C bond scission can roam around the HCO moiety at long range and subsequently abstract a

hydrogen atom to form CH_4 and CO.[65] This could be another way that would lead to the formation of methane in our experiments.

However, in our case, formation of methane was explained by direct molecular elimination of methane from acetaldehyde or by C-C bond scission followed by recombination of methyl and formyl radicals in our simulation. The CH_3CHO being produced by the isomerization of $CH_2=CHOH$ is "chemically active" and the threshold energy for reaction R13 is expected to be less. Hence, activation barrier for this reaction was reduced by 4.20kcal/mol as compared to reported value in order to best fit the methane concentration.

$CH_3CHO \rightarrow CH_4 + CO$ $k_{13} = 1.21\times10^{13}\exp[(-53.00 \times 10^3)/(RT)]\ s^{-1}$ (R13)

$CH_3CHO \rightarrow CH_3 + CHO$ $k_{10}=3.60\times10^{13}\exp[(-55.00 \times 10^3)/(RT)]\ s^{-1}$ (R10)

$CH_3 + CHO \rightarrow CH_4 + CO$ $k_{16} = 2.00\times10^{14}\ cm^3mol^{-1}s^{-1}$ (R16)
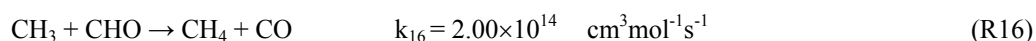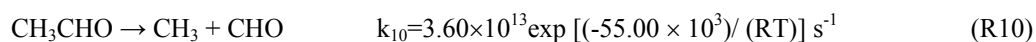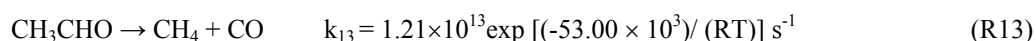
III.4.B.2.Ethane

The important reactions contributing to the formation of the ethane are R10 and R12. First, breaking of C-C bond in the acetaldehyde leads to the formation of methyl and formyl radical. The decomposition of formyl radical leads to formation of CO and hydrogen atom. The hydrogen atom produced is involved in several free radical reactions in our mechanism.

$CH_3CHO \rightarrow CH_3 + CHO$ $k_{10}=3.60\times10^{13}\exp[(-55.00 \times 10^3)/(RT)]\ s^{-1}$ (R10)
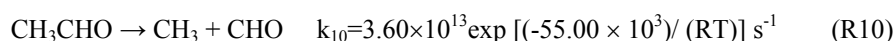
Concentration profile of C_2H_6 was underestimated using the proposed value for the rate constant of reaction R10 used to describe the pyrolysis mechanism of ethene oxide behind the reflected shock waves by Lifshitz et al.[41] However, CH_3CHO being produced by the isomerization of $CH_2=CHOH$ is "chemically active" and the threshold energy for reaction R10 is expected to be less. Thereby, activation barrier of the reaction R10 was reduced by 2.20kcal/mol as compared to reported value in order to best fit the ethane concentration. Reaction R10 followed by R12 corresponding to recombination of methyl radicals was taken into account to explain the formation of ethane as in the case of 2-fluoroethanol. The reported rate coefficient of methyl radical recombination is 2.30×10^{13}. This has been refined as shown below.
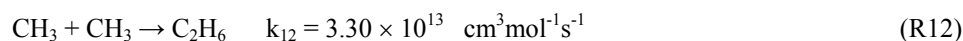
$$CH_3 + CH_3 \rightarrow C_2H_6 \quad k_{12} = 3.30 \times 10^{13} \quad cm^3 mol^{-1} s^{-1} \tag{R12}$$

The enthalpy of formation for CH_3CHO (-39.7 kcal mol-1) is 10 kcal mol^{-1} less than that of $CH_2=CHOH$ (-29.8 kcal mol-1). The barrier for isomerization is estimated to be 55.1 kcal mol^{-1} at B3LYP/6-311++G** level of theory. The enthalpy of formation of CEOH determined using isodesmic reaction at B3LYP/6- 311++G** level of theory was found to be -61.37 kcal/mol. The $C_2H_4ClOH \rightarrow CH_3CHO + HCl$ reaction is 4.24kcal/mol exoergic at the same level. The activation energy for HCl elimination from CEOH is determined to be 53.84 kcal mol^{-1} at B3LYP/6- 311++G** level of theory. Therefore most of the energy would remain as internal energy in the acetaldehyde.

It is clear from the Table III.1 that the concentration of ethane is increasing with rise in temperature. In fact, the observed ethane concentration was very low till 944K.

However, in case of 2-fluoroethanol, ethane were found to be product only above 1100 K. Other reactions having contribution to the formation of ethane are as follows:

$CH_3CHO + C_2H_5 \rightarrow C_2H_6 + CH_3CO \ k_{14} = 2.25(T)^{3.65} \exp[(-9.14 \times 10^3)/(RT)] \ cm^3mol^{-1}s^{-1}$ (R14)

$C_2H_5 + C_2H_5 \rightarrow C_2H_4 + C_2H_6$ $k_{21} = 1.39 \times 10^{12} \ cm^3mol^{-1}s^{-1}$ (R21)

$C_2H_5 + H \rightarrow C_2H_6$ $k_{23} = 4.80 \times 10^{12} \ cm^3mol^{-1}s^{-1}$ (R23)

$C_2H_5 + CHO \rightarrow C_2H_6 + CO$ $k_{25} = 1.20 \times 10^{14} \ cm^3mol^{-1}s^{-1}$ (R25)

$C_2H_5 + CH_4 \rightarrow CH_3 + C_2H_6 \ k_{26} = 1.50 \times 10^6 \ (T)^{4.14} \exp[(-6.32 \times 10^3)/(RT)] \ cm^3mol^{-1}s^{-1}$ (R26)

$C_2H_4 + C_2H_5 \rightarrow C_2H_6 + C_2H_3 \ k_{28} = 6.32 \times 10^2 \ (T)^{3.13} \exp[(-18.01 \times 10^3)/(RT)] \ cm^3mol^{-1}s^{-1}$ (R28)

$C_2H_5 + H_2 \rightarrow C_2H_6 + H \ k_{29} = 1.41 \times 10^{12} \exp[(-13.10 \times 10^3)/(RT)] \ s^{-1}$ (R29)
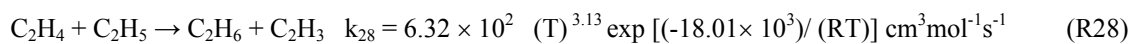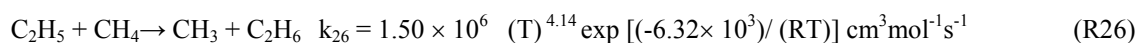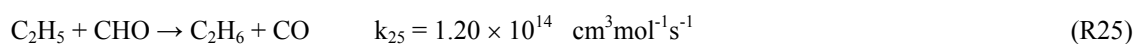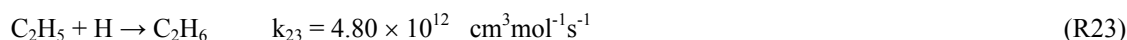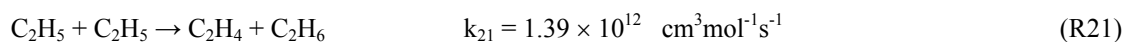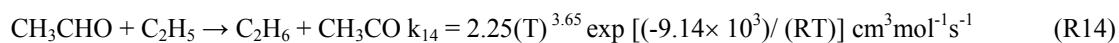
However, their contribution to the total production of ethane is negligible because their production depends on the concentration of the ethyl radical which is very low. However, these reactions were included for completeness and their importance in higher temperature range. This can be noticed from the sensitivity factors as reported in the Table III.3.

III.4.B.3.Ethene

Formation of ethene could be explained through C-Cl dissociation followed by C-OH bond scission. The C-Cl bond dissociation energy in CEOH is calculated at DFT/6-311++G** level and found to be 75.89 kcal mol^{-1}. The preexponential factor, 5.01×10^{15} s^{-1}, for reactions 5 was deduced from analogous bond fission reaction $C_2H_5Cl \rightarrow C_2H_5 +$ Cl available from reported literature. However, the preexponential factor was modified to

5.50×10^{16} s^{-1} to best fit the concentration profile of ethene where as the activation

energy, 75.89 kcal mol^{-1}, was evaluated at B3LYP/6-311++G** level of theory. The

preexponential factor, 8.00×10^{17} s^{-1}, for bond breaking reaction, ClC$_2$H$_4$OH $\rightarrow$ ClC$_2$H$_4$

+ OH, was derived from fitting to complex mechanism which is quite high. However, its

activation energy, 84.84 kcal/mol, was estimated at B3LYP/6-311++G** level of theory.

These bond scission reactions have been found to be the important reactions to describe

the ethene production and are as follows:

$$ClC_2H_4OH \rightarrow Cl + C_2H_4OH \quad k_5 = 5.50 \times 10^{16} \exp\left[(-75.89 \times 10^3)/ (RT)\right] \text{ s}^{-1} \qquad (R5)$$

$$C_2H_4OH \rightarrow C_2H_4 + OH \quad k_6 = 6.19 \times 10^{11} \exp\left[(-23.65 \times 10^3)/ (RT)\right] \text{ s}^{-1} \qquad (R6)$$

$$ClC_2H_4OH \rightarrow OH + C_2H_4Cl \quad k_7 = 8.00 \times 10^{17} \exp\left[(-84.84 \times 10^3)/ (RT)\right] \text{ s}^{-1} \qquad (R7)$$

$$C_2H_4Cl \rightarrow C_2H_4 + Cl \quad k_8 = 3.90 \times 10^{13} \exp\left[(-21.66 \times 10^3)/ (RT)\right] \text{ s}^{-1} \qquad (R8)$$
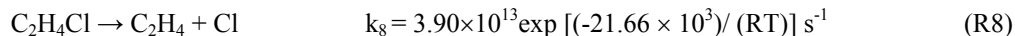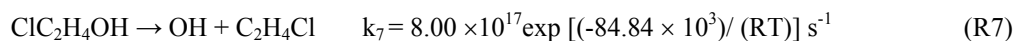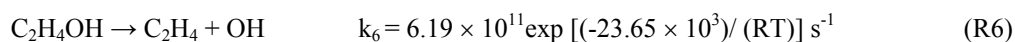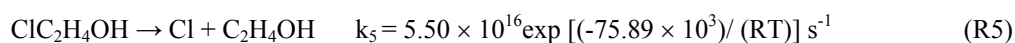
This can be explained in another way by considering the roaming radical

mechanism. Formation of C$_2$H$_4$ can equally be described by unimolecular elimination of

HOCl from CEOH as well directly in reaction mechanism as in the case of 2-

fluoroethanol.

$$Cl\text{-}CH_2CH_2\text{-}OH \rightarrow C_2H_4 + HOCl \qquad (R4)$$

The rate constant determined using the simulation for HOCl unimolecular

elimination was found to be $5.46 \times 10^{17} \exp\left[(-81.50 \times 10^3) / (RT)\right]$ s^{-1}. The

preexponential factor for the HOCl elimination reaction is significantly higher than the

HCl and H$_2$O elimination reactions. The barrier for HOF elimination from 2-

fluoroethanol was found to be almost 4.40 kcal/mol higher than the HOCl elimination

from CEOH. However, the theoretically determined energy of activation at MP2 (FULL)/6-311++g** for HOCl elimination is 100.45 kcal/mol which is 18.95 kcal/mol higher than the value determined using simulations. However, there is no experimental evidence available for HOCl elimination directly.

Following secondary reactions involving radical decomposition and radical recombination reactions have also been included in order to describe the ethene production. But their contribution to the total production of ethene is negligible because their production depends on the concentration of the C_2H_5 and C_2H_3 radical which is very low.

$$C_2H_5 \rightarrow C_2H_4 + H \qquad\qquad k_{19} = 4.00 \times 10^{14} \exp[(-40.50 \times 10^3)/(RT)]\ s^{-1} \qquad\qquad (R19)$$

$$C_2H_5 + CH_3 \rightarrow C_2H_4 + CH_4 \qquad k_{20} = 9.80 \times 10^{12}\ (T)^{-0.50}\ cm^3 mol^{-1} s^{-1} \qquad\qquad (R20)$$

$$C_2H_5 + C_2H_5 \rightarrow C_2H_4 + C_2H_6 \qquad k_{21} = 1.39 \times 10^{12}\ cm^3 mol^{-1} s^{-1} \qquad\qquad (R21)$$

$$C_2H_3 + H \rightarrow C_2H_4 \qquad k_{34} = 1.50 \times 10^{13} \exp[(-98.20 \times 10^3)/(RT)]\ cm^3 mol^{-1} s^{-1} \qquad (R34)$$

$$C_2H_3 + CHO \rightarrow C_2H_4 + CO \qquad k_{35} = 9.05 \times 10^{13}\ cm^3 mol^{-1} s^{-1} \qquad\qquad (R35)$$

$$C_2H_3 + C_2H_5 \rightarrow 2\ C_2H_4 \qquad\qquad k_{21} = 6.46\ cm^3 mol^{-1} s^{-1} \qquad\qquad (R36)$$
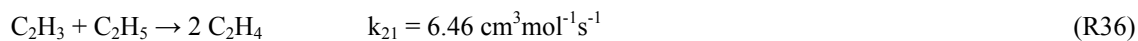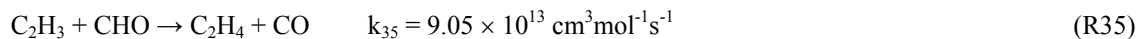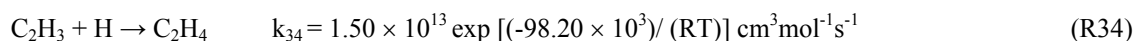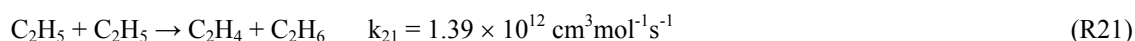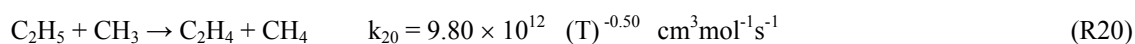
The consumption of the ethene formed in the reaction scheme is taken into account in the following reaction.

$$C_2H_4 + C_2H_4 \rightarrow C_2H_5 + C_2H_3 \qquad k_9 = 4.82 \times 10^{14} \exp[(-71.54 \times 10^3)/(RT)]\ cm^3 mol^{-1} s^{-1} \qquad (R9)$$

$$C_2H_4 + C_2H_5 \rightarrow C_2H_6 + C_2H_3 \qquad k_{28} = 6.32 \times 10^2\ (T)^{3.13} \exp[(-18.01 \times 10^3)/(RT)]\ cm^3 mol^{-1} s^{-1} \qquad (R28)$$

$$C_2H_4 \rightarrow C_2H_3 + H \qquad\qquad k_{30} = 2.00 \times 10^{16} \exp[(-110.0 \times 10^3)/(RT)]\ s^{-1} \qquad (R30)$$

$C_2H_4 + H \rightarrow C_2H_3 + H_2$ $k_{31} = 5.00 \times 10^{15} \exp [(-23.00 \times 10^3)/ (RT)]$ $cm^3mol^{-1}s^{-1}$ (R31)

$C_2H_4 + H_2 \rightarrow C_2H_5 + H$ $k_{32} = 1.02 \times 10^{13} \exp [(-68.16 \times 10^3)/ (RT)]$ $cm^3mol^{-1}s^{-1}$ (R32)

$C_2H_4 + CO \rightarrow C_2H_3 + CHO$ $k_{33} = 1.51 \times 10^{14} \exp [(-90.62 \times 10^3)/ (RT)]$ $cm^3mol^{-1}s^{-1}$ (R33)
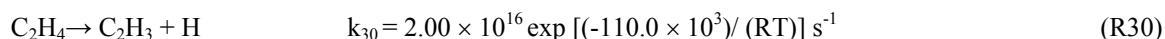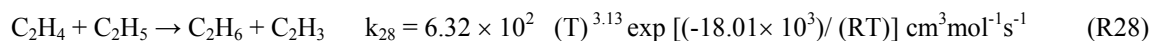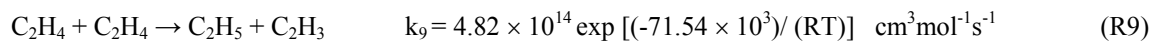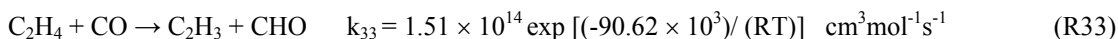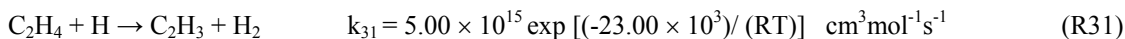
III.4.B.4.Acetylene

The unimolecular elimination of HCl from vinyl chloride leads to the formation of acetylene (R3). Acetylene has been observed experimentally but too low to be quantified that can be seen from the gas chromatogram as shown in the Figure III.1. In fact, the concentration of acetylene predicted by simulation is also negligible owing to its high energy barrier.

$CH_2CHCl \rightarrow C_2H_2 + HCl$ $k_3 = 1.00 \times 10^{14} \exp [(-69.35 \times 10^3)/ (RT)] \, s^{-1}$ (R3)
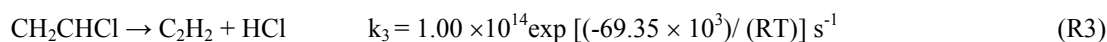
III.4.B.5.Butane

Butane has been observed experimentally but too low to be quantified that can be seen from the gas chromatogram as shown in the Figure III.1. In fact, the concentration of butane predicted by simulation is also negligible attributed to lower concentration of ethyl radicals.

$C_2H_5 + C_2H_5 \rightarrow C_4H_{10}$ $k_{22} = 1.08 \times 10^{13}$ (R22)

In general, the proposed reaction mechanism of thermal decomposition of CEOH is very similar to that of the 2-fluoroethanol.

The chemical kinetic modeling of the thermal decomposition mechanism of both 2-chloroethanol and 2-bromoethanol which is discussed in next chapter at high temperature was performed using a chemical kinetics simulator (CKS-1.01) program which is a scientific software tool developed by chemists at IBM's Almaden Research Center . The CKS program has rigorously accurate stochastic algorithm to propagate a reaction for the accurate simulation of chemical reactions.[66]

III.5. Sensitivity analysis

The presented reaction scheme was subjected to sensitivity analyses for the thermal decomposition of CEOH by increasing the rate coefficients by the factor of 3 as explained by Lifshitz[43]. These analyses have been carried out at two temperatures 1040 and 1100 K. This analysis has been carried out manually in excel sheet using the results obtained by chemical kinetic simulation by increasing the rate constant of each reaction by 3 times one by one and observing the corresponding change in the concentration of all the products at two different temperatures. The sensitivity spectrums of the six products and the reactants have been shown in the Table III.3. The reactions having the sensitivity factor less than 0.1% have been excluded from the scheme. This was a criterion for the reactions to be considered unimportant. Formation of particular product by certain reactions can easily be understood by following the sensitivity coefficient values as displayed in the sensitivity spectrum Table III.3. The sensitivity coefficient has been defined as $S_{ij} = \Delta \log C_i / \Delta \log k_j$. These numerical simulations were carried out for dwell time of 1.3ms. The negative sensitivity indicates decrease in concentration with the rise in the rate coefficient of a particular reaction by 3 times and *vice versa*. The values of

sensitivity factors given in the Table III.3 are self-explanatory. It is clear from Table 3 that the sensitivity factor of the products methane, ethane, and ethene formed by the free radical mechanism increases with rise in temperature. This can obviously be accounted by the higher concentrations of free radicals involved at high temperatures.

Table III.3. Sensitivity factors of 2-chloroethanol at 1040K/1100K with rate constant (k increased by 3 times)

R. No.	Reactions	C_2H_4	C_2H_6	CH_2CHCl	CH_3CHO	CH_4
R1	$ClC_2H_4OH \rightarrow CH_3CHO + HCl$	-0.169/-0.542	0.882/0.584	-0.185/-0.546	0.823/0.327	0.896/0.621
R2	$ClC_2H_4OH \rightarrow CH_2CHCl + H_2O$	-0.003/-0.025	-0.003/-0.017	0.990/0.976	-0.005/-0.028	-0.001/-0.018
R3	$CH_2CHCl \rightarrow C_2H_2 + HCl$	-/-0.001	-/-	-/-0.002	-/-	-/-
R4	$ClC_2H_4OH \rightarrow C_2H_4 + HOCl$	0.516/0.470	-0.002/0.012	-0.012/-0.034	-0.005/-0.041	-0.005/-0.040
R5	$ClC_2H_4OH \rightarrow Cl + C_2H_4OH$	0.639/0.575	-0.001/0.018	-0.009/-0.049	-0.008/-0.054	-0.001/-0.052
R6	$C_2H_4OH \rightarrow C_2H_4 + OH$	-/-	0.001/-	-0.007/-0.001	-/-	0.002/-
R7	$ClC_2H_4OH \rightarrow OH + C_2H_4Cl$	0.164/0.182	0.002/0.003	-0.008/-0.011	-0.001/-0.013	-/-0.013
R8	$C_2H_4Cl \rightarrow C_2H_4 + Cl$	0.001/-	0.001/-	-0.005/-0.002	-/-	-/-
R9	$2\ C_2H_4 \rightarrow C_2H_5 + C_2H_3$	-/-0.021	0.004/0.035	-0.001/-0.001	-/0.001	-0.002/-0.013
R10	$CH_3CHO \rightarrow CH_3 + HCO$	0.008/0.075	0.930/0.773	0.005/0.073	-0.107/-0.390	0.066/0.062
R11	$CHO \rightarrow CO + H$	0.001/0.002	0.041/0.039	-0.004/0.003	-/0.003	-0.041/-0.038
R12	$2\ CH_3 \rightarrow C_2H_6$	0.002/-	0.005/0.011	-0.001/0.001	-/0.002	-0.005/-0.011
R13	$CH_3CHO \rightarrow CH_4 + CO$	0.001/-0.013	-0.062/-0.246	-0.008/-0.011	-0.103/-0.409	0.894/0.709
R16	$CH_3 + CHO \rightarrow CH_4 + CO$	-0.001/-0.007	-0.112/-0.101	-0.005/-0.006	-0.001/-0.006	0.099/0.087
R17	$2\ CH_3 \rightarrow H + C_2H_5$	-/-	0.003/0.002	-/-0.001	-/0.001	-0.002/-0.002
R18	$CH_3 + OH \rightarrow CH_3OH$	0.001/-	-/-	-0.002/-0.002	-/-	-/-
R32	$C_2H_4 + H_2 \rightarrow C_2H_5 + H$	-/-0.002	-/0.002	-/0.001	-/-	-/-0.001
R35	$C_2H_3 + CHO \rightarrow C_2H_4 + CO$	0.003/0.001	0.001/-	-0.003/-	-/-	-0.001/-0.001
R38	$C_2H_6 \rightarrow 2\ CH_3$	-/-0.001	0.001/-	-/-0.001	-/-	-/-
R41	$2\ Cl \rightarrow Cl_2$	0.002/-	0.001/-0.001	-0.007/-	-/-	-/-
R42	$OH + Cl_2 \rightarrow HOCl + Cl$	0.001/-	-/-	-0.001/-0.001	-/-	-/-

III.6. Computational results and discussions

The optimization of both ground state and the TS structures for H_2O and HCl elimination reaction from CEOH were carried out at HF, MP2 (FULL) and DFT(B3LYP) levels of theory with the standard 6-31G*, 6-31G**, and 6-311++G** basis sets internally available in the Gaussian 03 suite of program.[67] These calculations were

performed for evaluating the pre-exponential factor and activation energy for these reactions using conventional transition-state theory. Extensive calculation was performed for evaluating the energies of different conformers of CEOH at different level of theory as mentioned above. There are five conformers of CEOH namely, G_g', G_g, G_t, T_g and T_t where the capital letters refers to the gauche and trans conformers for the rotation about C-C bond and small letters refers to the gauche and trans conformers for the rotation about C-O bond. The global rate coefficient was evaluated considering these five conformers of 2-chloroethaol. To verify the effect of β-substitution of OH on the barrier for HCl elimination, activation barrier have been compared with ethyl chloride. To understand the same phenomenon, experimental and theoretical E_a for H_2O elimination have been compared with that of ethyl alcohol and 2-fluoroethanol. Percentage change of four bond lengths involved in the reaction coordinate of HCl and H_2O elimination processes as compared to reactant have been performed in order to understand the structure of the TS and will be discussed in detail in next section. The structural parameters of the transition states for the HCl elimination and H_2O elimination from CEOH were compared with that of C_2H_5Cl and C_2H_5OH respectively.

The pre-exponential factors calculated depends on how the torsional mode in the reactant is treated. Hence, the rate parameters were estimated using harmonic oscillator, hindered rotor and free rotor models for torsional motion and will be discussed in detail in next section.

Optimized structures, normal mode vibrational frequencies, molecular energies and moment of inertia of five conformers of CEOH and those of HCl and H_2O

elimination reactions for the formation of CH_3CHO and CH_2CHCl respectively at different level of theories have been included in Table from III.A.1-III.A.20. (These Tables are given at the end of this Chapter). Figure III.6 shows the structures of transition states of HCl and H_2O eliminations including most stable ground state conformer $G_{g'}$ at B3LYP/6-311++g** level and TS of HOCl elimination for the formation of ethene at MP2/6-311++g** level. The optimized structures of ground state T_g, T_t, G_t and G_g conformations of CEOH B3LYP/6-311++g** level of theory have been reported in the Figure III.A.1 at the end of this chapter.
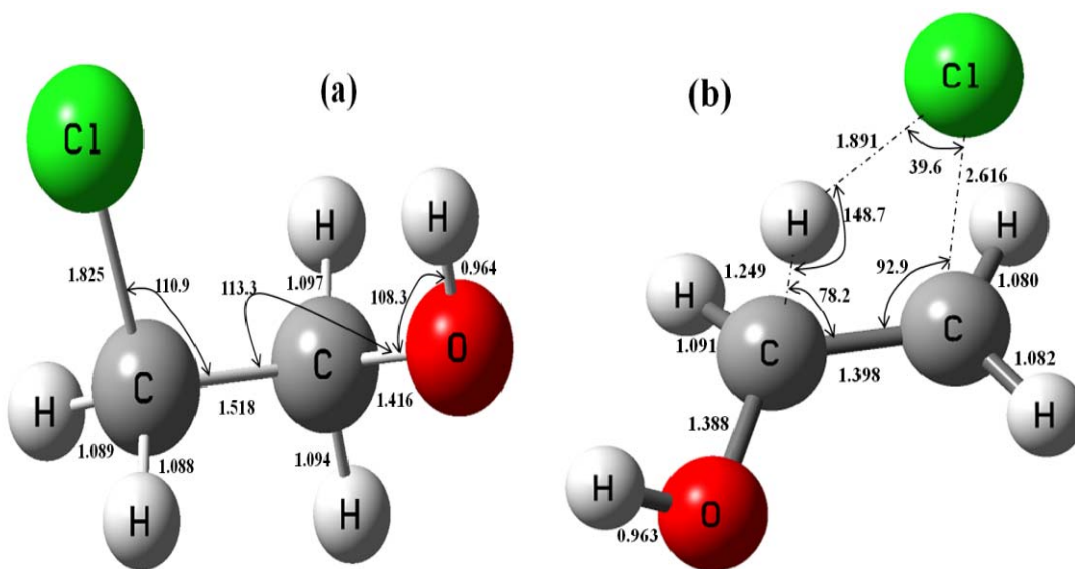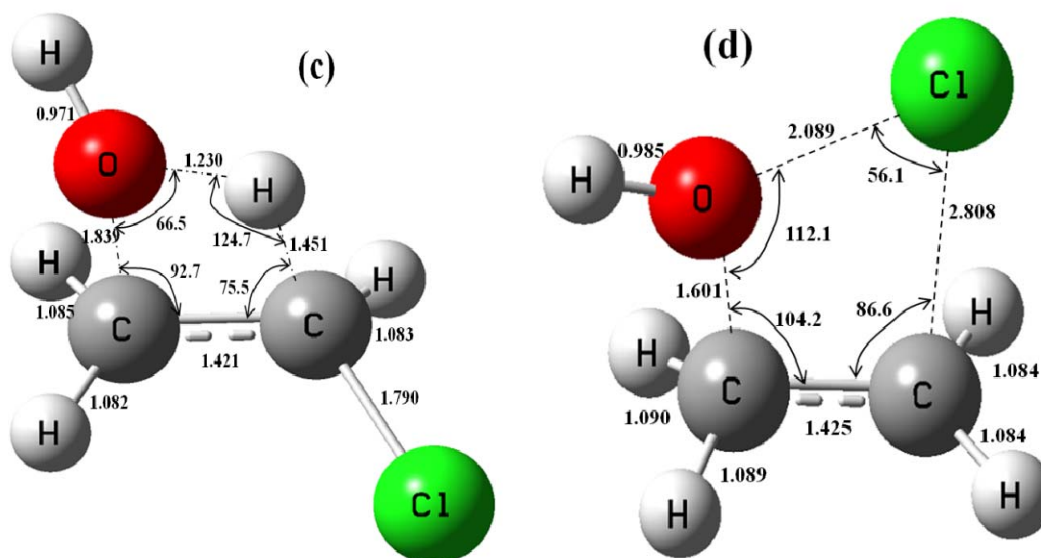
Figure III.6. Optimized geometries for $G_{g'}$ conformer of 2-chloroethanol (a) TS for HCl (b) and H_2O (c) elimination pathways at B3LYP/6-311++g** level. The units for bond lengths and bond angles have been given in angstrom and degrees, respectively. The optimization of HOCl elimination (d) was performed at MP2/6-311++g** level.

III.6.A.Transition state for HCl elimination

The TS for HCl elimination involves the formation of C=C and H-Cl bonds and the cleavage of C-Cl and C-H bonds. These bond distances are very important to understand the geometry of the TS. The C–C distance at the TS for HCl elimination was 1.381 and 1.383 A° with 6-31G** and 6-311++G** basis sets at HF level. Inclusion of electron correlation results in an increased but nearly similar C-C bond distance. It is 1.397 Å at MP2 (FULL) and 1.398 Å at B3LYP level respectively with 6-311++G** basis set. The optimized molecular structural parameters reported by Holmes et al. for the TS of HCl elimination from the $CF_3CFClCH_3$ molecule are in good agreement with our

result.[68] The calculated structural parameters for TS of HCl elimination from ethyl chloride and dichloroethane were found to be very similar in nature with that of the CEOH.[36]

The C-Cl and C-H bond distances involved in the HCl elimination are significantly different at different level of theory. At HF/6-31G** level of calculations, they are 2.695 and 1.213 Å, respectively. Adding diffuse function increases the C-Cl bond distance to 2.708 Å but decreases the C-H bond distance to 1.209 Å at HF/6-311++G** level. Moreover, results at B3LYP level are very different from the HF level with 6-311++G** basis set. The C-Cl distance is 2.437 Å at MP2 (FULL) and 2.616 Å at B3LYP level with 6-311++G** basis set. The C-H distance is 1.259Å at MP2 (FULL)/6-311++G** and 1.249Å at B3LYP/ (6-311++G**). The TS of HCl elimination reaction at HF level is comparatively tighter than that predicted at DFT level. The optimized molecular structural parameters reported by the Setser et al. for the TS of HCl elimination from the CH_2ClCH_2Br and CH_2ClCH_2Br molecule are in good agreement with our result.[69,70] These variations in bond distances results in change in the frequency factor as shown in the Table III.5. The larger A value corresponds to loose TS and vice versa. Summary of C-C, C-X, C-H, and H-X bond distances and percent changes calculated for the transition states for HCl/H_2O elimination reactions is shown in Table III.4.

The H-Cl distances evaluated using the 6-311++G** basis set at HF, MP2, and B3LYP levels are 2.071, 1.856, and 1.891 Å respectively. The bond distance of the free HCl molecule (1.286 Å at B3LYP/6-31G**) is smaller than the bond distance of HCl at TS at all levels of calculations as shown in the Table III.4.

Comparison of the transition states for the four bond distances involved in HCl elimination between ethyl chloride and CEOH have been reported in the Table III.A.34.

The TS has a plane of symmetry for ethyl chloride, containing all the four atoms involved in the reaction, i.e., two carbon, hydrogen, and chlorine. The $\angle ClCCH$ dihedral angle for HCl elimination from ethyl chloride is 0.0^0 at B3LYP/6-311++G** levels of theory indicating planarity of TS. At DFT/6-311++G** level of theory the $\angle OCCH$ dihedral angle for H_2O elimination from ethyl alcohol is 3.22^0 however it is 2.65^0 and 1.92^0 at HF and MP2 levels with the 6-311++G** basis set respectively.

Table III.4. Summary of C-C, C-X, C-H, and H-X distances and percent changes calculated for the transition states for HCl/H$_2$O elimination reactions from 2-chloroethanol[a]

Bond(H-X)	HF		MP2		B3LYP	
	6-31G**	6-311++G**	6-31G**	6-311++G*	6-31G**	6-311++G*
C-C (HCl)	1.381(-9.0)	1.383(-8.7)	1.399(-7.6)	1.397(-7.8)	1.401(-8.0)	1.398(-7.9)
C-C (H$_2$O)	1.454(-4.2)	1.467(-3.2)	1.419(-6.3)	1.425(-5.9)	1.428(-6.2)	1.421(-6.4)
C-Cl (HCl)	2.695(49.6)	2.708(50.1)	2.419(35.4)	2.437(36.4)	2.613(43.2)	2.616(43.3)
C-O (H$_2$O)	1.650(18.5)	1.607(15.4)	1.773(25.4)	1.756(24.3)	1.797(27.4)	1.839(29.9)
C-H (HCl)	1.213(11.6)	1.209(11.2)	1.275(16.7)	1.259(14.8)	1.251(13.7)	1.249(13.9)
C-H (H$_2$O)	1.610(49.2)	1.636(51.6)	1.503(38.5)	1.511(38.6)	1.493(36.8)	1.451(33.4)
HCl (HCl)	2.071(63.6)	2.071(63.1)	1.811(42.8)	1.856(45.8)	1.883(46.4)	1.891(47.0)
O-H (H$_2$O)	1.084(15.0)	1.078(14.5)	1.176(22.4)	1.178(22.9)	1.194(23.7)	1.230(27.9)

[a]For C-C, C-X, and C-H bonds, the percent changes (in parentheses) give the change in these distances compared to the reactant. For the H-X bond, percent change gives the change compared to free HCl and H_2O.

The dihedral angle for HCl elimination from 2-chlorothanol is a round 3.41^0-6.05^0 at all levels of theory with the 6-311++G** basis set. Dihedral angles for the 4 atoms involved in the reaction coordinate for HCl and H_2O elimination reactions from CEOH, ethyl alcohol and ethyl chloride are listed in the Table III.A.23 at end of this chapter. Comparisons of the four bond lengths of transition states for the HCl from CEOH as compared to that of HF eliminations from 2-fluoroethanol have been given in Table III.A.33.

III.6.B.Transition state for H_2O elimination

At all levels of calculation, the C-O and C-H bond lengths involved in the four centered TS was found to be longer than C-C and O-H bond lengths for H_2O elimination reactions. The C-C and C-H bond distances for H_2O elimination are longer than that of the HCl elimination indicating that the TS for the HCl and H_2O elimination reactions are very different from each other. At all levels of calculation, the C-X and H-X bond lengths(X=O/Cl) involved in the four centered TS for H_2O elimination was found to be shorter than that of the HCl elimination. These trends are very similar to what was observed in our previous work on 2-fluoroethanol[33]. Moreover, at all levels of calculations, the C-O bond is more broken for H_2O elimination in 2-fluoroethanol than in CEOH.[33] For HX elimination the C-H bond have been found to be more broken in 2-fluoroethanol than in CEOH at all levels of calculations.[33] The comparisons of the four

bond lengths of transition states for H_2O elimination between CEOH and 2-fluoroethanol have been given in Table III.A.33.

The C-O distances are 1.607 Å, 1.756 Å and 1.839 Å at HF, MP2 (FULL) and DFT level of theories respectively with 6-311++G** basis set for H_2O elimination from CEOH. The optimized molecular structural parameters reported by the Setser et al. for the TS of H_2O elimination from the 1-propanol are in good agreement with our result.[71] At all levels of calculations C-O bond lengths are smaller than the C-Cl distances resulting in a tighter TS for H_2O as compared to HCl elimination. Thereby, the pre-exponential factor for HCl elimination is expected to be greater than that of the H_2O elimination as shown in Table III.5. Lin et al. have reported optimized geometry of TS for water elimination computed at the B3LYP/6-311(d, p) level and is in closer agreement with our results.[16]

The C-O bond distance in the ground state Gg' conformer of CEOH is predicted almost constant. They are 1.393Å, 1.413 Å and 1.416 Å at HF, MP2 (FULL) and DFT theories respectively with 6-311++G** basis set. The increase in the bond distance from ground state to TS's is 0.214 Å at HF, 0.339 Å at MP2 (FULL) and is 0.423 Å at DFT level for H_2O elimination. This describes that the "looseness" of TS increases from HF to DFT through MP2 (FULL). This clearly reflects an increase in the value of pre-exponential factors from HF to DFT through MP2 (FULL) as shown in Table III.5. The C-O bond distance in the TS of ethanol was found to be more than that in the TS of CEOH. This may be attributed to the β-substitution effect of chlorine on the OH group.

The C-H bond distances for HCl and H_2O elimination are 1.249 Å and 1.451 Å respectively at B3LYP/6-311++G** level. Similar trend was observed at HF and MP2 (FULL) level as well. The C-H bond (the leaving hydrogen) is more broken in TS for H_2O elimination compared to that of HCl elimination. The C-H bond length is changed by 13.9% from ground state to TS for HCl and for H_2O elimination the change is 33.4% at DFT/6-311++G** level. The C-H bond is broken by 51.6% and 38.6% at HF and MP2 with 6-311++G** basis set for H_2O elimination. The similar trend was observed in case of 2-fluoroethanol also. We observed that O-H bond in TS for H_2O elimination is stronger than H-Cl bond in TS for HCl elimination. The dihedral angle for H_2O elimination from 2-chlorothanol is around 3.45^0-4.89^0 at all levels of theory with the 6-311++G** basis set indicating the non-planarity of TSs of CEOH for HCl and H_2O elimination reactions. This distortion of the TSs is attributed to the β-substitution effect.

III.6.C. Transition state for HOCl elimination

Our results show that the dihedral angle for HOCl elimination from 2-chlorothanol is around -12.2^0 at MP2/6-311++G** level indicating highly distorted non-planar geometry of HOCl transition state. The C-Cl bond distance for HCl is smaller than that of HOCl elimination and are 2.437 and 2.808 Å at MP2/6-311++G** level respectively. The C-OH bond distance for H_2O is longer than that of HOCl elimination and are 1.756 and 1.601 Å at MP2/6-311++G** level respectively as shown in the figure III.6. However, the C-C bond length is very similar to that of HCl and H_2O elimination. The Cl-OH bond distance in the transition state is much longer as compared to that of the free HOCl molecule and is 2.089 and 1.667Å at same level respectively. Thereby, the

transition state of H_2O elimination is tighter than that of the HOCl. This reflects in the higher preexponential factor of HOCl elimination ($10^{15.05}$) than that of H_2O ($10^{13.97}$).

III.6.D. Intrinsic reaction coordinate calculations

Minimum energy reaction pathways (reaction coordinate) have been obtained for transition state of HCl and H_2O elimination reaction from 2-chloroethaonl using the IRC calculations for the verification of transition state. These calculations were carried out in 61 steps and found to be well connecting reactant and products. However, IRC calculation of HOCl elimination was performed in 81 steps at MP2/6-311++G** level. These results have been displayed in Figure III.7 including the corresponding geometries of reactant, transition states and products. Comparison of the reaction coordinates of HCl, H_2O and HOCl elimination reaction pathways illustrates that the three reactions follow distinctly different reaction paths. We have found close agreement between the energies obtained using the IRC calculations and independently optimized values.

For the HCl elimination, IRC calculations indicate that the C-Cl bond cleaves first and virtually broken fully at transition state. This is followed by dissociation of C-H bond starting at 1.093 Å with simultaneous formation of H-Cl single bond. The C-Cl and C-H bonds are fully ruptured at transition state. Figure III.7 represents that this process proceeds with smooth conversion of C-C single bond to C-C double bond.

For the H_2O elimination, these calculations predict that the C-O bond is almost ruptured first at 1.727 Å. This is followed by formation of H-OH single bond begins at 1.205 Å with simultaneous cleavage of C-H bond starting at 1.086 Å. In fact, the

dissociation of C-OH and C-H bond is fully completed at transition state resulting in fully

formed bond of H-OH as shown in Figure III.7.

It is clear from the IRC plot of HOCl elimination that the C-Cl bond cleaved first

at 2.354 Å precedes with breaking of C-O bond starting at 1.415 Å. This is attributed to

the fact that the bond dissociation energy of the former (75.89 kcal mol^{-1}) is less than the

C-OH bond (84.84 kcal mol^{-1}). This is accompanied by the formation of HO-Cl single

bond beginning at 2.430 Å with simultaneous conversion of C-C single bond uniformly

proceeding to C-C double bond as displayed in Figure III.7.
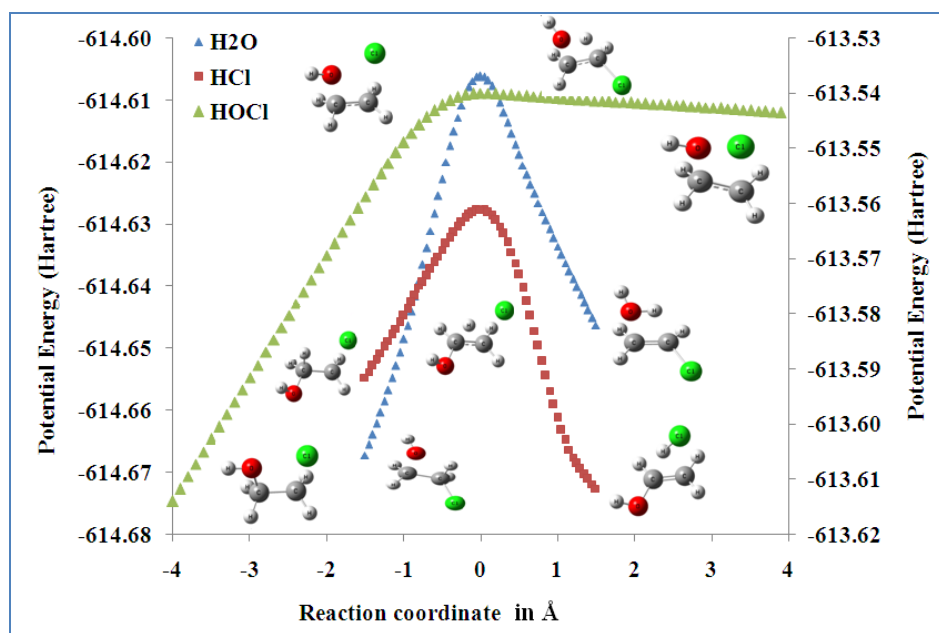
Figure III.7. Minimum energy reaction pathways for transition state of HCl and H$_2$O

elimination reactions from 2-chloroethaonl obtained using the intrinsic reaction

coordinate (IRC) calculations performed in 61 steps at B3LYP/6-311++G** level of the

theory for the verification of transition states and found to be well connecting reactant

and products represented at primary Y axis. However, IRC calculation of HOCl

elimination was performed in 81 steps at MP2/6-311++G** level shown in secondary Y axis. This plot also describes that the two transition states are following the distinctly different reaction paths.

III.6.E. Transition state theory calculations

Frequency calculations were carried out at all levels of calculations for both the ground and transition states to perform transition state theory calculations. Transition states have been characterized by one imaginary frequency corresponding to the reaction coordinate. The reaction coordinate corresponds to the motion of H away from C toward Cl/O in both cases. The motion of the reaction coordinates when visualized with Chemcraft clearly shows that the TS correspond to the reaction of interest. The transition–state theory expression was used for evaluating the thermal rate constants for both HCl and H_2O elimination from CEOH. The A and E_a were estimated between 930 and 1100 K (at 10 K intervals) at the HF, MP2 (FULL), and DFT level of theory with the 6-311++G** basis set. Details of which are given in the chapter II.

In this subsection, Arrhenius parameters for formation of CH_2CHOH and CH_2CHCl by unimolecular elimination of HCl and H_2O from CEOH will be discussed in detail.

Inspection of Figure III.8 demonstrates that HOCl elimination reaction is highly endothermic by 65.06 kcal mol^{-1} at MP2/6-311++G** level of theory. The HCl and H_2O elimination processes are exothermic and endothermic by 4.24 and 8.04 kcal mol^{-1} at B3LYP level, respectively. However, exothermicity of HCl elimination predicted at MP

level is too small, 0.24 kcal mol^{-1}. Schematic potential energy level diagram illustrating

the forward and backward activation energies including the enthalpy of reactions for

unimolecular HCl and H$_2$O elimination channels evaluated at HF, MP2 (FULL) and

B3LYP level using the 6-311++G** basis set have been represented in Figure III.8. For

HOCl elimination results have been estimated only at MP2 (FULL) /6-311++G** level

as our attempts failed to optimize the HOCl transition state at all other levels.
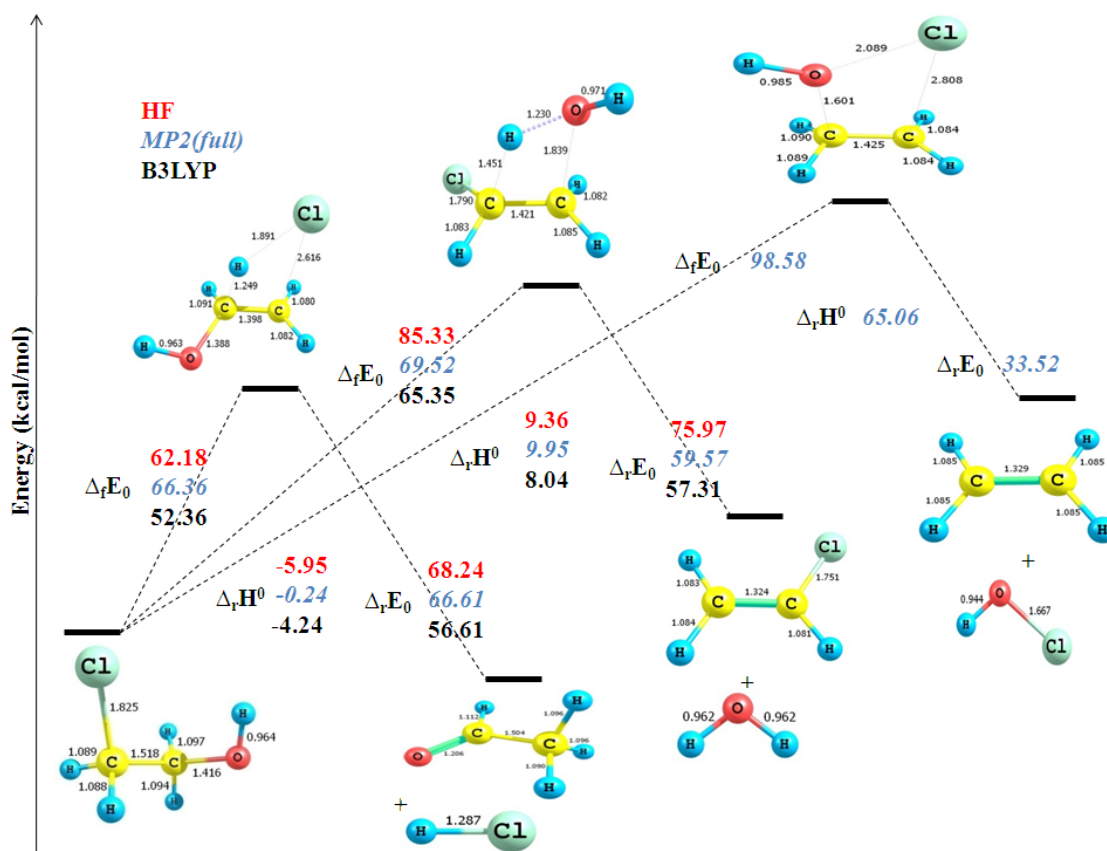
Figure III.8. Schematic potential energy level diagram showing the forward and

backward activation energies including the enthalpy of reactions for unimolecular HCl

and H$_2$O elimination channels from 2-chloroethanol evaluated at HF, MP2 (FULL) and

B3LYP level of theory using the 6-311++G** basis set. The E_a shown for HOCl elimination calculated only at MP2 (FULL) /6-311++G** level as our attempts failed to optimize the HOCl transition state at other levels. The $\Delta_f E_0$ and $\Delta_r E_0$ corresponds to difference in sum of electronic and zero point energies for forward reaction and reverse reactions respectively. $\Delta_r H^0$ denotes the enthalpy change of reaction. The geometries shown here are all at B3LYP/6-311++G** level except that of TS of HOCl and corresponding product that is at MP2 (FULL) /6-311++G** level. The units for bond lengths and bond angles have been given in angstrom and degrees, respectively.

Three potential energy surfaces (PES) scan have also been performed for the CEOH about the C-C and C-O bonds to identify no. of conformers (all energy minima) as well as difference in their energy. Present study has shown that the five conformers are distinctly different in energy and structure. Potential energy curves evaluated at B3LYP/6-311++G** level of theory corresponding to (a) rotation around the C-C bond in T_t structure (b) rotation around the C-O bond in G_g structure and (c) rotation around the C-O bind in T_g structure have been depicted in Figure III.9. It can be seen from Figure III.9 that the rotation around the C-O bond in Gg structure gives rise to three minima whereas rotation around the C-C bond produces two minima, therefore five conformers are possible for CEOH. The difference in energy between different rotamers can easily be noticed from the Figure III.9. We have found that the Gg' conformer is lower in energy by 1.0-2.5 kcal mol^{-1} as compared to other four conformers at B3LYP/6-311++G** the level theory. These results have been found to be in good agreement with the results reported by Souza et al. at B3LYP/6-31g (d, p) level of theory.[72] In general,

106

the energies were found to be increasing in the order $G_g'< T_t < T_g <G_t <G_g$. It is so because in case of the G_g conformer the hydroxyl hydrogen is pointing away from the chlorine whereas that of the G_g' conformer is pointing towards the chlorine side which permits the electrostatic interaction between the chlorine and hydroxyl hydrogen. As a result of this Gg' conformer is more stable than other four forms of CEOH and G_g is least stable conformer.
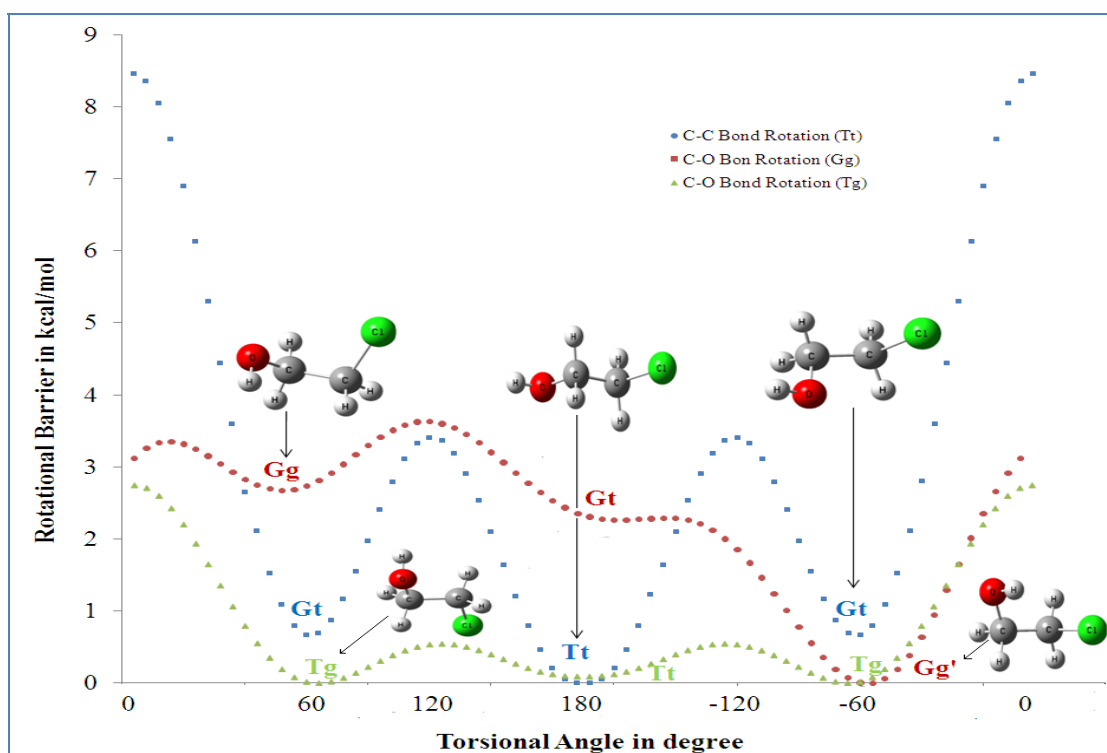
Figure III.9. The potential energy barriers for internal rotation about C-C bond for T_t conformer (filled blue squares), rotation around C-O bond for G_g conformer (filled maroon circles) and rotation around C-O bond for T_g conformer (filled green triangle) evaluated at B3LYP/6-311++G (d, p) level of theory for 2-chloroethanol. Fully optimized

detailed structural parameters of five conformers have been given in the Figure III.A.1 at the end of this chapter.

If their contributions are included, the activation energy calculated will be reduced depending upon the level of the theory. Hence, the total rate constant for HCl elimination was estimated as the sum of the values for the five conformers weighted by the Boltzmann factor.

$$k = k_{G_{g'}} w_{G_{g'}} + k_{G_t} w_{G_t} + k_{G_g} w_{G_g} + k_{T_t} w_{T_t} + k_{T_g} w_{T_g}$$

Here the w corresponds to the Boltzmann factor. The total rate constant for H_2O elimination was determined by taking all conformers except G_g conformer into account owing to inhibiting interactions between the C-H and O-H hydrogen's in the transition state and were calculated as follows:

$$k = k_{G_{g'}} w_{G_{g'}} + k_{G_t} w_{G_t} + k_{T_t} w_{T_t} + k_{T_g} w_{T_g}$$

To avoid any ambiguity, the reaction path degeneracy (l) considered for each conformer in any case is one.

The E_a for HCl elimination from ethyl chloride at HF, MP2, and DFT /6-311++G** level are 62.26, 66.23, and 53.59 kcal mol^{-1}, respectively.[36] At similar levels the E_a for HCl elimination from CEOH are 63.72, 67.85, and 53.84 kcal mol^{-1}, respectively. This slight increase at all levels basically implies that β-substitution of OH does not have a significant effect on the E_a of HCl elimination. The E_a for HCl

elimination from chlorofluoroethane at HF, MP2, and DFT /6-311++G** level are 70.45, 72.97, and 57.86 kcal mol^{-1}, respectively.[73] The experimental determined E_a for HCl elimination from CEOH, chloroethane, dichloroethane and chlorofluoroethane are 58.70, 57.7, 57.8, and 63.8 kcal mol^{-1}, respectively.[36, 73] This clearly reveals the fact both experimentally and theoretically that the fluorine substitution increases the activation barrier, however, Cl and OH substitution do not.

These thermal activation experiments results indicates that the β-substitution of Cl does not bring about a significant change in HCl elimination barrier. However, the chemical activation results show an increase of 7 kcal/mol on β-substitution on Cl on ethyl chloride.[70] This clearly indicate the difference between chemical and thermal activation experiments.

The thermal HCl elimination barrier from chloroethane found to be 55.8 kcal/mol using a single-pulse shock tube at 990–1200 K by Roux and co-workers.[75] Dai et al. has found the Arrhenius parameter E_a for unimolecular HCl elimination reaction to be 49.48 kcal/mol from trichloroethane experimentally by IR laser pyrolysis which is almost 5 kcal/mol lower than the results reported by Roux et al.[75-76]

It was found that the HF and MP2 (FULL) level calculations overestimate experimental E_a by 5.92, 9.15 kcal mol^{-1} for HCl elimination from CEOH respectively. However, a DFT result underestimates E_a by 3.96 kcal/mol in temperature range of investigation. The comparison of experimental and theoretical A and E_a values of HCl elimination from CEOH determined at HF, MP2 (FULL), B3LYP/6-311++G** level with ethyl chloride and chlorofluoroethane have been summarized in the Table III.6.[36, 73]

Table III.5. Comparison of theoretical and experimental rate parameters for unimolecular H_2O and HCl elimination reactions from 2-chloroethanol[a]

Theory/Basis set (6-311++g**)	$ClCH_2CH_2OH \rightarrow CH_3CHO+HCl$			$ClCH_2CH_2OH \rightarrow CH_2CHCl+H_2O$		
	log A	E_a	k^b	*log A*	E_a	k^b
HF (HO)	14.54±0.03	63.72±0.03	68.68	13.78±0.02	86.75±0.03	3.05×10^{-4}
HF (HR)	13.26±0.04	62.91±0.06	5.23	12.64±0.04	85.74±0.05	3.51×10^{-5}
HF (FR)	13.38±0.04	65.14±0.05	2.47	12.60±0.04	88.15±0.04	1.06×10^{-5}
MP2(FULL)(HO)	14.37±0.03	67.85±0.04	6.97	13.97±0.03	71.32±0.05	5.64×10^{-1}
MP2(FULL)(HR)	13.20±0.03	66.27±0.05	0.97	12.99±0.02	69.55±0.02	1.33×10^{-1}
MP2(FULL)(FR)	13.32±0.03	67.91±0.04	0.60	12.93±0.02	71.43±0.04	4.89×10^{-2}
B3LYP (HO)	14.48±0.02	53.84±0.02	5583.18	14.08±0.03	67.13±0.03	4.97
B3LYP (HR)	13.19±0.02	52.80±0.03	461.34^c	12.93±0.01	65.90±0.02	6.19×10^{-1}
B3LYP (FR)	13.39±0.03	55.31±0.03	230.98	12.98±0.03	68.58±0.03	2.03×10^{-1}
Experiment[d]	14.37±0.35	58.70±1.55	510.10	14.95±0.33	67.95±1.50	2.53×10^{1}

[a] The entropy of activation considering hindered rotor model, $\Delta S^{\neq}$, at 1100 K are -1.0, -0.7, and -1.2 cal K^{-1} mol^{-1} for HCl elimination at HF, MP2, and DFT levels, respectively. For H_2O elimination, the corresponding values are -3.7, 1.7, and 2.5 cal K^{-1} mol^{-1}. The entropy of activation considering free rotor model, $\Delta S^{\neq}$, at 1100 K are -6.7, -6.1, and -5.7 cal K^{-1} mol^{-1} for HCl elimination at HF, MP2, and DFT levels, respectively. For H_2O elimination, the corresponding values are -4.1, -5.0, and -4.3 cal K^{-1} mol^{-1}. HO, HR, and FR in the parentheses corresponds to harmonic oscillator, hindered rotor and free rotor models for the torsional mode. *A* is in s^{-1} and E_a are in kcal mol^{-1}. [b] Rate constant calculated at 1100 K in s^{-1}. [c] Predicts better agreement with experimental results for HR model. [d] Experimental values are from present study. The theoretical results given for CEOH are Boltzmann weighted averages for the five G_g', G_g, G_t, T_g and T_t forms for both HCl and H_2O elimination. Hindered rotor partition function is from a full

approximation following Truhlar's method. Detailed information on E_0 values of HCl and H_2O elimination in given in the Table III.A.21 at the end of this chapter.

It is clear from Table III.5 that the Arrhenius parameters for unimolecular HCl elimination deduced from experimental results have no satisfactory agreement , on both A and E_a together, with TST determined data at HF, MP2(FULL) and B3LYP level with 6-311++G** basis set. Experimentally determined preexponential factor for HCl elimination from CEOH, ethyl chloride, and 1, 2-dichloroethane are $10^{14.37}$, $10^{13.84}$, and $10^{13.98}$ s^{-1}, respectively.[36] We have observed in our previous analysis for HCl elimination from chlorofluoroethane and dichloroethane that the preexponential factors reduces by an order of magnitude when the C-C bond rotations were treated as free internal rotors.[73] The calculated preexponential factor for HCl elimination from ethyl chloride, chlorofluoroethane, and 1, 2-dichloroethane are $10^{13.96}$, $10^{13.53}$, and $10^{13.68}$ s^{-1}, respectively.[73] There are two low frequency torsional motion in case of CEOH corresponding to C-C and C-O bond rotations. These two internal rotors have been treated as either harmonic oscillator (HO) or hindered internal rotor (HR) or free rotor (FR) for estimating the preexponential factor. Hindered rotor partition function calculation was done only for the reactant not for TS. In the case of transition state, C-O internal motion for HCl elimination was found to be coupled with other modes in the transition state and hence was not treated as hindered rotor. Truhlar's detailed methodology[74] was followed for treating the torsional modes as hindered rotor that results in decrease of preexponential factor by an order of magnitude from $10^{14.48}$ to $10^{13.19}$ at B3LYP/6-311++G** level. This brings about an order of magnitude difference between experimental and theoretical preexponential factor at DFT level. In fact, this difference

leads to excellent quantitative agreement between experimental and theoretical rate coefficient of HCl elimination reaction as shown in Table III.5. However, DFT (HO) calculations overestimates and FR result underestimates the total rate coefficient of HCl elimination. It can be noticed from Table III.5 that the theoretical results at all other levels exhibit considerable deviation from the shock tube data. This fact is clear from a comparison of Arrhenius plots of the present shock tube determined and TST calculated results at HF, MP2(full) and B3LYP level with 6-311++G** basis set for the HCl elimination reaction as well in the temperature range of 930-1100 K that has been displayed in the Figure III.10.
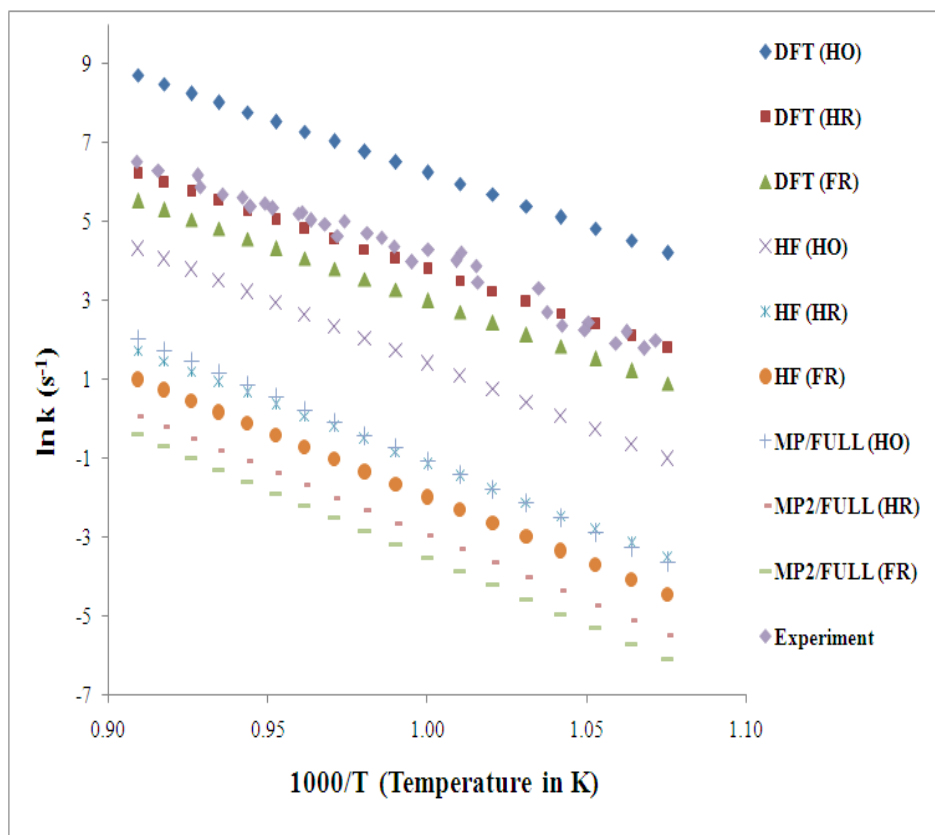
Figure III.10. Comparison of Arrhenius plot for rate coefficient data obtained from experimental and theoretical results for unimolecular elimination of HCl from 2-chloroethanol at HF, MP2(FULL) and DFT(B3LYP) level of theory with 6-311++G** basis set using HO, HR and FR models over the temperature range of 930-1100 K. The HO, HR, and FR given in parentheses correspond to harmonic oscillator, hindered rotor and free rotor. The data are labeled with different symbols and are designated in figure above.

A comparison of Arrhenius parameters determined at HF, MP2 (FULL) and B3LYP level of theories using the 6-311++G** basis set using HO, HR and FR models for both HCl and H_2O elimination reactions with experimental results have been compiled in Table III.5. We have observed excellent agreement between experiment and theoretical results at all levels of theory for the preexponential factor treating internal rotor as harmonic oscillator. However, it was found that the hindered and free rotor calculations at all levels predict decrease in preexponential factor by an order of magnitude.

The predicted rate coefficient for HCl elimination determined considering harmonic oscillator model at G3B3 and CBS-QB3 higher level of calculations are $10^{14.50\pm0.01}$ exp $[-(62.12\pm0.02)/(RT)]$ s^{-1} and $10^{14.40\pm0.01}$ exp $[-(62.34\pm0.01)/(RT)]$ s^{-1} respectively. These calculations also overestimate the E_a approximately by 3.5 kcal mol^{-1}.

The activation energies for H_2O elimination in case of C_2H_5OH are 85.2, 68.5, and 64.5 kcal mol^{-1} at HF, MP2 (FULL), and DFT theories, respectively.[33] However, the theoretical value reported by Lin and co-workers is 66.6 kcal mol^{-1} that is close to

predicted MP2 and DFT level values.[16] The E_a at the same levels for H_2O elimination

from CEOH are 86.75, 71.32, and 67.13 kcal mol^{-1}, respectively. This increase of ~ 1-3

kcal mol^{-1} at all levels basically represents the fact that β-substitution of Cl does not have

a significant effect on the E_a of H_2O elimination within the experimental uncertainty.

However, at similar level, the E_a for H_2O elimination from 2-floroethanol are 92.43,

75.52, and 70.07 kcal mol^{-1}, respectively.[33] This study certainly unveils the fact that the

β-substitution of F brings about the significantly large increase in activation barrier by ~

6-7 kcal/mol for H_2O elimination. The experimental E_a for H_2O elimination from CEOH,

2-fluoroethanol,[33] and ethyl alcohol[16] are 67.9, 69.7, and 67.9 kcal mol^{-1}, respectively

also describes the fact that the F substitution leads to an increase in E_a not the Cl.

Table III.6. Comparison of the rate parameters for the unimolecular elimination of

HCl from 2-chloroethanol with that from chlorofluoroethane and ethyl chloride *[a]*

Theory/6-311++G**	$ClC_2H_4OH \rightarrow CH_3CHO + HCl$			$FC_2H_4Cl \rightarrow HCl + CH_2CHF$			$C_2H_5Cl \rightarrow C_2H_4 + HCl$		
	log A	E_a	k ^{b}	log A	E_a	k ^{b}	log A	E_a	k ^{b}
HF	14.54±0.03	63.72±0.03	68.68	14.7	70.45	45.19	14.63±0.00	62.26±0.02	165.18
MP2(full)	14.37±0.03	67.85±0.04	6.97	14.75	72.97	1.59	14.54±0.01	66.23±0.02	21.69
DFT	14.48±0.02	53.84±0.02	5583.18	14.64	57.86	1274.44	14.29±0.00	53.59±0.02	4042.94
Experiment ^{c}	14.37±0.35	58.70±1.55	510.1	13.47	63.33	6.99	13.84±0.2	57.8±2.0	207.56

[a] The E_0 ($G_{g'}$) values are 62.18, 66.36, and 52.36 kcal mol^{-1} computed at HF, MP2, and DFT levels for HCl

elimination, respectively. The entropy of activation considering harmonic oscillator model, $\Delta S^{\neq}$, at 1100 K

are 3.3, 2.6, and 2.9 cal K^{-1} mol^{-1} for HCl elimination at HF, MP2, and DFT levels, respectively. *A* is in s^{-1}

and E_a are in kcal mol^{-1}. *[b]* Rate constant calculated at 1100 K in s^{-1}. *[c]* Experimental values are from present

study. *[c]* Chlorofluoroethane and chloroethane data are taken from ref 73.

From Table III.7 it is clear that the HF, MP2 (FULL) level calculations overestimate E_a, H_2O elimination, by 18.80 and 3.37 kcal mol^{-1} respectively. However, the DFT predictions underestimate E_a by 0.82 kcal/mol in temperature range of 930-1100 K. It can be concluded that the E_a estimated at DFT level have been found to be in good agreement with experimental results. This is also the case in ethanol and 2-fluoroethanol that can be noticed from Table III.7.[33] It must be emphasized here that the predicted as well as experimental value of E_a for H_2O elimination is higher than that of HCl at all levels of theory considered here.

Table III.7. Comparison of the rate parameters for the unimolecular elimination of H_2O from 2-chloroethanol with that from 2-fluoroethanol and ethyl alcohol [a]

Theory/6-311++g**	$ClC_2H_4OH \rightarrow H_2O + CH_2CHCl$			$FC_2H_4OH \rightarrow H_2O + CH_2CHF$			$C_2H_5OH \rightarrow H_2O + CH_2CH_2$		
	log A	E_a	k [b]	*log A*	E_a	k [b]	*log A*	E_a	k [b]
HF	13.78±0.02	86.75±0.03	3.05×10^{-4}	14.32± 0.01	92.43 ± 0.02	7.80×10^{-5}	14.79±0.00	85.24±0.02	6.25×10^{-3}
MP2(full)	13.97±0.03	71.32±0.05	5.64×10^{-1}	14.72 ±0.01	75.52 ±0.03	4.61×10^{-1}	13.97±0.00	68.56±0.02	2.00
DFT	14.08±0.03	67.13±0.03	4.97	14.71± 0.01	70.07± 0.03	5.50	14.39±0.00	64.47±0.02	3.45×10^1
Experiment[c]	14.95±0.33	67.95±1.50	2.53×10^1	14.30± 0.13	69.69 ±1.70	2.55	13.74	67.90	1.60

[a] The E_0 (G$_{g'}$) values are 85.33, 69.52, and 65.35 kcal mol^{-1} computed at HF, MP2, and DFT levels for H_2O elimination, respectively. The entropy of activation considering harmonic oscillator model, $\Delta S^{\neq}$, at 1100 K are 0.6, 1.5, and 1.6 cal K^{-1} mol^{-1} for H_2O elimination at HF, MP2, and DFT levels, respectively. A is in s^{-1} and E_a are given in units of kcal mol^{-1}. [b] Rate constant calculated at 1100 K is given in units of s^{-1}. [c] Experimental values are from present study. [c] Fluoroethanol and ethanol data are taken from ref 33.

It should be noticed here that the E_a values predicted considering free rotor model at all levels for both HCl and H_2O elimination reactions have been underestimated by ~1-3 kcal mol^{-1} than that estimated by HO and HR models as given in Table III.5.

The experimental pre-exponential factor for H_2O elimination from CEOH, ethyl alcohol, and 2-fluoroethanol are $10^{14.95}$, $10^{13.74}$, and $10^{14.30}$ s^{-1}, respectively. Our TST calculations at HF, MP2, and B3LYP/6-311++G** level underestimates preexponential factors by an order of magnitude for H_2O elimination from CEOH. They are $10^{13.78}$, $10^{13.97}$, and $10^{14.08}$ s^{-1}, respectively. However, treating the torsional modes, both C-C and C-O bond rotation, as hindered rotor results in a further decrease of preexponential factor by an order of magnitude. It is $10^{12.64}$, $10^{12.99}$, and $10^{12.93}$ s^{-1} at the same level, respectively. These calculations lead to further decrease of the rate coefficient in the temperature range of investigation. A free rotor calculation underestimates the rate coefficient of H_2O elimination to a large extent as illustrated in the Figure III.11.

Table III.5 reveals that the DFT/6-311++G** calculations using harmonic oscillator model underestimates the rate coefficient for H_2O elimination by 5 times as compared to experimental results. However, the theoretical result at all other levels uniformly underestimates the rate coefficients for H_2O elimination. The same can be observed from a combined Arrhenius plot of the present shock tube and TST fitted results calculated at all levels for the H_2O elimination reaction in the temperature range of 930-1100 K as represented in the Figure III.11.

In order to gain better insight into the Arrhenius parameters, the rate coefficient for H_2O elimination were determined considering harmonic oscillator model at higher

G3B3 and CBS-QB3 level of theory. They are $10^{13.93\pm0.01}$ exp [-(71.49±0.01)/(RT)] s^{-1} and $10^{13.95\pm0.01}$ exp [-(72.21±0.02)/(RT)] s^{-1} respectively. However, these calculations also overestimate the E_a approximately by 4 kcal mol^{-1}. The comparison of experimental and theoretical A and E_a values determined at HF, MP2 (FULL), B3LYP level of theory with the 6-311++G** basis set of H_2O elimination from CEOH with that from ethyl alcohol and 2-fluoroethanol have been summarized in the Table III.7.
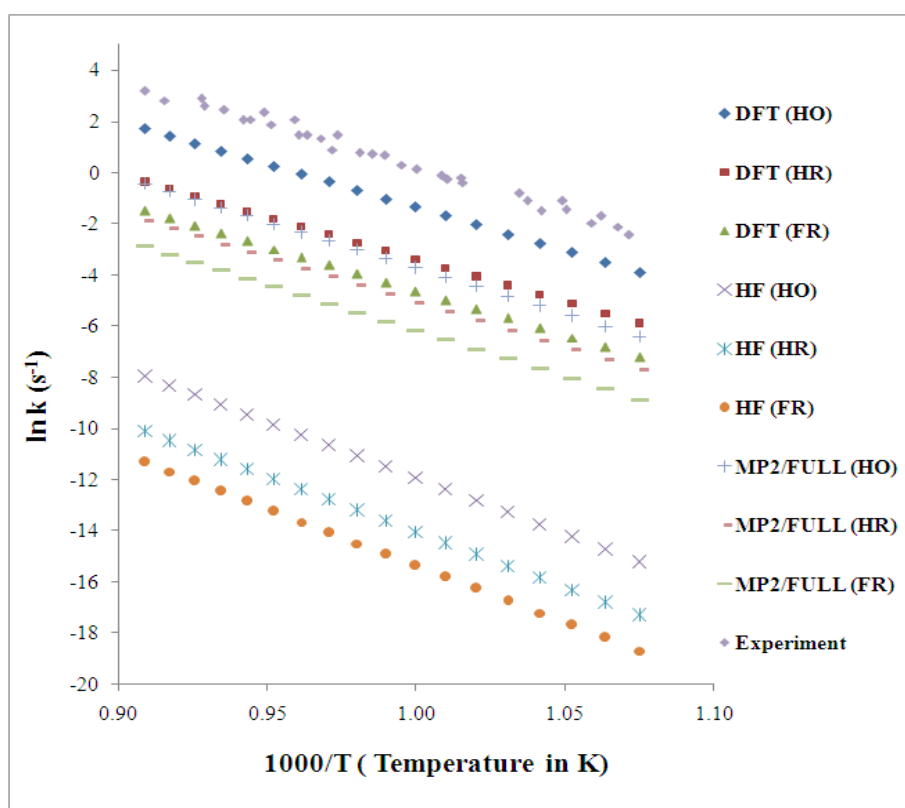
Figure III.11. Comparison of Arrhenius plot for rate coefficient data obtained from experimental and theoretical results for unimolecular elimination of H_2O from 2-chloroethanol at HF, MP2(FULL) and DFT(B3LYP) level of theory with 6-311++G** basis set using HO, HR and FR models. The HO, HR, and FR given in parentheses

correspond to harmonic oscillator, hindered rotor and free rotor. The data are labeled with different symbols and are designated in figure above.

In case of HOCl elimination total rate coefficient was estimated by taking the sum over the three conformers, $G_{g'}$, G_t, G_g , weighted by Boltzmann factor (*w*). Since the T_t and T_g conformers cannot lead to HOCl elimination. However the reaction path degeneracy considered for each conformer in any case is one.

$$k = k_{G_{g'}} w_{G_{g'}} + k_{G_t} w_{G_t} + k_{G_g} w_{G_g}$$

The rate coefficient estimated for HOCl elimination reaction at MP2 (FULL)/6-311++g** level of theory employing TST calculation is given by $10^{15.05\pm0.01}$ exp [-(100.45±0.02)/(RT)] s^{-1}. The HOCl elimination channel from CEOH was invoked because the kinetic simulations with well established rate constants could not explain the experimentally observed high C_2H_4 concentration. For the FCH_2CH_2OH, earlier attempts to identify a transition state for HOF elimination theoretically did not succeed[33]. However, for the FCH_2CH_2Cl the barrier for the analogous ClF elimination[77] channel was significantly higher, 145 kcal mol^{-1}. For HOCl elimination from chloroethanol, the calculated barrier is 100.45 kcal mol^{-1}. However, in order to fit the experimental concentration of C_2H_4, activation barrier of 81.50 kcal mol^{-1} was used for the HOCl elimination channel.

Recently, there has been a lot of interest in "roaming mechanism" which describes the abnormal molecular dissociation of vibrationally excited molecules.[78-79]

Based on the experimental and theoretical results it was described that, in roaming mechanism, the partially dissociated radicals which are separated by the 3 or 4 Å can roam around and may spend several hundred femtoseconds before they achieve an orientation which has the barrierless path leading to an internal abstraction and finally to molecular products.[78-79] This roaming mechanism has been observed most commonly in hydrogen atom.[80] However, there has been an example of its evidence in heavy atoms as well. In fact, there are reports available where shock tube technique has been used to investigate the roaming mechanism.[81-82] Hence, to explain the unusually high C_2H_4 concentration, it was speculated that the roaming mechanism may be operating in CEOH as well. It is clear from above discussion that the HOCl elimination barrier is very close to the C-Cl bond energy in chloroethanol. Therefore, the C-Cl bond may break and Cl may abstract the OH forming HOCl before drifting away from CH_2CH_2OH. The difference between experimental and theoretical activation energies for the HOCl elimination channel clearly point out that roaming pathway may be operating for chloroethanol as well. It would be interesting to do the high resolution imaging studies for the haloethanols. Comparison of Arrhenius plot obtained from modeling and TST fitted results for unimolecular elimination of HOCl at same level using harmonic oscillator model is depicted in Figure III.12. The rate coefficient obtained from fitting to complex mechanism is given by $10^{17.73\pm1.60}$ exp $[-(81.50\pm3.50)/(RT)]$ s^{-1}.
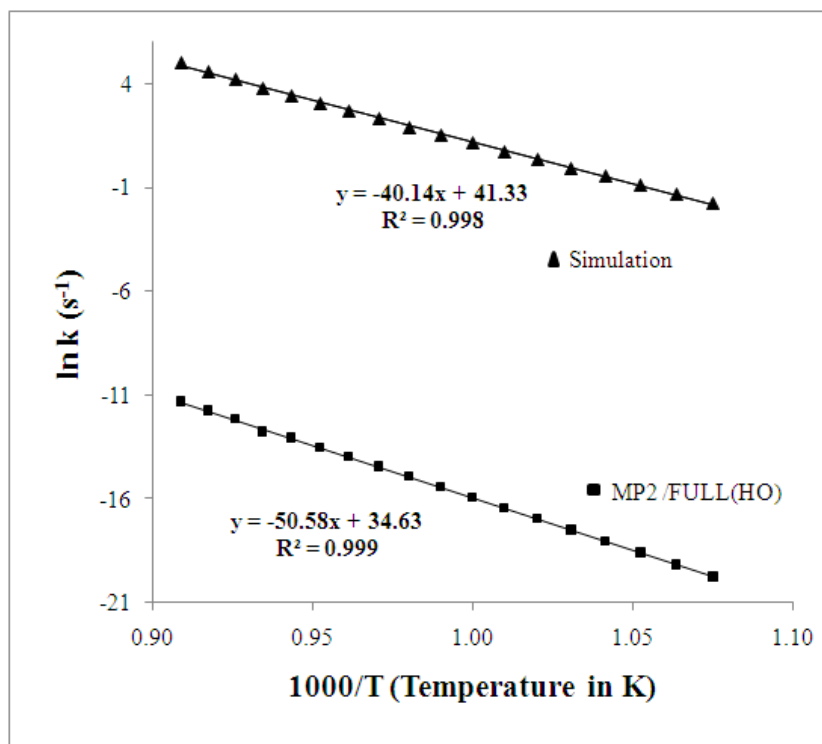
Figure III.12. Comparison of Arrhenius plot for rate coefficient data obtained from modeling and theoretical results for unimolecular elimination of HOCl from 2-chloroethanol at MP2 (FULL) with 6-311++G** basis set using harmonic oscillator model. The data are labeled with different symbols and are designated in figure above.

III.7. Conclusions

The rate coefficients for unimolecular HCl and H_2O elimination from CEOH studied over temperature range 930-1100 K behind single pulse reflected shock wave have been reported both experimentally and theoretically. The first order overall decomposition rate constant is given by $10^{14.61\pm0.34}$ exp $[-(58.70\pm1.55)/(RT)]$ s^{-1}. Experimentally determined gas phase first order rate coefficients for major HCl and H_2O elimination channels are $10^{14.37\pm0.35}$ exp $[-(57.50\pm1.64)/(RT)]$ s^{-1} and $10^{14.95\pm0.33}$ exp $[-$

$(67.95\pm1.50)/(RT)]$ s^{-1} respectively. Experimental results show that the reaction rates for HCl and H$_2$O elimination reactions are faster than those of the 2-fluoroethanol. The production of ethene was explained through HOCl elimination reaction. More experimental and spectroscopic investigations would be needed to verify the occurrence of HOCl elimination process. A kinetic model comprising of 45 elementary steps and 28 species both stable and unstable was constructed. This scheme was validated by the comparison to experimental results. The model predictions are satisfactory for the concentrations of all products in the temperature range of investigation. Sensitivity analyses reveals that only 21 steps and 23 species are needed to justify our pyrolysis mechanism. The rate coefficient for HOCl elimination reaction derived from fitting to complex mechanism is $10^{17.73\pm1.60}$ exp $[-(81.50\pm3.50)/ (RT)]$ s^{-1}. The mechanism proposed here is similar to that of the fluoroethanol.

Arrhenius parameters for the three unimolecular elimination channels have been evaluated using the TST calculations employing both ab initio and DFT methods to support our experimental results. The calculated values of activation energies at level HF, and MP2 (FULL) with 6-311++G** basis set for H$_2$O elimination was overestimated by 18.80 and 3.37 kcal mol^{-1}, respectively. Higher level G3B3 and CBS-QB3 calculations also overestimate the barrier for both HCl and H$_2$O elimination reaction. However, DFT underestimates by 0.82 kcal mol^{-1}. The calculated values of activation energies at level HF, and MP2 (FULL) with 6-311++G** basis set for HCl elimination was overestimated by 5.92 and 10.05 kcal mol^{-1}, respectively. However, DFT underestimates by 3.96 kcal mol^{-1}. The predicted rate coefficient at DFT (HR) level gives good agreement with

experimental k value for the HCl elimination. However experimental k for H_2O elimination is approximately 5 times faster than that calculated using DFT harmonic oscillator results. Experimental A of HCl elimination is higher by an order of magnitude than that of the ethyl chloride and chlorofluoroethane. Transition states structures have been verified by performing the IRC calculations. Present study has revealed both experimentally and theoretically that the fluorine substitution leads to an increase in E_a, however, Cl and OH substitution do not.

III.8.References

1. Kaphalia, B. S.; Khan, M. F.; Carroll, R. M.; Aronson, J.; Ansari, G. A. S. *Res. Commun. Pharmacol. Toxicol*., **1996**, *1*,173.

2. Chaigneau, M.; Muraz, B. *Ann. Pharm. Fr*., **1993**, *51*, 47.

3. Knippschild, M.; Rehm, H.-J, *Appl. Microbiol. Biotechnol*., **1995**, *44*, 253.

4. Overmeyer, C.; Rehm, H.-J. *Appl. Microbiol. Biotechnol*., **1995**, *43*, 143.

5. Pace, G.; Berton, A.; Calligaro, L.; Mantovani, A.; Uguagliati, P. *J. Chromatogr. A*, **1995,** *706*, 345.

6. Barnard, J.A.; Hughes, H.W.D. *Trans. Faraday. Soc*. **1960**, *56*, 55.

7. Norton, T.S.; Dryer, F.L. *Chem. Phys. Process. Combust*., Combustion Institute, Pittsburgh, **1985**, paper 36.

8. Hayashi, K.A.; Dryer, F.L. Chem. *Phys. Process. Combust*., Combustion Institute, Pittsburgh, **1981**, paper 13.

9. Natarajan, K.; Bhaskaran, K.A. *Proc. 13th Int. Shock Tube Symp*., Niagara Falls, **1981**, 834.

10. Borisov, A.A.; Zamanskii, V.M.; Konnov, A.A.; Lisyanskii, V.V. *Sov. J. Phys.* **1992**, *9*, 2527.

11. Bansal, K.M.; Freeman, G.R. *J. Am. Chem. Soc*. **1968**, *90*, 7183.

12. Danen, W.C. *J. Am. Chem. Soc*. **1979**, *101*, 1187.

13. Butkovskaya, N.I.; Zhao, Y.; Setser, D.W. *J. Phys. Chem*. **1994**, *98*, 10779.

14. Butkovskaya, N.I.; Setser, D.W. *J. Chem. Phys*. **1996**, *105*, 8064.

15. Yamabe, T.; Koizumi, M.; Yamashita. K.; Tachibana, A. *J. Am. Chem. Soc.* **1984**, *106*, 2255.

16. Park, J.; Zhu, R. S.; Lin, M. C.; *J. Chem. Phys*. **2002**, *117*, 3224.

17. Maccoll, A. *Chem. Rev.* **1969**, *33*.

18. Cadman, P.; Day, M.; Trotman-Dickenson, A.F. *J. Chem. Soc. A*. **1971**, 1356.

19. Evans, P. J.; Ichimura, T.; Tschuikow-Roux, E. *Int. J. Chem. Kinet.* **1978**, *10*, 855.

20. Weissman, M.; Benson, S. W. *Int. J. Chem. Kinet.* **1984**, *16*, 941.

21. Jones, Y.; Holmes, B. E.; Duke, D. W.; Tipton, D. L. *J. Phys. Chem*. **1990**, *94*, 4957.

22. Rakestraw, D. J.; Holmes, B. E. *J. Phys. Chem.* **1991**, *95*, 3968.

23. McDoniel, J. B.; Holmes, B. E. *J. Phys. Chem.* **1996**, *100*, 3044.

24. Srivatsa, A.; Arunan, E.; Manke, G. II.; Setser, D. W.; Sumathi, R. *J. Phys. Chem. A*. **1998**, *102*, 6412.

25. Sudbo, Aa. S.; Schulz, P. A.; Shen, Y. R.; Lee, Y. T. *J. Chem. Phys.* **1978**, *69*, 2312.

26. Quick C. R.; Wittig, C. *J. Chem. Phys.* **1980**, *72*, 1694.

27. Tsang, W. *J. Chem. Phys.* **1964**, *41*, 2487.

28. Toto, J. L.; Pritchard, G. O.; Kirtman, B. *J. Phys. Chem.* **1994**, *98*, 8359.

29. Chuchani, G.; Martin, I.; Rotinov, A.; Hernandez, A.; Reikonnen, N. *J. Phys. Chem.* **1984**, *88*, 1563.

30. Skingle, D. C.; Stimson, V. R. *Aust. J. Chem.* **1976**, *29*, 609.

31. Kelly, T.; Manning, M.; Bonard, A.; Wenger, J.; Treacy, J.; Sidebottom, H. Transport and Chemical Transformation in the Troposphere, *Proceedings of EUROTRAC Symposium, 6th*, Garmisch-Partenkirchen, Germany, **2000**, 410.

32. Buemi, G. *J. Chem. Soc. Faraday Trans.* **1994**, *90*, 1211.

33. Rajakumar, B.; Reddy, K. P. J.; Arunan, E. *J. Phys. Chem. A* **2003**,*107*, 9782.

34. Rajakumar, B.; Reddy, K. P. J.; Arunan, Proceedings of the 24th International symposium on shock waves, **2004**, 1, 621.

35. Krockenberger, D.; Lorkowski, H.; Rohrschneider,L. *Chromatographia* **1979**, 12, 787.

36. Rajakumar, B.; Reddy, K. P. J.; Arunan, E. *J. Phys. Chem. A*, 2002, 106, 8366.

37. Manion, J.A.; Louw, R. *J. Chem. Soc. Perkin Trans. 2*, **1988**, 1547.

38. Diau, E.W-G.; Lee, Y-P. *J. Chem. Phys*. **1992**, 96, 377.

39. Barat, R.B.; Bozzelli, J.W. *J. Phys. Chem,* **1992**, 96, 2494.

40. Tsang, W.; Hampson, R.F. *J. Phys. Chem. Ref. Data*, **1986**, 15, 1087.

41. Lifshitz, A.; Ben-Hamou, H. *J.Phys.Chem.***1983**, 87, 1782.

42. Krasnoperov, L.N.; Chesnokov, E.N.; Stark, H.; Ravishankara, A.R. *J.Phys. Chem. A*, **2004**, 108, 11526.

43. Lifshitz, A.; Tamburu,C.; Suslensky, A. *J. Phys. Chem.* **1990**, 94, 2966.

44. Davidson, D.F.; DiRosa, M.D.; Chang, E.J.; Hanson, R.K.; Bowman, C.T. *Int. J. Chem. Kinet*. **1995**, 27, 1179.

45. Baulch, D.L.; Cobos, C.J.; Cox, R.A.; Frank, P.; Hayman, G.; Just, Th.; Kerr, J.A.; Murrells, T.; Pilling, M.J.; Troe, J.; Walker, R.W.; Warnatz, J. *J. Phys. Chem. Ref. Data*, **1994**, 23, 847.

46. Allara, D.L.; Shaw, R. *J. Phys. Chem. Ref. Data*, **1980**, 9, 523.

47. Fagerstrom, K.; Lund, A.; Mahmoud, G.; Jodkowski, J.T.; Ratajczak, E. *Chem. Phys. Lett*., **1993**, 208, 321.

48. Zhang, Y-X.; Bauer, S. H. *J. Phys. Chem. B,* **1997,** 101, 8717.

49. Baulch, D.L.; Cobos, C.J.; Cox, R.A.; Esser, C.; Frank, P.; Just, Th.; Kerr, J.A.; Pilling, M.J.; Troe, J.; Walker, R.W.; Warnatz, J. *J. Phys. Chem. Ref. Data*, **1992**, 21, 411.

50. Dean, A.M. *J. Phys. Chem*. **1985**, 89, 4600.

51. Skinner, G.B.; " *Shock Waves in Chemistry*" ; Lifshitz, A. Ed.: Marcel Dekker: New York, **1981**.

52. Back, M.H. *Int. J. Chem. Kinet*. **1970**, 2, 409.

53. Back, R.A. *Can. J. Chem*. **1983**, 61, 916.

54. Oehlschlaeger, M.A.; Davidson, D.F.; Hanson, R.K. *Proc. Combust. Inst*. **2005**, 30, 1119

55. Tsang, W. *J. Phys. Chem. Ref. Data*, **1987**, 16,471.

56. Tsang, W. *Int. J. Chem. Kinet*. **2004**, 36, 456.

57. Baulch, D.L.; Duxbury, J.; Grant, S.J.; Montague, D.C. J. *Phys. Chem. Ref. Data*, **1981**, 10.

58. Bryukov, M.G.; Knyazev, V.D.; Lomnicki, S.M.; McFerrin, C.A.; Dellinger, B. *J. Phys. Chem. A*, **2004**, 108, 10464.

59. Xie, T.; Bowman, J.M.; Peterson, K.A.; Ramachandran, B. *J. Chem. Phys*., **2003**, 119, 9601.

60. Gupte, K. S.; Kiefer, J. H.; Tranter, R. S.; Klippenstein, S. J.; Harding, L. B. *Proc. Combust. Inst.* **2007**, *31*, 167.

61. Yasunaga, K.; Kubo, S.; Hoshikawa, H.; Kamesawa, T.; Hidaka, Y. *Int. J. Chem. Kinet.* **2008**, *40*, 73.

62. Yadav, J. S.; Goddard, J. D. *J. Chem. Phys.* **1986**, *84*, 2682. Martell, J. M.; Yu, H.; Goddard, J. D. *Mol. Phys.* **1997**, *92*, 497.

63. Smith, B. J.; Nguyen, M. T.; Bouma, W. J.; Radom, L. *J. Am. Chem. Soc.* **1991**, *113*, 6452.

64. Townsend, D.; Lahankar, S.A.; Lee, S.K.; Chambreau, S.D.; Suits, A.G.; Zhang, X.; Rheimecker, J.; Harding, L.B.; Bowman, J.M. *Science*, 2004, 306, 1158.

65. Harding, L. B.; Georgievskii, Y.; Klippenstein, S. J. *J. Phys. Chem.A*, **2010,** *114,* 765.

66. A chemical kinetics simulator (CKS-1.01) program, IBM's Almaden Research Center.

67. Frisch, M. J.; Trucks, G. W.; Schlegel, H. B.; Scuseria, G. E.; Robb, M. A.; Montgomery, J. R. C. J. A.; Vreven, T.; Kudin, K. N.; Burant, J. C.; Millam, J. M.; Iyengar, S. S.; Tomasi, J.; Barone, V.; Mennucci, B.; Cossi, M.; Scalmani, G.; Rega, N.; Petersson, G. A.; Nakatsuji, H.; Ehara, M. H. M.; Toyota, K.; Fukuda, R.; Hasegawa, J.; Ishida, M.; Nakajima, T.; Honda, Y.; Kitao, O.; Nakai, H.; Klene, M.; Li, X.; Knox, J. E.; Hratchian, H. P.; Cross, J. B.; Adamo, C.; Jaramillo, J.; Gomperts, R.; Stratmann, R. E.; Yazyev, O.; Austin, A. J.; Cammi, R.; Pomelli, C.; Ochterski, J. W.; Ayala, P. Y.; Morokuma, K.; Voth, G. A.; Salvador, P.; Dannenberg, J. J.; Zakrzewski, V. G.; Dapprich, S.; Daniels, A. D.; Strain, M. C.; Farkas, O.; Malick, D. K.; Rabuck, A. D.; Raghavachari, K.; Foresman, J. B.; Ortiz, J. V.; Cui, Q.; Baboul, A. G.; Clifford, S.; Cioslowski, J.;

Stefanov, B. B.; Liu, G.; Liashenko, A.; Piskorz, P.; Komaromi, I.; Martin, R. L.; Fox, D. J.; Keith, T.; Al-Laham, M. A.; Peng, C. Y.; Nanayakkara, A.; Challacombe, M.; Gill, P. M. W.; Johnson, B.; Chen, W.; Wong, M. W.; Gonzalez, C.; Pople, J. A. *Gaussian 03*, Revision A.1; Gaussian, Inc.: Pittsburgh, PA, 2003.

68. Holmes, D. A.; Holmes, B. E.; *J. Phys. chem. A* **2005**, 109, 10726.

69. Duncan, J.R.; Solaka, S.A.; Setser, D.W.; Holmes, B.E. *J. Phys. Chem. A,* **2010**, 114, 794.

70. Friederich, L.; Duncan, J.R.; Heard, G.L.; Setser, D.W.; Holmes, B.E. *J. Phys. Chem. A,* **2010**, 114, 4138.

71. Ferguson, H.A.; Caroline L. Parworth, C,L.; Traci Berry Holloway, T.B.; Aaron G.; Midgett, A.G.; Heard, G.L.; Setser, D.W.; Holmes, B.E .*J. Phys. Chem. A,* **2009**, 113, 10013.

72. Souza, F. R.; Freitas, M. P.; *Comp. Theo. Chem.* **2011**, *964*, 155.

73. Rajakumar, B.; Arunan, E. *Phys. Chem. Chem. Phys.,* **2003**, 5, 3897.

74. Chuang, Y.Y.; Truhlar, D. G.; *J. Chem. Phys.* **2000**, 112, 1221.

75. Tschuikow, R. E.; Quiring, W. J.; *J Phys Chem*, **1971**, 75, 295.

76. Dai, H. L.; Specht, E.; Berman, M.R.; *J. Chem. Phys.* **1982,** 77, 4494.

77. Zhu, L.; Bozzelli, J. W.; *Chem. Phys. Lett.* **2002**, *357*, 65.

78. Shepler, B. C.; Han, Y.; Bowman, J. M. *J. Phys. Chem. Lett.* **2011**, 2, 834.

79. Bowman, J. M.; Shepler, B. C. *Annu. Rev. Phys. Chem.* **2011**, *62*, 531.

80. Bowman, J. M.; Zhang, X. *Phys. Chem. Chem. Phys.* **2006**, 321.

81. Saxena, S.; Kiefer, J.; Klippenstein, S. *Proc. Combust. Inst.* **2009**, *32*, 123.

82. Sivaramakrishnan, R.; Michael, J. V.; Klippenstein, S. J.; *J. Phys. Chem. A*, **2010**, *114*, 755.

Table III.A.1. Optimized structures of 2-chloroethanol in $G_{g'}$ conformer at DFT, HF and MP2 (FULL) levels of theory with 6-31G*, 6-31G** and 6-311++G** basis sets.

Coordinate(Å)	B3LYP			HF			MP2(FULL)		
	6-31G*	6-31G**	6-311++G**	6-31G*	6-31G**	6-311++G**	6-31G*	6-31G**	6-311++G**
R(1,2)	1.523	1.522	1.518	1.518	1.517	1.515	1.515	1.514	1.515
R(1,3)	1.092	1.091	1.089	1.079	1.080	1.080	1.091	1.087	1.091
R(1,4)	1.091	1.091	1.088	1.078	1.079	1.079	1.090	1.085	1.090
R(1,5)	1.825	1.825	1.825	1.801	1.802	1.804	1.790	1.787	1.787
R(2,6)	1.101	1.100	1.097	1.086	1.087	1.087	1.098	1.093	1.097
R(2,7)	1.097	1.097	1.094	1.083	1.085	1.085	1.094	1.089	1.093
R(2,8)	1.412	1.411	1.416	1.393	1.392	1.393	1.416	1.414	1.413
R(8,9)	0.971	0.968	0.964	0.948	0.944	0.942	0.973	0.965	0.962
A(2,1,3)	111.8	111.8	111.4	111.4	111.4	111.1	111.5	111.3	110.9
A(2,1,4)	111.1	111.2	111.4	110.9	111.0	111.3	110.3	110.2	110.4
A(2,1,5)	110.6	110.7	110.9	111.1	111.1	111.2	110.4	110.5	110.1
A(3,1,4)	110.2	110.2	110.4	110.0	110.1	110.2	109.9	109.9	110.4
A(3,1,5)	106.6	106.6	106.4	106.6	106.6	106.4	107.5	107.5	107.6
A(4,1,5)	106.2	106.1	106.0	106.5	106.5	106.4	107.2	107.2	107.4
A(1,2,6)	109.6	109.5	109.8	109.9	109.8	109.8	109.8	109.6	109.5
A(1,2,7)	107.7	107.6	107.9	107.8	107.7	107.7	108.4	108.3	108.5
A(1,2,8)	113.1	113.1	113.3	112.8	112.8	113.1	112.4	112.5	112.5
A(6,2,7)	107.8	107.6	108.0	108.0	107.9	108.0	108.2	108.1	108.6
A(6,2,8)	112.1	112.2	111.5	111.6	111.7	111.4	111.8	112.0	111.4
A(7,2,8)	106.3	106.5	106.1	106.5	106.7	106.6	106.0	106.2	106.2
A(2,8,9)	107.1	107.2	108.3	109.5	109.7	110.0	106.9	106.8	106.8
D(3,1,2,6)	57.2	57.1	58.5	59.2	59.1	59.6	59.1	59.0	59.2
D(3,1,2,7)	-59.8	-59.6	-59.0	-58.2	-58.1	-57.8	-58.9	-58.7	-59.1
D(3,1,2,8)	-176.9	-176.9	-176.1	-175.5	-175.6	-175.3	-175.7	-175.8	-176.3
D(4,1,2,6)	-179.2	-179.2	-177.7	-177.8	-177.8	-177.1	-178.5	-178.7	-178.1
D(4,1,2,7)	63.8	64.1	64.8	64.8	65.0	65.4	63.5	63.5	63.6
D(4,1,2,8)	-53.3	-53.2	-52.3	-52.6	-52.5	-52.0	-53.3	-53.5	-53.6
D(5,1,2,6)	-61.5	-61.6	-59.8	-59.5	-59.6	-58.7	-60.2	-60.4	-59.7
D(5,1,2,7)	-178.5	-178.3	-177.3	-177.0	-176.8	-176.2	-178.2	-178.1	-178.1
D(5,1,2,8)	64.4	64.4	65.6	65.7	65.8	66.4	65.0	64.9	64.8
D(1,2,8,9)	-62.8	-62.8	-62.2	-66.9	-67.0	-65.5	-64.1	-63.8	-59.0
D(6,2,8,9)	61.7	61.7	62.3	57.3	57.3	58.8	59.9	60.1	64.4
D(7,2,8,9)	179.2	179.2	179.6	175.0	175.0	176.4	177.6	177.9	-177.5

1-C ,2-C,3-H(1),4-H(1),5-Cl(1),6-H(2),7-H(2),8-O(2),9-H(O)

Table III.A.2. Optimized structures of 2-chloroethanol in G_g conformer at DFT, HF and MP2 (FULL) levels of theory with 6-31G*, 6-31G** and 6-311++G** basis sets.

Coordinate(Å)	B3LYP			HF			MP2(FULL)		
	6-31G*	6-31G**	6-311++G**	6-31G*	6-31G**	6-311++G**	6-31G*	6-31G**	6-311++G**
R(1,2)	1.524	1.523	1.519	1.520	1.519	1.517	1.517	1.515	1.516
R(1,3)	1.094	1.094	1.091	1.081	1.082	1.082	1.093	1.088	1.093
R(1,4)	1.093	1.092	1.090	1.080	1.081	1.081	1.092	1.087	1.092
R(1,5)	1.812	1.812	1.814	1.789	1.790	1.793	1.779	1.778	1.777
R(2,6)	1.094	1.094	1.091	1.080	1.082	1.081	1.091	1.087	1.091
R(2,7)	1.105	1.104	1.101	1.090	1.091	1.091	1.101	1.096	1.100
R(2,8)	1.412	1.412	1.416	1.393	1.392	1.393	1.416	1.414	1.414
R(8,9)	0.970	0.967	0.963	0.947	0.943	0.941	0.972	0.964	0.961
A(2,1,3)	111.4	111.4	111.7	111.3	111.4	111.6	110.8	110.7	110.7
A(2,1,4)	110.4	110.4	110.2	110.3	110.3	110.1	110.2	110.1	109.8
A(2,1,5)	112.7	112.7	112.9	112.5	112.6	112.7	112.0	112.1	111.8
A(3,1,4)	108.6	108.6	108.9	108.7	108.8	109.0	108.5	108.4	108.8
A(3,1,5)	106.5	106.4	106.3	106.7	106.7	106.6	107.4	107.5	107.6
A(4,1,5)	107.0	107.0	106.6	107.0	107.0	106.7	107.8	107.9	108.0
A(1,2,6)	109.9	109.8	110.1	109.9	109.8	109.9	109.9	109.8	109.9
A(1,2,7)	106.8	106.7	107.1	107.3	107.2	107.2	107.7	107.5	107.6
A(1,2,8)	114.6	114.5	114.6	113.8	113.9	114.1	113.7	113.7	113.6
A(6,2,7)	107.6	107.5	107.8	107.9	107.8	107.9	108.0	108.0	108.4
A(6,2,8)	106.0	106.2	106.0	106.5	106.7	106.6	105.7	105.9	105.9
A(7,2,8)	111.8	112.0	111.2	111.3	111.4	111.0	111.7	111.8	111.4
A(2,8,9)	108.3	108.4	109.4	110.2	110.4	110.7	107.9	107.8	107.7
D(3,1,2,6)	177.5	177.7	175.3	176.5	176.8	175.1	177.2	177.6	176.5
D(3,1,2,7)	-66.1	-66.1	-67.8	-66.5	-66.4	-67.8	-65.4	-65.2	-65.6
D(3,1,2,8)	58.4	58.4	56.0	57.1	57.2	55.5	58.9	59.1	58.2
D(4,1,2,6)	-61.8	-61.5	-63.5	-62.7	-62.4	-63.7	-62.8	-62.5	-63.3
D(4,1,2,7)	54.7	54.7	53.4	54.3	54.4	53.3	54.6	54.7	54.5
D(4,1,2,8)	179.1	179.2	177.2	177.9	178.1	176.6	178.9	179.0	178.3
D(5,1,2,6)	57.9	58.1	55.6	56.7	57.0	55.3	57.2	57.5	56.5
D(5,1,2,7)	174.3	174.3	172.5	173.8	173.8	172.3	174.7	174.8	174.4
D(5,1,2,8)	-61.3	-61.2	-63.7	-62.7	-62.5	-64.4	-61.0	-60.9	-61.8
D(1,2,8,9)	-60.6	-60.5	-60.4	-63.9	-63.8	-63.3	-62.7	-62.6	-57.6
D(6,2,8,9)	178.1	178.2	178.1	174.8	174.9	175.2	176.6	176.7	-178.3
D(7,2,8,9)	61.2	61.1	61.3	57.5	57.5	57.9	59.4	59.4	64.1

1-C ,2-C,3-H(1),4-H(1),5-Cl(1),6-H(2),7-H(2),8-O(2),9-H(O)

Table III.A.3.Optimized structures of 2-chloroethanol in G_t conformer at DFT, HF and MP2 (FULL) levels of theory with 6-31G*, 6-31G** and 6-311++G** basis sets.

Coordinate(Å)	B3LYP			HF			MP2(FULL)		
	6-31G*	6-31G**	6-311++G**	6-31G*	6-31G**	6-311++G**	6-31G*	6-31G**	6-311++G**
R(1,2)	1.516	1.515	1.512	1.512	1.512	1.510	1.509	1.507	1.510
R(1,3)	1.092	1.091	1.089	1.079	1.079	1.079	1.090	1.086	1.090
R(1,4)	1.092	1.091	1.089	1.080	1.080	1.080	1.091	1.087	1.091
R(1,5)	1.814	1.815	1.816	1.791	1.792	1.795	1.781	1.779	1.779
R(2,6)	1.100	1.099	1.096	1.086	1.087	1.086	1.097	1.093	1.095
R(2,7)	1.105	1.105	1.101	1.090	1.091	1.090	1.101	1.096	1.099
R(2,8)	1.416	1.415	1.421	1.396	1.395	1.397	1.419	1.417	1.418
R(8,9)	0.968	0.965	0.961	0.946	0.942	0.940	0.971	0.963	0.959
A(2,1,3)	110.4	110.4	110.6	110.3	110.3	110.6	109.7	109.6	109.6
A(2,1,4)	110.6	110.6	110.6	110.6	110.6	110.5	110.4	110.2	110.2
A(2,1,5)	112.5	112.5	112.5	112.3	112.3	112.4	111.9	112.0	111.5
A(3,1,4)	109.7	109.7	109.9	109.6	109.7	109.9	109.5	109.4	109.8
A(3,1,5)	106.7	106.6	106.5	107.0	106.9	106.8	107.7	107.7	107.8
A(4,1,5)	106.8	106.7	106.4	106.8	106.8	106.5	107.6	107.7	107.8
A(1,2,6)	109.6	109.5	109.9	109.9	109.7	109.8	109.8	109.6	109.6
A(1,2,7)	107.0	106.9	107.3	107.5	107.4	107.4	107.8	107.7	108.1
A(1,2,8)	108.8	108.8	109.0	108.7	108.8	109.1	107.7	107.8	108.0
A(6,2,7)	107.7	107.6	108.2	108.1	108.0	108.3	108.2	108.1	108.7
A(6,2,8)	112.2	112.3	111.7	111.7	111.8	111.5	112.0	112.1	111.6
A(7,2,8)	111.4	111.5	110.7	110.9	111.0	110.6	111.3	111.4	110.8
A(2,8,9)	108.3	108.4	109.4	110.0	110.3	110.6	108.1	108.0	108.2
D(3,1,2,6)	172.3	172.3	170.2	171.9	172.1	170.9	172.6	173.1	171.4
D(3,1,2,7)	-71.2	-71.3	-72.3	-70.7	-70.8	-71.6	-69.7	-69.5	-70.3
D(3,1,2,8)	49.3	49.2	47.5	49.4	49.4	48.4	50.5	50.9	49.7
D(4,1,2,6)	-66.2	-66.0	-67.8	-66.7	-66.3	-67.2	-66.7	-66.3	-67.6
D(4,1,2,7)	50.4	50.4	49.7	50.7	50.8	50.3	50.9	51.1	50.7
D(4,1,2,8)	170.8	170.9	169.6	170.8	171.0	170.3	171.1	171.4	170.6
D(5,1,2,6)	53.2	53.3	51.1	52.6	52.8	51.6	53.2	53.6	52.1
D(5,1,2,7)	169.7	169.7	168.6	170.0	170.0	169.1	170.8	171.0	170.4
D(5,1,2,8)	-69.8	-69.8	-71.5	-69.9	-69.8	-70.9	-69.0	-68.6	-69.7
D(1,2,8,9)	166.0	164.8	163.0	167.3	166.2	166.2	167.8	167.9	158.7
D(6,2,8,9)	44.6	43.4	41.4	45.9	44.8	44.7	47.1	47.2	38.2
D(7,2,8,9)	-76.3	-77.5	-79.2	-74.8	-75.9	-75.8	-74.2	-74.2	-83.1

1-C,2-C,3-H(1),4-H(1),5-Cl(1),6-H(2),7-H(2),8-O(2),9-H(O)

Table III.A.4.Optimized structures of 2-chloroethanol in T$_g$ conformer at DFT, HF and MP2 (FULL) levels of theory with 6-31G*, 6-31G** and 6-311++G** basis sets.

Coordinate(Å)	B3LYP			HF			MP2(FULL)		
	6-31G*	6-31G**	6-311++G**	6-31G*	6-31G**	6-311++G**	6-31G*	6-31G**	6-311++G**
R(1,2)	1.527	1.527	1.524	1.522	1.521	1.520	1.519	1.517	1.519
R(1,3)	1.093	1.093	1.090	1.080	1.081	1.081	1.092	1.087	1.091
R(1,4)	1.091	1.090	1.088	1.078	1.079	1.079	1.090	1.085	1.089
R(1,5)	1.815	1.816	1.816	1.792	1.793	1.796	1.784	1.781	1.780
R(2,6)	1.093	1.093	1.091	1.081	1.082	1.081	1.091	1.087	1.090
R(2,7)	1.420	1.420	1.424	1.399	1.398	1.400	1.423	1.420	1.420
R(2,8)	1.099	1.099	1.096	1.086	1.086	1.086	1.097	1.092	1.096
R(7,9)	0.970	0.966	0.962	0.947	0.943	0.941	0.971	0.964	0.961
A(2,1,3)	111.6	111.6	111.8	111.5	111.5	111.7	111.0	110.9	111.0
A(2,1,4)	110.8	110.9	111.0	110.7	110.8	111.0	110.1	110.1	110.2
A(2,1,5)	110.8	110.8	110.5	110.7	110.7	110.4	110.6	110.7	110.0
A(3,1,4)	109.2	109.2	109.6	109.2	109.2	109.5	109.0	109.0	109.4
A(3,1,5)	106.8	106.7	106.5	107.0	106.9	106.7	107.6	107.6	107.7
A(4,1,5)	107.5	107.4	107.2	107.6	107.5	107.3	108.3	108.3	108.5
A(1,2,6)	109.8	109.7	109.9	109.8	109.7	109.8	109.9	109.8	109.8
A(1,2,7)	110.3	110.3	110.5	110.1	110.1	110.3	110.1	110.3	110.8
A(1,2,8)	110.1	110.0	110.2	110.2	110.1	110.1	110.3	110.0	109.9
A(6,2,7)	106.5	106.7	106.3	107.0	107.2	107.0	106.3	106.4	106.2
A(6,2,8)	107.8	107.7	108.1	107.9	107.8	108.0	108.0	108.0	108.2
A(7,2,8)	112.3	112.4	111.7	111.7	111.9	111.6	112.1	112.2	111.8
A(2,7,9)	108.1	108.2	109.3	110.0	110.3	110.6	107.7	107.6	107.7
D(3,1,2,6)	179.9	179.5	179.2	-179.9	179.8	179.5	-179.4	-179.7	179.5
D(3,1,2,7)	-63.1	-63.3	-63.8	-62.4	-62.5	-62.8	-62.6	-62.7	-63.4
D(3,1,2,8)	61.4	61.3	60.2	61.3	61.3	60.8	61.7	61.7	60.6
D(4,1,2,6)	-58.2	-58.5	-58.1	-58.1	-58.3	-57.9	-58.5	-58.9	-59.1
D(4,1,2,7)	58.8	58.8	58.9	59.5	59.4	59.7	58.2	58.1	57.9
D(4,1,2,8)	-176.7	-176.7	-177.1	-176.8	-176.8	-176.7	-177.5	-177.6	-178.0
D(5,1,2,6)	61.1	60.7	60.7	61.1	60.9	60.9	61.2	60.9	60.4
D(5,1,2,7)	178.1	178.0	177.7	178.7	178.6	178.6	178.0	177.9	177.5
D(5,1,2,8)	-57.4	-57.5	-58.3	-57.6	-57.6	-57.9	-57.8	-57.8	-58.5
D(1,2,7,9)	74.7	75.6	75.2	78.5	78.9	78.2	75.5	74.9	68.1
D(6,2,7,9)	-166.3	-165.4	-165.6	-162.2	-161.9	-162.5	-165.5	-166.1	-172.7
D(8,2,7,9)	-48.5	-47.6	-48.0	-44.3	-43.9	-44.5	-47.7	-48.1	-54.9

1-C,2-C,3-H(1),4-H(1),5-Cl(1),6-H(2),8-H(2),7-O(2),9-H(O)

Table III.A.5. Optimized structures of 2-chloroethanol in T_t conformer at DFT, HF and MP2 (FULL) levels of theory with 6-31G*, 6-31G and 6-311++G** basis sets.**

Coordinate(Å)	B3LYP			HF			MP2(FULL)		
	6-31G*	6-31G**	6-311++G**	6-31G*	6-31G**	6-311++G**	6-31G*	6-31G**	6-311++G**
R(1,2)	1.522	1.522	1.519	1.516	1.516	1.515	1.513	1.512	1.514
R(1,3)	1.091	1.090	1.088	1.078	1.079	1.078	1.090	1.085	1.089
R(1,4)	1.091	1.090	1.088	1.078	1.079	1.078	1.090	1.085	1.089
R(1,5)	1.811	1.811	1.813	1.792	1.792	1.796	1.782	1.779	1.779
R(2,6)	1.100	1.100	1.096	1.086	1.087	1.086	1.098	1.093	1.096
R(2,7)	1.100	1.100	1.096	1.086	1.087	1.086	1.098	1.093	1.096
R(2,8)	1.422	1.421	1.427	1.401	1.400	1.401	1.424	1.421	1.422
R(8,9)	0.969	0.965	0.962	0.947	0.943	0.940	0.972	0.963	0.960
A(2,1,3)	110.9	110.9	111.1	110.8	110.8	111.1	110.2	110.2	110.4
A(2,1,4)	110.9	110.9	111.1	110.8	110.8	111.1	110.2	110.2	110.4
A(2,1,5)	110.4	110.5	110.2	110.5	110.5	110.2	110.4	110.5	109.7
A(3,1,4)	109.4	109.5	109.9	109.5	109.6	109.8	109.3	109.2	109.7
A(3,1,5)	107.6	107.5	107.2	107.5	107.5	107.2	108.3	108.4	108.3
A(4,1,5)	107.6	107.5	107.2	107.5	107.5	107.2	108.3	108.4	108.3
A(1,2,6)	109.5	109.4	109.7	109.8	109.7	109.8	109.7	109.6	109.5
A(1,2,7)	109.5	109.4	109.7	109.8	109.7	109.8	109.7	109.6	109.5
A(1,2,8)	105.7	105.8	105.9	105.9	106.0	106.2	105.2	105.5	106.1
A(6,2,7)	108.0	107.9	108.6	108.3	108.2	108.5	108.2	108.1	108.5
A(6,2,8)	112.0	112.1	111.4	111.5	111.6	111.3	111.9	112.0	111.6
A(7,2,8)	112.0	112.1	111.4	111.5	111.6	111.3	111.9	112.0	111.6
A(2,8,9)	108.0	108.1	109.1	109.9	110.1	110.4	107.9	107.8	107.7
D(3,1,2,6)	60.0	60.1	59.0	59.6	59.7	59.2	60.3	60.5	59.8
D(3,1,2,7)	178.2	178.1	178.3	178.6	178.4	178.3	179.0	178.9	178.7
D(3,1,2,8)	-60.9	-60.9	-61.3	-60.9	-60.9	-61.3	-60.4	-60.3	-60.7
D(4,1,2,6)	-178.2	-178.1	-178.3	-178.6	-178.4	-178.3	-179.0	-178.9	-178.7
D(4,1,2,7)	-60.0	-60.1	-59.0	-59.6	-59.7	-59.2	-60.3	-60.5	-59.8
D(4,1,2,8)	60.9	60.9	61.3	60.9	60.9	61.3	60.4	60.3	60.7
D(5,1,2,6)	-59.1	-59.0	-59.6	-59.5	-59.4	-59.6	-59.4	-59.2	-59.5
D(5,1,2,7)	59.1	59.0	59.6	59.5	59.4	59.6	59.4	59.2	59.5
D(5,1,2,8)	180.0	180.0	180.0	-180.0	180.0	180.0	180.0	-180.0	180.0
D(1,2,8,9)	180.0	180.0	180.0	180.0	180.0	180.0	180.0	180.0	180.0
D(6,2,8,9)	60.8	60.8	60.7	60.6	60.6	60.6	60.8	60.8	60.8
D(7,2,8,9)	-60.8	-60.8	-60.7	-60.6	-60.6	-60.6	-60.8	-60.8	-60.8

1-C,2-C,3-H(1),4-H(1),5-Cl(1),6-H(2),7-H(2),8-O(2),9-H(O)

135

Table III.A.6. Optimized structures of 2-chloroethanol in its transition state for HCl elimination at DFT, HF and MP2 (FULL) levels of theory with 6-31G*, 6-31G** and 6-311++G** basis sets.

Coordinate(Å)	B3LYP			HF			MP2(FULL)		
	6-31G*	6-31G**	6-311++G**	6-31G*	6-31G**	6-311++G**	6-31G*	6-31G**	6-311++G**
R(1,3)	1.401	1.401	1.398	1.379	1.381	1.383	1.392	1.399	1.397
R(1,6)	1.084	1.084	1.082	1.072	1.073	1.073	1.082	1.083	1.082
R(1,7)	1.083	1.082	1.080	1.070	1.071	1.071	1.080	1.081	1.081
R(2,5)	1.883	1.883	1.891	2.078	2.071	2.071	1.983	1.811	1.856
R(3,4)	1.387	1.385	1.388	1.360	1.360	1.361	1.379	1.389	1.382
R(3,5)	1.246	1.251	1.249	1.212	1.213	1.209	1.243	1.275	1.259
R(3,8)	1.096	1.094	1.092	1.079	1.079	1.079	1.090	1.088	1.088
R(4,9)	0.970	0.967	0.963	0.949	0.945	0.943	0.973	0.961	0.961
A(3,1,6)	120.7	120.6	120.8	120.5	120.5	120.8	120.0	120.2	119.9
A(3,1,7)	120.7	120.8	120.5	120.7	120.7	120.4	120.6	119.8	119.8
A(6,1,7)	118.6	118.6	118.6	118.7	118.7	118.6	119.0	119.1	119.3
A(1,3,4)	117.1	117.3	117.2	118.0	117.9	117.9	117.6	120.0	117.2
A(1,3,5)	79.9	77.7	78.2	71.6	71.9	73.2	68.1	71.6	70.3
A(1,3,8)	118.1	118.2	118.7	119.6	119.3	119.1	120.0	120.3	119.8
A(4,3,5)	112.3	112.7	112.3	112.6	112.9	112.9	112.7	106.2	112.4
A(4,3,8)	116.9	117.3	116.8	117.9	117.9	117.7	118.8	118.0	118.5
A(5,3,8)	105.1	105.5	105.7	105.5	105.7	105.7	106.0	104.9	106.5
A(3,4,9)	108.7	108.8	109.6	110.9	111.1	111.1	109.1	107.8	108.5
A(2,5,3)	149.0	149.4	148.7	156.4	154.7	153.9	152.1	148.6	149.6
D(6,1,3,4)	-15.0	-13.6	-13.2	-14.0	-13.7	-14.2	-7.1	1.9	-4.6
D(6,1,3,5)	95.0	95.8	96.1	92.4	93.2	93.3	97.9	100.5	101.1
D(6,1,3,8)	-163.2	-163.1	-162.4	-169.8	-168.5	-167.7	-165.7	-162.6	-160.7
D(7,1,3,4)	166.5	166.0	166.3	170.5	169.8	169.6	165.2	170.5	163.7
D(7,1,3,5)	-83.5	-84.6	-84.5	-83.1	-83.3	-82.9	-89.7	-90.9	-90.6
D(7,1,3,8)	18.3	16.5	17.0	14.7	15.0	16.1	6.6	6.0	7.6
D(1,3,4,9)	145.7	145.2	146.4	140.2	139.3	140.8	143.5	-99.1	139.3
D(5,3,4,9)	55.9	57.8	58.6	59.7	58.3	58.4	67.2	-176.9	60.8
D(8,3,4,9)	-65.7	-65.0	-63.8	-63.6	-65.5	-65.3	-57.7	65.8	-64.2
D(1,3,5,2)	-10.2	-10.9	-11.0	-7.6	-9.4	-10.1	-9.8	-10.0	-15.6
D(4,3,5,2)	105.1	103.7	103.8	105.8	104.0	103.6	102.1	106.9	96.6
D(8,3,5,2)	-126.7	-127.1	-127.7	-124.2	-125.7	-126.4	-126.3	-127.5	-132.1

1-C,2-Cl(1),3-C,4-O(3),5-H(3),6-H(1),7-H(1),8-H(3),9-H(O)

Table III.A.7. Optimized structures of 2-chloroethanol in its transition state for H₂O elimination at DFT, HF and MP2 (FULL) levels of theory with 6-31G*, 6-31G** and 6-311++G** basis sets.

Coordinate(Å)	B3LYP			HF			MP2(FULL)		
	6-31G*	6-31G**	6-311++G**	6-31G*	6-31G**	6-311++G**	6-31G*	6-31G**	6-311++G**
R(1,2)	1.427	1.428	1.421	1.455	1.454	1.467	1.419	1.419	1.425
R(1,3)	1.085	1.085	1.083	1.075	1.075	1.076	1.084	1.079	1.083
R(1,4)	1.500	1.493	1.451	1.624	1.610	1.636	1.531	1.503	1.511
R(1,6)	1.791	1.793	1.790	1.794	1.795	1.804	1.763	1.762	1.762
R(2,5)	1.089	1.088	1.085	1.078	1.078	1.079	1.089	1.084	1.088
R(2,7)	1.085	1.085	1.083	1.074	1.075	1.075	1.086	1.081	1.086
R(4,8)	1.203	1.194	1.230	1.094	1.084	1.078	1.189	1.176	1.178
R(8,9)	0.979	0.975	0.971	0.956	0.951	0.949	0.983	0.974	0.973
A(2,1,3)	118.8	118.7	119.2	115.6	115.7	115.0	118.6	118.4	118.7
A(2,1,4)	74.2	73.5	75.5	70.9	70.5	69.9	73.4	72.3	75.4
A(2,1,6)	117.5	117.3	117.8	114.1	114.1	113.2	117.5	117.6	117.4
A(3,1,4)	117.1	117.9	115.6	125.8	126.0	128.6	116.9	117.2	117.8
A(3,1,6)	111.3	111.0	111.2	108.9	108.9	108.0	112.3	112.4	112.7
A(4,1,6)	113.4	113.8	113.1	116.4	116.5	116.4	112.8	113.3	112.1
A(1,2,5)	118.9	118.7	118.7	117.5	117.3	116.3	118.6	118.5	117.5
A(1,2,7)	121.1	121.0	121.4	120.5	120.5	120.0	120.8	120.8	120.8
A(5,2,7)	115.0	114.9	115.7	113.6	113.7	113.4	114.7	114.8	115.3
A(1,4,8)	123.3	123.9	124.7	114.6	116.0	113.2	121.1	123.9	122.3
A(4,8,9)	110.5	112.2	119.0	113.1	115.0	115.4	109.6	110.4	113.7
D(3,1,2,5)	-11.4	-11.7	-12.4	-16.3	-16.7	-18.5	-9.7	-9.7	-10.9
D(3,1,2,7)	142.5	141.2	143.5	129.8	129.3	124.3	141.8	141.9	139.7
D(4,1,2,5)	101.3	101.5	99.1	105.1	104.7	105.6	102.4	102.2	101.7
D(4,1,2,7)	-104.8	-105.6	-105.0	-108.8	-109.3	-111.5	-106.1	-106.2	-107.7
D(6,1,2,5)	-150.2	-149.8	-152.2	-143.7	-144.2	-143.4	-150.1	-150.2	-152.1
D(6,1,2,7)	3.7	3.1	3.8	2.4	1.8	-0.6	1.4	1.4	-1.5
D(2,1,4,8)	5.4	5.9	7.8	4.2	4.8	5.6	5.8	6.3	8.6
D(3,1,4,8)	120.1	120.1	123.5	112.5	113.0	112.1	120.0	119.7	122.3
D(6,1,4,8)	-108.2	-107.2	-106.7	-104.0	-103.1	-101.1	-107.6	-106.8	-104.5
D(1,4,8,9)	-109.7	-110.7	-117.1	-116.3	-117.8	-120.4	-109.7	-109.6	-115.1

1-C,2-C,3-H(1),4-H(1),5-H(2),6-Cl(1),7-H(2),8-O(2),9-H(O)

Table III.A.8. Optimized structures of 2-chloroethanol in its transition state for HOCl elimination at MP2 (FULL) levels of theory with 6-311++G** basis set.

R(1,2)	1.424
R(1,3)	1.083
R(1,4)	1.084
R(1,5)	2.803
R(2,5)	3.063
R(2,6)	1.090
R(2,7)	1.089
R(2,8)	1.596
R(2,9)	2.223
R(3,5)	3.075
R(4,5)	3.112
R(5,8)	2.087
R(8,9)	0.984
A(2,1,3)	120.6
A(2,1,4)	120.3
A(3,1,4)	118.7
A(1,2,6)	115.5
A(1,2,7)	115.5
A(1,2,8)	104.3
A(1,2,9)	127.1
A(5,2,6)	124.9
A(5,2,7)	113.3
A(5,2,9)	61.2
A(6,2,7)	113.5
A(6,2,8)	101.4
A(6,2,9)	92.7
A(7,2,8)	104.4
A(7,2,9)	88.6
A(1,5,8)	56.2
A(2,5,3)	41.7
A(2,5,4)	41.4
A(3,5,4)	35.100
A(3,5,8)	70
A(4,5,8)	65.7
A(5,8,9)	126.6
L(3,5,8,4,-2)	89.5
D(3,1,2,6)	-148.7
D(3,1,2,7)	-13
D(3,1,2,8)	101
D(3,1,2,9)	96.1

D(4,1,2,6)	23.8
D(4,1,2,7)	159.5
D(4,1,2,8)	-86.6
D(4,1,2,9)	-91.4
D(6,2,5,3)	-132.3
D(6,2,5,4)	-78.3
D(7,2,5,3)	81.6
D(7,2,5,4)	135.7
D(9,2,5,3)	156.1
D(9,2,5,4)	-149.8
D(1,5,8,9)	162.5
D(3,5,8,9)	145.3
D(4,5,8,9)	-176.9

1-C,2-C,3-H(1),4-H(1),5-Cl(1),6-H(2),7-H(2),8-O(2),9-H(O)

Table III.A.9. Normal mode vibrational frequencies of 2-chloroethanol in G$_{g'}$ conformer at DFT, HF and MP2 (FULL) levels of theory with 6-31G*, 6-31G** and 6-311++G** basis sets (cm^{-1}).

B3LYP			HF			MP2 (FULL)		
6-31G*	6-31G**	6-311++G**	6-31G*	6-31G**	6-311++G**	6-31G*	6-31G**	6-311++G**
152.3	150.6	144.4	163.2	162.5	161.0	166.5	165.5	166.5
283.0	282.1	282.3	301.1	300.5	300.8	294.6	292.0	295.3
402.2	396.7	383.5	403.7	398.8	394.3	404.5	398.9	421.0
472.5	471.4	470.3	510.4	509.8	508.4	486.4	484.4	483.5
654.5	652.4	648.3	712.6	710.2	707.0	719.1	721.2	722.5
869.9	866.0	859.8	940.3	936.5	932.0	894.5	893.0	884.8
938.6	934.1	931.4	1022.4	1018.1	1013.8	980.8	979.1	973.5
1065.5	1058.8	1051.8	1154.3	1148.6	1143.7	1103.0	1100.5	1090.9
1105.9	1102.7	1086.8	1220.3	1218.4	1210.5	1133.4	1134.2	1130.1
1207.2	1201.3	1191.3	1300.2	1293.0	1285.1	1232.4	1231.6	1222.9
1235.1	1226.3	1218.3	1346.3	1337.5	1329.4	1272.0	1270.7	1250.8
1341.3	1328.8	1321.7	1466.1	1453.5	1445.8	1387.5	1386.0	1371.2
1411.1	1401.2	1382.1	1523.6	1511.0	1499.8	1430.6	1426.5	1408.1
1437.0	1425.8	1415.4	1568.1	1557.4	1550.8	1460.8	1462.0	1446.0
1496.6	1481.5	1466.4	1621.4	1605.4	1596.1	1531.9	1529.2	1481.8
1523.7	1509.2	1490.8	1654.8	1638.9	1625.5	1561.4	1558.3	1511.9
3018.4	3010.2	3008.2	3216.9	3190.7	3178.9	3090.4	3112.8	3075.9
3087.5	3077.7	3067.3	3272.6	3246.3	3229.1	3157.7	3179.7	3132.2
3111.1	3103.3	3088.1	3293.4	3268.4	3251.1	3174.1	3198.7	3154.9
3176.8	3172.5	3151.5	3359.1	3336.8	3314.8	3235.0	3261.1	3208.3
3724.9	3793.1	3808.6	4097.9	4172.0	4164.1	3759.9	3877.3	3871.2

Table III.A.10. Normal mode vibrational frequencies of 2-chloroethanol in G_g conformer at DFT, HF and MP2 (FULL) levels of theory with 6-31G*, 6-31G** and 6-311++G** basis sets (cm^{-1}).

B3LYP			HF			MP2 (FULL)		
6-31G*	6-31G**	6-311++G**	6-31G*	6-31G**	6-311++G**	6-31G*	6-31G**	6-311++G**
135.0	136.0	132.9	143.8	151.2	143.4	145.8	147.0	163.1
254.4	255.4	241.7	270.6	290.7	261.4	261.2	261.3	292.8
329.7	329.0	307.6	342.7	400.2	328.9	338.9	336.0	462.2
482.8	482.5	478.1	517.5	517.5	514.3	495.4	494.7	528.0
669.3	667.9	660.1	731.4	726.5	723.4	731.2	732.4	729.8
862.9	859.3	852.8	935.7	928.4	927.7	888.4	887.1	875.0
958.9	955.0	952.4	1043.8	1038.0	1035.8	1003.6	1002.5	993.5
1031.9	1025.5	1017.3	1120.1	1116.9	1110.2	1060.8	1056.8	1060.5
1121.4	1118.6	1097.9	1223.9	1217.3	1209.4	1151.3	1153.8	1134.2
1166.5	1157.1	1152.3	1271.0	1263.4	1258.5	1195.9	1192.2	1196.7
1275.1	1267.1	1261.1	1385.4	1375.7	1370.3	1306.9	1306.6	1291.0
1350.1	1337.6	1330.8	1473.5	1457.9	1454.0	1395.0	1391.8	1380.2
1401.6	1391.0	1370.9	1514.7	1502.6	1490.5	1421.4	1417.8	1408.3
1441.2	1429.6	1419.8	1570.8	1558.4	1553.7	1463.0	1463.3	1452.0
1504.7	1489.5	1473.5	1628.7	1611.3	1601.0	1540.2	1536.2	1486.6
1522.1	1507.4	1489.4	1653.4	1635.8	1624.1	1559.8	1556.4	1508.4
2974.7	2969.0	2969.0	3177.9	3166.8	3141.9	3061.2	3087.1	3039.8
3086.3	3079.5	3066.8	3269.1	3256.6	3228.8	3138.4	3161.3	3109.4
3120.9	3110.8	3097.3	3304.2	3294.0	3259.2	3191.9	3215.5	3162.5
3147.0	3143.0	3125.5	3330.6	3320.8	3289.3	3207.9	3234.9	3177.7
3737.4	3806.2	3827.3	4102.8	4128.2	4173.8	3769.7	3889.0	3741.6

Table III.A.11. Normal mode vibrational frequencies of 2-chloroethanol in G$_t$ conformer at DFT, HF and MP2 (FULL) levels of theory with 6-31G*, 6-31G** and 6-311++G** basis sets (cm^{-1}).

B3LYP			HF			MP2 (FULL)		
6-31G*	6-31G**	6-311++G**	6-31G*	6-31G**	6-311++G**	6-31G*	6-31G**	6-311++G**
141.9	142.0	137.2	152.6	153.0	149.7	152.0	152.8	134.3
187.0	174.0	154.1	211.8	200.0	198.4	212.4	210.3	153.2
290.8	289.1	287.9	313.4	311.8	311.0	304.0	301.7	298.9
464.2	463.3	461.3	501.1	500.9	497.3	478.2	475.9	474.3
667.9	665.6	659.6	731.8	728.6	723.4	732.6	734.3	733.2
872.4	868.0	861.1	946.6	942.7	938.0	897.0	895.0	885.5
967.4	963.2	959.9	1047.7	1043.4	1038.7	1011.5	1010.5	1002.8
1060.4	1053.2	1039.2	1151.2	1144.4	1134.6	1096.7	1094.8	1067.9
1109.5	1105.6	1085.8	1224.9	1223.7	1213.6	1139.8	1141.4	1125.9
1194.3	1186.2	1175.3	1288.3	1278.4	1270.2	1223.3	1220.2	1207.0
1274.4	1269.3	1265.7	1387.5	1381.2	1377.8	1293.1	1292.8	1296.3
1315.7	1303.6	1292.4	1425.6	1413.5	1406.0	1343.2	1339.1	1322.7
1354.2	1342.3	1337.4	1479.0	1466.5	1461.4	1399.0	1397.5	1385.1
1474.1	1462.1	1444.3	1605.9	1592.5	1580.5	1500.6	1500.5	1468.9
1498.2	1483.2	1466.9	1626.8	1612.2	1601.4	1533.5	1530.3	1481.7
1538.3	1523.5	1502.0	1669.1	1652.4	1637.2	1576.6	1574.4	1522.7
2972.4	2963.9	2969.4	3179.5	3151.9	3143.3	3056.6	3079.4	3050.9
3042.1	3035.8	3035.1	3237.5	3212.2	3199.8	3122.1	3147.7	3116.1
3110.7	3103.3	3088.8	3289.3	3265.2	3248.9	3158.6	3180.6	3133.7
3171.9	3168.1	3148.3	3353.6	3332.2	3311.2	3229.6	3255.8	3202.1
3770.2	3841.2	3859.4	4124.5	4201.1	4196.3	3791.1	3911.6	3919.6

Table III.A.12. Normal mode vibrational frequencies of 2-chloroethanol in T$_t$ conformer at DFT, HF and MP2 (FULL) levels of theory with 6-31G*, 6-31G** and 6-311++G** basis sets (cm^{-1}).

B3LYP			HF			MP2 (FULL)		
6-31G*	6-31G**	6-311++G**	6-31G*	6-31G**	6-311++G**	6-31G*	6-31G**	6-311++G**
124.7	124.0	118.8	142.0	142.1	141.1	137.4	137.9	48.3
217.0	208.3	191.1	258.1	251.8	239.4	251.1	244.2	151.8
248.6	247.9	247.4	271.7	271.4	270.0	257.3	255.6	253.9
386.2	385.8	384.2	418.4	418.4	417.0	403.2	403.4	403.0
762.1	760.3	753.4	826.1	824.2	818.2	824.8	827.1	822.1
810.9	806.7	803.4	866.0	862.1	859.6	830.7	827.9	826.7
1023.3	1019.3	1015.3	1099.7	1096.3	1090.3	1067.8	1066.5	1055.5
1076.2	1067.1	1048.1	1173.9	1166.0	1158.0	1106.8	1111.3	1094.4
1080.1	1079.7	1060.2	1196.2	1196.5	1181.8	1117.6	1114.8	1096.0
1218.1	1212.2	1204.5	1331.6	1324.8	1319.0	1247.4	1248.9	1225.9
1246.0	1235.2	1227.0	1345.2	1332.4	1325.1	1270.8	1263.5	1255.3
1314.9	1306.9	1302.2	1431.0	1422.7	1419.5	1346.3	1347.5	1326.3
1322.0	1308.7	1303.5	1442.6	1428.9	1422.2	1361.0	1357.3	1342.5
1474.9	1464.2	1443.2	1607.0	1595.3	1581.6	1502.5	1502.7	1472.1
1521.1	1507.0	1491.6	1644.7	1630.6	1621.9	1555.2	1553.6	1511.7
1557.4	1543.6	1523.3	1683.6	1667.9	1653.2	1594.4	1592.9	1538.8
3014.3	3005.0	3006.8	3209.1	3181.9	3173.9	3081.0	3103.1	3071.2
3050.4	3043.6	3045.7	3248.1	3222.7	3212.3	3133.3	3159.3	3125.0
3118.9	3111.2	3097.3	3301.8	3276.9	3259.5	3172.5	3193.5	3144.4
3182.1	3177.6	3160.2	3368.4	3345.7	3324.7	3244.7	3269.9	3216.4
3759.3	3830.5	3847.8	4116.0	4192.2	4187.8	3781.1	3902.5	3903.2

Table III.A.13. Normal mode vibrational frequencies of 2-chloroethanol in T$_g$ conformer at DFT, HF and MP2 (FULL) levels of theory with 6-31G*, 6-31G** and 6-311++G** basis sets (cm^{-1}).

B3LYP			HF			MP2 (FULL)		
6-31G*	6-31G**	6-311++G**	6-31G*	6-31G**	6-311++G**	6-31G*	6-31G**	6-311++G**
133.5	132.6	128.1	143.5	143.5	143.2	144.5	145.3	144.2
240.4	240.0	238.0	266.2	266.0	261.2	249.5	247.9	243.2
327.9	317.1	288.0	318.3	312.5	285.4	322.6	320.0	329.1
386.4	385.9	384.5	419.3	419.4	418.8	403.2	404.2	408.0
749.4	747.6	743.4	826.8	825.2	820.1	810.4	807.5	807.4
791.9	787.3	788.1	847.0	843.4	842.8	819.8	822.9	824.8
1036.2	1030.6	1023.1	1122.9	1118.7	1113.7	1065.1	1061.5	1053.2
1060.7	1055.7	1049.1	1144.2	1139.0	1132.7	1100.7	1100.5	1088.6
1080.7	1077.9	1056.5	1197.8	1198.0	1183.3	1116.3	1119.1	1111.4
1150.0	1140.8	1134.3	1245.1	1235.1	1228.7	1181.5	1179.2	1172.2
1294.7	1282.2	1282.2	1414.7	1402.9	1398.0	1331.9	1330.1	1313.4
1319.5	1309.6	1304.9	1430.4	1420.5	1414.6	1352.7	1353.2	1340.5
1403.3	1391.6	1372.3	1516.4	1502.4	1490.2	1421.9	1416.4	1396.5
1428.1	1417.2	1407.5	1563.7	1553.7	1546.2	1455.8	1458.2	1440.4
1515.5	1501.0	1485.8	1639.2	1623.9	1614.6	1550.4	1548.0	1500.0
1538.7	1524.4	1509.5	1666.4	1651.2	1638.8	1575.9	1573.0	1523.7
3038.3	3032.3	3028.5	3227.1	3202.0	3191.7	3105.2	3128.5	3091.4
3098.9	3093.2	3080.1	3282.6	3258.0	3241.5	3155.9	3177.3	3128.4
3126.6	3117.2	3105.5	3306.7	3280.0	3264.3	3198.9	3222.5	3179.1
3170.7	3167.1	3149.3	3354.5	3331.7	3311.8	3234.7	3260.0	3207.0
3746.0	3818.5	3835.8	4110.1	4185.7	4181.2	3779.4	3898.0	3894.6

Table III.A.14. Normal mode vibrational frequencies of the transition state for the H$_2$O elimination from 2-chloroethanol at DFT, HF and MP2 (FULL) levels of theory with 6-31G*, 6-31G** and 6-311++G** basis sets (cm^{-1}).

B3LYP			HF			MP2 (FULL)		
6-31G*	6-31G**	6-311++G**	6-31G*	6-31G**	6-311++G**	6-31G*	6-31G**	6-311++G**
-1923.2	-1878.8	-2002.3	-1591.9	-1508.6	-1416.4	-2002.4	-1971.0	-1952.9
144.7	143.7	145.6	136.5	137.9	129.7	147.4	147.5	143.0
332.1	334.1	293.7	331.3	338.3	346.9	348.4	350.2	338.4
424.4	435.0	367.7	431.1	437.3	446.0	454.6	463.8	428.3
510.1	491.0	423.0	552.0	536.2	521.5	521.3	525.1	437.2
585.4	590.2	555.5	669.6	671.9	663.5	615.6	623.1	607.1
685.4	684.4	674.8	792.3	797.3	802.2	735.2	736.3	724.5
748.2	743.9	735.0	847.1	842.5	864.1	777.8	769.6	748.7
810.4	815.9	793.2	956.5	952.7	969.0	840.3	839.8	826.1
1019.0	1019.4	985.7	1125.8	1119.7	1111.8	1056.6	1056.7	1041.4
1072.8	1072.1	1055.3	1202.2	1199.8	1175.9	1119.5	1121.7	1104.4
1141.7	1142.4	1125.2	1253.1	1245.9	1262.5	1187.5	1190.7	1184.3
1239.6	1237.7	1226.9	1399.8	1392.6	1384.8	1278.9	1284.1	1258.9
1321.8	1314.1	1305.4	1419.2	1412.9	1414.1	1373.7	1378.7	1346.7
1452.0	1438.0	1361.3	1575.8	1552.5	1519.9	1481.1	1490.9	1399.3
1503.9	1491.4	1478.6	1623.7	1610.2	1597.2	1542.9	1548.7	1504.1
1684.7	1714.6	1661.6	2154.7	2196.6	2243.1	1717.6	1740.0	1749.9
3150.5	3138.0	3132.3	3316.4	3289.9	3260.7	3186.7	3211.3	3161.7
3206.7	3202.2	3180.8	3360.8	3342.9	3309.5	3267.3	3294.6	3240.6
3254.6	3243.5	3234.6	3422.2	3395.3	3361.0	3295.4	3323.9	3269.3
3656.9	3722.4	3726.8	4016.4	4093.0	4073.4	3656.4	3771.2	3744.4

Table III.A.15. Normal mode vibrational frequencies of the transition state for the HCl elimination from 2-chloroethanol at DFT, HF and MP2 (FULL) levels of theory with 6-31G*, 6-31G** and 6-311++G** basis sets (cm^{-1}).

B3LYP			HF			MP2 (FULL)		
6-31G*	6-31G**	6-311++G**	6-31G*	6-31G**	6-311++G**	6-31G*	6-31G**	6-311++G**
-1378.9	-1406.9	-1397.8	-1032.1	-1068.7	-1044.1	-1359.3	-1746.9	-1612.6
128.0	126.2	131.2	107.9	109.9	116.1	127.4	135.5	131.2
230.7	227.3	228.3	219.1	229.0	233.1	242.9	178.0	263.4
317.0	318.2	312.8	300.1	299.3	290.9	347.4	282.5	355.5
325.3	329.6	333.6	361.9	367.4	364.6	397.4	402.7	416.4
457.0	455.4	456.3	501.6	499.6	496.8	465.4	465.2	460.0
696.1	709.8	713.7	801.1	797.9	802.2	806.6	771.3	812.4
879.6	874.0	873.6	1013.8	1004.5	993.6	915.3	884.6	897.1
988.1	984.0	991.8	1191.8	1182.8	1180.1	1012.5	983.0	1004.9
1023.1	1014.3	1015.2	1199.0	1184.2	1184.3	1082.8	1071.2	1072.0
1157.5	1153.6	1138.6	1266.8	1262.1	1250.5	1183.0	1157.4	1166.9
1203.5	1193.5	1182.6	1354.9	1346.3	1339.1	1232.8	1176.3	1211.5
1262.0	1250.6	1240.1	1399.9	1389.8	1384.0	1290.6	1275.0	1274.5
1327.7	1316.1	1306.6	1470.0	1453.1	1442.9	1366.7	1315.5	1330.7
1434.0	1428.2	1414.8	1575.8	1564.3	1550.3	1472.4	1414.9	1433.8
1474.7	1479.5	1478.0	1723.3	1714.1	1698.0	1572.5	1465.2	1515.9
1642.3	1653.3	1649.8	2112.4	2129.6	2151.4	1903.4	1661.0	1746.8
3099.3	3101.0	3092.7	3343.8	3318.8	3296.2	3211.9	3201.5	3194.7
3220.4	3208.2	3181.5	3407.8	3377.8	3347.4	3275.2	3224.7	3231.9
3330.9	3322.7	3294.6	3526.5	3498.0	3466.9	3395.0	3347.2	3354.7
3749.4	3818.2	3831.4	4089.0	4166.6	4157.5	3766.1	3882.6	3888.7

Table III.A.16. Normal mode vibrational frequencies of the transition state for the HOCl elimination from 2-chloroethanol at MP2 (FULL) levels of theory with 6-311++G** basis set (cm^{-1}).

-466.4
57.1
197.4
305.1
398.3
446.3
564.7
685.2
841.7
1134.3
1165.5
1207.9
1249.9
1289.5
1483.5
1549.5
3138.0
3192.2
3220.4
3304.7
3572.0

Table III.A.17. Energies of 2-chloroethanol in G_g', T_g, T_t, G_t, G_g conformers at various levels of theory (in Hartree).

Theory	Basis set	$G_{g'}$	T_g	T_t	G_t	G_g
B3LYP	**6-31G***	-614.558996	-614.556566	-614.555955	-614.555064	-614.554997
	6-31G**	-614.569938	-614.567541	-614.566950	-614.566167	-614.566042
	6-311++G**	-614.647658	-614.645413	-614.645537	-614.644588	-614.643714
HF	**6-31G***	-612.901352	-612.899452	-612.899946	-612.898104	-612.897283
	6-31G**	-612.914371	-612.912484	-612.912986	-612.911234	-612.910185
	6-311++G**	-612.981471	-612.979678	-612.980561	-612.978693	-612.977425
MP2 (FULL)	**6-31G***	-613.496011	-613.493562	-613.493510	-613.492324	-613.491882
	6-31G**	-613.539891	-613.537651	-613.537549	-613.536423	-613.536027
	6-311++G**	-613.737089	-613.734671	-613.735372	-613.734340	-613.732962

Table III.A.18. Energies of 2-chloroethanol in its transition state for HCl and H_2O elimination at various levels of theory (in Hartree).

Theory	Basis set	TS-HCl	TS-H_2O
B3LYP	6-31G*	-614.469408	-614.448597
	6-31G**	-614.483401	-614.463576
	6-311++G**	-614.564211	-614.543520
HF	6-31G*	-612.794718	-612.758908
	6-31G**	-612.811572	-612.777663
	6-311++G**	-612.882216	-612.845486
MP2(FULL)	6-31G*	-613.384114	-613.378541
	6-31G**	-613.627235	-613.425285
	6-311++G**	-613.631333	-613.626304

Table III.A.19. Moments of inertia of 2-chloroethanol in $G_{g'}$, G_g, G_t, T_g and T_t conform--ers at various levels of theory (a.m.u. $\mathring{A}^2$).

Theory/ Basis set	$G_{g'}$	G_g	G_t	T_g	T_t
HF/6-31G*	38.43622 147.64991 171.75510	37.81113 151.96172 174.09215	36.83204 152.43979 173.45818	29.34192 2.43355 2.32587	16.89389 205.43781 216.08570
HF/6-31G**	38.39333 147.76388 171.83219	37.90645 151.76822 174.00404	36.85589 152.39061 173.46890	29.35202 2.43492 2.3271	16.88853 205.37353 216.00904
HF/6-311++G**	38.25505 148.71745 172.60038	37.44020 153.81403 175.36376	36.64796 153.70316 174.43285	29.32097 2.43238 2.32449	16.91120 205.63760 216.27990
MP2/6-31G*	39.31094 144.93941 169.71217	38.88698 149.25813 172.36843	37.78679 149.57752 171.25747	17.39412 208.14367 217.74477	17.10880 205.04273 215.78308
MP2/6-31G**	39.11981 144.80817 169.51805	38.72399 149.04244 172.13242	37.64981 149.30090 171.03201	17.27597 207.76460 217.33369	16.99666 204.75198 215.43905
MP2/6-311++G**	39.21692 144.07664 168.80518	38.88698 149.25813 172.36843	37.84710 149.19380 170.74944	17.43750 206.86230 216.66563	17.13589 204.46205 215.20878
B3LYP/6-31G*	39.63950 148.61031 173.85380	38.89500 154.32977 177.50599	37.71168 155.27479 176.85995	17.52916 212.26299 222.00218	17.24221 209.11170 219.96434
B3LYP/6-31G**	39.59267 148.68857 173.90285	38.88566 154.22098 177.42435	37.71097 155.26859 176.88223	17.50479 212.22466 221.95050	17.21999 209.09527 219.93467
B3LYP/6-311++G**	39.33980 149.96634 174.81842	38.37193 156.54359 178.89715	37.44569 156.68337 177.76448	17.48542 212.20060 221.94855	17.19733 209.31870 220.12722

Table III.A.20. Moments of inertia of 2-Chloroethanol in its transition state for H_2O and HCl elimination at various levels of theory (a.m.u. Å^2).

Theory/ Basis set	H_2O	HCl
HF/6-31G*	30.30350 182.95060 191.36043	38.03741 232.04667 253.15154
HF/6-31G**	30.39598 182.32950 190.92739	37.76468 229.86404 250.64801
HF/6-311++G**	30.20355 181.20895 189.40753	38.26762 229.20206 250.43189
MP2/6-31G*	32.93292 181.03499 193.06668	35.83885 220.57397 238.96800
MP2/6-31G**	32.72053 180.54798 192.54737	37.68738 200.03130 220.72329
MP2/6-311++G**	33.46622 177.47794 190.28543	37.68791 203.51190 223.57158
B3LYP/6-31G*	33.54677 185.04259 197.36744	41.50245 210.39228 234.23205
B3LYP/6-31G**	33.28068 184.82266 196.91756	40.46341 210.49393 233.27952
B3LYP/6-311++G**	34.56385 183.14021 196.77112	40.51668 210.54742 233.37324
MP2/6-311++G**	49.02053 135.58415 177.22277	**HOCl elimination**

Table III.A.21. Activation energies (E_0) for HCl and H_2O elimination from 2-chloroethanol at various levels of theory (in kcal/mol).

Theory	Basis set	TS-HCl	TS-H_2O
HF	6-31G*	66.914	89.385
	6-31G**	64.507	85.786
	6-311++G**	62.284	85.332
MP2(FULL)	6-31G*	70.216	73.714
	6-31G**	67.249	71.916
	6-311++G**	66.363	69.519
B3LYP	6-31G*	56.217	69.276
	6-31G**	54.303	66.743
	6-311++G**	52.364	65.348

Table III.A.22. Entropy of activation $(\Delta S^{\#})$ evaluated using different models for HCl and H_2O elimination from 2-chloroethanol at various levels of theory (in cal/mol/K).

Theory/ Basis set	$\Delta S^{\#}(HO)$	$\Delta S^{\#}(HR)$	$\Delta S^{\#}(FR)$
HF/6-311++G (H_2O)**	0.63	-3.70	-6.71
MP2/6-311++G (H_2O)**	1.53	-1.73	-6.06
B3LYP/6-311++G (H_2O)**	1.63	-2.49	-5.56
HF/6-311++G (HCl)**	3.29	-1.04	-4.05
MP2/6-311++G (HCl)**	2.59	-0.67	-5.00
B3LYP/6-311++G (HCl)**	2.93	-1.19	-4.26

Table III.A.23. Dihedral angle for the 4 atoms involved in the reaction coordinate for HCl and H$_2$O elimination reactions from 2-chloroethanol, ethyl alcohol and ethyl chloride.

Molecule	HF/ 6-311++G**	MP2(FULL)/ 6-311++G**	B3LYP/ 6-311++G**
CEOH (HCl)	3.41	6.05	4.11
EtCl (HCl)	0.04	0.03	0.07
CEOH (H$_2$O)	3.45	4.89	4.28
EtOH (H$_2$O)	2.65	1.92	3.22

Table III.A.24. Low frequency torsional modes of C-C and C-O rotors for the five different conformations of 2-chloroethanol at both ab initio and DFT (B3LYP) levels of theory with the 6-311++G* basis set.

Theory/ Basis Set	Rotors	$G_{g'}$	T_g	T_t	G_t	G_g
B3LYP/ 6-311++G	C-C rotor	144.4	128.1	118.8	137.2	132.9
	C-O rotor	383.5	288.0	191.1	154.1	241.7
HF/ 6-311++G	C-C rotor	161.0	143.2	141.1	149.7	143.4
	C-O rotor	394.3	285.4	239.4	198.4	261.4
MP2(FULL)/ 6-311++G	C-C rotor	166.5	144.2	48.3	153.2	163.1
	C-O rotor	421.0	329.1	151.8	134.3	462.2

Table III.A.25. Moment of inertia (Kg-m^2) calculated about the C-C and C-O bonds of the different conformers of the 2-chloroethanol at both ab initio and DFT (B3LYP) levels of theory with the 6-311++G* basis set.

Conformers	C-C bond			C-O bond		
	B3LYP	HF	MP2(FULL)	B3LYP	HF	MP2(FULL)
$G_{g'}$	2.98E-46	2.90E-46	2.95E-46	1.38E-47	1.29E-47	1.40E-47
G_g	3.10E-46	3.12E-46	3.09E-46	1.36E-47	1.28E-47	1.38E-47
G_t	3.11E-46	3.02E-46	3.09E-46	1.35E-47	1.28E-47	1.37E-47
T_t	3.15E-46	3.05E-46	3.12E-46	1.36E-47	1.28E-47	1.38E-47
T_g	3.15E-46	3.05E-46	3.12E-46	1.36E-47	1.28E-47	1.38E-47

Table III.A.26. Energies of various conformers relative to most stable $G_{g'}$ conformer of 2-chloroethanol in kcal/mol.

Theory	$G_{g'}$ - T_g	$G_{g'}$ - T_t	$G_{g'}$ - G_t	$G_{g'}$ - G_g
HF	1.125125	0.571034	1.743223	2.538905
MP2	1.517319	1.077435	1.725025	2.589734
DFT	1.408760	1.330949	1.926456	2.474899

Table III.A.27. Hindered rotor partition function in temperature range of 930-1100K calculated at 10K intervals at both ab initio and DFT (B3LYP) levels of theory with the 6-311++G* basis set for low frequency torsional modes of C-C and C-O bonds of 2-chloroethanol.

Temperature	B3LYP		MP2 (FULL)		HF	
	C-C	C-O	C-C	C-O	C-C	C-O
930	12.387	5.921	8.468	4.471	12.610	5.971
940	12.596	6.007	8.608	4.545	12.806	6.048
950	12.806	6.093	8.749	4.618	13.002	6.124
960	13.017	6.178	8.891	4.692	13.199	6.199
970	13.228	6.262	9.033	4.765	13.396	6.274
980	13.440	6.346	9.175	4.838	13.594	6.349
990	13.652	6.429	9.318	4.912	13.792	6.423
1000	13.865	6.512	9.461	4.985	13.991	6.497
1010	14.079	6.594	9.605	5.057	14.189	6.570
1020	14.293	6.676	9.749	5.130	14.388	6.643
1030	14.507	6.757	9.894	5.203	14.588	6.716
1040	14.722	6.838	10.039	5.275	14.788	6.788
1050	14.937	6.918	10.185	5.348	14.988	6.859
1060	15.153	6.998	10.331	5.420	15.188	6.930
1070	15.369	7.077	10.477	5.492	15.388	7.001
1080	15.586	7.155	10.624	5.563	15.589	7.071
1090	15.803	7.233	10.771	5.635	15.790	7.141
1100	16.020	7.311	10.919	5.706	15.991	7.210

Table III.A.28. Free rotor partition function at various temperatures calculated at different level of theory with the 6-311++G* basis set for low frequency torsional modes of C-C and C-O bonds of $G_{g'}$ confirmation of 2-chloroethanol.

Temperature	$G_{g'}$ (C-C)			$G_{g'}$ (C-O)		
	B3LYP	**HF**	**MP2(FULL)**	**B3LYP**	**HF**	**MP2(FULL)**
930	46.43680	45.85910	46.25404	9.99948	9.67355	10.06164
940	46.68579	46.10499	46.50206	10.05310	9.72542	10.11559
950	46.93347	46.34958	46.74875	10.10643	9.77701	10.16926
960	47.17984	46.59289	46.99416	10.15948	9.82833	10.22264
970	47.42493	46.83493	47.23828	10.21226	9.87939	10.27574
980	47.66876	47.07573	47.48115	10.26476	9.93018	10.32858
990	47.91135	47.31530	47.72279	10.31700	9.98072	10.38114
1000	48.15272	47.55367	47.96321	10.36898	10.03100	10.43344
1010	48.39289	47.79084	48.20243	10.42069	10.08103	10.48548
1020	48.63186	48.02685	48.44047	10.47215	10.13081	10.53726
1030	48.86967	48.26170	48.67734	10.52336	10.18035	10.58878
1040	49.10633	48.49542	48.91307	10.57432	10.22965	10.64006
1050	49.34186	48.72801	49.14766	10.62504	10.27872	10.69109
1060	49.57626	48.95950	49.38115	10.67552	10.32755	10.74188
1070	49.80956	49.18990	49.61353	10.72575	10.37615	10.79243
1080	50.04178	49.41922	49.84483	10.77576	10.42452	10.84275
1090	50.27292	49.64749	50.07506	10.82553	10.47267	10.89283
1100	50.50300	49.87471	50.30424	10.87508	10.52060	10.94268

Table III.A.29. Free rotor partition function at various temperatures calculated at different level of theory with the 6-311++G* basis set for low frequency torsional modes of C-C and C-O bonds of G_g conformation of 2-chloroethanol.

Temperature	G_g (C-C)			G_g (C-O)		
	B3LYP	HF	MP2(FULL)	B3LYP	HF	MP2(FULL)
930	47.42039	47.51790	47.27921	9.92361	9.61948	10.00207
940	47.67465	47.77268	47.53272	9.97682	9.67106	10.05570
950	47.92757	48.02612	47.78489	10.02975	9.72237	10.10905
960	48.17916	48.27823	48.03573	10.08240	9.77341	10.16212
970	48.42944	48.52903	48.28527	10.13478	9.82418	10.21491
980	48.67844	48.77854	48.53352	10.18688	9.87469	10.26743
990	48.92617	49.02677	48.78051	10.23873	9.92494	10.31968
1000	49.17265	49.27376	49.02626	10.29031	9.97494	10.37167
1010	49.41790	49.51952	49.27078	10.34163	10.02469	10.42340
1020	49.66194	49.76406	49.51410	10.39270	10.07420	10.47487
1030	49.90479	50.00741	49.75622	10.44352	10.12346	10.52609
1040	50.14646	50.24957	49.99717	10.49409	10.17248	10.57707
1050	50.38697	50.49058	50.23697	10.54443	10.22127	10.62780
1060	50.62634	50.73044	50.47562	10.59452	10.26983	10.67828
1070	50.86458	50.96918	50.71316	10.64438	10.31816	10.72853
1080	51.10172	51.20680	50.94958	10.69400	10.36626	10.77855
1090	51.33775	51.44332	51.18492	10.74340	10.41414	10.82834
1100	51.57271	51.67876	51.41918	10.79256	10.46181	10.87790

Table III.A.30. Free rotor partition function at various temperatures calculated at different level of theory with the 6-311++G* basis set for low frequency torsional modes of C-C and C-O bonds of G_t conformation of 2-chloroethanol.

Temperature	G_t (C-C)			G_t (C-O)		
	B3LYP	**HF**	**MP2(FULL)**	**B3LYP**	**HF**	**MP2(FULL)**
930	47.47785	46.75887	47.29046	9.90589	9.61778	9.95607
940	47.73243	47.00959	47.54403	9.95900	9.66935	10.00945
950	47.98565	47.25898	47.79625	10.01184	9.72065	10.06255
960	48.23754	47.50706	48.04715	10.06439	9.77167	10.11538
970	48.48813	47.75385	48.29675	10.11668	9.82244	10.16792
980	48.73743	47.99938	48.54506	10.16869	9.87294	10.22020
990	48.98546	48.24365	48.79211	10.22044	9.92318	10.27221
1000	49.23224	48.48669	49.03792	10.27193	9.97317	10.32396
1010	49.47779	48.72852	49.28250	10.32316	10.02291	10.37545
1020	49.72212	48.96916	49.52587	10.37414	10.07241	10.42669
1030	49.96526	49.20862	49.76805	10.42487	10.12166	10.47768
1040	50.20723	49.44692	50.00906	10.47535	10.17068	10.52842
1050	50.44803	49.68407	50.24892	10.52559	10.21946	10.57891
1060	50.68769	49.92010	50.48763	10.57560	10.26801	10.62917
1070	50.92622	50.15502	50.72522	10.62537	10.31633	10.67919
1080	51.16364	50.38885	50.96170	10.67490	10.36442	10.72898
1090	51.39997	50.62159	51.19709	10.72421	10.41230	10.77853
1100	51.63521	50.85327	51.43140	10.77329	10.45995	10.82786

Table III.A.31. Free rotor partition function at various temperatures calculated at different level of theory with the 6-311++G* basis set for low frequency torsional modes of C-C and C-O bonds of T_t conformation of 2-chloroethanol.

Temperature	T_t (C-C)			T_t (C-O)		
	B3LYP	HF	MP2(FULL)	B3LYP	HF	MP2(FULL)
930	47.79305	47.02583	47.57401	9.93578	9.63161	9.99539
940	48.04932	47.27798	47.82910	9.98906	9.68325	10.04898
950	48.30422	47.52879	48.08284	10.04205	9.73462	10.10230
960	48.55779	47.77829	48.33525	10.09476	9.78572	10.15533
970	48.81004	48.02649	48.58634	10.14720	9.83656	10.20808
980	49.06099	48.27342	48.83614	10.19938	9.88713	10.26057
990	49.31067	48.51908	49.08467	10.25128	9.93745	10.31278
1000	49.55908	48.76351	49.33195	10.30293	9.98751	10.36474
1010	49.80626	49.00672	49.57800	10.35431	10.03733	10.41643
1020	50.05222	49.24873	49.82283	10.40544	10.08689	10.46787
1030	50.29698	49.48956	50.06647	10.45633	10.13622	10.51906
1040	50.54055	49.72922	50.30892	10.50696	10.18530	10.57000
1050	50.78295	49.96773	50.55021	10.55736	10.23415	10.62069
1060	51.02420	50.20511	50.79036	10.60751	10.28277	10.67115
1070	51.26432	50.44137	51.02937	10.65743	10.33116	10.72137
1080	51.50331	50.67653	51.26727	10.70711	10.37933	10.77135
1090	51.74120	50.91060	51.50407	10.75657	10.42727	10.82110
1100	51.97801	51.14360	51.73979	10.80580	10.47499	10.87063

Table III.A.32. Free rotor partition function at various temperatures calculated at different level of theory with the 6-311++G* basis set for low frequency torsional modes of C-C and C-O bonds of T_g conformation of 2-chloroethanol.

Temperature	T_g (C-C)			T_g (C-O)		
	B3LYP	HF	MP2(FULL)	B3LYP	HF	MP2(FULL)
930.0	47.73620	47.01240	47.51790	9.92220	9.62797	10.00432
940.0	47.99216	47.26448	47.77268	9.97541	9.67959	10.05796
950.0	48.24677	47.51522	48.02612	10.02833	9.73095	10.11132
960.0	48.50003	47.76464	48.27823	10.08097	9.78203	10.16440
970.0	48.75198	48.01277	48.52903	10.13334	9.83284	10.21720
980.0	49.00264	48.25963	48.77854	10.18544	9.88340	10.26973
990.0	49.25202	48.50522	49.02677	10.23727	9.93370	10.32200
1000.0	49.50014	48.74959	49.27376	10.28885	9.98374	10.37400
1010.0	49.74702	48.99273	49.51952	10.34016	10.03353	10.42574
1020.0	49.99269	49.23467	49.76406	10.39122	10.08308	10.47722
1030.0	50.23715	49.47543	50.00741	10.44204	10.13239	10.52846
1040.0	50.48043	49.71502	50.24957	10.49260	10.18146	10.57944
1050.0	50.72255	49.95346	50.49058	10.54293	10.23029	10.63018
1060.0	50.96351	50.19077	50.73044	10.59301	10.27889	10.68068
1070.0	51.20334	50.42696	50.96918	10.64286	10.32726	10.73094
1080.0	51.44205	50.66206	51.20680	10.69248	10.37541	10.78097
1090.0	51.67966	50.89606	51.44332	10.74187	10.42333	10.83077
1100.0	51.91618	51.12900	51.67876	10.79103	10.47103	10.88034

Table III.A.33. Summary of C-C, C-X, C-H, and H-X bond distances for the transition states for HCl/H$_2$O elimination reactions from 2-chloroethanol and change in percent change calculated as compared to 2-HF/H$_2$O elimination from fluoroethanol given in the parenthesis.

Bond(H-X)	HF		MP2		B3LYP	
	6-31G**	6-311++G**	6-31G**	6-311++G**	6-31G**	6-311++G**
C-C(HCl)	1.381(1.2)	1.383(0.5)	1.399(0.2)	1.397(0.3)	1.401(0.6)	1.398(0.1)
C-C(H$_2$O)	1.454(-0.4)	1.467(-0.2)	1.419(-0.1)	1.425(-0.8)	1.428(-0.3)	1.421(-0.6)
C-Cl(HCl)	2.695(7.7)	2.708(0.1)	2.419(4.9)	2.437(3.0)	2.613(6.5)	2.616(0.6)
C-O(H$_2$O)	1.650(-3.2)	1.607(-1.0)	1.773(-1.5)	1.756(-1.5)	1.797(-2.5)	1.839(0.0)
C-H(HCl)	1.213(-8.4)	1.209(-3.8)	1.275(-6.8)	1.259(-4.8)	1.251(-8.7)	1.249(-4.1)
C-H(H$_2$O)	1.610(3.1)	1.636(0.3)	1.503(1.7)	1.511(1.9)	1.493(3.4)	1.451(4.6)
HCl(HCl)	2.071(21.9)	2.071(8.1)	1.811(7.6)	1.856(3.2)	1.883(8.7)	1.891(-1.0)
HO(H$_2$O)	1.084(-1.9)	1.078(-0.1)	1.176(-2.5)	1.178(-2.0)	1.194(-3.8)	1.230(-3.9)

Table III.A.34. Summary of C-C, C-X, C-H, and H-X bond distances for the transition states for HCl/H$_2$O elimination reactions from 2-chloroethanol and change in percent change calculated as compared to ethyl chloride given in the parenthesis.

Bond(H-X)	HF		MP2		B3LYP	
	6-31G**	6-311++G**	6-31G**	6-311++G**	6-31G**	6-311++G**
C-C(HCl)	1.381(-0.2)	1.383(-0.2)	1.399(-0.5)	1.397(0.0)	1.401(0.0)	1.398(-0.1)
C-Cl(HCl)	2.695(-2.3)	2.708(-1.9)	2.419(-4.5)	2.437(-1.4)	2.6139(-1.9)	2.616(-1.5)
C-H(HCl)	1.213(-2.3)	1.209(-2.1)	1.275(0.7)	1.259(-2.1)	1.251(-2.1)	1.249(-1.6)
HCl(HCl)	2.071(8.6)	2.071(7.4)	1.811(-1.3)	1.856(5.9)	1.883(5.0)	1.891(4.4)

Table III.A.35. Potential energy as function of torsional angle evaluated at B3LYP/6-311++G** level of theory for 2-chloroethanol around C-C (T_t) and C-O (G_t and T_t) bonds. Angles are in degree and energy in kcal/mol.

Around C-C (T_t) bond		Around C-O bond (G_t)		Around C-O bond (T_t)	
Torsional	Energy	Torsional	Energy	Torsional	Energy
0.00	3.12	0.00	8.46	0.00	2.75
5.00	3.26	5.00	8.35	5.00	2.71
10.00	3.33	10.00	8.04	10.00	2.60
15.00	3.35	15.00	7.55	15.00	2.43
20.00	3.32	20.00	6.90	20.00	2.20
25.00	3.25	25.00	6.13	25.00	1.94
30.00	3.15	30.00	5.30	30.00	1.65
35.00	3.04	35.00	4.44	35.00	1.35
40.00	2.93	40.00	3.59	40.00	1.06
45.00	2.83	45.00	2.80	45.00	0.79
50.00	2.75	50.00	2.11	50.00	0.55
55.00	2.70	55.00	1.52	55.00	0.35
60.00	2.67	60.00	1.08	60.00	0.19
65.00	2.69	65.00	0.80	65.00	0.08
70.00	2.73	70.00	0.67	70.00	0.02
75.00	2.81	75.00	0.69	75.00	0.00
80.00	2.92	80.00	0.87	80.00	0.02
85.00	3.04	85.00	1.17	85.00	0.07
90.00	3.17	90.00	1.54	90.00	0.14
95.00	3.29	95.00	1.97	95.00	0.22
100.00	3.41	100.00	2.40	100.00	0.31
105.00	3.51	105.00	2.80	105.00	0.39
110.00	3.58	110.00	3.11	110.00	0.45
115.00	3.62	115.00	3.33	115.00	0.50
120.00	3.63	120.00	3.41	120.00	0.54
125.00	3.60	125.00	3.37	125.00	0.55
130.00	3.54	130.00	3.19	130.00	0.54
135.00	3.45	135.00	2.90	135.00	0.50
140.00	3.33	140.00	2.53	140.00	0.46
145.00	3.20	145.00	2.09	145.00	0.40
150.00	3.06	150.00	1.64	150.00	0.33
155.00	2.91	155.00	1.20	155.00	0.27
160.00	2.77	160.00	0.80	160.00	0.21
165.00	2.64	165.00	0.46	165.00	0.16
170.00	2.53	170.00	0.21	170.00	0.12
175.00	2.43	175.00	0.05	175.00	0.10

-180.00	2.36	180.00	0.00	180.00	0.09
-175.00	2.31	-180.00	0.00	-180.00	0.09
-170.00	2.27	-175.00	0.05	-175.00	0.10
-165.00	2.26	-170.00	0.21	-170.00	0.12
-160.00	2.26	-165.00	0.46	-165.00	0.16
-155.00	2.27	-160.00	0.80	-160.00	0.21
-150.00	2.28	-155.00	1.20	-155.00	0.27
-145.00	2.29	-150.00	1.64	-150.00	0.33
-140.00	2.29	-145.00	2.09	-145.00	0.40
-135.00	2.26	-140.00	2.53	-140.00	0.46
-130.00	2.21	-135.00	2.90	-135.00	0.50
-125.00	2.12	-130.00	3.19	-130.00	0.54
-120.00	2.00	-125.00	3.37	-125.00	0.55
-115.00	1.85	-120.00	3.41	-120.00	0.54
-110.00	1.67	-115.00	3.33	-115.00	0.50
-105.00	1.46	-110.00	3.11	-110.00	0.45
-100.00	1.24	-105.00	2.80	-105.00	0.39
-95.00	1.01	-100.00	2.40	-100.00	0.31
-90.00	0.78	-95.00	1.97	-95.00	0.22
-85.00	0.56	-90.00	1.54	-90.00	0.14
-80.00	0.36	-85.00	1.17	-85.00	0.07
-75.00	0.19	-80.00	0.87	-80.00	0.02
-70.00	0.07	-75.00	0.69	-75.00	0.00
-65.00	0.00	-70.00	0.67	-70.00	0.02
-60.00	0.00	-65.00	0.80	-65.00	0.08
-55.00	0.06	-60.00	1.08	-60.00	0.19
-50.00	0.19	-55.00	1.52	-55.00	0.35
-45.00	0.39	-50.00	2.11	-50.00	0.55
-40.00	0.64	-45.00	2.80	-45.00	0.79
-35.00	0.95	-40.00	3.59	-40.00	1.06
-30.00	1.29	-35.00	4.44	-35.00	1.35
-25.00	1.65	-30.00	5.30	-30.00	1.65
-20.00	2.01	-25.00	6.13	-25.00	1.94
-15.00	2.35	-20.00	6.90	-20.00	2.20
-10.00	2.66	-15.00	7.55	-15.00	2.43
-5.00	2.92	-10.00	8.04	-10.00	2.60
0.00	3.12	-5.00	8.35	-5.00	2.71
0.00	3.12	0.00	8.46	0.00	2.75
		0.00	8.46	0.00	2.75

Table III.A.36. The energies evaluated using the IRC calculations along the reaction coordinate at DFT levels of theory with 6-311++G** basis set (in Hartree) for HCl (61 steps), H_2O (61 steps) and HOCl (81 steps) elimination reaction.

HOCl		HCl		H_2O	
Coordinate	Energy	Coordinate	Energy	Coordinate	Energy
0.000	-613.539971	-0.050	-614.627804	0.050	-614.606298
-0.097	-613.540094	-0.100	-614.628076	0.100	-614.606868
-0.196	-613.540339	-0.150	-614.628497	0.150	-614.607769
-0.296	-613.540750	-0.200	-614.629048	0.200	-614.608956
-0.396	-613.541350	-0.250	-614.629710	0.250	-614.610378
-0.496	-613.542154	-0.300	-614.630466	0.300	-614.611972
-0.596	-613.543162	-0.350	-614.631301	0.350	-614.613674
-0.696	-613.544364	-0.400	-614.632199	0.400	-614.615420
-0.796	-613.545745	-0.450	-614.633148	0.450	-614.617158
-0.896	-613.547287	-0.500	-614.634138	0.500	-614.618852
-0.996	-613.548968	-0.550	-614.635158	0.550	-614.620488
-1.096	-613.550765	-0.600	-614.636202	0.600	-614.622068
-1.196	-613.552658	-0.650	-614.637262	0.650	-614.623602
-1.296	-613.554627	-0.700	-614.638333	0.699	-614.625099
-1.396	-613.556656	-0.750	-614.639409	0.749	-614.626567
-1.496	-613.558732	-0.800	-614.640486	0.799	-614.628010
-1.596	-613.560840	-0.850	-614.641560	0.849	-614.629430
-1.696	-613.562976	-0.900	-614.642629	0.899	-614.630829
-1.796	-613.565131	-0.950	-614.643689	0.949	-614.632208
-1.896	-613.567299	-1.000	-614.644739	0.999	-614.633569
-1.996	-613.569476	-1.050	-614.645778	1.049	-614.634913
-2.096	-613.571663	-1.100	-614.646804	1.099	-614.636239
-2.196	-613.573856	-1.150	-614.647816	1.149	-614.637548
-2.296	-613.576054	-1.200	-614.648814	1.199	-614.638842
-2.396	-613.578258	-1.250	-614.649799	1.249	-614.640118
-2.496	-613.580465	-1.300	-614.650770	1.299	-614.641379
-2.596	-613.582678	-1.350	-614.651727	1.349	-614.642623
-2.696	-613.584894	-1.400	-614.652672	1.399	-614.643852
-2.796	-613.587115	-1.450	-614.653603	1.449	-614.645064
-2.896	-613.589339	-1.500	-614.654524	1.499	-614.646259
-2.996	-613.591567	0.050	-614.627806	-0.050	-614.606299
-3.096	-613.593800	0.100	-614.628116	-0.100	-614.606894
-3.196	-613.596036	0.150	-614.628637	-0.150	-614.607863
-3.296	-613.598276	0.200	-614.629376	-0.200	-614.609189
-3.396	-613.600520	0.250	-614.630336	-0.250	-614.610844
-3.496	-613.602767	0.300	-614.631514	-0.300	-614.612793
-3.596	-613.605017	0.350	-614.632901	-0.350	-614.614998
-3.696	-613.607270	0.400	-614.634484	-0.400	-614.617415

-3.796	-613.609525	0.450	-614.636249	-0.450	-614.619998
-3.896	-613.611783	0.500	-614.638180	-0.500	-614.622701
-3.996	-613.614042	0.550	-614.640259	-0.550	-614.625478
0.096	-613.540043	0.600	-614.642467	-0.600	-614.628287
0.196	-613.540129	0.650	-614.644780	-0.650	-614.631088
0.296	-613.540226	0.700	-614.647169	-0.700	-614.633846
0.396	-613.540327	0.750	-614.649602	-0.750	-614.636536
0.495	-613.540430	0.800	-614.652045	-0.800	-614.639139
0.595	-613.540534	0.84966	-614.6544645	-0.850	-614.641645
0.690	-613.540632	0.89966	-614.6568258	-0.900	-614.644051
0.786	-613.540729	0.94966	-614.6590894	-0.950	-614.646361
0.884	-613.540829	0.99965	-614.6612121	-1.000	-614.648581
0.983	-613.540927	1.04964	-614.663149	-1.050	-614.650718
1.083	-613.541022	1.0996	-614.6648615	-1.100	-614.652780
1.182	-613.541115	1.14954	-614.6663275	-1.150	-614.654774
1.282	-613.541204	1.19941	-614.6675544	-1.200	-614.656703
1.382	-613.541290	1.24923	-614.6685879	-1.250	-614.658574
1.480	-613.541373	1.29909	-614.669495	-1.300	-614.660392
1.580	-613.541455	1.34902	-614.6703299	-1.350	-614.662160
1.670	-613.541525	1.39899	-614.6711196	-1.400	-614.663883
1.755	-613.541588	1.44898	-614.6718747	-1.450	-614.665564
1.849	-613.541662	1.49897	-614.6726003	-1.500	-614.667208
1.948	-613.541742	0	-614.6276972	0.000	-614.606086
2.047	-613.541822				
2.146	-613.541903				
2.245	-613.541984				
2.344	-613.542066				
2.442	-613.542150				
2.541	-613.542234				
2.640	-613.542320				
2.738	-613.542408				
2.834	-613.542493				
2.928	-613.542577				
3.024	-613.542665				
3.119	-613.542754				
3.216	-613.542845				
3.314	-613.542940				
3.412	-613.543036				
3.510	-613.543134				
3.609	-613.543232				
3.705	-613.543327				
3.799	-613.543421				
3.895	-613.543518				

(a)   (b)

(c)   **(d)**
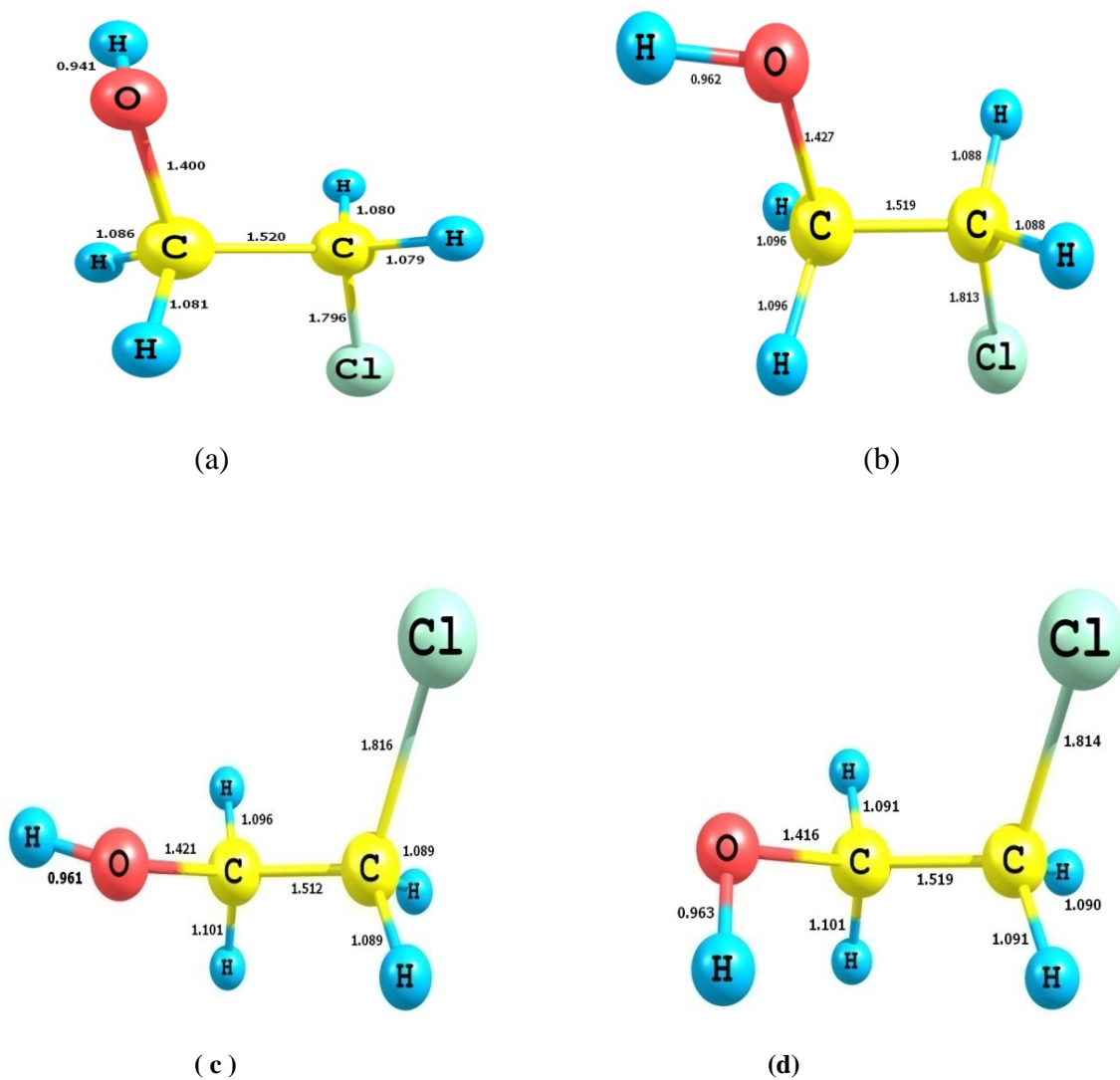
Figure III.A.1. Optimized structures of (a) ground state T_g conformation of 2-chloroethanol at B3LYP/6-311++g** level (b) ground state T_t conformation of 2-chloroethanol at B3LYP/6-311++g** level (c) ground state T_g conformation of 2-chloroethanol at B3LYP/6-311++g** level (d) ground state T_t conformation of 2-chloroethanol at B3LYP/6-311++g** level of theory (bond lengths are given in angstroms)

Chapter IV

Thermal Decomposition of 2-Bromoethanol

IV.1. Abstract

Kinetics of thermal decomposition of 2-bromoethanol highly diluted homogeneously in high purity argon was investigated using single pulse shock tube behind the reflected shock wave over the temperature range 910-1102K and the pressure varied between 9-14 atm. The distribution of reaction products in the post shock mixture was analyzed using standard qualitative FT-IR and quantitative gas chromatographic techniques revealing the presence of six reaction products. The products in the order of abundance in the post shock mixture were acetylene, vinyl bromide, methane, ethane, ethene and acetaldehyde. The kinetics of decomposition of 2-bromoethanol was simulated using a model containing 47 elementary reactions and 28 species in the temperature range of 910-1102K at 10K intervals. This scheme was later reduced to 32 reactions and 27 species using sensitivity analysis illustrating the relative importance of different kinds of reactions during the pyrolysis. This mechanism was validated by comparison to the shock tube measurements. The observed agreement is satisfactory between experimental and modeling results for the distribution of all the six reaction products with the accuracy of ±2%. The fundamental goal is to obtain the rate coefficient for the gas phase unimolecular HBr and H_2O elimination reactions from 2-bromoethanol. The possibilities of the direct HOBr elimination along with C-Br bond fission have been included to account for the formation of ethene. The formation of CH_4 and C_2H_6 was explained by the decomposition of vibrationally excited acetaldehyde. The first order overall thermal decomposition rate coefficient derived by using the Arrhenius expression is $10^{14.1\pm0.2}$ exp $[-(55.7\pm1.1)/(RT)]$ s^{-1}. The experimental rate coefficient for HBr

elimination is $10^{13.5\pm0.3}$ exp [(-53.4$\pm$1.4)/ (RT)] s^{-1}and that for the H_2O elimination is $10^{14.5\pm0.5}$ exp [-(66.5$\pm$2.2)/(RT)] s^{-1} where the activation energies are given in kcal/mol. This chapter also reports the HF, MP2 (FULL) and DFT computations that have been carried out to obtain the moment of inertia and frequencies of vibration of the reactant and the transition state to evaluate TST fitted A and E_a. Hindered and free rotor calculations have been performed for low frequency C-C and C-O bond torsional mode to obtain a better agreement with the experimental results. Present study has revealed both experimentally and theoretically for HBr elimination that the bromine, chlorine and fluorine substitution lead to an increase in E_a accounting for β-substitution effect, however, OH substitution does not. For H_2O elimination the Br substitution does not bring about significant variation but F substitution does increase the E_a. The higher level CBS-QB3 calculations for HBr elimination overestimates the *k*, however, underestimates for H_2O. Comparisons of the branching ratios for the HX, H_2O and HOX elimination reactions of haloethanols have also been performed. In this chapter, we have reported comparison of the overall thermal decomposition kinetics of three haloethanols.

IV.2. Introduction

The studies of halogenated alcohols have attracted great attention realizing their importance in the atmospheric and combustion chemistry.[1] The first order gas phase kinetics of thermal decomposition of 1, 1- and 1, 2-dibromoethanes in the static system at 415.5°C was studied by the Maccoll et al. in 1971.[2] The reaction observed in each case only HBr elimination leading to vinyl bromide. Will the thermal decomposition of 2-bromoethanol (BEOH) show unimolecular elimination of H_2O at higher temperatures?

With this question in mind, shock tube studies on BEOH have been performed in our laboratory. However, in the past, there have been many reports available on BEOH which includes the thermal decomposition of BEOH on metal surfaces like Cu (100) reported by Chang et al. where they identified the various possible surface intermediates generated from BEOH decomposition.[3] The identification of such intermediates helps in understanding the partial and selective oxidation of hydrocarbons and the deoxygenation of alcohols. Durig's group have reported infrared spectroscopic studies of BEOH for the assignment of vibrational, conformational and structural parameters.[4] Photodissociation of BEOH at 193 nm have been carried out by Hinsta et al. where they observed two dissociation channels i.e. primary dissociation by elimination of bromine atom to give C_2H_4OH radical which then undergo secondary dissociation to produce C_2H_4 and OH.[5] IR photolysis of BEOH in solid Argon matrices was studied by Hoffmann et al. where they found the quantum yield distribution for the photoisomerization of BEOH.[6] Flash vacuum thermolysis of BEOH have also been performed by Jenneskens et al. which resulted in the formation of α-bromoethylether via the formation of 1-bromoethanol.[7]

In fact, there have been many investigations both experimental and theoretical in the recent past on the kinetics of HBr elimination that includes kinetic study on the pyrolysis of vinyl bromide, performed by Laws et al. This study shows the predominant molecular elimination of HBr at higher temperatures.[8] The HX elimination and DX elimination from CH_3CH_2X and CD_3CD_2X systems respectively had also been reported by McGrath et al. where they found that 1,2- HX elimination barriers are 62.7 ± 0.6 kcal/mol for chloroethane and 60.7 ± 0.6 kcal/mol for bromoethane at QCISD/cc-pVDZ level of theory.[9] The studies on thermal gas phase decomposition of 2-bromopropene also

171

show the elimination of HBr as the only decomposition route to give propyne (E_a= 49.7 kcal/mol) as reported by Nisar et al. [10] Similar evidence of HBr elimination as the sole mode of decomposition was observed by King et al. during their studies on the thermal decomposition of bromocyclobutane (E_a= 52.0 kcal/mol). [11] Zou et al. have reported the photodissociation of bromoform at 248nm where HBr elimination is one of the secondary photodissociation processes from $CHBr_2$ radicals which were generated in the primary channel. [12]

Also, there are reports available in the literature both experimental and theoretical on the kinetics of H_2O elimination reaction.[13-16] The E_a for the elimination of H_2O from n-butanol to give butane has been found to be 67 kcal/mol computationally by Simmie et al. in their studies on the gas phase chemistry of enols.[13] Kinetic work on t-butyl alcohol (TBA) reported by Lewis and his group using a single-pulse shock tube over the temperature range 920-1175 K provided the Arrhenius parameters; log A=14.6 and E_a=66.2 kcal/mol. [14] This result was later showed to be matching with that obtained by Kalra et al. in their studies on the decomposition of TBA involving the determinations of deuterium kinetic isotope effects and DFT calculations to define the transition structure for the reaction and also k_H/k_D ratio.[15] The chemical activation experiment by Setser et al. have shown the threshold energies of unimolecular 1,2-H_2O elimination from $CH_2ClCH_2CH_2OH$ and $CF_3CH_2CH_2OH$ to be 59 and 62 kcal/mol respectively.[16] Recently, the kinetics of H_2O elimination from the ethyl alcohol have been reported experimentally using shock tube technique by Lin et al.[17]

However, to the best of our knowledge, the high temperature gas phase kinetics of the BEOH have never been investigated in the past which provides the best example for

the study of kinetics of both HBr and H_2O elimination reaction from the same molecule. Hence, thermal decomposition study of 2-bromoethanol was performed in our laboratory both experimentally and theoretically. This study will certainly provide a better insight into the β-substitution effect. In fact, among the haloethanols the articles on the pyrolysis of 2-chloroethanol[18] and 2-fluoroethanol[19] have been published from our laboratory by Arunan et al. using the single pulse shock tube elucidating Arrhenius parameters for the unimolecular HX (F, Cl) and H_2O elimination reactions as predominant channels including reaction mechanism of the thermal decomposition in the temperature range of investigation.

The plausible reaction mechanism has been proposed to explain the formation of different products for the thermal decomposition of the BEOH. This mechanism was validated by comparison to experimental shock tube results. The sensitivity analysis was also performed to understand the importance of the different elementary reactions in the mechanism. Finally, the major objective of this study was to estimate both experimental and theoretical Arrhenius parameters for the two elementary unimolecular elimination reactions i.e. 1,2-HBr and 1,2-H_2O from BEOH at high temperature. These kinetic and modeling data can provide better insight into the mechanism of thermal decomposition of BEOH.

IV.3. Experimental section

IV.3.A. Experimental details

Details of the shock tube facility used for the thermal decomposition study of BEOH are explained in the previous chapter. In this chapter, details specific to BEOH experiments have been mentioned. The Aluminum shock tube was heated to 70^0C with the variation of $\sim2^0C$. The reaction mixture loaded in shock tube contains 0.7% mixture of 2-bromoethanol in argon. The initial pressure used was in the range of 500 to 590 torr. The shock waves were generated by pressure bursting of the aluminum diaphragm of different grooves with helium as the driver gas to obtain the different temperature in the range of 910-1102K. The pressure behind the reflected wave was varied between 9 and 14atm in all runs. The observed cooling rates were found to be approximately 4×10^{-5} K/s. The reaction dwell time observed was typically in the range of 1120-1330 μs with an accuracy of ±3%. The sample section of the shock tube was connected to the gas chromatograph and 0.5mL of the mixture was injected through an online sampling valve. The Porapack Q column of 6 ft length was used for quantitative analysis of the reaction products with gas chromatograph. The gas chromatographic analyses of post-shock mixtures were performed at a column oven temperature of $80-140^0C$ having the temperature programming rate of 10^0C min^{-1} with flame ionization detector kept at 160^0C. The flow rate of carrier gas, nitrogen, was maintained at 22mL min^{-1} in all runs. Products were identified by comparing the retention times of the known pure authentic samples with those of unknown. The standard samples were used to determine the sensitivities of various reaction products to flame ionization detector. The typical gas

chromatogram of 0.7% bromoethanol shocked to 1092K has been shown in the Figure

IV.1. The FT-IR Spectra of post shocked mixture confirming the presence of all reaction

products were recorded for qualitative analyses using the Thermo Nicolet-870 model.
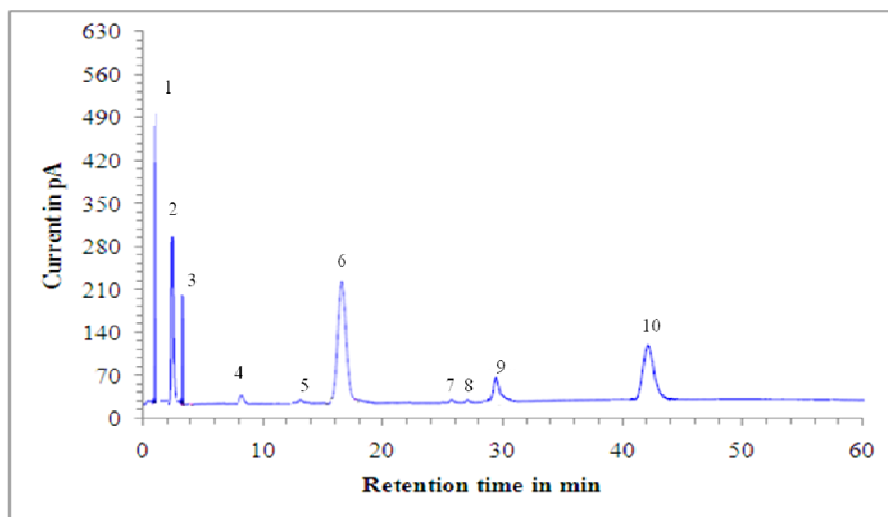
Figure IV.1.   A Gas chromatograph of the post shock mixture for the thermal

decomposition of the 0.7% mixture of 2-bromoethanol in argon on the 6 feet long

porapak-Q column recorded using the FID: (1) methane; (2) ethene; (3) ethane; (4)

acetylene; (5) propylene; (6) acetaldehyde; (7) methyl bromide; (8) ethyl bromide; (9)

vinyl bromide; (10) 2-bromoethanol. The reflected shock temperature is 1096K.

IV.3.B. Materials and analysis

BEOH was received from fluka specified to be 95% pure was used for sampling.

Before making the sample freeze-pump-thaw method was used many times for degassing

and further purification. Gas chromatographic analyses of the post shock gas mixture was

carried out using the HP 6890 gas chromatograph with FID. FT-IR spectra of the

compounds were recorded using Thermonicolet (Nexus 870) spectrometer for qualitative

analysis. The Porapack Q column used for separation of all the products was manufactured by the Chromatopak Analytical Instrumentation Pvt. Ltd, Mumbai, India. The FID sensitivity was evaluated for each of the compound with standard samples in order to determine the concentrations of all the species involved. These samples were bought from different sources. We bought acetaldehyde from Merck chemicals. Vinyl bromide was from the sigma aldrich. Ethyl bromide and methyl bromide were from sigma aldrich. Methane and ethane were supplied by the Bhoruka Gas Agency. Ethene was bought from hydrogas. The gases used in gas chromatogram analysis are from Bhoruka gases, India. These gases are argon, helium, oxygen, and hydrogen. All these gases are of high purity (UHP grade 99.999%).

IV.3.C. Theoretical details

The optimization of both equilibrium ground state and transition state structures for H_2O and HBr elimination reaction from BEOH have been performed at HF, MP2 (FULL) and DFT(B3LYP) levels of theory with the standard 6-31G*, 6-31G**, and 6-311++G** basis sets. The transition states are characterized by one imaginary frequency corresponding to the reaction coordinate. These calculations were done for estimating the pre-exponential factor and activation energy for H_2O and HBr reactions using transition-state theory. These theoretically estimated rate constants were then employed for comparison with experimentally calculated rate coefficient of elimination reactions under consideration. The zero point energies and vibrational frequencies were used without the scaling in these calculations. The transition state for HOBr elimination was also optimized successfully at HF, MP2 (FULL), B3LYP level with 6-311++g** basis

set. The activation energy of HOBr elimination from BEOH was compared with that of HOCl elimination from CEOH for which calculation were carried out at MP2/6-311++g** level of theory as discussed in the previous chapter. Optimizations of all the five conformer have been carried out to find out the minima and will be described in detail next. The calculation of enthalpy of formation was performed using isodesmic reaction for BEOH at B3LYP/6-311++g** level in order to estimate the internal energy of the products. The C-C, C-X, C-H, and H-X (O/Br) bond distances and percent changes calculated for the transition states for HBr and H_2O elimination reactions from BEOH have been discussed. For the verification of three transition states, intrinsic reaction coordinate calculations have also been carried out.

IV.4. Experimental results and discussions

27 experiments have been performed behind the reflected shocks with 2-bromoethanol diluted in argon between 910 and 1102 K. The total pressures were varied between 9 and 14 atm. The post-shock mixtures were analyzed with GC and FT-IR. Table IV.1 contains the information about the distribution of all the reaction products and the experimental conditions i. e. P_5, T_5 and dwell time. The notation P_5 and T_5 implies the pressure and temperature behind the reflected shock wave respectively.

The rate constant for the overall decomposition of 2-bromoethanol in the gas phase was calculated using the expression for the first order rate constant. The expression for which is given below.

$$k_{total} = -\ln\{[C_2H_4BrOH]_t / [C_2H_4BrOH]_0\}/t \qquad (1)$$

Table IV.1. Summary of the experimental conditions and distribution of the reaction products for the thermal decomposition of the 2-bromoethanol

S. No.	$T_5(K)$	P_5 (atm)	Dwell Time in µs	$[BEOH]_t/[BEOH]_0$	$[C2H2]_t/[BEOH]_0$	$[C2H4]_t/[BEOH]_0$	$[C2H6]_t/[BEOH]_0$	$[CH2CHBr]_t/[BEOH]_0$	$[CH3CHO]_t/[BEOH]_0$	$[CH4]_t/[BEOH]_0$
1	910	8.9	1240	0.993901	0.000000	0.000709	0.000000	0.000031	0.005345	0.000014
2	916	9.1	1220	0.992347	0.000000	0.000570	0.000000	0.000041	0.007023	0.000019
3	920	9.2	1145	0.992575	0.000000	0.001231	0.000000	0.000047	0.006079	0.000067
4	923	9.7	1130	0.988824	0.000000	0.002903	0.000000	0.000074	0.008100	0.000098
5	948	10.1	1220	0.983434	0.000000	0.004973	0.000014	0.000114	0.011305	0.000160
6	961	8.7	1260	0.969873	0.000000	0.003787	0.000096	0.000552	0.025531	0.000160
7	967	10.3	1310	0.958364	0.000000	0.009025	0.000132	0.000429	0.031927	0.000122
8	972	10.5	1220	0.953721	0.000000	0.008101	0.000113	0.000671	0.036939	0.000455
9	985	10.0	1290	0.906767	0.000000	0.008001	0.000310	0.000612	0.083607	0.000703
10	993	9.4	1220	0.922533	0.000000	0.010175	0.000451	0.001102	0.064741	0.000998
11	1005	11.2	1195	0.874995	0.000000	0.012021	0.000193	0.000761	0.111859	0.000171
12	1009	11.2	1220	0.879335	0.000000	0.025158	0.001986	0.001150	0.091011	0.001359
13	1017	11.5	1220	0.850629	0.000000	0.036290	0.002492	0.001806	0.107696	0.001087
14	1025	11.4	1305	0.824237	0.000000	0.010946	0.003189	0.002091	0.156492	0.003035
15	1028	11.7	1265	0.810299	0.000054	0.035266	0.004644	0.001440	0.146145	0.002152
16	1039	12.0	1220	0.691785	0.000123	0.081082	0.007026	0.003710	0.210252	0.006022
17	1048	12.8	1140	0.666486	0.000092	0.066272	0.006057	0.007011	0.241067	0.013015
18	1053	13.0	1220	0.685896	0.000212	0.095920	0.009236	0.004070	0.191465	0.013201
19	1058	12.3	1120	0.613328	0.000283	0.092305	0.013056	0.005040	0.254584	0.021403
20	1059	12.3	1320	0.601447	0.000256	0.120793	0.011648	0.007240	0.234890	0.023725
21	1067	12.6	1260	0.597217	0.000396	0.111105	0.019502	0.005662	0.246897	0.019220
22	1071	13.1	1280	0.476971	0.000418	0.172620	0.027193	0.004650	0.291837	0.026311
23	1075	12.9	1220	0.501490	0.000495	0.155024	0.022723	0.009093	0.277970	0.033205
24	1081	13.7	1229	0.494340	0.000653	0.133121	0.035704	0.005961	0.291187	0.039035
25	1084	13.1	1250	0.406783	0.000861	0.154718	0.041953	0.009180	0.338481	0.048025
26	1092	13.8	1330	0.358360	0.000897	0.184801	0.048403	0.011001	0.319308	0.077230
27	1102	14.1	1220	0.247830	0.001135	0.219219	0.061102	0.011701	0.357588	0.101025

Here the t corresponds to dwell time and $[C_2H_4BrOH]_t$ & $[C_2H_4BrOH]_0$ represents the final and initial concentration of the 2-bromoethanol respectively. The rate parameters A and E_a, in turn, were evaluated from the intercept and the slope of this straight line respectively. The straight of this plot indicates the overall thermal decomposition of 2-bromoethaol is of the first order. The value of the rate coefficient for overall decomposition of 2-bromoethanol was found to be $10^{14.08\pm23}$exp $[-(55.66\pm1.07)/(RT)]$ s^{-1}.The E_a is expressed in terms of the kcal/mol. Figure IV.2 shows the Arrhenius plot for the overall thermal decomposition of the BEOH in temperature range of investigation. The rate coefficient for the unimolecular elimination of H_2O and HBr was found to be 16.5s^{-1} and 6.84×10^2 s^{-1}at 1100K using our experimental result.
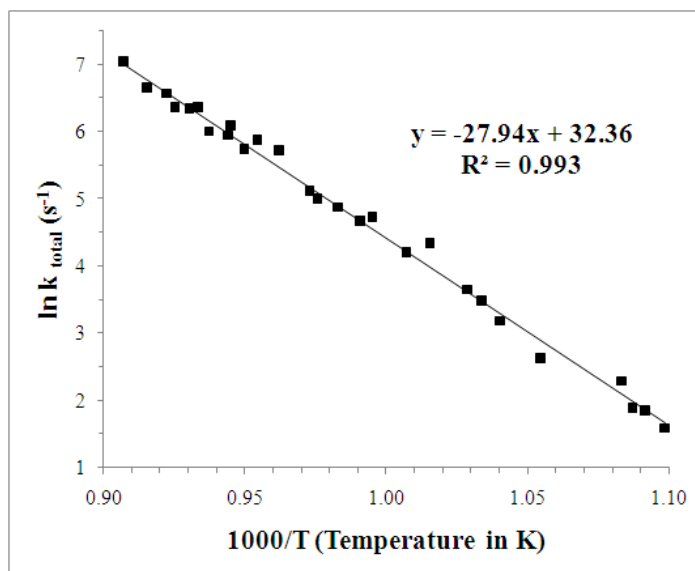
Figure IV.2. Arrhenius plot for the first order overall thermal decomposition of the 2-bromoethanol.

The Arrhenius plot for the unimolecular elimination of H_2O and HBr elimination from BEOH have been shown in the Figure IV.3 and IV.4.
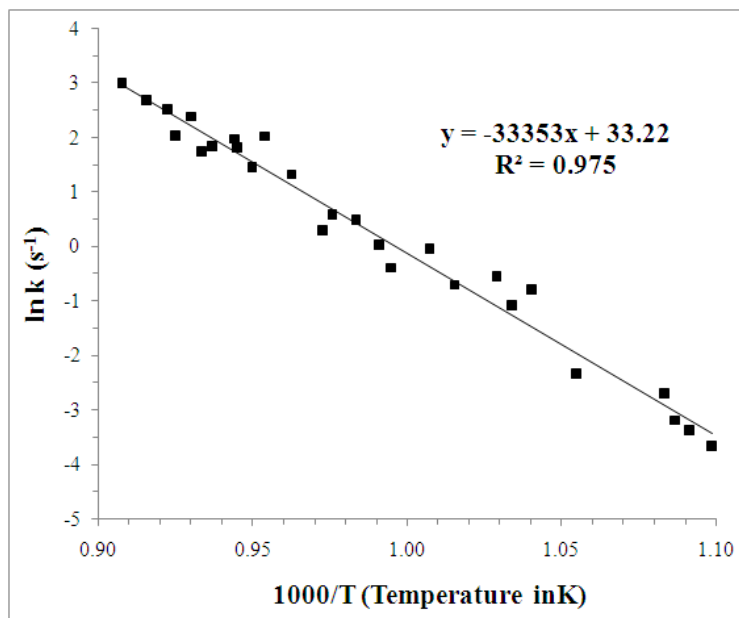
Figure IV.3. Arrhenius Plot for the unimolecular elimination of H_2O from 2-bromoethanol.
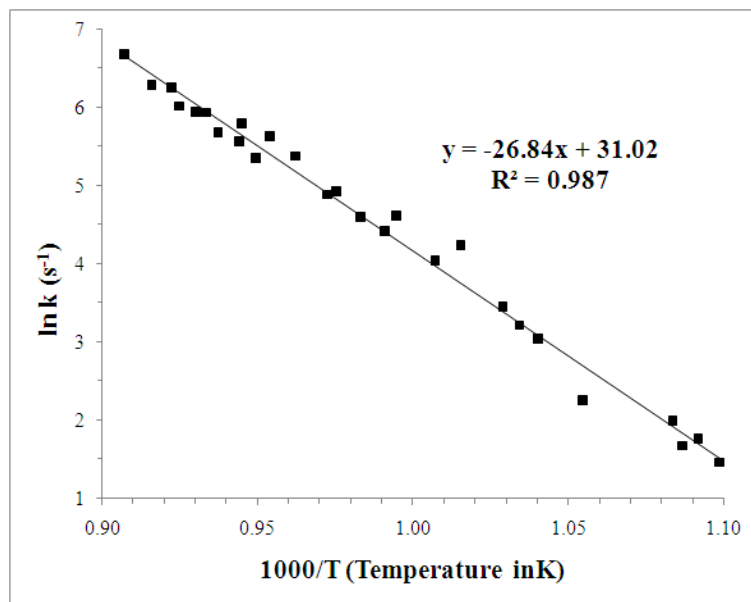
Figure IV.4. Arrhenius Plot for the unimolecular elimination of HBr from 2-bromoethanol.

The experimental results were described using the reaction scheme which contains unimolecular elimination reactions, unimolecular thermal decompositions of radical intermediates, bimolecular transfer reactions, abstractions, dissociation of stable reactant molecule. and radical-radical recombination reactions. The rate coefficients of most of the reactions were taken from literature and NIST chemical kinetic database for simulating the profiles of products. The rate constants listed in the Table IV.2 are given as either $k = A \exp(-E_0/RT)$ or $k = A\,T^n \exp(-E_0/RT)$ where the units are expressed in terms of kcal, mol^{-1}, cm^3, and K. A reaction scheme containing 28 species and 47 elementary reactions was composed in order to account for the formation of distribution of reaction products for the decomposition of 2-bromoethanol has been compiled in the Table IV.2. The references of all the reaction used in the kinetic mechanism have also been included in the in the Table IV.2. Among the 47 reactions that were introduced into kinetic scheme, 18 were unimolecular and 29 were bimolecular. The entire rate coefficients used in our mechanism are at high temperatures and pressures. The simulation was done within the experimentally determined reaction times i.e. 1.3ms. The consumption of all the radicals involved in the reaction mechanism was found to be complete within the reaction time. The chemical kinetic mechanism includes experimentally determined expression for rate constant of the H_2O and HBr elimination reaction and the rate expressions for HOBr elimination was derived from fitting to the complex mechanism in our simulation. The pre-exponential factor for reactions 4 and 35 were taken from available literature by comparison to similar reactions where as the activation energy was evaluated. The sensitivity analysis method was used to find the effect of different chemical reactions in our chemical kinetic mechanism on the

distribution of various reaction products. It was found that there are 12 reactions among 47 that have no appreciable influence on the distribution of any of the chemical species. This is attributed to the very low concentrations of the ethyl, methylene and other radicals involved in these chemical reactions. Hence, these chemical reactions were excluded from the kinetic scheme. It was verified by performing the simulations with the reduced kinetic mechanism that successfully reproduces the quantitative experimental profiles similar to the complete kinetic model containing 47 reactions within approximately 1-2%. The rate expression of the kinetic mechanism that includes 35 reactions and 26 species are given in the Table IV.5.

Around 75 percent of the 2-bromoethanol was found to be consumed at the highest temperature of the experiment and dwell times of our experiments. However, it was 28% and 65% in case of 2-fluoroethanol and 2-chloroethanol respectively in the temperature range of their investigation. The distributions in terms of logarithmic normalized concentrations of all the reaction products as a function of temperature have been shown in the Figure IV.5. The formation of CO was observed qualitatively under our experimental condition that is produced by the decomposition of the formyl radicals. The qualitative analysis of CO in post shock mixture was done using FT-IR spectroscopy. Carbon monoxide and hydrogen was not observed quantitatively in our analysis as it needs thermal conductivity detector. In fact the production of H_2 has also been predicted in our numerical simulations and it is around 4.2%.

Table IV.2. Reaction scheme proposed for the thermal decomposition of 2-bromoethanol.

S. No.	Reactions	A	n	E_a	k (1100K)	References
R1	$BrC_2H_4OH \rightarrow CH_3CHO + HBr$	3.70×10^{13}	0.00	53.42	6.84×10^2	Present study
R2	$BrC_2H_4OH \rightarrow CH_2CHBr + H_2O$	2.96×10^{14}	0.00	66.47	1.65×10^1	Present study
R3	$CH_2CHBr \rightarrow C_2H_2 + HBr$	1.70×10^{15}	0.00	65.58	1.42×10^2	20
R4	$BrC_2H_4OH \rightarrow Br + C_2H_4OH$	5.01×10^{15}	0.00	66.66	2.56×10^2	Present study
R5	$BrC_2H_4OH \rightarrow C_2H_4 + HOBr$	5.21×10^{15}	0.00	72.00	2.29×10^1	Present study
R6	$C_2H_4OH \rightarrow C_2H_4 + OH$	6.19×10^{11}	0.00	23.65	1.19×10^7	21
R7	$CH_3CHO \rightarrow CH_3 + CHO$	9.00×10^{13}	0.00	57.20	3.54×10^2	22
R8	$CH_3CHO + H \rightarrow H_2 + CH_2CHO$	2.40×10^1	3.50	5.17	9.88×10^{10}	23
R9	$CH_3CHO + H \rightarrow H_2 + CH_3CO$	8.70×10^{13}	0.00	4.20	1.26×10^{13}	24
R10	$CH_3CO \rightarrow CO + CH_3$	8.55×10^{14}	0.00	27.40	2.94×10^9	25
R11	$CH_2CHO \rightarrow CH_2CO + H$	1.45×10^{15}	-0.15	45.61	4.08×10^5	26
R12	$CH_2CO + H \rightarrow CO + CH_3$	3.01×10^{12}	1.45	2.78	2.16×10^{16}	26
R13	$CH_3 + CHO \rightarrow CH_4 + CO$	2.21×10^{14}	0.00	0.00	2.21×10^{14}	27
R14	$CHO \rightarrow CO + H$	2.04×10^{13}	0.66	14.87	2.25×10^{12}	28
R15	$2\ CH_3 \rightarrow C_2H_6$	2.30×10^{13}	-0.54	0.14	4.91×10^{11}	29
R16	$C_2H_5 \rightarrow C_2H_4 + H$	3.06×10^{10}	0.95	36.94	1.02×10^6	30
R17	$C_2H_5 + H \rightarrow C_2H_6$	1.35×10^{14}	0.16	0.00	4.14×10^{14}	31
R18	$C_2H_5 + CHO \rightarrow C_2H_6 + CO$	1.20×10^{14}	0.00	0.00	1.20×10^{14}	27
R19	$2\ CH_3 \rightarrow H + C_2H_5$	8.77×10^{12}	0.10	10.61	1.35×10^{11}	32
R20	$H + C_2H_4 \rightarrow C_2H_3 + H_2$	5.00×10^{15}	0.00	23.00	1.30×10^{11}	33
R21	$C_2H_3 + H \rightarrow C_2H_4$	1.52×10^{13}	0.00	98.30	3.81×10^{-7}	34
R22	$CH_2CO \rightarrow CO + CH_2$	3.00×10^{14}	0.00	70.94	2.14	35
R23	$2\ CH_2 \rightarrow C_2H_4$	1.00×10^{12}	0.00	0.00	1.00×10^{12}	36
R24	$C_2H_4 + C_2H_5 \rightarrow C_2H_6 + C_2H_3$	6.32×10^2	3.13	18.01	5.36×10^8	23
R25	$C_2H_3 + CHO \rightarrow C_2H_4 + CO$	9.04×10^{13}	0.00	0.00	9.04×10^{13}	27
R26	$CH_3 + H \rightarrow CH_4$	5.30×10^{18}	0.00	0.00	5.30×10^{18}	37
R27	$C_2H_6 + H \rightarrow CH_4 + CH_3$	5.40×10^1	0.00	11.63	2.59×10^{-1}	38
R28	$CH_4 \rightarrow CH_3 + H$	1.03×10^{16}	0.00	104.00	1.88×10^{-5}	39
R29	$C_2H_6 \rightarrow C_2H_4 + H_2$	6.93×10^{16}	0.00	82.07	2.99	40
R30	$C_2H_4 + H_2 \rightarrow C_2H_5 + H$	1.02×10^{13}	0.00	68.16	2.61×10^{-1}	27
R31	$2\ C_2H_4 \rightarrow C_2H_5 + C_2H_3$	4.82×10^{14}	0.00	71.54	2.62	27
R32	$C_2H_4 \rightarrow C_2H_3 + H$	2.00×10^{16}	0.00	110.00	2.33×10^{-6}	41
R33	$C_2H_6 \rightarrow 2\ CH_3$	1.15×10^{33}	-13.14	102.00	5.73×10^{-28}	42
R34	$C_2H_5 + H_2 \rightarrow C_2H_6 + H$	1.41×10^{12}	0.00	13.00	3.61×10^9	43
R35	$BrC_2H_4OH \rightarrow OH + C_2H_4Br$	2.01×10^{17}	0.00	82.51	7.09	Present study
R36	$C_2H_4Br \rightarrow C_2H_4 + Br$	6.81×10^{10}	0.00	6.50	3.44×10^9	44
R37	$2\ Br \rightarrow Br_2$	1.48×10^{14}	0.00	1.70	6.78×10^{13}	45
R38	$OH + Br \rightarrow HBr + O$	2.75×10^{12}	0.00	17.33	9.63×10^8	45
R39	$HBr + O \rightarrow OH + Br$	3.49×10^{12}	0.00	2.98	8.88×10^{11}	46
R40	$C_2H_3 \rightarrow C_2H_2 + H$	1.15×10^{23}	-7.50	45.51	1.50×10^{-9}	47
R41	$C_2H_3 + H_2 \rightarrow C_2H_4 + H$	2.04×10^{10}	2.56	5.03	1.24×10^{17}	48
R42	$C_2H_3 + CH_2 \rightarrow C_2H_2 + CH_3$	1.81×10^{13}	0.00	0.00	1.81×10^{13}	27
R43	$2\ CH_2 \rightarrow C_2H_2 + H_2$	1.58×10^{15}	0.00	11.94	6.57×10^{12}	49
R44	$C_2H_2 + CH_3 \rightarrow CH_4 + C_2H$	1.81×10^{11}	0.00	17.29	6.46×10^7	27
R45	$C_2H_5 + C_2H \rightarrow C_2H_4 + C_2H_2$	1.81×10^{12}	0.00	0.00	1.81×10^{12}	27
R46	$H_2 + C_2H \rightarrow H + C_2H_2$	3.36×10^{11}	2.39	0.86	4.21×10^{18}	50
R47	$C_2H_6 + C_2H \rightarrow C_2H_2 + C_2H_5$	3.61×10^{12}	0.00	0.00	3.61×10^{12}	27

IV.4.A. Major Channels

IV.4.A.1. HBr and H$_2$O elimination

The unimolecular eliminations of HBr and H$_2$O are found to be the major channel that account for the formation of acetaldehyde and vinyl bromide respectively. Experimentally determined rate coefficients of these two reaction channels were used in the modeling to explain their distribution. The concentration of vinyl bromide is almost 29.83 times smaller than that of the acetaldehyde. This is due to their different values of the Arrhenius parameters as shown below.

Br-CH$_2$CH$_2$-OH → CH$_3$CHO+ HBr $k_1=3.70\times10^{13}\exp[(-53.42\times10^3/(RT)]$ s^{-1} R1

Br-CH$_2$CH$_2$-OH → CH$_2$=CH-Br + H$_2$O $k_2=2.96\times10^{14}\exp[(-66.47\times10^3/(RT)]$ s^{-1} R2
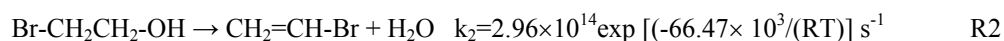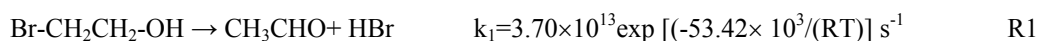
Reactions which were considered to explain the production of the minor products were found to have minor effect on concentration profile of acetaldehyde and vinyl bromide.

Table IV.3. Comparison of the experimental kinetic parameters of HX (X= F, Cl, Br), H$_2$O and HOX unimolecular elimination reactions evaluated at 1100K

Molecule*	HX			H$_2$O			HOX		
	A	E_a	k (s^{-1})	A	E	k (s^{-1})	A	E_a	k (s^{-1})
FEOH	1.50×10^{13}	59.45	2.31×10^1	2.00×10^{14}	69.69	2.84	2.01×10^{17}	85.91	1.72
CEOH	1.92×10^{14}	57.46	7.35×10^2	7.00×10^{14}	67.81	2.35×10^1	5.46×10^{17}	81.53	3.49×10^1
BEOH	3.70×10^{13}	53.42	8.99×10^2	2.96×10^{14}	66.47	1.84×10^1	5.21×10^{15}	72.02	2.57×10^1

*Here, FEOH, CEOH and BEOH stand for fluoroethanol, chloroethanol and bromoethanol respectively.

Table IV.4. Experimentally determined product branching ratios for the kinetics of HX (X= F, Cl, Br), H_2O and HOX unimolecular reactions at 1100K for haloethanols

Reactions of 2-fluoroethanol	Branching ratio (%)	Reactions of 2-chloroethanol	Branching ratio (%)	Reaction of 2-bromoethanol	Branching ratio (%)
HF	83.51	HCl	92.63	HBr	95.32
H_2O	10.28	H_2O	2.96	H_2O	1.95
HOF	6.21	HOCl	4.40	HOBr	2.73

Comparison of the experimental kinetic parameters of HX (X= F, Cl, Br), H_2O and HOX unimolecular elimination reactions evaluated at 1100K have been given in the Table IV.3. This table indicates that the both A and E_a increases from HX to HOX through H_2O. To the best of our knowledge, the branching ratios for three HX, H_2O and HOX channels leading to CH_3CHO, CH_2CHX and C_2H_4 have been quantified for the first time for haloethanols. The high temperature product branching ratio for the major channel HX elimination from 2-fluoroethanol, 2-chloroethanol and 2-bromoethanol leading to CH_3CHO was determined to be 83.51, 92.63 and 95.32 at 1100K as listed in Table IV.4 above. This implies that the HF elimination is slower than the HCl which, in turn, is slower than HBr. The values of branching ratios for H_2O elimination channel were 10.28, 2.96 and 1.95, respectively indicating that the significant amount of vinyl fluoride is produced as compared to vinyl chloride and bromide. The values of branching ratios for minor HOX elimination channel were 6.21, 4.40 and 2.73, respectively indicating the increase in rate coefficients of HOX pathway on going from 2-fluoroethanol to 2-bromoethanol. The branching ratio of HOCl as well as H_2O elimination channels are decreasing because of the increase in the rate coefficients of the HCl elimination on going from fluoroethanol to bromoethanol.

IV.4.B. Minor channels

IV.4.B.1.Ethane

The important reactions contributing in the formation of the ethane is R7. In this reaction, breaking of C-C bond in the acetaldehyde which is "chemically active species" leads to the formation of methyl radical and formyl radical.

$CH_3CHO \rightarrow CH_3 + CHO$ $k_7 = 9.00 \times 10^{13} exp\ [(-57.20 \times 10^3/(RT)]\ s^{-1}$ R7

It was found that the concentration profile of C_2H_6 is underestimated using the proposed value for the rate constant of reaction R7 that were used to describe the pyrolysis mechanism of ethylene oxide behind the reflected shock waves by Lifshitz et al.[22] However, the CH_3CHO that is produced by the isomerization of CH_2=CHOH is "chemically active" and the threshold energy for reactions R7 is expected to be less. The activation barrier of the reaction R7 was reduced by 2.0 kcal/mol than the reported value in order to best fit our data.

The enthalpy of formation for CH_3CHO (-39.7 kcal mol^{-1}) is 10 kcal mol^{-1} less than that of CH_2=CHOH (-29.8 kcal mol^{-1}). The barrier for isomerization is estimated to be 55.1 kcal mol^{-1} at B3LYP/6- 311++G** level of theory. The enthalpy of formation of 2-bromoethanol at CCSD/cc-PVDZ level of theory was found to be -50.71 kcal/mol. The $BrC_2H_4OH \rightarrow CH_3CHO$ + HBr reaction is 2.7 kcal/mol exoergic at the B3LYP/6-311++G** level of theory. The activation energy for HBr elimination from 2-bromoethanol is determined to be 51.38 kcal/mol at B3LYP/6- 311++G** level. Hence, most of the vibrational energy could remain as internal energy in the acetaldehyde.
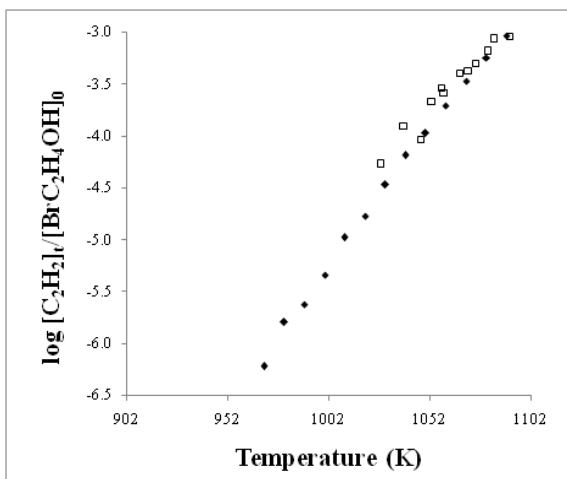
(a)
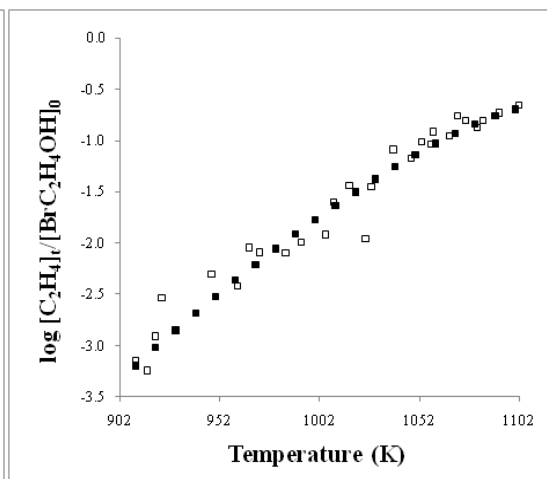
(b)
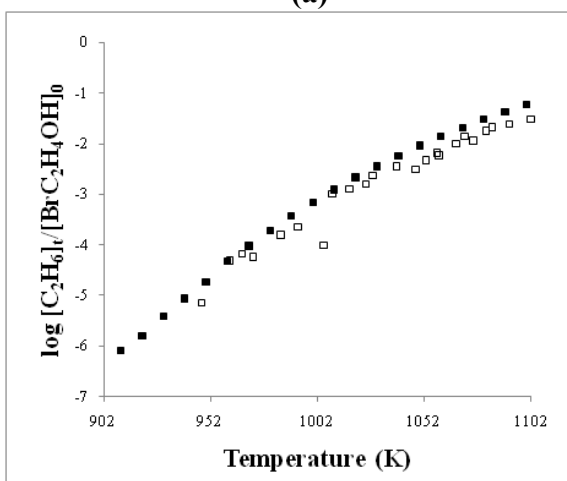
(c)
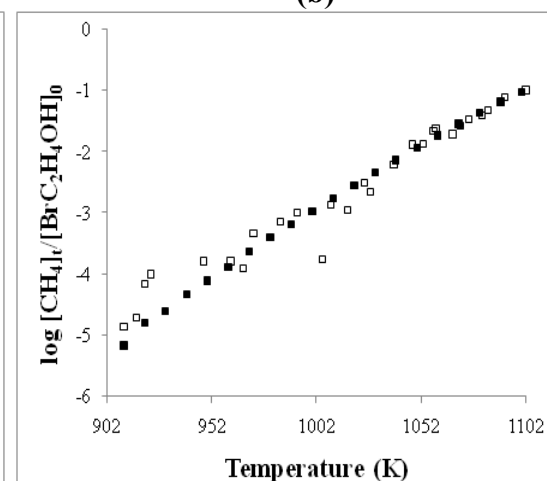
(d)
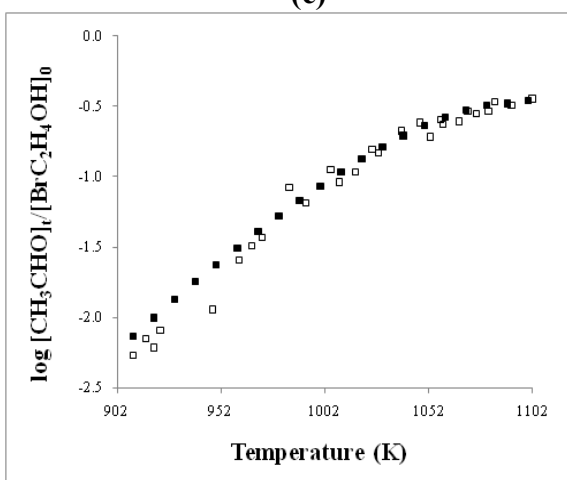
(e)
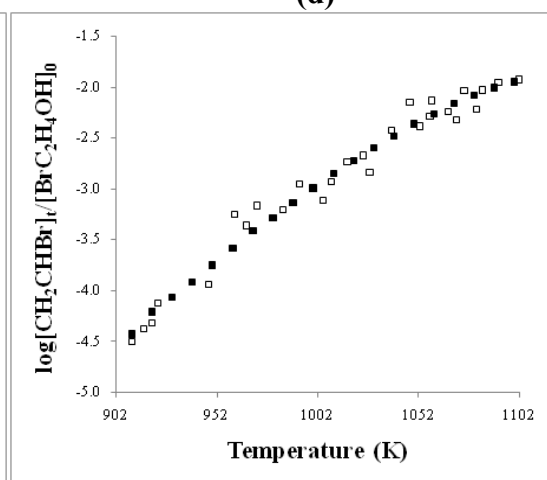
(f)

Figure IV.5. Experimental logarithmic normalized concentrations of the six reaction products plotted as a function of temperature. The open squares are the experimental concentrations and the filled squares are the model predicted values for which simulations were performed at 10K intervals in the temperature range of 910 to 1100K.
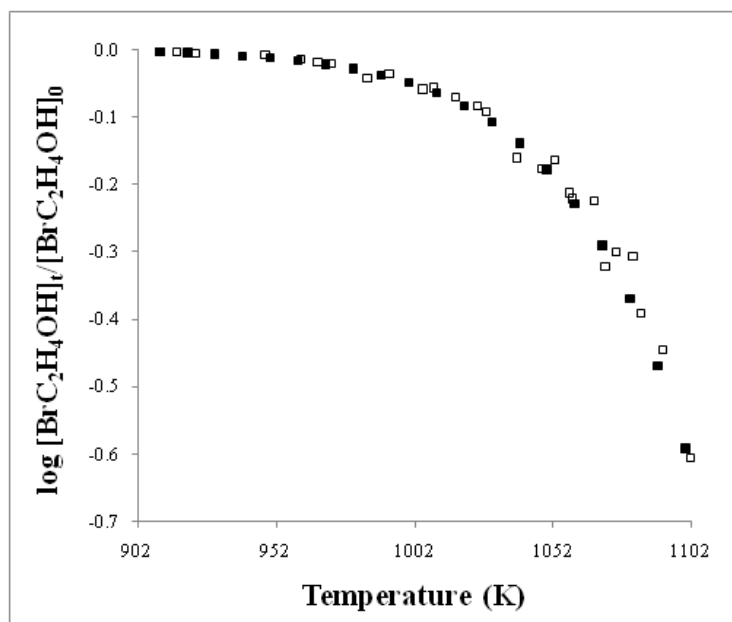
Figure IV.6. The total thermal decomposition of 2-bromoethanol plotted as a function of temperature. The open squares are the experimental concentrations and the filled squares represent the model predicted values where simulations were carried out at 10K intervals.

The formation of ethane was explained by the recombination of methyl radicals.

$$CH_3 + CH_3 \rightarrow C_2H_6 \quad k_{15} = 2.30 \times 10^{13} \ (T)^{-0.54} \exp{[(-0.14 \times 10^3 / (RT)]} \ cm^3mol^{-1}s^{-1} \qquad R15$$
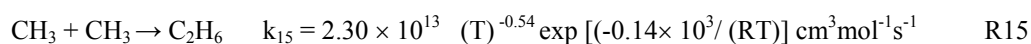
Reactions R17, R18, R24 and R34 also contribute to the formation of ethane.
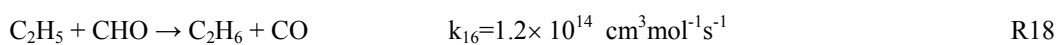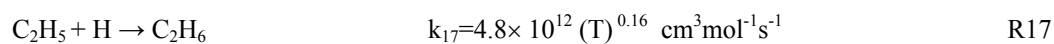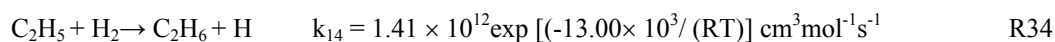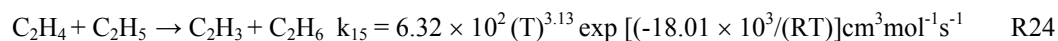
$$C_2H_5 + H \rightarrow C_2H_6 \qquad\qquad k_{17} = 4.8 \times 10^{12} \ (T)^{0.16} \ cm^3mol^{-1}s^{-1} \qquad\qquad R17$$

$$C_2H_5 + CHO \rightarrow C_2H_6 + CO \qquad k_{16} = 1.2 \times 10^{14} \ cm^3mol^{-1}s^{-1} \qquad\qquad R18$$

188

$C_2H_4 + C_2H_5 \rightarrow C_2H_3 + C_2H_6$ $k_{15} = 6.32 \times 10^2 (T)^{3.13} \exp[(-18.01 \times 10^3/(RT)]cm^3mol^{-1}s^{-1}$ R24

$C_2H_5 + H_2 \rightarrow C_2H_6 + H$ $k_{14} = 1.41 \times 10^{12} \exp[(-13.00 \times 10^3/(RT)] cm^3mol^{-1}s^{-1}$ R34

But their contribution to the total production of ethane is negligible because their production depends on the concentration of the ethyl radical which is very low. Ethane and methane are the secondary products in our temperature range of investigation. The ethene yields have been found to be 3.6 and 2.1 times greater than those of the ethane and methane respectively. The formation of ethane was observed in temperature range of 948-1102 K. It is clear from the Table IV.1 that the concentration of ethane which is a secondary product was found to be very low at lower temperatures. We observed the increasing concentration of ethane with rise in temperature. In case of 2-fluoroethanol ethane were found to be products only above 1100 K respectively. However, for 2-chloroethanol the ethane was observed above 950K. In fact, we did not observe ethane formation till 950K for 2-bromoethanol and its concentration was found to be significant only beyond this temperature.

IV.4.B.2.Ethene

The formation of ethene was explained through C-Br dissociation followed by C-OH bond dissociation. The pre-exponential factor of C-Br bond dissociation was taken from literature by comparison with similar reaction for which the activation energy was estimated. The C-Br bond dissociation energy calculated at DFT/6-311++G** level of theory is 66.70 kcal mol^{-1}. For this bond breaking reaction, the reference reaction used for the pre-exponential factor was $C_2H_5Cl \rightarrow C_2H_5 + Cl$. The C-Br bond dissociation energy

is lower than the activation energy determined using simulation for HOBr elimination reaction which is 72.00 kcal/mol. Therefore larger contribution to the production of ethene will be due to the reaction R29 and R30.

$BrC_2H_4OH \rightarrow Br + C_2H_4OH$ $k_4=5.01\times10^{15}exp\,[(-66.66\times 10^3/(RT)]\,s^{-1}$ R4

$C_2H_4OH \rightarrow C_2H_4 + OH$ $k_6=6.19\times10^{11}exp\,[(-23.65\times 10^3/(RT)]\,s^{-1}$ R6
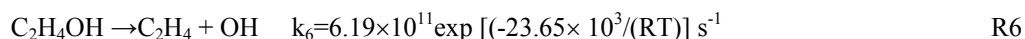
Therefore it is clear from our analysis that these C-Br followed by C-OH bond breaking reaction can account for larger C_2H_4 production than the C_2H_4 formation described by direct unimolecular elimination of HOBr from 2-bromoethanol in our reaction mechanism. This is also clear from the sensitivity analysis results which are described in detail at different temperatures in the next section. The rate constant determined by simulated fits for HOBr unimolecular elimination is given below.

$Br-CH_2-CH_2-OH \rightarrow C_2H_4 + HOBr$ $k_5 = 5.21 \times 10^{15} \exp\,[(-72.00 \times 10^3 / (RT)]\,s^{-1}$ R5
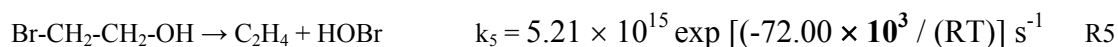
The barrier for HOF elimination from 2-fluoroethanol was found to be almost 14 kcal/mol higher than the HOBr elimination from 2-bromoethanol. However, the theoretically determined energy of activation at B3LYP/6-311++g** level of theory for HOBr elimination is 80.72 kcal/mol which is 8.72 kcal/mol higher than the value determined using simulations. However, there is no experimental evidence for HOBr elimination directly. Initially several reactions have also been included to explain the ethene production which can account for almost 2% of the overall ethene production. All these possibilities for its production have been described below.

$BrC_2H_4OH \rightarrow OH + C_2H_4Br$ $k_{18}=2.01\times10^{17}exp\,[(-82.51\times 10^3/ (RT)]\,s^{-1}$ R35

$C_2H_4Br \rightarrow C_2H_4 + Br$ $k_{18}=6.81\times10^{10} \exp\,[(-6.50\times10^3/ (RT)]\,s^{-1}$ R36
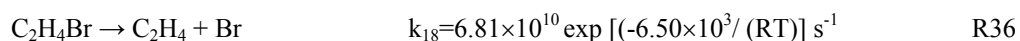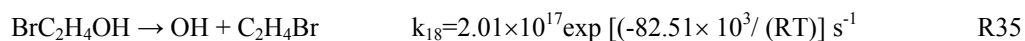
$C_2H_6 \rightarrow C_2H_4 + H_2$ $k_{18}=6.93\times10^{16}exp\ [(-82.07\times 10^3/ (RT)]\ s^{-1}$ R29

$C_2H_3 + CHO \rightarrow C_2H_4 + CO$ $k_{19} =9.04 \times 10^{13}\ cm^3mol^{-1}s^{-1}$ R25

$C_2H_5 \rightarrow C_2H_4 + H$ $k_{14} = 3.06 \times 10^{10}\ (T)^{0.95} exp\ [(-36.94\times 10^3/ (RT)]\ s^{-1}$ R16

$CH_2 + CH_2 \rightarrow C_2H_4$ $k_{19} =1.00 \times 10^{12}\ cm^3mol^{-1}s^{-1}$ R23

$C_2H_3 + H_2 \rightarrow C_2H_4 + H$ $k_{14} = 2.04 \times 10^{10}\ (T)^{2.56} exp\ [(-5.03\times 10^3/ (RT)]\ cm^3mol^{-1}s^{-1}$ R41

$C_2H_5 + C_2H \rightarrow C_2H_4 +C_2H_2$ $k_{19} =1.81 \times 10^{12}\ cm^3mol^{-1}s^{-1}$ R45

$C_2H_3 + CHO \rightarrow C_2H_4 + CO$ $k_{19} =9.04 \times 10^{13}\ cm^3mol^{-1}s^{-1}$ R25

In fact, we observed that these reactions had insignificant contribution about 1% to its formation which could not explain the experimentally determined concentration of ethene. Their contribution to the total production of ethene is negligible because their production depends on the concentration of the ethyl radical which is very low.

The following reaction has also been considered for the consumption of ethene.

$C_2H_4 + C_2H_4 \rightarrow C_2H_5 + C_2H_3$ $k_{18}= 4.82 \times 10^{14} exp\ [(-71.54\times10^3/ (RT)]\ cm^3mol^{-1}s^{-1}$ R31
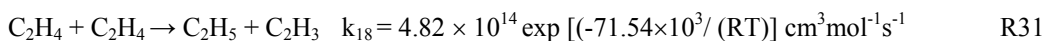
IV.4.B.3.Methane

The following reactions have been found to be important to account for the formation of the methane.

$CH_3 + H \rightarrow CH_4$ $k_{26} = 5.30 \times 10^{18}\ cm^3mol^{-1}s^{-1}$ R26

$CH_3 + CHO \rightarrow CH_4 + CO$ $k_{13} =2.21 \times 10^{14}\ cm^3mol^{-1}s^{-1}$ R13
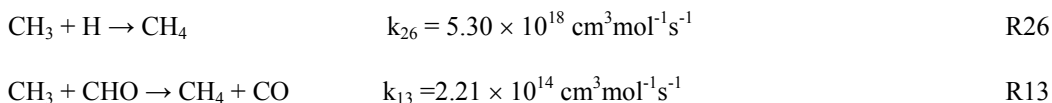
Other possibilities which have negligible contribution to its formation have been given below.

$C_2H_6 + H \rightarrow CH_4 + CH_3$ $k_{14} = 5.40 \times 10^1$ exp $[(-11.63 \times 10^3/ (RT)]$ cm^{3}mol^{-1}s^{-1} R27

$C_2H_2 + CH_3 \rightarrow CH_4 + C_2H$ $k_{19} = 1.81 \times 10^{11}$ exp $[(-17.29 \times 10^3/ (RT)]$ cm^{3}mol^{-1}s^{-1} R44
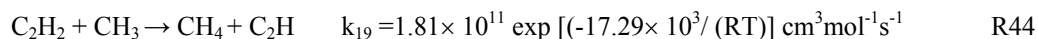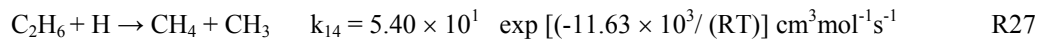
IV.4.B.4. Acetylene

The unimolecular elimination of HBr from vinyl bromide leads to the formation of acetylene (R3). The rate coefficient for this reaction considered in the kinetic modeling was taken from NIST and is given below.

$CH_2CHBr \rightarrow C_2H_2 + HBr$ $k_3 = 1.70 \times 10^{15}$ exp $[(-66.58 \times 10^3/ (RT)]$ s^{-1} R3
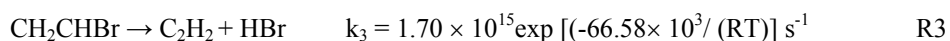
The energy barrier for this reaction derived from TST calculations is 66.75 kcal/mol at B3LYP/6-311++G** level of theory which is in good agreement with above reported value. This reaction in the scheme can successfully account for the experimentally observed concentration of the acetylene. Initially several reactions have been used to describe the acetylene formation. All these possibilities for the formation of the acetylene are shown below.

$C_2H_3 + CH_2 \rightarrow C_2H_2 + CH_3$ $k_{19} = 1.81 \times 10^{13}$ cm^{3}mol^{-1}s^{-1} R42

$CH_2 + CH_2 \rightarrow C_2H_2 + H_2$ $k_{14} = 1.58 \times 10^{15}$ exp $[(-11.94 \times 10^3/ (RT)]$ cm^{3}mol^{-1}s^{-1} R43

$C_2H_5 + C_2H \rightarrow C_2H_4 + C_2H_2$ $k_{19} = 1.81 \times 10^{12}$ cm^{3}mol^{-1}s^{-1} R45

$H_2 + C_2H \rightarrow H + C_2H_2$ $k_{14} = 3.36 \times 10^{11}$ (T)$^{2.39}$ exp $[(-0.86 \times 10^3/ (RT)]$ cm^{3}mol^{-1}s^{-1} R46

$C_2H_6 + C_2H \rightarrow C_2H_2 + C_2H_5$ $k_{19} = 3.61 \times 10^{12}$ cm^{3}mol^{-1}s^{-1} R47
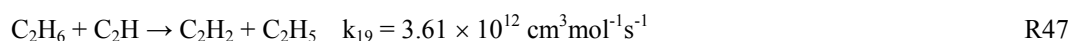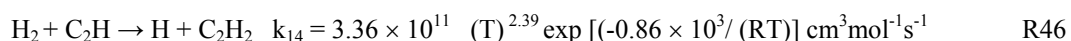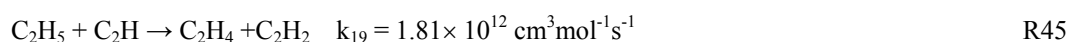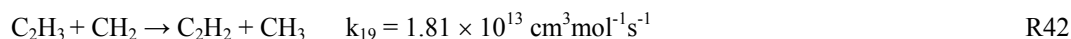
The following reaction had also been included for its consumption.

$C_2H_2 + CH_3 \rightarrow CH_4 + C_2H$ $k_{14} = 1.81 \times 10^{11}$ exp $[(-17.29 \times 10^3/ (RT)]$ cm^{3}mol^{-1}s^{-1} R44
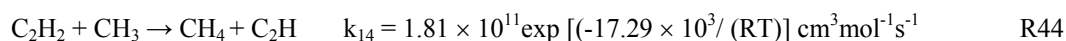
In fact, propyne, methyl bromide and ethyl bromide have also been observed experimentally but they were too low to be quantified that can be seen from the gas chromatogram as shown in the Figure III.1. These products were observed only above 1090K.

The final simulated results obtained from the reduced chemical kinetic model which contains only 32 reactions and 27 species have been found to be in good agreement with the experimental results. This reduced model was obtained using the sensitivity analysis results and has been discussed in detail in the next section.

The C-Br is the weakest among three haloethanols (X=F, Cl, Br) that have been studied in our laboratory. This is supported by the statement that the standard enthalpy of formation of three haloethanols are -96.78±0.03 (Fluoroethanol), -61.86±0.02 (Chloroethanol) and -50.91±0.96 (BEOH) kcal/mol at 298.15K. In the temperature range of investigation it is expected that the overall thermal decomposition of BEOH would be faster considering the fact that the bond energy of the C-Br bond is least. This proves kinetically least stability of BEOH. The characteristics of thermal decomposition are dependent on the C-X (F, Cl, and Br) bond length and the substituent's attached on the neighboring atom including the C-C bond strength. From the kineticist point of view the reactivity of BEOH was predicted to be faster than that of the fluoroethanol and chloroethanol as shown in the Figure IV.7 below.
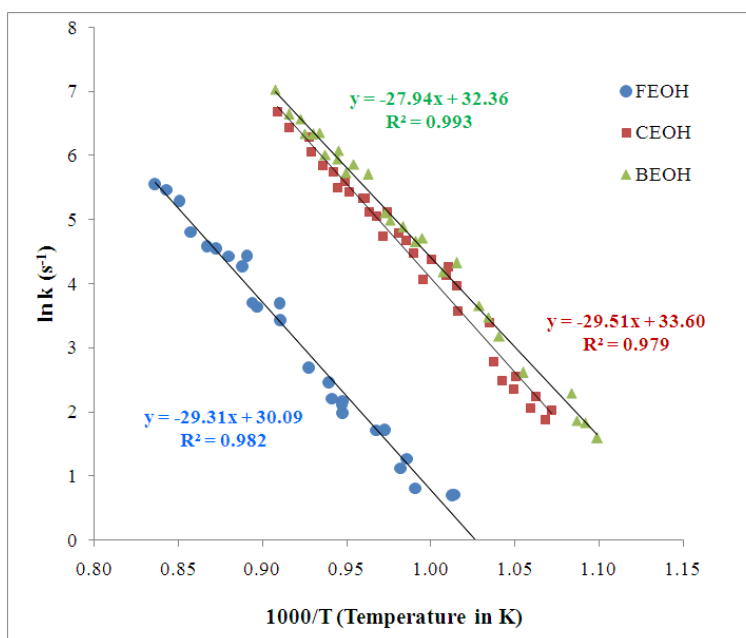
Figure IV.7. Comparison of rate for overall thermal decomposition of haloethanols.

IV.5. Sensitivity analysis

The reaction scheme was subjected to sensitivity analyses for the thermal decomposition of 2-bromoethanol by increasing the rate coefficients by the factor of 3 as explained by Lifshitz.[23] These analyses were carried out at two temperatures 1030 and 1100K. This analysis has been carried out using an excel spread sheet using the results obtained by chemical kinetic simulation by increasing the rate constant of each reaction by 3 times one by one and observing the corresponding change in the concentration of all the products at two different temperatures. The sensitivity factor has been defined as $S_{ij} = \Delta \log C_i / \Delta \log k_j$.

Table IV.5. Sensitivity factor obtained at 1030/1100K (k is changed by a factor of 3)

R. No.	Reactions	C_2H_2	C_2H_4	C_2H_6	CH_2CHBr	CH_3CHO	CH_4
R1	$BrC_2H_4OH \rightarrow CH_3CHO + HBr$	-0.119/-0.410	-0.155/-0.556	1.089/0.604	-0.163/-0.585	0.835/0.330	0.724/0.413
R2	$CH_2CHBr \rightarrow C_2H_2 + HBr$	1.010/0.869	-0.001/-	-0.008/-0.041	-0.028/-0.217	-/-0.009	-0.001/0.075
R3	$BrC_2H_4OH \rightarrow CH_2CHBr + H_2O$	1.039/0.973	-0.005/-0.016	-0.003/-0.062	1.001/0.983	-0.002/-0.028	-0.001/0.071
R4	$BrC_2H_4OH \rightarrow Br + C_2H_4OH$	-0.033/-0.171	0.904/0.632	0.037/0.264	-0.040/-0.250	-0.043/-0.309	0.003/-0.037
R5	$BrC_2H_4OH \rightarrow C_2H_4 + HOBr$	0.048/-0.017	0.116/0.108	0.002/0.016	-0.004/-0.026	-0.003/-0.032	-0.005/0.007
R6	$C_2H_4OH \rightarrow C_2H_4 + OH$	-/0.007	-/-	0.006/-	0.008/0.002	-/-	-0.003/-
R7	$CH_3CHO \rightarrow CH_3 + HCO$	0.015/-0.004	0.001/0.001	0.685/0.246	0.003/-0.002	-0.105/-0.586	1.050/0.724
R8	$CH_3CHO + H \rightarrow H_2 + CH_2CHO$	0.051/-0.014	-0.001/-	0.002/0.007	-0.001/0.002	-/-0.001	-0.006/-0.004
R9	$CH_3CHO + H \rightarrow H_2 + CH_3CO$	-0.012/-0.008	-/-	0.382/0.367	0.001/0.007	-0.012/-0.088	-0.391/-0.319
R10	$CH_3CO \rightarrow CO + CH_3$	-0.043/-	-0.001/0.001	-0.001/-	-0.001/0.001	-/-	-0.007/0.001
R11	$CH_2CHO \rightarrow CH_2CO + H$	0.005/-0.012	-/-	0.009/-	-0.001/0.001	-/-	-0.013/-
R12	$CH_2CO + H \rightarrow CO + CH_3$	0.046/-	-/-	-0.003/-	-0.002/0.002	-/-	-0.004/-0.001
R13	$CH_3 + CHO \rightarrow CH_4 + CO$	0.022/0.004	-0.001/-0.001	-0.006/-0.009	-0.004/0.002	-/0.002	0.002/0.004
R14	$CHO \rightarrow CO + H$	0.069/-0.004	-0.001/-	0.002/0.004	0.006/-	-/-0.001	-0.005/-0.003
R15	$2 CH_3 \rightarrow C_2H_6$	-0.075/0.006	-/-	0.107/0.183	0.002/0.004	-/-0.014	-0.175/-0.227
R17	$C_2H_5 + H \rightarrow C_2H_6$	-/-0.006	-/-	-/-	-/0.002	-/-	-/-
R18	$C_2H_5 + CHO \rightarrow C_2H_6 + CO$	-/0.003	-/-0.001	-/-	-/0.004	-/-	-/-0.002
R19	$2 CH_3 \rightarrow H + C_2H_5$	-0.054/-0.007	-0.001/-	0.098/0.064	0.002/0.004	-0.007/-0.042	0.081/0.054
R20	$H + C_2H_4 \rightarrow C_2H_3 + H_2$	0.039/0.001	-/-0.001	-0.002/-	0.002/0.003	-/0.001	-0.007/-0.001
R24	$C_2H_4 + C_2H_5 \rightarrow C_2H_6 + C_2H_3$	-0.005/-0.010	-/-	0.004/-	0.004/0.003	-/-	-0.003/-0.002
R26	$CH_3 + H \rightarrow CH_4$	0.029/0.006	-/0.001	-0.500/-0.448	-0.002/-	0.010/0.065	0.220/0.184
R29	$C_2H_6 \rightarrow C_2H_4 + H_2$	-0.020/0.006	-/0.001	-0.002/-0.003	0.002/0.002	-/-	-0.006/0.001
R30	$C_2H_4 + H_2 \rightarrow C_2H_5 + H$	0.007/-0.005	-/-0.001	-0.003/0.003	-0.001/0.005	-/-	-0.002/0.001
R31	$2 C_2H_4 \rightarrow C_2H_5 + C_2H_3$	-0.002/0.001	-0.002/-0.064	0.027/0.186	-/-	-0.001/-0.032	0.008/0.121
R34	$C_2H_5 + H_2 \rightarrow C_2H6 + H$	-0.020/-0.012	-/-	0.005/0.001	-/0.003	-/-	-0.008/-0.002
R35	$BrC_2H_4OH \rightarrow OH + C_2H_4Br$	0.034/-0.004	0.028/0.036	0.008/0.005	0.001/-0.005	-0.001/-0.010	-0.005/0.001
R36	$C_2H_4Br \rightarrow C_2H_4 + Br$	-0.051/0.001	-/-	0.003/0.001	-/0.004	-/-	-0.005/-
R37	$2 Br \rightarrow Br_2$	0.105/-0.004	-/0.001	0.009/-	-0.002/-	-0.001/-	-0.002/-
R38	$OH + Br \rightarrow HBr + O$	-0.012/-0.009	-0.002/-	-/0.002	0.004/0.001	-/-	-0.002/-0.001
R39	$HBr + O \rightarrow OH + Br$	0.078/0.009	-0.001/-0.001	-/-	-0.001/0.002	-/-	-0.006/-
R44	$C_2H_2 + CH_3 \rightarrow CH_4 + C_2H$	0.017/-0.005	-/-	-0.003/-0.048	-0.002/0.004	-/-0.010	-/0.087

It is important to throw some light on the details of the scheme in terms of the sensitivity factors given in the Table IV.5. The negative sensitivity explains the decrease in concentration with the rise in the rate coefficient of a particular reaction and vice versa in case of increase in k by 3 times. The same holds true for the sensitivity spectrum obtained by eliminating the reactions from the kinetic scheme.

The sensitivity spectrums of the six products and the reactants have been shown in the Table IV.5. The sensitivity of the products formed by the free radical mechanism becomes larger at higher temperatures. This can obviously be accounted by the greater yields of free radicals at high temperatures. The values of sensitivity factors given in the Table IV.5 are self explanatory.

The reactions having the sensitivity factor less than 0.1% for the concentration profile of any of the reaction products at these temperatures have been excluded from the scheme. This is the criterion that was used for the reactions to be considered as unimportant in the scheme. The sensitivity analysis reveals that the twelve reactions are not important and were removed from the reaction scheme. The rate expressions of the reduced kinetic mechanism that includes 32 reactions and 26 species are given in the Table IV.5.

The formation of different products by certain reactions can easily be understood by following the results shown in the sensitivity spectrum. The bar diagram have also been plotted at 1100K for better understanding of the sensitivity analysis and is given in the Figure IV.8.
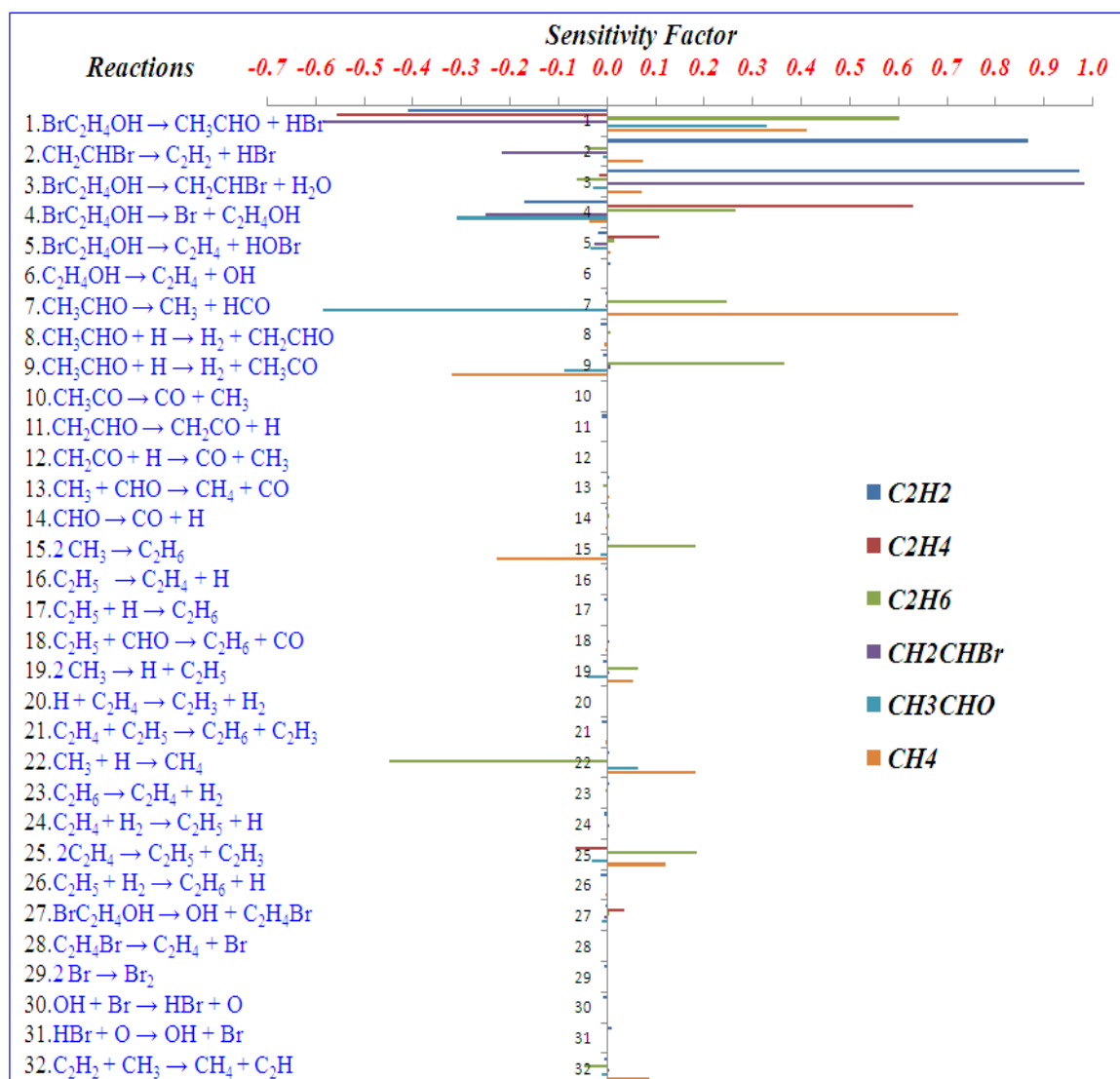
Figure IV.8. Sensitivity analysis bar diagram obtained at 1100K where k is changed by a factor of 3.

IV.6. Computational results and discussions

The major objective of this computational investigation was to get the transition states for HBr, H_2O and HOBr elimination reactions and to evaluate the activation energy and pre-exponential factor for these reactions using transition state

197

theory. Hence, the optimization of both ground state structure and the transition state (TS) structures for H_2O, HBr and HOBr elimination reaction from 2-bromoethanol were performed at HF, MP2 (FULL) and DFT(B3LYP) levels of theory with the standard 6-31G**, 6-31+G**, and 6-311++G** basis sets internally. Moreover, vibrational frequencies for the molecule and the transition state structures were evaluated to ascertain the nature of optimized structures. Five rotational isomers are possible because of the single bond rotation about both C-C and C-O bonds and there have been reports available on their relative energies, structures and vibrational frequencies. Similar to 2-chloroethanol, the $G_{g'}$ structure is found to be the most stable structure compared to other forms of 2-bromoethanol i. e. G_g, G_t, T_g and T_t where G and T is referred to gauche and trans geometry for rotation about the C-C bond, however, g and t is referred to gauche and trans for rotation about the C-O bond. The $G_{g'}$ conformer was found to be 1-3 kcal/mol lower in energy as compared to other four conformers of BEOH based on the calculated theoretical results at B3LYP/6-311++G** level of theory. It is so because in case of the G_g conformer the hydroxyl hydrogen is pointing away from the bromine whereas that of the G_g' conformer is pointing towards the bromine side which permits the electrostatic interaction between the bromine and hydroxyl hydrogen. As a result of this Gg' conformer is more stable than other four forms of BEOH and G_g is least stable conformer. However, these values would be different at different levels of theory used. The optimized structures of $G_{g'}$, G_g, G_t, T_g and T_t conformers are given in the Figure IV.9.b. In order to verify the β-substitution effect of Br on the barrier for H_2O elimination, kinetics of H_2O elimination has been compared with that of ethyl alcohol.[19]

The fully Optimized ground state structural parameters (bond length are in Å, angle in degree, normal mode vibrational frequencies (cm^{-1}) of the five confirmers of BEOH and of the TS structures for HBr, HOBr and H_2O elimination reaction at HF, MP2 (FULL), DFT (B3LYP) level of theories with the 6-31G*, 6-31G** and 6-311++G** basis sets have been included in the Table from IV.A.1-IV.A.17. These tables are given at the end of this chapter. The comparisons of these TS structures with those available in the literature have been discussed in detail in next section. Intrinsic Reaction Coordinate calculations have also been performed for the verification of these transition states. The four centered concerted transition state structures and barriers for the elimination of HBr, H_2O and HOBr are also compared. The TS structures for ethyl bromide for HBr elimination have been estimated and they are used for comparison with these results. Figure IV.9 shows structures of all the ground state conformers and of the transition states of HBr, HOBr and H_2O eliminations at B3LYP/6-311++G** theory. In general, variations in bond distances going from ground state to transition state results in change in the frequency factor as shown in the Table IV.7. The larger *A* value corresponds to loose TS and *vice versa*. Based on these results, it was found that the transition states for HBr & HOBr elimination were looser than that of the H_2O elimination. However, TS of HOBr elimination reaction is looser than that of the HBr elimination reaction. This will be discussed in detail next. The rate coefficients were estimated between 910 and 1102 K (at 10 K intervals) at the HF, MP2 (FULL), and DFT level of theory with the 6-311++G** basis set by TST calculations. The rate constants determined using TST calculations were independently fitted to Arrhenius expression to estimate values of A and E_a for HBr, H_2O and HOBr elimination reaction. The similar procedure was followed

to determine A and E_a for HBr elimination from ethyl bromide and dibromoethane at HF, MP2 (FULL) and DFT (B3LYP) levels of theory to understand β-substitution effect. We have used three models for treating the two torsional motions in reactant to compute the overall rate coefficients. Since the frequency factor depends on the partition function of the reactant and transition state. The Harmonic oscillator and rigid rotor partition functions were used for vibrational (3N-8) and rotational (3) degree of freedom. However, the two low frequency torsional motions about C-C and C-O bond were treated as either harmonic oscillator or hindered rotor or free rotor for estimating the frequency factor.

The TS for HBr elimination from BEOH do not have an effective plane of symmetry for the four atoms (Br, C, C and H) involved in the reaction. The four atoms at the TS is non-planar with ∠BrCCH dihedral angle varied from 3.3 to 4.6^0 depending upon the levels of theory as shown in the table IV.7. Similarly, the TS for H_2O elimination, the ∠OCCH dihedral angle is around 1.4 to 4.6^0 at HF and MP2 levels but at DFT (B3LYP) level, it is 0.2 to 1.3^0. However, the TS for H_2O elimination from ethyl alcohol was found to be planar (zero dihedral angle).[19] It is due to the β-substitution of Br/OH which distorts the planar transition state. To completely understand the structure of the transition state it is essential to analyze the important structural parameters which are involved in the reaction coordinate of HBr, HOBr and H_2O elimination processes from 2-bromoethanol. These structural parameters of all the TS would be discussed next.

IV.6.A.Transition state for HBr elimination

In the case of the TS for HBr elimination, C=C (newly formed), C-Br (leaving bromine atom) C-H (leaving hydrogen atom) and H-Br bond distances are very important to understand. The C-C bond distance at HF level of theory is 1.380 Å with 6-31G** basis set and with the addition of diffuse functions (6-311++G**), the bond length is increased to 1.384 Å. Adding electron correlation, the reverse trend is observed. Both at MP2 (FULL) and DFT levels the C-C bond is 1.399 Å with 6-311++G** basis set. From HF to DFT there is an increase of 0.06 Å in the C-C bond length. However, this bond distance is very much close to C=C bond length.

In case of the ground state i.e., $G_{g'}$ molecule, the C-C bond length is 1.517 Å at HF level with 6-31+G** basis set. And it decreases to 1.516 Å with the addition of diffuse functions 6-311++G**. With the addition of electron correlation by MP2 method, the C-C bond distance remains same as 1.516 Å with 6-311++G** basis sets. Whereas, in case of DFT level of theory there is a sudden raise in the bond distance of about 0.01 Å. Hence from ground state (GS) to transition state (TS) there is a decrease in the C-C bond length by about 0.118 Å. This is explained as the single bond (C-C) in the reactant becomes a double bond (C=C) in the product.
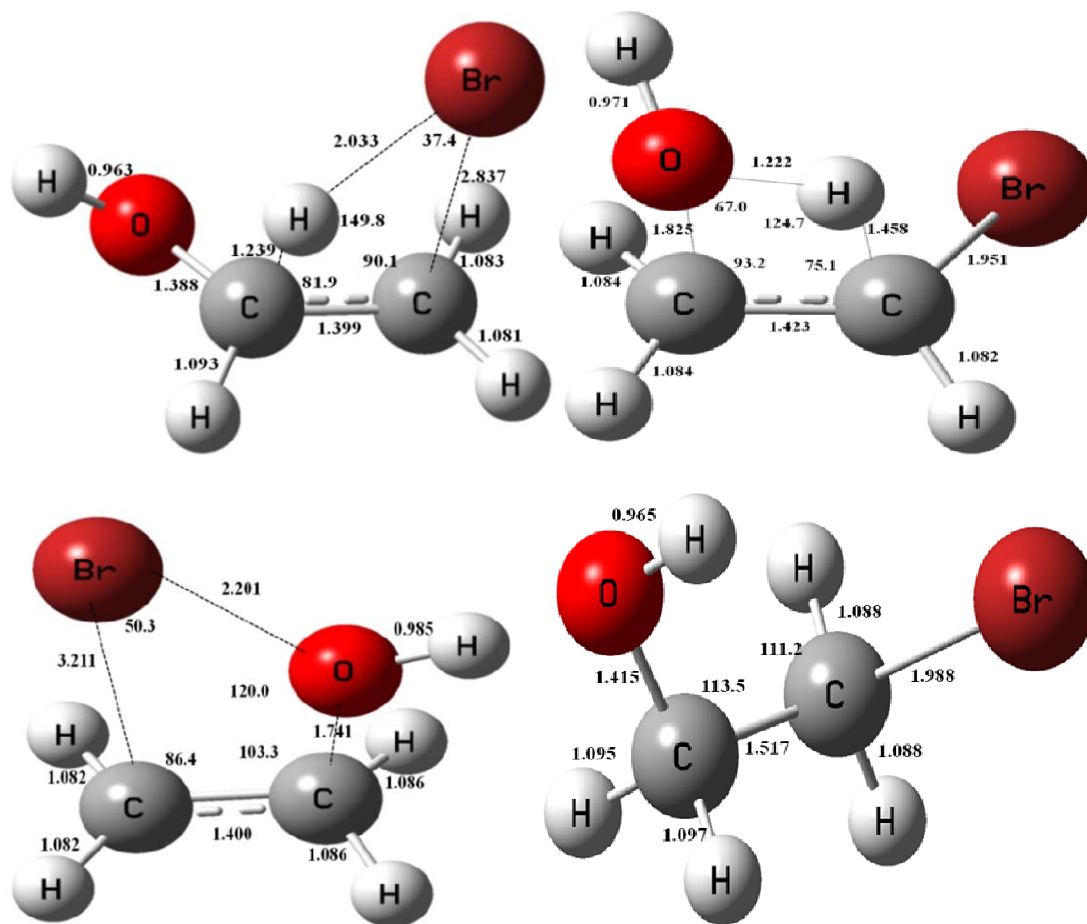
Figure IV.9. a. Optimized structures showing the bond distances of the concerted four centered transition state for (a) HBr elimination (b) H_2O elimination (c) HOBr elimination from 2- bromoethanol (d) ground state structure of 2-bromoethanol ($G_{g'}$) at the B3LYP/ 6-311++G** level of theory respectively.
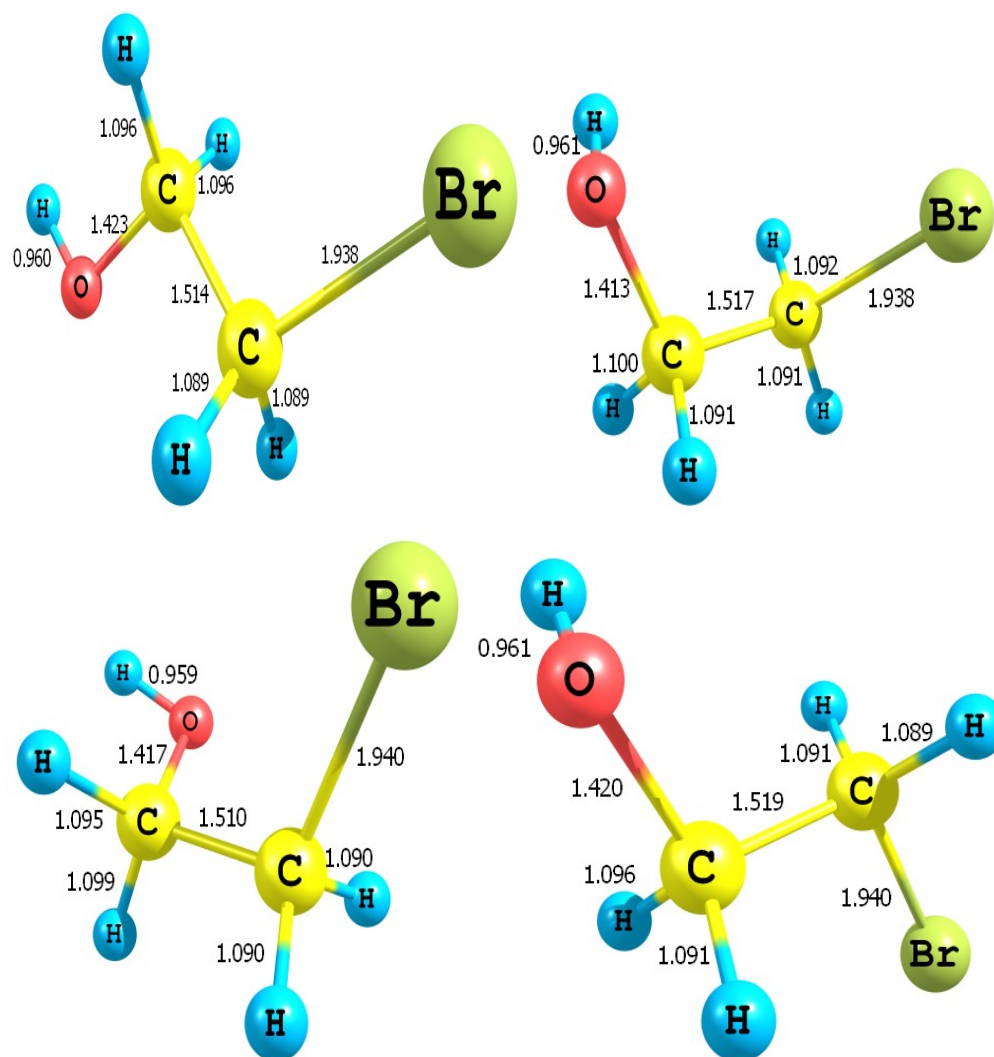
Figure IV.9.b. Optimized structures showing the bond distances of the ground state structure of the four conformers for (a) G_g conformer (b) G_t conformer (c) T_g conformer (d) T_t conformer of 2-bromoethanol at the B3LYP/ 6-311++G** level of theory respectively.

Ground state fully optimized structures showing the bond distances of the four conformers of 2-bromoethanol at the B3LYP level with 6-311++G** basis set respectively have been displayed in the Figure IV.9b.

The C-Br bond distance in the TS at HF level of theory with 6-31G** basis set is 2.821 and it is 2.727 Å for C-Cl bond in CEOH. It is 1.967 Å in the GS of BEOH. With the addition of diffuse functions (6-311++G**), the distance is increased to 2.884 Å where as in case of GS, it is reduced to 1.965 Å. With the addition of electron correlation, in the TS of BEOH at MP2(FULL) level of theory, there is a reduction of the distance from 6-31G** (2.615 Å) to 6-311++G** (2.613 Å), whereas at DFT level of theory, though there is increase from 6-31G** (2.713 Å) to 6-311++G** (2.837Å) and the distances are longer when compared to that of the distances at MP2(FULL) level. The "looseness" of the TS can be attributed to the C-Br distance. Hence the TS of BEOH is more "tighter" in MP2 (FULL) and "looser" in HF and it is in between at DFT level of the theories. These results have been found to be in good agreement with results reported by Setser et al.[52]

In the case of ethyl bromide the C-Br distance in the TS at the same level of theory and basis sets are 2.862 Å and 2.940Å respectively which is actually increasing with the diffuse function by 0.078 Å. When the TS of ethyl bromide is considered, with the addition of the electron correlation, the C-Br distance reduces from 6-31G** basis set (2.665 Å) to 6-311++G** (2.664 Å) at MP2 (FULL) level of theory. The same trend is observed in case of DFT theory also from 6-31G** (2.819 Å) to 6-311++G** (2.876 Å). Here also the TS is "tight" in case at MP2 (FULL), "loose" at HF level and it is in between at DFT level of theory. The loose or tightness affects the pre-exponential factors significantly. These values are compared in Table IV.8.

Table IV.6. Summary of C-C, C-X, C-H, and H-X distances and percent changes calculated for the transition states for HBr/H$_2$O/HOBr elimination reactions from 2-bromoethanol.^{a}

Bond	HF			MP2			B3LYP		
	6-31G**	6-31+G**	6-311++G**	6-31G**	6-31+G**	6-311++G**	6-31G**	6-31+G**	6-311++G**
C-C (H$_2$O)	1.4618 (-3.61)	1.4658 (-3.29)	1.4717 (-2.93)	1.4207 (-6.15)	1.4195 (-6.14)	1.4281 (-5.79)	1.4279 (-6.07)	1.4239 (-6.24)	1.4228 (-6.21)
C-C (HBr)	1.3803 (-8.99)	1.3828 (-8.76)	1.384 (-8.71)	1.3951 (-7.84)	1.3955 (-7.72)	1.3994 (-7.68)	1.4021 (-7.77)	1.4035 (-7.58)	1.3994 (-7.75)
C-C (HOBr)	1.3896 (-8.37)	1.3945 (-7.99)	1.3926 (-8.15)	1.3921 (-8.04)	1.3952 (-7.74)	1.4283 (-5.77)	1.3986 (-8.00)	1.4023 (-7.66)	1.4002 (-7.70)
C-Br (HBr)	2.8205 (43.37)	2.8777 (46.59)	2.8838 (46.77)	2.6154 (33.43)	2.6395 (34.87)	2.6125 (34.13)	2.7826 (39.89)	2.8243 (42.30)	2.8366 (42.69)
C-Br (HOBr)	2.7171 (38.11)	2.7524 (40.21)	2.7795 (41.46)	2.860 (45.90)	2.936 (50.03)	3.050 (56.59)	2.9698 (49.30)	3.0143 (51.88)	3.2114 (61.54)
C-O (H$_2$O)	1.6207 (16.52)	1.6046 (15.17)	1.5856 (13.90)	1.7595 (24.55)	1.7833 (25.64)	1.737 (22.97)	1.7919 (27.05)	1.8343 (29.49)	1.8245 (28.90)
C-O (HOBr)	1.8015 (29.52)	1.7882 (28.35)	1.7924 (28.76)	1.841 (30.32)	1.847 (30.13)	1.568 (11.01)	1.7715 (25.60)	1.7727 (25.14)	1.7414 (23.03)
C-H (H$_2$O)	1.6278 (51.03)	1.6307 (51.23)	1.634 (51.55)	1.5175 (39.90)	1.4893 (37.16)	1.5307 (40.48)	1.4937 (37.14)	1.4521 (33.22)	1.4577 (34.03)
C-H (HBr)	1.221 (12.34)	1.2065 (11.08)	1.2071 (11.10)	1.2455 (13.89)	1.2351 (13.02)	1.2512 (14.07)	1.2529 (13.85)	1.238 (12.63)	1.2394 (12.97)
H-OH (H$_2$O)	1.0739 (13.86)	1.0777 (14.26)	1.0774 (14.46)	1.1653 (21.31)	1.1882 (23.45)	1.1645 (21.45)	1.1907 (23.36)	1.2197 (26.38)	1.2216 (26.99)
H-Br (HBr)	2.1966 (56.94)	2.2376 (59.70)	2.2698 (61.16)	2.0766 (47.65)	2.0898 (48.85)	2.068 (46.70)	1.978 (39.58)	2.0027 (41.08)	2.0328 (42.49)
HO-Br (HOBr)	2.1192 (17.26)	2.1147 (17.37)	2.1271 (17.84)	2.1185 (13.82)	2.124 (14.26)	2.1843 (17.46)	2.1506 (15.19)	2.1638 (16.15)	2.2006 (17.58)

^{a} For C-C, C-X, and C-H bonds, the percent changes (in parentheses) give the change in these distances compared to the reactant. For the H-X bond, percent change gives the change compared to free HBr, H$_2$O and HOBr.

A significantly different trend is observed for C-H (the hydrogen atom involved in the reaction coordinate) in both the TS and GS of BEOH and ethyl bromide. The percentage changes of these bond lengths are tabulated in the Table IV.6.

Another important structural parameter which has to be considered carefully is the dihedral angle containing all the four atoms i.e., ∠Br-C-C-H. In TS of BEOH, this dihedral angle is increasing at each level of the theory with the basis set as shown in the Table IV.7. At HF/6-31G** it is 3.3^0 and it is 3.7^0 with 6-311++G** basis set. At MP2 (FULL) it increases from 5.2^0 to 6.8^0, where as in DFT level of theory the increase is from 4.5^0 to 4.6^0 through 5.1^0. In case of ethyl bromide, these four atoms are in the same plane at every level of theory and basis set. On an overall look the TS for the HBr elimination from BEOH and ethyl bromide follow the similar structural parameters.

Table IV.7. Dihedral angle for the 4 atoms involved in the reaction coordinate for HBr, HOBr and H_2O elimination reactions from 2-bromoethanol at different level of theory.

Elimination reactions	HF			MP2 (Full)			DFT		
	6-31G**	6-31+G**	6-311++G**	6-31G**	6-31+G**	6-311++G**	6-31G**	6-31+G**	6-311++G**
HBr	3.3	3.3	3.7	5.2	5.9	6.8	4.5	5.1	4.6
H_2O	4.4	4.1	4.6	3.3	1.4	2.3	1.3	0.8	0.2
HOBr	0.0	0.0	0.0	0.0	0.0	0.0	9.0	0.1	0.0

IV.6.B. Transition state for H_2O elimination

The TS for H_2O elimination involves five atoms whose structural parameters have to be followed carefully. These parameters are compared with those corresponding to ethanol in its TS to eliminate H_2O. The C-C bond length in TS is changing differently with different basis sets and different levels of the theories. This distance is 1.471Å at HF level, it is 1.428 Å at MP2 (FULL) level and it is 1.423 Å at DFT level of calculations

with 6-311++G** basis set. In the GS the distances are about 1.516 Å, 1.516 Å and 1.517 Å at HF, MP2 (FULL) and DFT levels of the theories respectively, with the same basis set. In case of the TS of ethanol the distances are 1.413 Å, 1.422 Å and 1.414Å at HF, MP2 (FULL) and DFT level of theories, respectively. The C-C bond distance in TS of ethanol is quite different at all level of theory than that of BEOH. In the GS of ethanol the C-C bond distances are 1.519 Å, 1.513Å and 1.517 Å at HF, MP2(FULL) and DFT levels of the theories respectively with 6-311++G** basis set. In both the GS of BEOH and ethanol the C-C distance is almost the same in all levels of theory. There is a decrease in the C-C bond distance from GS to TS in both BEOH and ethanol and the decrease is almost similar. The percentage changes of C-C bond from GS to TS in BEOH are given in Table IV.6. However, this C-C distance is slightly smaller than for HX elimination in TS.

Very important structural parameter which plays a significant role in the nature of the TS is C-O (oxygen involved in the reaction coordinate) bond distance. In the TS of BEOH the C-O bond distance is reducing with the basis set, except in case of DFT theory with 6-311++G**. The C-O distance is 1.586 Å, 1.737 Å and 1.825 Å at HF, MP2 (FULL) and DFT level of theories with 6-311++G** respectively. The C-O distance in the GS of BEOH is 1.392 Å HF level of the theory. However, adding electron correlation, the C-O bond distance increases to 1.413 Å and 1.415 Å at MP2(FULL) and DFT level of theory with 6-311++G** the basis sets respectively.

The increase in the bond distance from GS to TS is 13.90% at HF, 22.97% at MP2 (FULL) and 28.905% at DFT level of theories. The "looseness" of the TS increases from HF to DFT through MP2 (FULL). This reflects in the pre-exponential factors,

which can be seen in Table IV.6. There is an increase in the pre-exponential factors from HF to DFT level of theories. In case of the ethanol, the C-O distances in the TS are 1.879 Å, 1.798 Å and 1.925 Å at HF, MP2(FULL) and DFT level of theories at 6-311++G** basis set. If we compare these bond distances at the same level of the theories the C-O bond distance in the TS of ethanol is more than that in the TS of BEOH. This may be attributed to the β-bromine effect on the OH group.

All the four atoms namely H, C, C and O which are directly involved in the reaction coordinate in BEOH are not in a single plane as shown in the Table IV.7. At HF/6-31G** it is 4.4^0 and it is 4.6^0 with 6-311++G** basis set. At MP2 (FULL) it decreases from 3.3^0 to 2.3^0, where as in DFT level of theory the decrease is from 1.3^0 to 0.2^0 through 0.8^0. In case of ethanol also the four atoms are not in one plane, but the trend in the dihedral angles is not similar to that of BEOH. A gradual increase is observed in each level of the theory with the basis set. In HF the dihedral angle is increasing from 1.6^0 (6-31G**) to 3.2^0 (6-311++G**), in MP2(FULL) it is from 1.0^0 to 2.4^0 and in case of DFT the increase is from 1.6^0 to 3.8^0.

The frequency calculations have been carried out at all levels of theories and basis sets for both the GS and TS. The TS are characterized by one imaginary frequency corresponding to the reaction coordinate. The reaction coordinate corresponds to the motion of H away from C towards Br/O in the HBr elimination and H_2O elimination respectively. The motion along the reaction coordinate is very similar to that described by Holmes and coworker[53] for the HBr elimination reaction of CH_2ClCH_2Br. The motion of the reaction coordinate when visualized in Chemcraft clearly shows the TS corresponding to the reaction of interest. The energies and moments of inertia of 2-bromoethanol in

ground state (Gg', G_g, G_t and T_t, T_g conformers) and transition state for HBr and H_2O elimination are given in Table from IV.A.18 to IV.A.21(These tables are given at the end of this chapter).

The comparisons of TS for HBr and H_2O eliminations have been discussed. The C-H bond (the leaving hydrogen) is more broken in TS for HBr elimination compared to TS for H_2O elimination. When the C-H bond length is changed by 11.10% from GS to TS for HBr, the change is 51.55% when compared with TS for H_2O elimination at HF/6-311++G**. The C-H bond is broken more by 14.07 and 12.97% at MP2 and DFT with 6-311++G** basis set for HBr elimination. However, the C-H bond is broken more by 40.48 and 34.03% at MP2 and DFT with 6-311++G** basis set for H_2O elimination. The same kind of trend is observed in case of FEOH and CEOH also. The C-Br bond in TS for HBr elimination is more broken than the C-O bond in TS for H_2O elimination. This can be clearly seen in Figure IV.9a respectively. The percentage changes are given in Table IV.6.

The comparisons of TS for H_2O elimination from FEOH, CEOH and BEOH have been discussed. At HF level, the C-O bond decreases for H_2O elimination from FEOH to BEOH through CEOH. When the electron correlation is added, at MP2 level the change in C-O bond is almost similar in BEOH, CEOH and FEOH. At DFT, with 6-311++G** basis set, the change is almost identical in all three haloethanols. The C-H bond is more broken in CEOH than in FEOH at MP2 and DFT theories. However, the C-H bond is less broken in BEOH than in CEOH at MP2 and DFT theories in the TS. However, at HF level the change in the C-H bond length is almost same for three haloethanols. The

comparisons of percentage change in the C-O and C-H bond lengths for FEOH, CEOH and BEOH indicates that the variations are within 2-3%.

IV.6.C. Transition state for HOBr elimination

In the case of the TS for HOBr elimination, C=C (newly formed), C-Br (leaving bromine atom) C-OH (leaving hydroxyl group) and HO-Br bond distances are very important to understand. The TS of HOBr elimination reaction from BEOH have been successfully optimized at HF, MP2 (FULL) and DFT level with the three basis sets. The TS structure for HOBr elimination has been shown in Figure IV.9a.

The C-C bond length in TS is almost similar with different basis sets and different levels of the theories. The C-C bond distances calculated with the three basis sets at HF, MP2 (FULL) and DFT level were found to be close to the TS for HBr elimination. They were 1.392, 1.428 and 1.400 Å, HF, MP2 (FULL) and DFT level with 6-311++G** basis set respectively. However, the C-C bond is longer in the TS of H_2O elimination than that in HOBr at all level of theory with all basis sets. In the GS the distances are about 1.516 Å, 1.516 Å and 1.517 Å at HF, MP2 (FULL) and DFT levels of the theories respectively, with the 6-311++G** basis set.

The C-Br distance at the TS was 2.970, 3.014 and 3.211Å with 6-31G**, 6-31+G** and 6-311++G** basis sets at DFT level. At the TS for HBr elimination, the corresponding distances were 2.783, 2.824 and 2.837 Å. Thus, with both smaller and larger basis sets, the C-Br distances look very different. This indicates that the C-Br bond is more broken in TS of HOBr than TS of HBr. Similar trend have been observed at MP2 level with three basis set. However, at HF level, the TS structure for HOBr elimination

has shorter C-Br bond than that of HBr elimination. The increase in the bond distance

from GS to TS is 41.46% at HF, 56.59% at MP2 (FULL) and 61.54% at DFT level of

theories. The "looseness" of the TS increases from HF to DFT through MP2 (FULL).

This reflects in the pre-exponential factors, which can be seen in Table IV.8. There is an

increase in the pre-exponential factors from HF to DFT level of theories.

The C-O bond distance in TS of HOBr elimination is longer at HF and MP2 level

of theory except MP2/6-311++G** level as compared to that of H_2O elimination.

However, reverse trend is observed at DFT level with all the basis set used.   The C-O

bond distance is 1.792, 1.568 and 1.741Å, HF, MP2 (FULL) and DFT level with 6-

311++G** basis set respectively.

Another important structural parameter which has to be considered carefully is the

dihedral angle containing all the four atoms i.e., $\angle$Br-C-C-OH. In TS of BEOH, this

dihedral angle is calculated to be zero at each level of the theory with the basis set as

shown in the Table IV.7. except at B3LYP/6-311G** and it is 9.0^0 indicating great

distortion. In case of ethyl bromide, these four atoms are in the same plane. The dihedral

angle is 0^0 at every level of theory and basis set. On an overall look the TS for the HOBr

elimination from BEOH and HBr elimination from ethyl bromide has the same dihedral

angle.

IV.6.D. Intrinsic reaction coordinate calculations

Minimum energy reaction pathways (reaction coordinate) have been obtained for

transition state of HBr and H_2O elimination reaction from 2-bromoethaonl using the

intrinsic reaction coordinate (IRC) calculations for the verification of transition state at HF, MP2 (FULL) and DFT level with 6-311++G** basis set. These calculations were carried out in 61 steps and found to be well connecting reactant and products. However, IRC calculation of HOBr elimination was performed in 81 steps at the same level. These results have been displayed in Figure IV.10 including the corresponding geometries of reactant, transition states and products. Comparison of the reaction coordinates of HBr, H_2O and HOBr elimination reaction pathways illustrates that the three reactions follow distinctly different reaction paths. We have found close agreement between the energies obtained using the IRC calculations and independently optimized values.
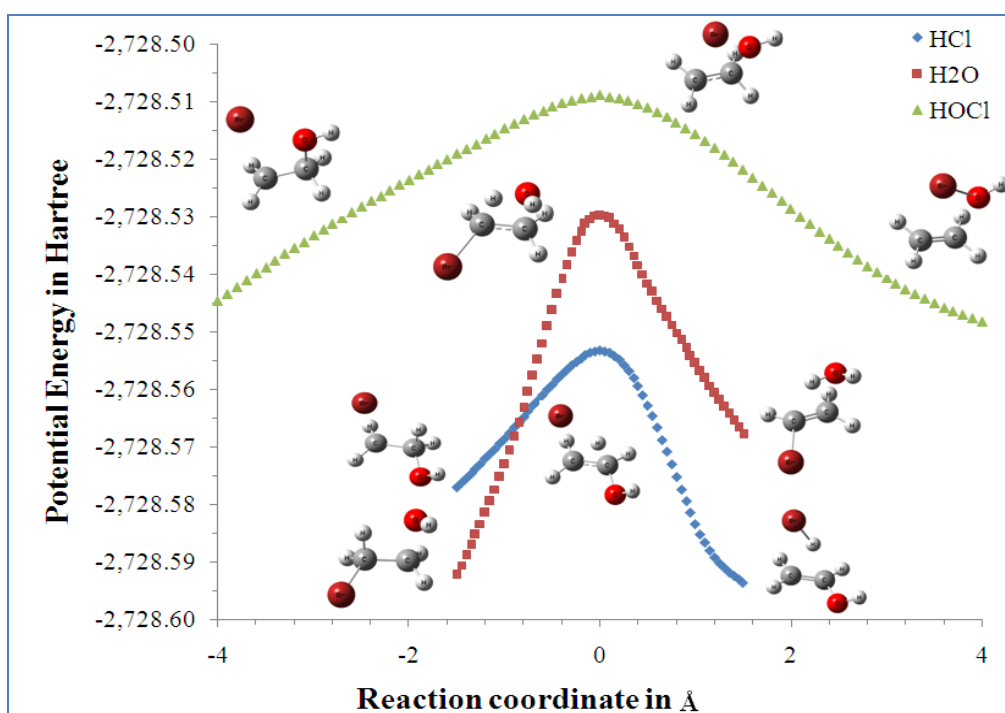
Figure IV.10. Minimum energy reaction pathways for transition state of HBr, H_2O and HOBr elimination reactions from 2-bromoethaonl obtained using the intrinsic reaction coordinate (IRC) calculations performed in 61 steps at B3LYP/6-311++G** level of the

theory for the verification of transition states and found to be well connecting reactant and products. However, IRC calculation of HOBr elimination was performed in 81 steps at same level. This plot also describes that the two transition states are following the distinctly different reaction paths.

For the HBr elimination, IRC calculations indicate that the C-Br bond cleaves first and virtually broken fully at transition state at B3LYP/6-311++G** level. This is followed by dissociation of C-H bond starting at 1.258 Å with simultaneous formation of H-Br single bond. The C-Br and C-H bonds are fully ruptured at transition state having bond distances of 1.839 and 2.885 Å. Figure IV.10 also represents that this process proceeds with smooth conversion of C-C single bond to C-C double bond.

For the H_2O elimination, these calculations predicts that the C-O bond is almost ruptured first at 1.827 Å at B3LYP/6-311++G** level. This is followed by formation of H-OH single bond begins at 1.197 Å with simultaneous cleavage of C-H bond starting at 1.481 Å. In fact, the dissociation of C-OH and C-H bond is fully completed at transition state resulting in fully formed bond of H-OH as shown in Figure IV.10 having a bond distance of 0.968 Å.

It is clear from the IRC plot of HOBr elimination that the C-Br bond cleaved first at 3.218 Å precedes with breaking of C-O bond starting at 1.777 Å at B3LYP/6-311++G** level. This is attributed to the fact that the bond dissociation energy of the former (75.89 kcal mol^{-1}) is lesser than the C-OH bond (84.84 kcal mol^{-1}) . This is accompanied by the formation of HO-Br single bond begins at 2.182 Å with

simultaneous conversion of C-C single bond uniformly proceeding to C-C double bond beginning at 1.393 Å as displayed in Figure IV.10.

IV.6.E. Transition state theory calculations

Frequency calculations were carried out at all levels of calculations for both the ground and transition states to perform transition state theory calculations. Transition states have been characterized by one imaginary frequency corresponding to the reaction coordinate. The reaction coordinate corresponds to the motion of H away from C toward Br/O in both cases. The motion of the reaction coordinates when visualized with Chemcraft clearly shows that the TS correspond to the reaction of interest. The transition–state theory was used for evaluating the thermal rate constants for both HBr and H_2O elimination from BEOH. The A and E_a were estimated between 930 and 1100 K (at 10 K intervals) at the HF, MP2 (FULL), and DFT level of theory with the 6-311++G** basis set. Details of which are given in the chapter II.

For the evaluation of free rotor and hindered rotor partition function, a similar procedure has been followed as discussed in the previous chapter. Hindered rotor and free rotor partition function in the temperature range of 910-1102K at 10K intervals calculated at HF, MP2 (FULL), B3LYP levels of theory with the 6-311++G** basis set for low frequency torsional modes of C-C and C-O bonds of BEOH are listed in the Tables from IV.A.36 to IV.A.37 at the end of this chapter.

In this subsection, Arrhenius parameters for formation of CH_2CHOH, CH_2CHBr and C_2H_4 by unimolecular elimination of HBr, H_2O and HOBr from BEOH will be described in detail.

Schematic potential energy level diagram illustrating the forward and backward activation energies including the enthalpy of reactions for unimolecular HBr, HOBr and H_2O elimination channels evaluated at HF, MP2 (FULL) and B3LYP level using the 6-311++G** basis set have been represented in Figure IV.11. Inspection of Figure IV.11 demonstrates that the HBr elimination reaction is exothermic by 3.74, 2.88 and 1.37 kcal mol^{-1} at HF, MP2 (FULL) and DFT level with 6-311++G** basis set. The H_2O elimination reaction is endothermic by 11.46, 12.27 and 10.36 kcal mol^{-1} at HF, MP2 (FULL) and DFT level with 6-311++G** basis set. However, endothermicity of HOBr elimination predicted at HF, MP2 (FULL) and B3LYP level with same basis set have been predicted very high and it is 53.16, 56.71 and 47.72 kcal mol^{-1} respectively. In fact, the potential energy level diagram indicating the values of forward and reverse activation energies is self explanatory.

Figure IV.11. Schematic potential energy level diagram showing the forward and backward activation energies including the enthalpy of reactions for unimolecular HBr, H_2O and HOBr elimination channels from 2-bromoethanol evaluated at HF, MP2 (FULL) and B3LYP level of theory using the 6-311++G** basis set. The $\Delta_f E_0$ and $\Delta_r E_0$ corresponds to difference in sum of electronic and zero point energies for forward reaction and reverse reactions respectively. $\Delta_r H^0$ denotes the enthalpy change of reaction. The geometries shown here are all at B3LYP/6-311++G** level of theory. All values are given in units of kcal mol^{-1}.

Three potential energy surfaces (PES) scan have also been performed for the BEOH about the C-C and C-O bonds to identify no. of conformers as well as difference

in their energy. Present study has shown that the five conformers are distinctly different in energy and structure. Potential energy curves evaluated at B3LYP/6-311++G** level of theory corresponding to (a) rotation around the C-C bond in T_t structure (b) rotation around the C-O bond in G_g structure and (c) rotation around the C-O bind in T_g structure have been depicted in Figure IV.12.

It can be seen from Figure IV.12 that the rotation around the C-O bond in G_g structure gives rise to three minima whereas rotation around the C-C bond produces two minima, therefore five conformers are possible for BEOH similar to the case of FEOH and CEOH. The difference in energy between different rotamers can easily be noticed from the Figure IV.12. We have found that the $G_{g'}$ conformer is lower in energy by 1.0-3.0 kcal mol^{-1} as compared to other four conformers at B3LYP/6-311++G** the level theory.
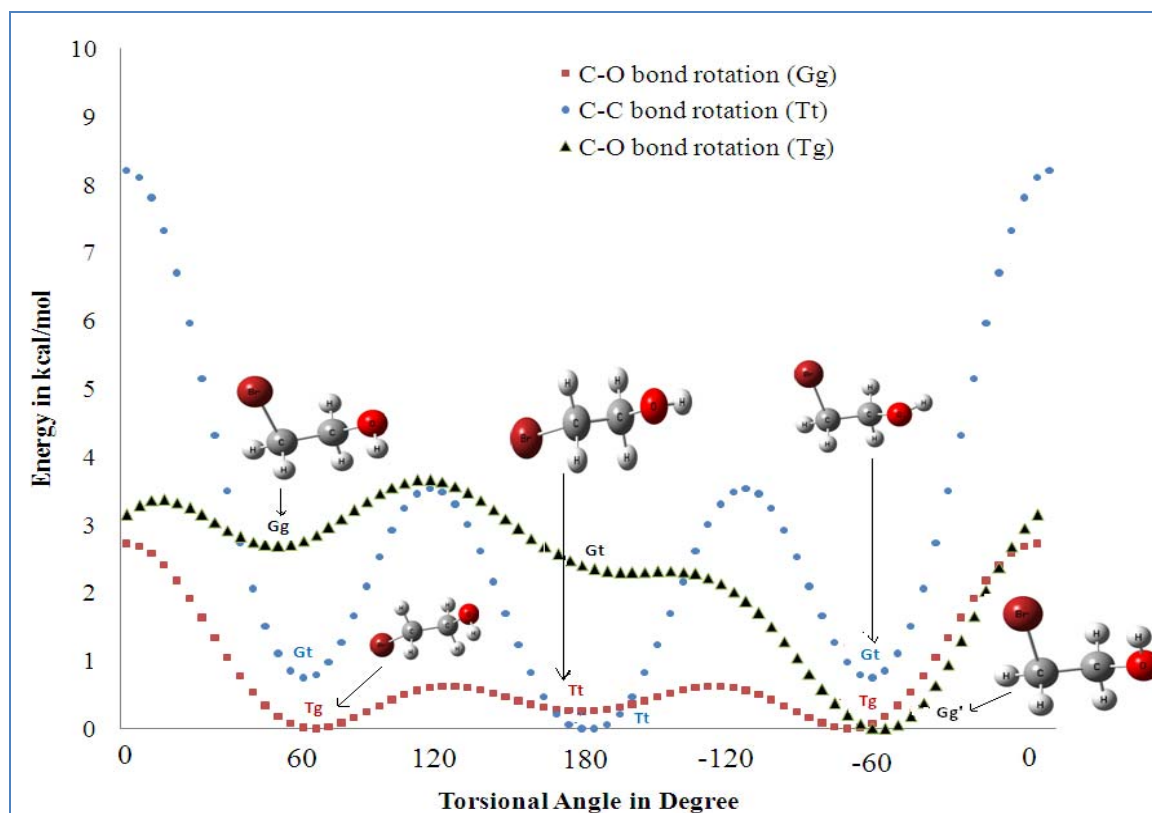
Figure IV.12. The potential energy barriers for internal rotation about C-C bond for T_t conformer (filled blue circle), rotation around C-O bond for G_g conformer (filled maroon squares) and rotation around C-O bond for T_g conformer (filled black triangle) evaluated at B3LYP/6-311++G (d, p) level of theory for 2-bromoethanol.

In general, the energies were found to be increasing in the order $G_g' < T_t < T_g < G_t < G_g$. It is so because in case of the G_g conformer the hydroxyl hydrogen is pointing away from the bromine whereas that of the G_g' conformer is pointing towards the bromine side which permits the electrostatic interaction between the bromine and hydroxyl hydrogen. As a result of this G_g' conformer is more stable than other four forms of BEOH and G_g is least stable conformer. These results have been found to be in good agreement with the results reported by Souza et al. at B3LYP/6-31g (d, p) level of theory[51].

If their contributions are included, the activation energy calculated will be reduced depending upon the level of the theory. Hence, the total rate constant for HBr elimination was estimated as the sum of the values for the five conformers weighted by the Boltzmann factor.

$$k = k_{G_{g'}} w_{G_{g'}} + k_{G_t} w_{G_t} + k_{G_g} w_{G_g} + k_{T_t} w_{T_t} + k_{T_g} w_{T_g}$$

Here the w corresponds to the Boltzmann factor. The total rate constant for H_2O elimination was determined by taking all conformers except G_g conformer into account owing to inhibiting interactions between the C-H and O-H hydrogen's in the transition state and were calculated as follows:

$$k = k_{G_{g'}} w_{G_{g'}} + k_{G_t} w_{G_t} + k_{T_t} w_{T_t} + k_{T_g} w_{T_g}$$

The reaction path degeneracy (l) considered for each conformer is one.

The potential energy profile corresponding to different unimolecular elimination, isomerization and decomposition pathways with zero point energy correction obtained at the B3LYP/6-311++G (d, p) level of theory involved in the pyrolysis of 2-bromoethanol have been displayed in the Figure IV.13. Relative energies are given in kilocalories per mole.
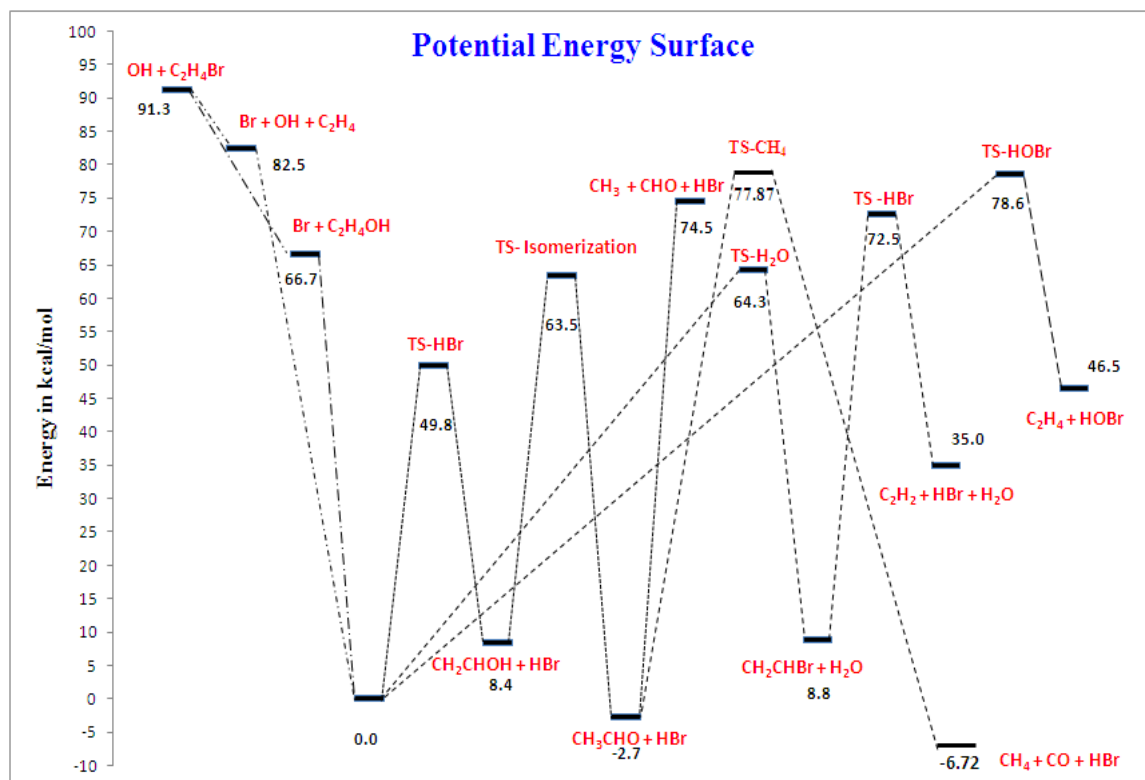
Figure IV.13. Potential energy profile corresponding to different unimolecular elimination, isomerization and decomposition pathways with zero point energy correction obtained at the B3LYP/6-311++G (d, p) level of theory involved in the pyrolysis of 2-bromoethanol. Relative energies are given in kilocalories per mole.

The E_a for HBr elimination from ethyl bromide at HF, MP2, and DFT with 6-311++G** level are 58.23, 63.10, and 51.14 kcal mol^{-1}, respectively. At similar levels the E_a for HBr elimination from BEOH are 59.42, 64.21, and 51.38 kcal mol^{-1}, respectively. This slight increase at all levels basically implies that β-substitution of OH does not have a significant effect on the E_a of HBr elimination. The E_a for HBr elimination from bromofluoroethane at HF and DFT with 6-311++G** level are 67.21 and 56.22 kcal mol^{-1}, respectively. This implies that the β-substitution of F results in the increase of E_a for

HBr elimination. The E_a for HBr elimination from bromochloroethane at HF, MP2 (FULL) and DFT with 6-311++G** level are 66.48, 67.64 and 55.96 kcal mol^{-1}, respectively. This implies that the β-substitution of Cl results in the increase of E_a for HBr elimination. Similarly, the β-substitution of Cl in the ethyl chloride predicts an increase in HCl elimination barrier at all level of theory.[53] However, there was no evidence of increase in activation barrier experimentally.[53]Hence, experimental data on the kinetics of HCl and HBr elimination from bromochloroethane would be useful. The experimentally determined E_a for HBr elimination from BEOH, bromoethane[52], dibromoethane[2] and bromochloroethane[53] are 53.42, 53.70, 56.00 and 58.00 kcal mol^{-1}, respectively. This clearly reveals the fact both experimentally and theoretically that the β-substitution of bromine and chlorine increases the activation barrier. However, both experiment and theory predicts that the OH substitution does not bring about a significant change in the value of E_a for HBr elimination.

Tschuikow-Roux have reported the value of E_a for HBr elimination from C_2H_5Br to be 53.4 kcal/mol using thermal activation experiments using shock tube from a temperature range of 660-706 K.[54] This result is in excellent agreement with the result reported by Tsang for the pyrolysis study on C_2H_5Br using shock tube for the E_a (53.5 kcal/mol) of HBr elimination in the temperature range of 740-1000 K.[55] The E_a value for HBr elimination from BEOH obtained from present investigation in the temperature range of 910-1102K also shows it to be 53.42 kcal/mol. These thermal activation results indicate no difference in the E_a value for HBr elimination. Similarly, the experimental result for E_a obtained using the shock tube on C_2H_5Cl, ClC_2H_4Cl and ClC_2H_4OH was

found to be approximately 58 kcal/mol.[56] The chemical activation experiment show an increase in the value of E_0 of the order of 4-5 kcal/mol for HBr elimination on going from ethyl bromide to dibromoethane. However, this difference between ethyl chloride and dichloroethane was found to be approximately 7 kcal/mol.[53]

These results on thermal activation using shock tube confirm that the β-substitution Cl and OH bring about no change in the E_a value. However, a chemical activation experiment predicts an increase in the barrier on β-substitution Cl and Br.

It was found that the HF and MP2 (FULL) level calculations overestimate experimental E_a by 5.00 and 10.79kcal mol^{-1} for HCl elimination respectively. However, a DFT result underestimates E_a by 2.04 kcal/mol in our temperature range of investigation.

The comparison of experimental and theoretical kinetic parameters A and E_a values of HBr elimination from BEOH determined at HF, MP2 (FULL), B3LYP/6-311++G** level with ethyl bromide and dibromoethane, bromochloroethane and chlorofluoroethane have been summarized in the Table IV.10.

Table IV.8. Comparison of the rate parameters for the unimolecular elimination of HBr, H_2O and HOBr from 2-bromoethanol calculated at HF, MP2 (full), and DFT/6-311++G level of theory considering harmonic oscillator, hindered rotor and free rotor model**

Theory/6-311++g**	BrCH$_2$CH$_2$OH→CH$_3$CHO+HBr			BrCH$_2$CH$_2$OH→CH$_2$CHBr+H$_2$O			BrCH$_2$CH$_2$OH→CH$_2$CH$_2$ + HOBr		
	log A	E$_a$	k	log A	E$_a$	k	log A	E$_a$	k
HF (HO)	14.41±0.01	59.42±0.02	$3.67×10^2$	13.71±0.02	84.43±0.03	$7.53×10^{-4}$	14.52±0.03	119.19±0.04	$5.70×10^{-10}$
MP2(FULL)(HO)	14.19±0.02	64.21±0.03	$2.45×10^1$	13.90±0.01	69.63±0.01	$1.04×10^0$	15.82±0.04	370.06±0.05	$1.08×10^{-58}$
B3LYP (HO)	14.44±0.01	51.38±0.02	$1.58×10^4$	13.97±0.02	66.08±0.03	$6.25×10^0$	15.81±0.03	80.72±0.03	$5.21×10^{-01}$
HF (HR)	13.33±0.01	58.71±0.01	$4.22×10^1$	12.64±0.02	83.60±0.02	$9.38×10^{-5}$	13.37±0.01	118.55±0.03	$5.41×10^{-11}$
MP2(FULL)(HR)	13.08±0.04	63.54±0.05	$2.58×10^0$	12.83±0.01	68.80±0.02	$1.30×10^{-1}$	13.00±0.02	368.17±0.04	$3.88×10^{-61}$
B3LYP (HR)	13.23±0.02	50.04±0.03	$1.80×10^3$	12.95±0.03	65.09±0.04	$9.40×10^{-1}$	14.52±0.03	79.17±0.05	$5.45×10^{-2}$
HF (FR)	13.59±0.00	61.62±0.02	$2.02×10^1$	12.90±0.01	86.47±0.04	$4.57×10^{-5}$	13.32±0.02	121.39±0.04	$1.31×10^{-11}$
MP2(FULL)(FR)	13.40±0.01	66.59±0.02	$1.33×10^0$	13.15±0.03	71.85±0.05	$6.69×10^{-2}$	13.02±0.04	371.21±0.04	$1.01×10^{-61}$
B3LYP (FR)	13.70±0.02	53.87±0.03	$9.14×10^2$	13.30±0.01	68.39±0.01	$4.63×10^{-1}$	14.69±0.01	83.00±0.01	$1.39×10^{-2}$
Experiment[a]	13.48±0.30	53.42±1.39	$6.84×10^2$	14.47±0.46	66.47±2.15	$1.65×10^1$	15.91±0.63	67.70±3.20	$2.59×10^2$

The HO, HR, and FR in the parentheses correspond to harmonic oscillator, hindered rotor and free rotor models for the torsional mode. The entropy of activation considering harmonic oscillator model, $\Delta S^{\neq}$, at 1100 K are 3.44, 2.64, and 3.39 cal K^{-1} mol^{-1} for HBr elimination at HF, MP2 (FULL), and DFT levels, respectively. For H$_2$O elimination, the corresponding values are 0.52, 1.37, and 1.49 cal K^{-1} mol^{-1}. For HOBr elimination, the corresponding values are 3.15, 6.34, and 8.90 cal K^{-1} mol^{-1}. The entropy of activation considering hindered rotor model, $\Delta S^{\neq}$, at 1100 K are 0.15, -0.91, and 0.38 cal K^{-1} mol^{-1} for HBr elimination at HF, (FULL), and DFT levels, respectively. For H$_2$O elimination, the corresponding values are -3.74, -3.15, and -1.54 cal K^{-1} mol^{-1}. For HOBr elimination, the corresponding values are -1.09, -2.25, and 4.61 cal K^{-1} mol^{-1}. The entropy of activation considering free rotor model, $\Delta S^{\neq}$, at 1100 K are -3.56, -4.54, and -3.43 cal K^{-1} mol^{-1} for HBr elimination at HF, (FULL), and DFT levels, respectively with 6-311++G** basis set. For H$_2$O elimination, the corresponding values are -6.47, -5.80, and -5.31 cal K^{-1} mol^{-1}. For HOBr elimination, the corresponding values are -3.84, -0.35, and 2.09 cal K^{-1} mol^{-1}. The change in

entropy of activation values from positive to negative indicates the transition in the structure of transition state from loose and big to tight and stiff structure. A is in s^{-1} and E_a is in kcal mol^{-1}. Rate constant calculated at 1100 K in s^{-1}. [a]Experimental results are in better agreement with theoretical results for HBr elimination using FR model. Experimental values are from present study. The theoretical results given for BEOH are Boltzmann weighted averages for the five G_g, G_g, G_t, T_g and T_t forms for HBr elimination. However, for H_2O elimination averaged over four conformers except G_g and for HOBr elimination only over three gauche conformers. Hindered rotor partition function is from a full approximation following Truhlar's method. The E_0 values are 58.05, 62.90, and 48.85 kcal mol^{-1} at HF, MP2, and DFT levels for HBr elimination, respectively. For H_2O elimination, the corresponding values are 83.14, 68.02, and 64.34 kcal mol^{-1}. For HOBr elimination, the corresponding values are 117.32, 367.50, and 78.57 kcal mol^{-1}. The E_0 values given here are relative to $G_{g'}$ conformer.

Table IV.9. Entropy of activation ($\Delta S^{\#}$) in cal/mol/K and ratio of partition function evaluated using three different models for HBr, H_2O and HOBr elimination from 2-bromoethanol at HF, MP2(FULL) and DFT level with 6-311++G basis set using harmonic oscillator, hindered rotor and free rotor model at 1100 K.**

Theory/6-311++G**basis Set	Elimination reactions	Ratio of Partition function considering all modes at 1100K			$\Delta S^{\#}$ at 1100 K using three models		
		$Q^{\#}/Q^R$ (HO)	$Q^{\#}/Q^R$ (HR)	$Q^{\#}/Q^R$ (FR)	Harmonic oscillator	Hindered rotor	Free rotor
HF	HBr	5.65	1.08	0.17	3.44	0.15	-3.56
MP2(FULL)	HBr	3.78	0.63	0.10	2.64	-0.91	-4.54
DFT	HBr	5.50	1.21	0.18	3.39	0.38	-3.43
HF	H_2O	1.30	0.15	0.04	0.52	-3.74	-6.47
MP2(FULL)	H_2O	1.99	0.21	0.05	1.37	-3.15	-5.80
DFT	H_2O	2.12	0.46	0.07	1.49	-1.54	-5.31
HF	HOBr	4.89	0.58	0.15	3.15	-1.09	-3.84
MP2(FULL)	HOBr	24.30	0.32	0.84	6.34	-2.25	-0.35
DFT	HOBr	88.30	10.20	2.87	8.90	4.61	2.09

The entropy of activation ($\Delta S^{\#}$) in cal/mol/K evaluated using different models for HBr, H_2O and HOBr elimination reaction from 2-bromoethanol at HF, MP2(FULL) and DFT level with 6-311++G** basis set using harmonic oscillator, hindered rotor and free rotor model at 1100 K have been listed in Table IV.9.

It can be noticed from Table IV.8 that the Arrhenius parameters for unimolecular HBr elimination deduced from experimental results have no satisfactory agreement with TST determined data at HF, MP2(FULL) and B3LYP level with 6-311++G** basis set using harmonic oscillator model. Experimentally determined preexponential factor for HBr elimination from BEOH, ethyl bromide[52], bromochloroethane[53] and 1, 2-dibromoethane[2] are $10^{13.48}$, $10^{13.60}$, $10^{9.04}$ and $10^{13.40}$ s^{-1}, respectively.

Table IV.10. Comparison of the rate parameters for the unimolecular elimination of HBr with dibromoethane and ethyl bromide considering harmonic oscillator model

Theory/basis set	$BrC_2H_4OH \rightarrow HBr + CH_3CHO$		$BrC_2H_4Br \rightarrow HBr + CH_2=CHBr$		*$C_2H_5Br \rightarrow HBr + CH2=CH2$	
	log A	E_a	log A	E_a	log A	E_a
HF/6-311++g**	14.41±0.01	59.42±0.02	14.69±0.02	66.47±0.03	14.66±0.02	58.23±0.02
MP2(FULL)/6-311++g**	14.19±0.02	64.21±0.03	14.78±0.01	67.84±0.01	14.66±0.01	63.10±0.02
DFT/6-311++g**	14.44±0.01	51.38±0.02	14.64±0.02	56.16±0.04	14.64±0.02	51.14±0.03
Experiment	13.5±0.3	53.4±1.4	13.40	56.00	13.3	53.5

*Experimental values are from reference 51.

Table IV.11. Comparison of the rate parameters for the unimolecular elimination of HBr with chlorobromoethane and fluorobromoethane considering harmonic oscillator model

Theory/basis set	$BrC_2H_4OH \rightarrow HBr+ CH_3CHO$		$BrC_2H_4Cl \rightarrow HBr + CH_2=CHCl$		$BrC_2H_4F \rightarrow HBr + CH_2=CHF$	
	log A	E_a	log A	E_a	log A	E_a
HF/6-311++g**	14.41±0.01	59.42±0.02	14.65±0.03	66.48±0.03	14.71±0.01	67.21±0.01
MP2(FULL)/6-311++g**	14.19±0.02	64.21±0.03	14.72±0.02	67.64±0.04	[b] -	-
DFT/6-311++g**	14.44±0.01	51.38±0.02	14.64±0.01	55.96±0.02	14.67±0.01	56.22±0.02
Experiment	13.5±0.3	53.4±1.4	-	[a]58.00	-	-

[a]58.00 is the E_0 value(reference 52) [b] could not be optimized.

Table IV.12. Comparison of the rate parameters for the unimolecular elimination of HBr from vinyl bromide

Theory/basis set	$CH_2CHBr \rightarrow CH_2CH_2 + HBr$	
	log A	E_a
HF/6-311++g**	14.89±0.01	74.93±0.01
MP2(FULL)/6-311++g**	14.87±0.01	77.75±0.02
DFT/6-311++g**	14.76±0.01	66.75±0.01
*Literature	15.22	65.58

*Reference 20

Table IV.10 indicates that the TST fitted rate coefficient for HBr elimination from the vinyl bromide resulting in the formation of acetylene has good agreement with the literature reported value[20]. This rate coefficient has been used in the modeling in order to

predict experiment C_2H_2 concentration. We have found good agreement between experimental and modeled concentration for the same.

We have observed in our previous analysis for HCl elimination from chlorofluoroethane and dichloroethane that the preexponential factors reduces by an order of magnitude when the C-C bond rotations were treated as free internal rotors.[57] The calculated preexponential factor for HCl elimination from ethyl chloride, chlorofluoroethane, and 1, 2-dichloroethane are $10^{13.96}$, $10^{13.53}$, and $10^{13.68}$ s^{-1}, respectively.[57] In fact, there are two low frequency torsional motion in case of BEOH corresponding to C-C and C-O bond rotations. Hence, these two internal rotors have been treated as either harmonic oscillator (HO) or hindered internal rotor (HR) or free rotor (FR) for estimating the preexponential factor for HBr, H_2O and HOBr elimination reactions from BEOH. Hindered rotor partition function calculation was done only for the reactant not for TS. In the case of transition state, C-O internal motion for HCl elimination was found to be coupled with other modes in the transition state and hence was not treated as hindered rotor. Truhlar's detailed methodology[58] was followed for treating the torsional modes as hindered rotor that results in decrease of preexponential factor by an order of magnitude from $10^{14.44}$ to $10^{13.23}$ at B3LYP/6-311++G** level for HBr elimination. This brings about an order of magnitude difference between experimental and theoretical preexponential factor at DFT level. In fact, DFT free rotor calculations leads to excellent quantitative agreement between experimental and theoretical rate coefficient of HBr elimination reaction as shown in Table IV.8. However, DFT level calculations using harmonic oscillator and free rotor model overestimates the

total rate coefficient of HBr elimination. It can be noticed from Table IV.8 that the theoretical results at all other levels exhibit considerable deviation from the shock tube data and underestimates significantly. This fact is clear from a comparison of Arrhenius plots of the present shock tube determined and TST calculated results at HF, MP2(full) and B3LYP level with 6-311++G** basis set using three models for the HBr elimination reaction as well in the temperature range of 910-1102 K that has been displayed in the Figure IV.14.

A comparison of Arrhenius parameters determined at HF, MP2 (FULL) and B3LYP level of theories using the 6-311++G** basis set using HO, HR and FR models for both HBr, HOBr and H_2O elimination reactions with experimental results have been compiled in Table IV.8. We have observed close agreement between experiment and theoretical results at all levels of theory for the preexponential factor treating internal rotors as hindered and free rotor. However, it was found that the harmonic oscillator calculations at all levels predicts an increase in preexponential factor by an order of magnitude. The predicted rate coefficient for HBr elimination determined considering harmonic oscillator model at CBS-QB3 higher level of calculation are $10^{14.67\pm0.02}$ exp [-(48.73±0.03)/(RT)] s^{-1}. This calculation also underestimates the E_a approximately by 4.7 kcal mol^{-1}. However, the predicted preexponential factor is an order of magnitude higher than experimental value.
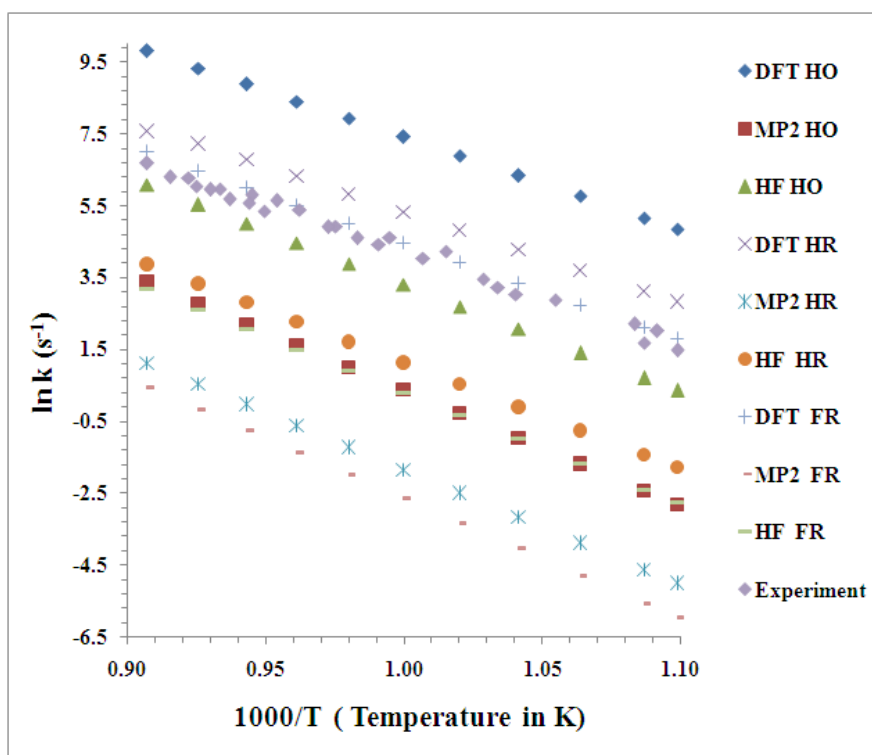
Figure IV.14. Comparison of Arrhenius plot for rate coefficient data obtained from experimental and theoretical results for unimolecular elimination of HBr from 2-bromoethanol at HF, MP2(FULL) and DFT(B3LYP) level of theory with 6-311++G** basis set using HO, HR and FR models. The HO, HR, and FR correspond to harmonic oscillator, hindered rotor and free rotor. The data are labeled with different symbols and are designated in Figure above.

The activation energies for H_2O elimination in case of C_2H_5OH are 85.2, 68.5, and 64.5 kcal mol^{-1} at HF, MP2 (FULL), and DFT level with 6-311++G** basis set, respectively.[18] However, the theoretical value reported by Lin and co-workers is 66.6 kcal mol^{-1} that is close to predicted MP2 and DFT level values.[59] The E_a at the same

levels for H_2O elimination from BEOH are 84.43, 69.63, and 66.08 kcal mol^{-1}, respectively.

This variation of $\sim$ 1-2 kcal mol^{-1} at all levels basically represents the fact that β-substitution of Br does not have a significant effect on the E_a of H_2O elimination within the experimental uncertainty. However, at similar level, the E_a for H_2O elimination from 2-floroethanol are 92.43, 75.52, and 70.07 kcal mol^{-1}, respectively. The E_a at the same levels for H_2O elimination from CEOH are 86.75, 71.32, and 67.13kcal mol^{-1}, respectively. This study certainly unveils the fact that the β-substitution of F brings about the significantly large increase in activation barrier by $\sim$ 6-7 kcal/mol for H_2O elimination. The experimental E_a for H_2O elimination from BEOH, 2-chloroethanol, 2-fluoroethanol,[18] and ethyl alcohol[59] are 66.47, 67.9, 69.7, and 67.9 kcal mol^{-1}, respectively also describes the fact that the β-substitution of F leads to an increase of $\sim$2 kcal/mol in E_a accounting for β-substitution effect, however, Br and Cl do not.

From Table IV.13 it is clear that the HF, MP2 (FULL) level calculations overestimate E_a for H_2O elimination, by 17.96 and 3.16 kcal mol^{-1} respectively. However, the DFT predictions underestimate E_a by 0.39 kcal/mol in temperature range of 910-1102 K. It can be concluded that the E_a estimated at DFT level have been found to be in good agreement with experimental results. This is also the case in ethanol, 2-chloroethanol and 2-fluoroethanol[18] that can be noticed from Table IV.13. It must be emphasized here that the predicted as well as experimental value of E_a for H_2O elimination is higher than that of HBr at all levels of theory considered here.

It should be noticed here that the E_a values predicted considering free rotor model at all levels for both HBr, HOBr and H_2O elimination reactions have been underestimated by ~1-3 kcal mol^{-1} than that estimated by harmonic oscillator and hindered rotor models as given in Table IV.8.

The experimental pre-exponential factor for H_2O elimination from BEOH, 2-chloroethanol, ethyl alcohol, and 2-fluoroethanol[18] are $10^{14.47}$, $10^{14.95}$, $10^{13.74}$, and $10^{14.30}$ s^{-1}, respectively. We observed that the TST calculations at all HF, MP2(FULL), and B3LYP level with 6-311++G** basis set underestimates preexponential factors by an order of magnitude by harmonic oscillator model for HBr elimination from BEOH. They are $10^{13.71}$, $10^{13.90}$, and $10^{13.97}$ s^{-1}, respectively. However, treating the torsional modes, both C-C and C-O bond rotation, as hindered rotor results in a further decrease of preexponential factor by an order of magnitude. It is $10^{12.64}$, $10^{12.83}$, and $10^{12.95}$ s^{-1} at the same level, respectively. These calculations lead to further decrease of the rate coefficient in the temperature range of investigation. A free rotor calculation underestimates the rate coefficient of H_2O elimination to a large extent as illustrated in the Figure IV.15.

Table IV.8 reveals that the present shock tube investigations overestimates the rate coefficient for H_2O elimination reaction by 2.6 times as compared to that estimated at DFT/6-311++G** level using harmonic oscillator model. However, the theoretical result at all other levels uniformly underestimates the rate coefficients for H_2O elimination. The same can be observed from a combined Arrhenius plot of the present shock tube and TST fitted results calculated at all levels for the H_2O elimination reaction in the temperature range of 910-1102 K as represented in the Figure IV.15.
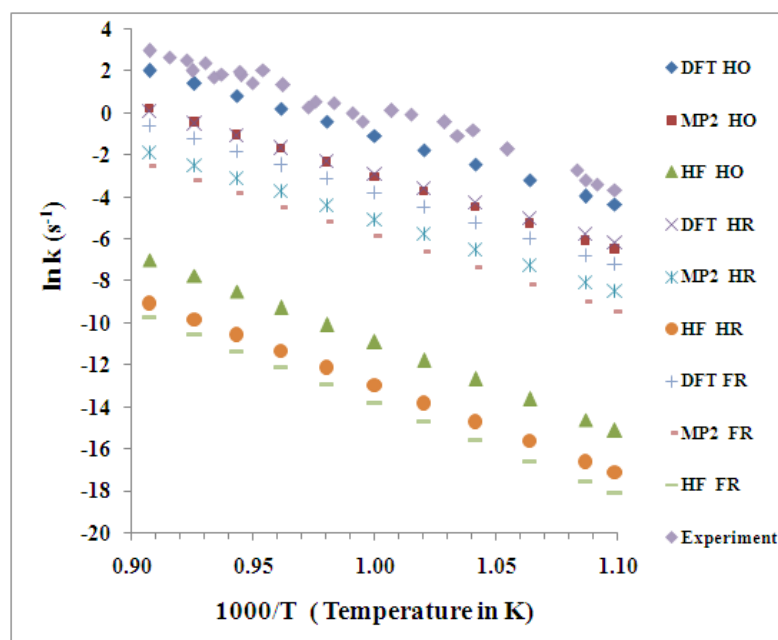
Figure IV.15. Comparison of Arrhenius plot for rate coefficient data obtained from experimental and theoretical results for unimolecular elimination of H_2O from 2-bromoethanol at HF, MP2(FULL) and DFT(B3LYP) level of theory with 6-311++G** basis set using HO, HR and FR models. The HO, HR, and FR correspond to harmonic oscillator, hindered rotor and free rotor. The data are labeled with different symbols and are designated in Figure above.

In order to gain better insight into the Arrhenius parameters, the rate coefficient for H_2O elimination were determined to be $10^{14.24\pm0.02}$ exp [-(185.45±0.01)/(RT)] s^{-1} considering harmonic oscillator model at higher CBS-QB3 level of theory. However, these calculations also overestimate the E_a to a large extent. The comparison of experimental and theoretical A and E_a values determined at HF, MP2 (FULL), B3LYP level of theory with the 6-311++G** basis set of H_2O elimination from BEOH with that from ethyl alcohol and 2-fluoroethanol[18] have been summarized in the Table IV.13.

232

Table IV.13. Comparison of rate parameters for the unimolecular elimination of H$_2$O with fluoroethanol, chloroethanol and ethyl alcohol

Theory/ basis set	BrC$_2$H$_4$OH → H$_2$O + CH2=CHBr		FC$_2$H$_4$OH → H$_2$O + CH2=CHF		ClC$_2$H$_4$OH → H$_2$O + CH2=CHCl		C$_2$H$_5$OH → H$_2$O + CH$_2$CH$_2$	
	log A	E$_a$	log A	E$_a$	log A	E$_a$	log A	E$_a$
HF/ 6-311++g**	13.71±0.02	84.43±0.03	14.32± 0.01	92.43 ± 0.02	13.78±0.02	86.75±0.03	14.79±0.00	85.24±0.02
MP2/ 6-311++g**	13.90±0.01	69.63±0.01	14.72 ±0.01	75.52 ±0.03	13.97±0.03	71.32±0.05	13.97±0.00	68.56±0.02
DFT/ 6-311++g**	13.97±0.02	66.08±0.03	14.71± 0.01	70.07± 0.03	14.08±0.03	67.13±0.03	14.39±0.00	64.47±0.02
Experiment	14.47±0.46	66.47±2.15	14.30± 0.13	69.69 ±1.70	14.95±0.33	67.95±1.50	13.74	67.90

233

In case of HOBr elimination total rate coefficient was estimated by taking the sum over the three conformers, $G_{g'}$, G_t, G_g , weighted by Boltzmann factor (*w*). Since the T_t and T_g conformers cannot lead to HOBr elimination. However the reaction path degeneracy considered for each conformer in any case is one.

$$ k = k_{G_{g'}} w_{G_{g'}} + k_{G_t} w_{G_t} + k_{G_g} w_{G_g} $$

The rate coefficient estimated for HOBr elimination reaction at HF, MP2 (FULL) and DFT level with 6-311++g** basis set have been given in the Table IV.8. However, the experimentally observed C_2H_4 is significantly more than what could be accounted for using kinetic simulations with well established rate constants. Therefore, a direct HOBr elimination channel was invoked to account for the C_2H_4 concentration. For the FCH_2CH_2OH, earlier attempts to identify a transition state for HOF elimination theoretically did not succeed.[19] However, the rate coefficient estimated for HOCl elimination reaction at MP2 (FULL)/6-311++g** level of theory is given by $10^{15.05\pm0.01}$ exp $[-(100.45\pm0.02)/(RT)]$ s^{-1}. In fact, for the FCH_2CH_2Cl the barrier for the analogous ClF elimination channel was significantly higher, 145 kcal mol^{-1}.[60] For HOBr elimination from bromoethanol, the calculated barrier is 80.72 kcal mol^{-1} DFT/6-311++g** level of theory. However, in order to fit the experimental concentration of C_2H_4, it was needed to use activation energy barrier of 72.00 kcal mol^{-1} for the HOBr elimination channel. Comparison of Arrhenius plot obtained from modeling and TST fitted results using DFT/6-311++g** calculations for unimolecular elimination of HOBr using harmonic oscillator model is depicted in Figure IV.16. The rate coefficient obtained

from fitting to complex mechanism is given by $10^{15.71\pm0.52}$ exp [-(66.72±2.60)/(RT)] s^{-1}. DFT predicted value of A using harmonic oscillator model for HOBr elimination form 2-bromoethanol was found to be in close agreement with experimentally determined one. However, the calculated E_a is overestimated by approximately 13 kcal/mol as shown in the Table IV.8. Hence, the calculated rate constant is too slow as compared to experimentally determined one.
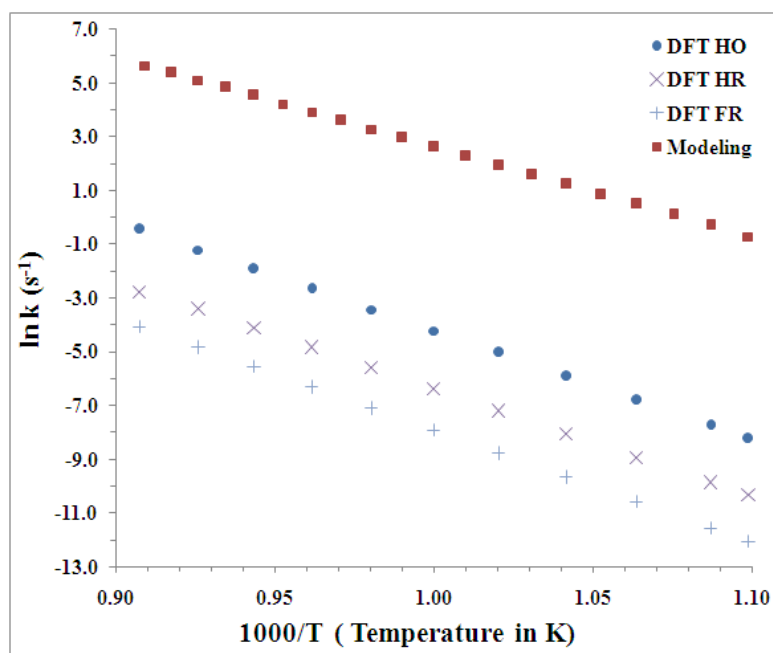
Figure IV.16. Comparison of Arrhenius plot for rate coefficient data obtained from modeling and theoretical results for unimolecular elimination of HOBr from 2-bromoethanol at B3LYP with 6-311++G** basis set using HO, HR and FR models. The data are labeled with different symbols and are designated in Figure above.

IV.7. Conclusions

In the present study, the thermal decomposition of 2-bromoethaonl has been investigated in the temperature range of 910-1102 K using shock tube apparatus. The Arrhenius parameters for all of the unimolecular elimination channels have been evaluated using the TST calculations employing both ab initio and DFT methods to support our experimental results. The experimental first order overall thermal decomposition rate coefficient derived by using the Arrhenius expression is $10^{14.08\pm0.23}$ exp [-(55.66±1.07)/(RT)] s^{-1}. The experimental rate coefficient for HBr elimination is $10^{13.48\pm0.30}$ exp [(-53.42±1.39)/(RT)] s^{-1} and that for the H_2O elimination is $10^{14.47\pm0.46}$ exp [-(66.47±2.15)/(RT)] s^{-1}. These experimental results have been found to be in very good agreement with the earlier reported data within the uncertainty limit for HBr and H_2O elimination reactions. The reaction scheme proposed for the thermal decomposition of 2-bromoethanol containing the 47 elementary reactions and 28 species can successfully account for the yields of products as a function of temperature. The reduced kinetic model proposed here using sensitivity analysis contains 32 reactions and 27 species. This mechanism was ultimately validated by the comparison to experimental results. The mechanism proposed here is similar to that of the fluoroethanol and chloroethanol. The reported experimental rate coefficients for the unimolecular elimination reactions of HBr and H_2O can adequately be described by the TST fitted results. More specifically, the estimated activation energies for H_2O elimination at MP2 (FULL) and DFT level of theory with 6-311++G** basis set were overestimated by +3.16 and underestimated by -0.39 kcal mol^{-1} respectively. The calculated activation energies for HBr elimination at HF

and DFT level with 6-311++G** basis set were overestimated by +6.00 and underestimated by -2.04 kcal mol^{-1} respectively. The pre-exponential factor evaluated using the hindered rotor approximation for low frequency torsional mode resulted in good agreement between theoretical and experimental values for the HBr elimination. The formation of ethene was explained by considering the possibility of HOBr elimination. The expression for the rate coefficient derived from fitting to complex mechanism for HOBr elimination reaction is $10^{15.91\pm0.63}$ exp [(-67.70±3.20)/(RT)] s^{-1}. Additionally, the TST fitted Arrhenius parameters for HOBr elimination reaction has also been estimated using both ab initio and DFT methods. This study also provides the IRC results performed for the verification of the three transition states. Present study has revealed both experimentally and theoretically for HBr elimination that the bromine, chlorine and fluorine substitution leads to an increase in E_a, however, OH substitution do not. For H_2O elimination the Br substitution does not bring about significant variation but F substitution does increase the E_a.

IV.8.References

1. Indulkar, Y.N.; Upadhayaya, H.P.; Kumar,A.; Waghmode, S,B.; Naik, P.D. *J. Phys. Chem. A* **2009**, 113, 8462.

2. Good, P.T.; Maccoll, A. *J. Chem. Soc. (B),* **1971,** 268.

3. Chang, P.-T.; Shih, J.-J.; Kuo, K.-H.; Chen, C.-Y.; Fu, T.-W.; Shieh, D.-L.; Liao, Y.-H.; Lin, J.-L. *J. Phys. Chem. B* **2004,** 108, 13320

4. Durig, J.R.; Shen, S.; Guirgis, G.A. *J. Mol. Struc.*, **2001**, 560,, 295.

5. Hinsta, E.J.; Zhao, X.; Lee, Y.T. *J. Chem. Phys*. **1990**, 4, 2280.

6. Hoffman III, W.F. *J. Mol. Struc.*, **1987**, 157, 275.

7. Jenneskens, L.W.; Wiersum, U.E.; Ripoll, J.-L. *Tetrahedron Letters*, **1988**, 29, 6489.

8. Laws, P.A.; Hayley, B.D.; Anthony, L.M.; Roscoe, J.M. *J. Phys. Chem. A* **2001**, 105, 1830.

9. McGrath, M.P.; Rowland, F.S. *J. Phys. Chem. A* **2002**, 106, 8191.

10. Nisar, J.; Awan, I.A. *Int. J. chem. Kinet.* **2007**, 39, 1.

11. King, K.D.; Gilbert, R.G. *Int. J. Chem. Kinet*, **1980**, XII, 339.

12. Zou, P.; Shu, J.; Sears, T.J.; Hall, G.E.; North, S.W. *J. Phys. Chem. A* **2004**, 108, 1482

13. Simmie, J.M.; Curran, H.J. *J. Phys. Chem. A* **2009**, 113, 7834.

14. Lewis, D.; Keil, M.; Sarr, M. *J. Am. Chem. Soc.* **1974**, 96, 4398.

15. Kalra, B.L.; Lewis, D.K.; Singer, S.R.; Raghavan, A.S.; Baldwin, J.E.; B.Andes H. Jr. *J. Phys. Chem. A* **2004**, 108, 11554.

16. Ferguson, H.A.; Parworth, C.L.; Holloway, T.B.; Midgett, A.G.; Heard, G.L.; Setser, D.W.; Holmes, B.E. *J. Phys. Chem. A* **2009**, 113, 10013.

17. Wu, C.-W.; Matsui, H.; Wang, N.-S.; Lin, M. C. *J. Phys. Chem. A* **2011**, 115, 8086.

18. Chakravarty, H. K.; Reddy, K. P. J., Arunan, E.: Proceedings of 27th international symposium on shock waves, **2009**, 32.

19. Rajakumar, B.; Reddy, K. P. J.; Arunan, E. *J. Phys. Chem. A* **2003**, 107, 9782.

20. Shilov, A. E.; Sabirova, R. D.; *Kinet. Catal.* **1964**, 5, 32.

21. Diau, E.W-G; Lee, Y-P. *J. Chem. Phys.* **1992**, 96, 377.

22. Lifshltz, A.; B-H, Halm**.** *J. Phys. Chem.* **1983**, 87, 1782.

23. Lifshitz, A.; Tamburu,C.; Suslensky, A. *J. Phys. Chem.* **1990**, 94, 2966.

24. Kern, R.D.; Singh, H.J.; Xie, K. *AIP Conf. Proc. (Curr. Top. Shock Waves),* **1990**, 487.

25. Wakamatsu, H.; Hidaka, Y. *Int. J. Chem. Kinet*. **2008**, 40, 320.

26. Senosiain, J.P.; Klippenstein, S.J.; Miller, J.A. J. *Phys. Chem. A.* **2006**, 110, 5772.

27. Tsang, W.; Hampson, R.F. *J. Phys. Chem. Ref. Data*, **1986**, 15, 1087.

28. Li, J.;Zhao, Z.W.; Kazakov, A.; Chaos, M.; Dryer, F.L.; Scire, J.J. *Int. J. Chem. Kinet.* **2007**, 39,109.

29. Klippenstein, S.J.; Georgievskii, Y.; Harding, L.B. Phys. *Chem. Chem. Phys.* **2006**, 8,1133.

30. Curran, H.J. *Int. J. Chem. Kinet.* **2006**, 38, 250.

31. Harding, L.B.; Georgievskii, Y.; Klippenstein, S.J. *J. Phys. Chem. A.***2005**, 109, 4646.

32. Stewart, P.H.; Larson, C.W.; Golden, D.M. *Combust. Flame*, **1989**, 75, 25.

33. Just, Th.; Roth, P.; Damm, R. *Symp. Int. Combust. Proc.***1977**, 16.

34. Skinner, G.B.; " *Shock Waves in Chemistry*" ; Lifshitz, A. Ed.: Marcel Dekker: New York, **1981.**

35. Warnatz, J. *Combustion Chemistry*, ed. W.C. Gardiner,Jr., pub. Springer-Verlag,NY, **1984**.

36. Mackie, J.C.; Doolan, K.R. *Int. J. Chem. Kinet.* **1984**, 16, 525.

37. Pratt, G.; Veltman, I. *J. Chem. Soc. Faraday Trans. 1*, **1974**, 70, 1840.

38. Back, R.A. *Can. J. Chem.* **1983**, 61, 916.

39. Takahashi, J.; Momose, T.; Shida, T. *Bull. Chem. Soc. Jpn*. **1994**, 67, 74.

40. Brodsky, A.M.; Kalinenko, R.A.; Lavrovsky, K.P. *J. Chem. Soc*. **1960**, 4443.

41. Dean, A.M. *J. Phys. Chem*, **1985**, 89, 4600.

42. Oehlschlaeger, M.A.; Davidson, D.F.; Hanson, *R.K. Proc. Combust. Inst*. **2005**, 30, 1119.

43. Manion, J.A.; Louw, R. *J. Chem. Soc. Perkin Trans. 2*, **1988**, 1547.

44. Jung, K-H.; Choi, Y.S.; Yoo, H.S.; Tschuikow-Roux, E. *J. Phys. Chem.* **1986,** *90,* 1816.

45. Baulch, D.L.; Duxbury, J.; Grant, S.J.; Montague, D.C. J. *Phys. Chem. Ref. Data*, **1981**, 10.

46. DeMore, W.B.; Sander, S.P.; Golden, D.M.; Hampson, R.F.; Kurylo, M.J.; Howard, C.J.; Ravishankara, A.R.; Kolb, C.J.; Molina, M.J. *JPL Publication 94-26*, **1994**, 1.

47. Baulch, D.L.; Cobos, C.J.; Cox, R.A.; Esser, C.; Frank, P.; Just, Th.; Kerr, J.A.; Pilling, M.J.; Troe, J.; Walker, R.W.; Warnatz, J. *J. Phys. Chem. Ref. Data*. **1992**, 21, 411.

48. Knyazev, V.D.; Bencsura, A.; Stoliarov, S.I.; Slagle, I.R. *J. Phys. Chem*. **1996**, 100, 11346.

49. Bauerle, S.; Klatt, M.; Wagner, H.Gg. *Ber. Bunsenges. Phys. Chem.* **1995**, 99, 870.

50. Harding, L.B.; Schatz, G.C.; Chiles, R.A. *J. Chem. Phys*, **1982**, 76, 5172.

51. Souza, F. R.; Freitas, M. P.; *Comp. Theo. Chem.* **2011**, *964*, 155.

52. Tsang, W.; *J. Chem. Phys.,* **1964**, 41, 2487.

53. Friedrich, L.; Duncan, J.R.; Heard, G.L.; Setser, D.W.; Holmes, B.E. *J. Phys. Chem. A* **2010,** 114, 4138.

54. Jung, K.-H.; Kang, S.H.; Ro, C.U.; Tschuikow-Roux, E. *J. Phys. Chem.* **1987,** 91, 2354.

55. Tsang, W. J.; Int. J. Chem. Kinet 1970, 2, 311.

56. Rajakumar, B.; Reddy, K. P. J.; Arunan, E. *J. Phys. Chem. A*, 2002, 106, 8366.

57. Rajakumar, B.; Arunan, E. *Phys. Chem. Chem. Phys.,* **2003**, 5, 3897.

58. Chuang, Y.Y.; Truhlar, D. G .; *J. Chem. Phys.* **2000**, 112, 1221.

59. Park, J.; Zhu, R. S.; Lin, M. C.; *J. Chem. Phys.* **2002**, *117*, 3224.

60. Zhu, L.; Bozzelli, J. W.; *Chem. Phys. Lett.* **2002**, *357*, 65.

Table IV.A.1. Normal mode vibrational frequencies of 2-bromoethanol in G_g, conformer at DFT, HF AND MP2 (FULL) levels of theory with 6-31G**, 6-31+G** and 6-311++G** basis sets (cm^{-1}).

HF			MP2 (FULL)			B3LYP		
6-31G**	6-31+G**	6-311++G**	6-31G**	6-31+G**	6-311++G**	6-31G**	6-31+G**	6-311++G**
156.0	141.9	144.4	160.8	149.7	147.2	148.8	132.3	129.9
275.0	277.1	274.6	269.2	272.1	271.7	257.6	260.7	258.0
413.6	386.5	386.4	420.0	406.8	418.0	409.1	388.8	374.7
486.9	490.3	485.6	465.0	468.5	465.2	452.7	454.8	449.0
606.1	606.3	604.7	605.0	604.7	613.5	562.4	562.0	556.1
914.8	919.6	912.3	868.1	870.7	862.8	844.9	848.5	841.0
1000.7	1002.2	998.3	958.2	956.1	954.2	921.3	921.6	918.2
1115.2	1123.9	1113.8	1059.2	1063.0	1055.2	1021.7	1030.0	1019.4
1213.6	1209.4	1207.4	1130.4	1119.3	1127.9	1100.4	1091.3	1085.5
1286.1	1275.4	1274.0	1219.8	1206.7	1211.2	1193.0	1183.0	1180.5
1314.6	1316.7	1311.7	1242.2	1236.0	1224.9	1203.4	1202.3	1198.7
1411.4	1418.7	1409.8	1335.2	1338.8	1329.2	1289.9	1294.2	1287.7
1510.6	1493.3	1499.3	1427.1	1398.0	1405.9	1399.6	1375.8	1380.8
1555.4	1551.6	1547.4	1457.3	1447.7	1440.0	1426.2	1416.3	1413.5
1600.2	1599.0	1590.3	1519.8	1511.4	1476.0	1475.9	1471.9	1461.8
1639.6	1634.8	1626.5	1557.4	1545.8	1514.2	1508.1	1498.1	1490.3
3191.1	3197.5	3180.0	3109.2	3114.2	3073.5	3007.1	3019.7	3008.2
3241.3	3246.3	3224.5	3184.2	3174.9	3133.8	3069.5	3077.8	3059.7
3279.8	3275.2	3257.0	3193.2	3193.7	3148.2	3115.0	3108.0	3095.9
3355.5	3347.8	3325.9	3275.1	3260.3	3213.1	3190.6	3180.0	3164.3
4160.4	4165.5	4160.8	3853.5	3837.4	3859.1	3766.5	3779.9	3795.9

Table IV.A.2. Normal mode vibrational frequencies of 2-bromoethanol in G$_g$ conformer at DFT, HF AND MP2 (FULL) levels of theory with 6-31G**, 6-31+G** and 6-311++G** basis sets (cm^{-1})

HF			MP2 (FULL)			B3LYP		
6-31G**	6-31+G**	6-311++G**	6-31G**	6-31+G**	6-311++G**	6-31G**	6-31+G**	6-311++G**
130.3	114.8	129.2	132.3	126.0	134.3	117.8	104.6	116.5
241.3	230.7	241.3	234.3	236.1	246.5	222.7	215.7	223.9
329.9	309.6	319.2	327.4	317.8	331.4	312.9	292.8	299.5
493.5	497.6	493.0	471.1	474.6	475.3	457.2	460.0	455.2
617.9	616.6	616.5	612.8	610.6	620.1	570.4	567.0	562.2
908.9	914.3	907.6	861.7	864.0	856.6	836.8	840.0	833.4
1018.1	1022.0	1016.3	976.0	975.8	971.6	937.3	939.8	935.1
1091.7	1095.0	1091.0	1029.9	1029.5	1028.1	998.8	1002.3	995.5
1203.1	1200.5	1195.4	1146.3	1134.3	1136.6	1112.5	1102.8	1094.6
1249.9	1246.5	1244.9	1162.1	1155.3	1158.3	1136.0	1133.1	1131.1
1355.6	1359.1	1352.4	1278.9	1277.4	1269.9	1240.4	1245.0	1237.3
1421.8	1428.0	1419.5	1347.2	1349.4	1337.8	1305.1	1307.5	1300.6
1498.4	1483.2	1488.1	1412.1	1386.1	1392.5	1385.5	1362.9	1368.1
1557.6	1554.3	1551.0	1459.1	1451.2	1444.9	1429.1	1421.1	1418.8
1607.2	1606.2	1596.3	1528.8	1519.6	1482.3	1483.8	1479.1	1469.1
1637.5	1633.7	1625.5	1555.2	1545.2	1512.4	1506.1	1497.2	1489.6
3146.7	3154.1	3137.3	3078.7	3083.5	3043.4	2961.3	2973.8	2960.9
3258.5	3255.0	3237.5	3170.4	3159.4	3118.4	3092.6	3087.7	3077.0
3280.7	3284.4	3262.3	3215.3	3214.8	3167.4	3111.6	3116.3	3099.2
3328.9	3322.8	3302.1	3249.7	3237.6	3190.3	3162.7	3154.7	3140.4
4179.7	4182.7	4174.7	3886.4	3870.3	3888.5	3808.4	3818.5	3826.8

Table IV.A.3. Normal mode vibrational frequencies of 2-bromoethanol in G_t conformer at DFT, HF AND MP2 (FULL) levels of theory with 6-31G**, 6-31+G** and 6-311++G** basis sets (cm^{-1})

HF			MP2 (FULL)			B3LYP		
6-31G**	6-31+G**	6-311++G**	6-31G**	6-31+G**	6-311++G**	6-31G**	6-31+G**	6-311++G**
139.6	133.4	133.5	140.3	117.9	118.4	126.7	119.0	119.1
195.5	192.2	193.8	200.4	135.1	135.1	178.6	151.4	146.6
282.5	282.0	282.1	276.1	271.2	271.2	262.2	259.5	259.3
479.8	477.7	477.8	455.9	455.2	455.1	442.8	441.5	441.5
615.1	613.7	613.8	610.7	617.3	617.3	565.5	558.0	557.9
916.8	915.4	915.5	865.2	860.6	860.5	841.4	838.8	838.8
1025.3	1022.3	1022.5	987.8	982.1	982.1	949.5	946.1	946.2
1119.4	1112.8	1112.8	1063.5	1042.4	1042.4	1026.4	1015.0	1014.8
1215.0	1207.3	1207.1	1132.5	1115.2	1115.3	1096.5	1078.8	1078.4
1259.3	1251.2	1251.3	1196.7	1182.5	1182.5	1169.8	1156.2	1156.1
1365.7	1366.2	1366.3	1276.9	1283.5	1283.5	1246.5	1247.7	1247.9
1404.6	1397.3	1397.3	1325.1	1314.4	1314.3	1294.5	1284.9	1285.1
1432.6	1432.2	1432.2	1352.0	1348.4	1348.4	1311.9	1309.1	1309.1
1585.6	1575.1	1575.1	1492.5	1461.8	1461.8	1456.1	1439.8	1439.7
1610.3	1598.1	1598.2	1523.0	1477.9	1477.9	1479.1	1462.6	1462.6
1652.1	1638.4	1638.4	1572.1	1523.7	1523.7	1522.7	1502.1	1502.0
3145.3	3137.9	3137.9	3072.9	3046.4	3046.4	2957.4	2961.5	2961.6
3213.8	3200.7	3200.7	3146.5	3116.1	3116.1	3034.6	3035.7	3036.2
3278.2	3256.7	3256.6	3190.2	3137.5	3137.5	3116.3	3098.6	3098.5
3351.3	3323.0	3322.9	3272.0	3209.1	3209.1	3187.2	3162.6	3162.6
4200.8	4196.4	4195.9	3908.9	3921.3	3921.3	3840.5	3860.1	3860.3

Table IV.A.4. Normal mode vibrational frequencies of 2-bromoethanol in T$_t$ conformer at DFT, HF AND MP2 (FULL) levels of theory with 6-31G**, 6-31+G** and 6-311++G** basis sets (cm^{-1})

HF			MP2 (FULL)			B3LYP		
6-31G**	6-31+G**	6-311++G**	6-31G**	6-31+G**	6-311++G**	6-31G**	6-31+G**	6-311++G**
137.0	138.4	135.1	131.6	116.3	87.4	120.2	120.1	114.6
238.9	237.7	233.2	226.0	172.4	145.9	196.4	187.2	174.8
247.9	240.3	239.3	229.8	223.2	227.2	217.4	215.6	217.8
358.9	358.3	359.0	345.1	343.6	347.6	331.0	329.9	329.3
725.6	727.3	726.9	713.8	714.1	723.6	672.8	673.6	668.6
843.0	848.9	844.7	805.8	811.0	805.5	787.2	791.7	788.9
1092.1	1088.0	1085.5	1049.8	1051.8	1039.3	1010.4	1013.6	1012.1
1108.4	1123.0	1109.6	1060.9	1057.8	1052.1	1018.5	1024.4	1013.4
1191.4	1178.3	1175.8	1102.7	1075.1	1085.7	1072.4	1048.5	1039.6
1318.5	1312.6	1313.2	1240.7	1229.2	1218.4	1207.2	1204.9	1199.5
1319.7	1318.8	1315.5	1249.3	1238.0	1248.8	1217.0	1212.2	1215.2
1391.2	1393.8	1388.0	1308.5	1306.3	1302.0	1275.8	1271.6	1268.2
1421.3	1420.8	1419.9	1341.6	1332.2	1324.9	1303.9	1302.4	1302.1
1585.7	1578.2	1574.8	1490.3	1471.7	1462.9	1456.2	1439.4	1437.8
1627.5	1622.8	1618.2	1546.1	1535.3	1507.3	1501.5	1495.6	1487.5
1666.9	1659.3	1652.8	1590.3	1573.6	1539.0	1542.2	1527.2	1522.7
3184.1	3193.1	3175.8	3103.1	3112.1	3072.0	3005.6	3020.4	3008.0
3225.3	3235.8	3214.7	3159.8	3173.3	3126.8	3043.7	3063.1	3046.8
3287.2	3285.3	3265.8	3201.1	3190.5	3148.3	3121.9	3117.6	3105.5
3362.4	3358.2	3335.0	3284.5	3272.4	3223.3	3194.4	3188.0	3172.5
4189.1	4191.2	4184.3	3900.6	3881.2	3902.5	3827.9	3837.7	3844.9

Table IV.A.5. Normal mode vibrational frequencies of 2-bromoethanol in T$_g$ conformer at DFT, HF AND MP2 (FULL) levels of theory with 6-31G**, 6-31+G** and 6-311++G** basis sets (cm^{-1})

HF			MP2 (FULL)			B3LYP		
6-31G**	6-31+G**	6-311++G**	6-31G**	6-31+G**	6-311++G**	6-31G**	6-31+G**	6-311++G**
138.1	138.8	136.8	138.5	137.2	138.6	127.1	126.7	123.7
234.1	233.0	233.8	218.9	216.1	219.0	210.1	209.1	210.3
313.6	280.3	284.2	324.5	284.5	321.7	318.6	282.9	292.5
363.7	361.4	364.0	351.5	346.9	365.7	341.1	332.9	334.9
726.3	727.9	728.0	708.7	708.4	719.8	661.9	663.0	657.2
826.2	832.7	829.6	788.4	795.2	793.0	770.8	776.6	775.3
1086.6	1093.5	1086.9	1027.8	1029.4	1028.7	994.5	1001.3	995.0
1123.9	1125.2	1117.9	1079.4	1065.4	1067.0	1043.7	1039.6	1032.9
1192.1	1180.4	1177.4	1113.5	1104.8	1103.7	1071.4	1058.2	1050.7
1212.9	1210.0	1209.9	1154.3	1140.4	1153.8	1125.5	1116.6	1118.3
1359.1	1370.8	1362.2	1276.9	1285.4	1277.7	1235.2	1247.3	1241.5
1413.0	1411.3	1406.6	1342.2	1333.9	1323.5	1303.7	1299.1	1297.2
1501.0	1486.2	1490.6	1413.1	1386.5	1393.3	1387.2	1366.1	1369.5
1543.7	1542.3	1539.1	1444.4	1438.2	1432.4	1410.5	1404.7	1403.0
1619.1	1616.2	1609.7	1540.1	1529.4	1496.1	1495.3	1490.1	1481.5
1649.5	1644.1	1638.1	1570.1	1557.2	1524.7	1522.7	1512.7	1508.6
3206.1	3212.9	3194.2	3127.4	3133.1	3088.7	3032.4	3044.0	3030.5
3270.5	3269.5	3249.0	3185.3	3176.5	3131.2	3104.0	3101.6	3089.5
3284.9	3289.3	3267.8	3222.2	3226.1	3177.7	3119.4	3125.2	3108.8
3349.5	3346.2	3322.3	3273.2	3263.1	3211.3	3183.3	3177.7	3162.3
4185.7	4191.7	4180.1	3893.6	3878.4	3890.2	3814.9	3828.5	3832.3

Table IV.A.6. Normal mode vibrational frequencies of the transition state for the H$_2$O elimination from 2-bromoethanol at DFT, HF AND MP2 (FULL) levels of theory with 6-31G, 6-31+G** and 6-311++G** basis sets (cm^{-1})**

HF			MP2 (FULL)			B3LYP		
6-31G**	6-31+G**	6-311++G**	6-31G**	6-31+G**	6-311++G**	6-31G**	6-31+G**	6-311++G**
-1318.8	-1355.0	-1347.5	-1892.6	-1986.7	-1854.9	-1862.8	-1949.8	-1979.1
91.8	100.0	102.2	112.0	126.3	123.0	115.6	129.9	127.5
325.4	327.4	326.2	314.7	309.2	309.5	298.8	287.4	275.5
393.5	402.8	430.9	410.5	357.2	373.9	381.5	327.9	321.2
524.8	532.1	533.8	520.9	493.0	482.4	485.9	460.0	450.6
589.6	586.9	595.3	601.1	595.8	600.3	557.5	553.5	545.9
833.5	834.0	839.5	679.5	654.3	673.0	655.7	637.0	632.5
878.8	868.9	876.4	770.6	754.8	748.1	741.6	724.9	721.3
965.4	975.2	983.7	828.7	810.8	815.3	801.0	787.1	782.0
1090.5	1094.0	1085.7	1044.3	1033.2	1034.0	1008.3	987.5	986.5
1183.8	1177.8	1166.3	1110.7	1085.6	1103.2	1057.7	1037.8	1036.2
1271.2	1274.5	1287.5	1195.6	1185.8	1184.7	1144.4	1134.1	1133.0
1344.1	1351.4	1339.5	1260.7	1256.0	1246.4	1224.0	1223.0	1216.6
1419.3	1419.3	1421.3	1346.5	1341.3	1320.6	1284.6	1286.9	1275.0
1594.0	1569.6	1563.9	1516.8	1435.1	1431.3	1448.8	1383.4	1378.2
1614.3	1611.1	1603.6	1541.9	1537.0	1500.4	1488.7	1487.8	1475.2
2256.1	2242.9	2251.3	1752.2	1711.1	1772.6	1720.5	1687.8	1678.7
3289.5	3288.6	3262.1	3208.0	3211.2	3156.2	3139.6	3151.0	3130.7
3354.6	3352.7	3321.6	3303.3	3294.0	3244.4	3214.0	3210.6	3191.3
3378.7	3377.5	3346.9	3316.4	3319.6	3260.4	3233.9	3247.7	3223.8
4086.9	4081.3	4072.1	3771.4	3745.0	3747.1	3727.6	3728.8	3732.1

Table IV.A.7. Normal mode vibrational frequencies of the transition state for the HBr elimination from 2-bromoethanol at DFT, HF AND MP2 (FULL) levels of theory with 6-31G**, 6-31+G** and 6-311++G** basis sets (cm^{-1})

HF			MP2 (FULL)			B3LYP		
6-31G**	6-31+G**	6-311++G**	6-31G**	6-31+G**	6-311++G**	6-31G**	6-31+G**	6-311++G**
-1114.3	-1045.9	-1015.4	-1457.7	-1423.9	-1473.8	-1454.9	-1372.4	-1362.6
91.2	88.4	95.0	105.2	102.3	108.0	105.5	109.1	108.6
213.9	211.6	213.3	237.0	235.7	248.4	213.7	218.0	200.2
267.0	243.8	247.4	317.0	301.6	311.7	274.4	261.1	250.5
355.9	349.3	356.5	376.2	381.6	400.7	304.7	315.6	316.8
499.8	499.2	496.9	460.9	462.0	460.5	454.5	456.9	456.2
781.5	781.3	789.4	775.2	767.2	789.3	654.1	666.0	665.3
1005.4	1005.8	996.5	904.1	912.1	899.8	869.8	881.7	875.4
1160.6	1185.2	1168.7	989.5	1003.3	986.6	959.1	989.4	982.4
1175.6	1192.5	1193.0	1061.8	1067.9	1063.8	1006.0	1023.0	1015.0
1259.7	1254.3	1247.6	1179.7	1169.4	1163.8	1152.1	1143.3	1136.7
1342.7	1340.6	1334.2	1226.5	1219.2	1206.4	1182.5	1185.2	1174.7
1386.9	1380.3	1381.4	1282.6	1270.5	1274.5	1244.5	1238.0	1235.1
1449.2	1448.8	1445.8	1354.3	1345.7	1331.5	1312.3	1302.9	1303.9
1564.4	1560.0	1551.4	1473.5	1461.8	1438.0	1395.5	1403.9	1404.5
1710.7	1705.9	1697.7	1561.2	1556.9	1525.2	1444.2	1457.2	1450.4
2069.9	2156.7	2200.0	1870.7	1894.8	1838.2	1616.3	1629.6	1631.5
3322.0	3320.0	3297.9	3238.1	3237.5	3196.4	3084.8	3090.0	3076.9
3379.8	3370.7	3344.9	3295.5	3284.2	3233.3	3205.8	3196.9	3177.8
3499.3	3492.7	3465.3	3419.8	3410.4	3356.4	3319.9	3311.8	3291.0
4165.5	4162.2	4154.8	3885.0	3866.1	3883.4	3816.3	3822.5	3830.1

Table IV.A.8. Normal mode vibrational frequencies of the transition state for the HOBr elimination from 2-bromoethanol at DFT, HF AND MP2 (FULL) levels of theory with 6-31G**, 6-31+G** and 6-311++G** basis sets (cm^{-1})

HF			MP2 (FULL)			B3LYP		
6-31G**	6-31+G**	6-311++G**	6-31G**	6-31+G**	6-311++G**	6-31G**	6-31+G**	6-311++G**
-1063.2	-1047.7	-1043.7	-664.2	-649.3	-124.4	-615.6	-594.1	-549.2
142.7	148.8	142.0	90.4	78.4	107.5	55.8	76.0	37.8
168.2	151.4	142.1	101.8	96.0	272.0	89.7	81.8	41.9
299.5	278.0	311.9	254.4	204.8	381.9	183.5	211.6	236.0
332.9	324.0	323.4	328.8	322.9	450.8	322.5	297.4	280.0
533.3	530.7	522.2	460.9	446.9	507.1	454.7	463.0	403.2
605.4	618.4	595.0	488.7	477.9	574.7	477.5	481.4	444.9
900.2	902.3	895.6	847.7	852.8	652.4	825.5	839.2	836.3
965.3	978.9	966.4	850.0	868.0	829.5	834.5	865.6	863.5
1119.9	1125.5	1115.5	1024.2	1023.2	1134.2	1033.6	1041.2	1047.9
1184.8	1197.8	1187.1	1055.2	1068.3	1146.0	1078.5	1084.4	1090.5
1213.8	1211.7	1211.0	1076.9	1072.8	1198.1	1110.9	1119.4	1139.8
1311.0	1301.2	1294.7	1262.4	1261.9	1257.3	1236.5	1237.9	1235.8
1340.3	1341.5	1331.4	1284.0	1274.6	1331.3	1249.1	1241.3	1236.2
1594.1	1592.3	1581.7	1516.3	1508.8	1472.6	1479.8	1475.9	1470.2
1681.4	1674.4	1662.0	1604.2	1592.8	1533.4	1559.1	1551.8	1540.8
3319.2	3320.0	3294.7	3235.0	3228.3	3113.3	3137.5	3139.9	3113.0
3353.7	3350.3	3322.3	3267.5	3254.3	3182.6	3192.1	3187.0	3163.7
3409.2	3410.0	3382.5	3337.7	3331.4	3196.5	3221.1	3224.7	3192.7
3457.4	3456.2	3427.8	3381.3	3370.5	3295.2	3294.7	3291.6	3266.6
3885.4	3886.4	3889.6	3479.2	3464.5	3611.3	3509.7	3516.1	3546.7

Table IV.A.9. Optimized structures of 2-bromoethanol in $G_{g'}$ conformer at DFT, HF AND MP2 (FULL) levels of theory with 6-31G**, 6-31+G** and 6-311++G** basis sets

Coordinate (Å)	HF			MP2 (FULL)			B3LYP		
	6-31G**	6-31+G**	6-311++G**	6-31G**	6-31+G**	6-311++G**	6-31G**	6-31+G**	6-311++G**
R(1,2)	1.517	1.516	1.516	1.514	1.512	1.516	1.520	1.519	1.517
R(1,3)	1.085	1.085	1.085	1.090	1.090	1.094	1.097	1.097	1.095
R(1,4)	1.087	1.086	1.087	1.094	1.093	1.097	1.101	1.099	1.097
R(1,7)	1.391	1.393	1.392	1.413	1.419	1.413	1.410	1.417	1.415
R(2,5)	1.079	1.079	1.079	1.086	1.087	1.090	1.090	1.091	1.088
R(2,6)	1.078	1.078	1.078	1.085	1.086	1.090	1.089	1.090	1.088
R(2,9)	1.967	1.963	1.965	1.960	1.957	1.948	1.989	1.985	1.988
R(7,8)	0.945	0.945	0.942	0.967	0.968	0.963	0.969	0.969	0.965
A(2,1,3)	107.8	107.6	107.4	108.4	108.4	108.1	107.9	107.9	107.7
A(2,1,4)	109.7	110.1	110.0	109.4	110.1	109.8	109.4	110.0	110.1
A(2,1,7)	112.8	113.0	113.3	112.4	112.4	112.7	112.9	113.2	113.5
A(3,1,4)	107.9	108.0	107.9	108.3	108.5	108.4	107.7	107.9	107.8
A(3,1,7)	106.7	106.4	106.4	106.2	105.7	106.1	106.5	106.0	105.9
A(4,1,7)	111.8	111.4	111.5	112.0	111.4	111.5	112.2	111.5	111.5
A(1,2,5)	112.2	111.6	111.4	112.5	111.7	111.3	112.8	111.9	111.9
A(1,2,6)	111.8	111.7	111.6	111.3	111.3	110.8	112.0	112.0	111.9
A(1,2,9)	110.4	111.3	111.7	109.5	110.4	110.6	109.8	110.8	111.2
A(5,2,6)	110.8	110.6	110.5	110.8	110.6	110.6	111.0	110.7	110.7
A(5,2,9)	105.8	105.7	105.6	106.4	106.4	106.8	105.8	105.7	105.5
A(6,2,9)	105.5	105.7	105.6	105.9	106.2	106.5	105.0	105.4	105.2
A(1,7,8)	109.4	110.2	110.0	106.4	107.4	106.7	106.7	107.9	108.2
D(3,1,2,5)	-60.1	-59.4	-58.2	-61.3	-61.7	-59.8	-62.1	-61.5	-59.9
D(3,1,2,6)	65.1	65.0	65.9	63.7	62.5	63.7	64.0	63.5	65.1
D(3,1,2,9)	-177.8	-177.2	-176.1	-179.4	-179.8	-178.4	-179.8	-179.2	-177.6
D(4,1,2,5)	57.1	58.2	59.0	56.5	56.9	58.3	54.7	56.0	57.4
D(4,1,2,6)	-177.7	-177.5	-176.9	-178.4	-179.0	-178.2	-179.2	-179.0	-177.6
D(4,1,2,9)	-60.6	-59.6	-58.8	-61.6	-61.3	-60.3	-62.9	-61.7	-60.3
D(7,1,2,5)	-177.6	-176.5	-175.4	-178.4	-178.2	-176.7	-179.5	-178.5	-176.8
D(7,1,2,6)	-52.4	-52.2	-51.3	-53.3	-54.1	-53.2	-53.4	-53.5	-51.9
D(7,1,2,9)	64.7	65.7	66.7	63.5	63.6	64.7	62.8	63.8	65.5
D(2,1,7,8)	-63.2	-64.5	-66.2	-60.5	-59.4	-58.9	-58.8	-59.0	-62.0
D(3,1,7,8)	178.7	177.7	176.1	-178.9	-177.5	-177.0	-177.0	-177.1	-179.9
D(4,1,7,8)	60.9	60.1	58.6	63.1	64.8	65.1	65.4	65.7	63.0

1-C, 2-C, 3-H(1), 4-H(1), 7-O(1), 9-Br(2), 5-H(2), 6-H(2), 8-H(7)

Table IV.A.10. Optimized structures of 2-bromoethanol in G_g conformer at DFT, HF AND MP2 (FULL) levels of theory with 6-31G**, 6-31+G** and 6-311++G** basis sets

Coordinate (Å)	HF			MP2 (FULL)			B3LYP		
	6-31G**	6-31+G**	6-311++G**	6-31G**	6-31+G**	6-311++G**	6-31G**	6-31+G**	6-311++G**
R(1,2)	1.518	1.517	1.517	1.514	1.513	1.517	1.521	1.520	1.519
R(1,3)	1.091	1.091	1.091	1.097	1.096	1.100	1.105	1.104	1.102
R(1,4)	1.081	1.081	1.081	1.087	1.087	1.091	1.093	1.093	1.091
R(1,7)	1.392	1.394	1.393	1.414	1.419	1.413	1.411	1.417	1.416
R(2,5)	1.079	1.080	1.080	1.086	1.087	1.091	1.091	1.091	1.089
R(2,6)	1.080	1.081	1.081	1.087	1.088	1.092	1.092	1.093	1.090
R(2,9)	1.954	1.950	1.953	1.949	1.946	1.938	1.975	1.972	1.977
R(7,8)	0.943	0.943	0.941	0.964	0.966	0.961	0.967	0.967	0.963
A(2,1,3)	107.3	107.2	107.0	107.6	107.5	107.3	107.0	106.9	106.8
A(2,1,4)	109.8	110.3	110.1	109.7	110.5	110.2	109.8	110.4	110.3
A(2,1,7)	113.9	114.0	114.2	113.6	113.8	113.9	114.4	114.7	114.8
A(3,1,4)	107.8	107.9	107.8	108.1	108.3	108.2	107.5	107.8	107.7
A(3,1,7)	111.3	110.9	110.9	111.8	111.2	111.2	111.8	111.1	111.0
A(4,1,7)	106.6	106.4	106.6	105.8	105.5	106.0	106.1	105.8	106.0
A(1,2,5)	111.1	110.5	110.5	111.2	110.5	110.2	111.3	110.5	110.6
A(1,2,6)	112.1	111.9	111.9	111.7	111.5	111.2	112.2	112.1	112.2
A(1,2,9)	112.1	113.0	113.1	111.4	112.4	112.3	112.0	113.1	113.2
A(5,2,6)	109.4	109.2	109.2	109.3	109.1	109.0	109.3	109.2	109.3
A(5,2,9)	106.2	106.0	106.0	106.9	106.8	107.2	106.3	106.1	105.8
A(6,2,9)	105.7	105.9	105.9	106.2	106.4	106.8	105.4	105.6	105.5
A(1,7,8)	110.5	111.2	110.7	107.9	108.9	107.8	108.5	109.6	109.4
D(3,1,2,5)	-56.2	-55.2	-54.3	-57.5	-57.4	-55.7	-57.4	-56.0	-55.0
D(3,1,2,6)	66.5	66.8	67.7	64.8	64.1	65.3	65.4	66.0	67.3
D(3,1,2,9)	-174.7	-173.7	-172.9	-176.6	-176.5	-175.1	-176.2	-174.7	-173.6
D(4,1,2,5)	60.7	62.1	62.6	59.9	60.6	61.9	58.9	61.0	61.7
D(4,1,2,6)	-176.6	-176.0	-175.4	-177.7	-177.9	-177.1	-178.2	-177.0	-176.0
D(4,1,2,9)	-57.8	-56.5	-55.9	-59.2	-58.5	-57.5	-59.9	-57.7	-56.8
D(7,1,2,5)	-179.8	-178.3	-177.4	178.2	179.1	-179.3	178.1	-179.6	-178.6
D(7,1,2,6)	-57.1	-56.3	-55.5	-59.5	-59.4	-58.2	-59.1	-57.6	-56.3
D(7,1,2,9)	61.6	63.1	64.0	59.1	59.9	61.4	59.3	61.6	62.9
D(2,1,7,8)	62.7	62.1	62.5	60.8	57.6	57.0	59.4	57.6	59.7
D(3,1,7,8)	-58.8	-59.0	-58.5	-61.2	-63.9	-64.3	-62.5	-63.7	-61.6
D(4,1,7,8)	-176.1	-176.1	-175.6	-178.7	178.9	178.2	-179.4	179.6	-178.2

1-C, 2-C, 3-H(1), 4-H(1), 7-O(1), 9-Br(2), 5-H(2), 6-H(2), 8-H(7)

Table IV.A.11. Optimized structures of 2-bromoethanol in G_t conformer at DFT, HF AND MP2 (FULL) levels of theory with 6-31G**, 6-31+G** and 6-311++G** basis sets

Coordinate (Å)	HF			MP2 (FULL)			B3LYP		
	6-31G**	6-31+G**	6-311++G**	6-31G**	6-31+G**	6-311++G**	6-31G**	6-31+G**	6-311++G**
R(1,2)	1.511	1.511	1.511	1.506	1.510	1.510	1.513	1.511	1.511
R(1,3)	1.091	1.091	1.091	1.097	1.099	1.099	1.105	1.102	1.102
R(1,4)	1.086	1.086	1.086	1.093	1.095	1.095	1.099	1.096	1.096
R(1,7)	1.395	1.396	1.396	1.417	1.418	1.418	1.415	1.421	1.421
R(2,5)	1.079	1.079	1.079	1.086	1.090	1.090	1.090	1.088	1.088
R(2,6)	1.078	1.078	1.078	1.085	1.090	1.090	1.090	1.088	1.088
R(2,9)	1.956	1.955	1.955	1.950	1.940	1.940	1.977	1.979	1.979
R(7,8)	0.942	0.940	0.940	0.963	0.959	0.959	0.965	0.961	0.961
A(2,1,3)	107.5	107.2	107.2	107.8	107.7	107.7	107.2	107.1	107.1
A(2,1,4)	109.7	110.1	110.1	109.5	109.9	109.9	109.5	110.2	110.2
A(2,1,7)	108.8	109.2	109.2	107.7	108.4	108.4	108.7	109.2	109.2
A(3,1,4)	108.0	108.2	108.2	108.2	108.5	108.5	107.7	108.1	108.1
A(3,1,7)	110.9	110.5	110.5	111.4	110.5	110.5	111.4	110.5	110.5
A(4,1,7)	111.8	111.6	111.6	112.1	111.7	111.7	112.2	111.7	111.7
A(1,2,5)	111.4	110.9	110.9	111.4	110.7	110.7	111.5	111.1	111.1
A(1,2,6)	111.1	111.0	111.0	110.6	110.1	110.1	111.2	111.1	111.1
A(1,2,9)	111.8	112.8	112.7	111.2	111.9	112.0	111.9	112.8	112.8
A(5,2,6)	110.4	110.2	110.2	110.4	110.1	110.1	110.4	110.3	110.3
A(5,2,9)	106.0	105.7	105.7	106.7	107.0	107.0	106.0	105.6	105.6
A(6,2,9)	106.0	106.1	106.1	106.4	107.0	107.0	105.6	105.7	105.7
A(1,7,8)	110.3	110.6	110.5	108.0	108.1	108.1	108.4	109.4	109.4
D(3,1,2,5)	-52.5	-51.3	-51.3	-53.6	-51.9	-51.9	-52.9	-51.1	-51.1
D(3,1,2,6)	71.0	71.5	71.5	69.5	70.0	70.0	70.8	72.0	72.0
D(3,1,2,9)	-170.8	-169.7	-169.6	-172.4	-171.2	-171.1	-171.4	-169.5	-169.5
D(4,1,2,5)	64.7	66.1	66.1	64.0	66.2	66.2	63.6	66.2	66.2
D(4,1,2,6)	-171.7	-171.1	-171.1	-172.9	-172.0	-171.9	-172.7	-170.7	-170.7
D(4,1,2,9)	-53.6	-52.2	-52.2	-54.9	-53.1	-53.1	-54.9	-52.2	-52.2
D(7,1,2,5)	-172.6	-171.1	-171.0	-173.9	-171.5	-171.5	-173.4	-170.8	-170.8
D(7,1,2,6)	-49.1	-48.3	-48.2	-50.8	-49.6	-49.6	-49.7	-47.6	-47.6
D(7,1,2,9)	69.0	70.6	70.6	67.2	69.2	69.2	68.1	70.9	70.9
D(2,1,7,8)	-166.9	-166.0	-165.9	-168.6	-155.0	-155.1	-166.2	-162.0	-161.5
D(3,1,7,8)	75.2	76.4	76.4	73.4	87.1	87.0	76.0	80.5	81.0
D(4,1,7,8)	-45.5	-44.0	-43.9	-48.1	-33.9	-34.0	-44.9	-39.8	-39.3

1-C, 2-C, 3-H(1), 4-H(1), 7-O(1), 9-Br(2), 5-H(2), 6-H(2), 8-H(7)

Table IV.A.12. Optimized structures of 2-bromoethanol in T$_g$ conformer at DFT, HF AND MP2 (FULL) levels of theory with 6-31G**, 6-31+G** and 6-311++G** basis sets

Coordinate (Å)	HF			MP2 (FULL)			B3LYP		
	6-31G**	6-31+G**	6-311++G**	6-31G**	6-31+G**	6-311++G**	6-31G**	6-31+G**	6-311++G**
R(1,2)	1.520	1.520	1.521	1.516	1.516	1.519	1.525	1.524	1.523
R(1,3)	1.081	1.081	1.081	1.087	1.086	1.091	1.093	1.092	1.090
R(1,4)	1.086	1.085	1.086	1.092	1.092	1.096	1.099	1.097	1.095
R(1,7)	1.399	1.402	1.400	1.421	1.428	1.420	1.421	1.427	1.426
R(2,5)	1.079	1.080	1.080	1.086	1.087	1.091	1.091	1.091	1.089
R(2,6)	1.078	1.078	1.078	1.084	1.085	1.089	1.089	1.090	1.087
R(2,9)	1.956	1.953	1.955	1.952	1.949	1.940	1.977	1.974	1.978
R(7,8)	0.943	0.943	0.941	0.964	0.965	0.961	0.966	0.966	0.963
A(2,1,3)	109.7	110.1	109.9	109.7	110.3	110.0	109.7	110.2	110.1
A(2,1,4)	110.1	110.5	110.3	109.9	110.5	110.1	110.0	110.5	110.4
A(2,1,7)	110.2	109.8	110.2	110.3	109.9	110.5	110.5	110.2	110.3
A(3,1,4)	107.8	108.1	108.0	107.9	108.4	108.3	107.6	108.0	108.1
A(3,1,7)	107.2	106.9	106.9	106.6	105.9	106.2	106.6	106.2	106.2
A(4,1,7)	111.8	111.5	111.4	112.3	111.6	111.7	112.4	111.7	111.6
A(1,2,5)	112.2	112.0	112.1	111.9	111.6	111.5	112.4	112.1	112.3
A(1,2,6)	111.5	111.2	111.3	111.2	110.7	110.7	111.7	111.3	111.5
A(1,2,9)	110.2	110.9	110.7	109.9	110.7	110.3	110.2	110.9	110.6
A(5,2,6)	110.0	109.8	109.8	109.9	109.8	109.7	110.0	109.8	110.0
A(5,2,9)	106.0	106.0	106.0	106.5	106.5	106.9	105.8	105.8	105.7
A(6,2,9)	106.7	106.6	106.6	107.2	107.3	107.7	106.6	106.6	106.4
A(1,7,8)	110.2	111.1	110.6	107.6	108.8	107.7	108.1	109.4	109.2
D(3,1,2,5)	178.8	179.3	179.1	179.0	179.6	179.1	178.4	179.0	178.5
D(3,1,2,6)	-57.3	-57.5	-57.5	-57.6	-57.7	-58.5	-57.5	-57.6	-57.5
D(3,1,2,9)	60.9	61.0	60.9	60.9	61.1	60.5	60.8	60.9	60.7
D(4,1,2,5)	60.3	60.0	60.0	60.5	59.7	59.9	60.3	59.7	59.2
D(4,1,2,6)	-175.8	-176.7	-176.5	-176.1	-177.7	-177.7	-175.6	-176.9	-176.8
D(4,1,2,9)	-57.6	-58.2	-58.1	-57.6	-58.8	-58.7	-57.4	-58.4	-58.5
D(7,1,2,5)	-63.5	-63.3	-63.4	-63.9	-64.0	-64.0	-64.3	-64.2	-64.6
D(7,1,2,6)	60.4	59.9	60.0	59.5	58.7	58.4	59.8	59.3	59.4
D(7,1,2,9)	178.6	178.4	178.5	178.0	177.6	177.4	178.0	177.8	177.6
D(2,1,7,8)	78.8	80.6	77.7	74.9	74.2	67.8	74.3	76.1	74.2
D(3,1,7,8)	-162.0	-160.0	-162.9	-166.1	-166.6	-172.9	-166.6	-164.6	-166.5
D(4,1,7,8)	-44.0	-42.1	-45.1	-48.1	-48.8	-55.1	-48.9	-47.1	-49.0

1-C, 2-C, 3-H(1), 4-H(1), 7-O(1), 9-Br(2), 5-H(2), 6-H(2), 8-H(7)

Table IV.A.13. Optimized structures of 2-bromoethanol in T$_t$ conformer at DFT, HF AND MP2 (FULL) levels of theory with 6-31G**, 6-31+G** and 6-311++G** basis sets

Coordinate (Å)	HF			MP2 (FULL)			B3LYP		
	6-31G**	6-31+G**	6-311++G**	6-31G**	6-31+G**	6-311++G**	6-31G**	6-31+G**	6-311++G**
R(1,2)	1.515	1.514	1.515	1.511	1.510	1.514	1.519	1.519	1.518
R(1,3)	1.087	1.086	1.086	1.093	1.092	1.096	1.100	1.098	1.096
R(1,4)	1.087	1.086	1.086	1.093	1.092	1.096	1.100	1.098	1.096
R(1,7)	1.400	1.403	1.402	1.422	1.430	1.423	1.422	1.429	1.428
R(2,5)	1.077	1.078	1.078	1.084	1.085	1.089	1.089	1.089	1.087
R(2,6)	1.077	1.078	1.078	1.084	1.085	1.089	1.089	1.089	1.087
R(2,9)	1.955	1.951	1.954	1.950	1.946	1.938	1.972	1.968	1.974
R(7,8)	0.943	0.943	0.941	0.964	0.965	0.960	0.966	0.966	0.962
A(2,1,3)	109.7	110.1	109.9	109.5	110.1	109.8	109.4	110.0	109.9
A(2,1,4)	109.7	110.1	109.9	109.5	110.1	109.6	109.4	110.0	109.9
A(2,1,7)	106.1	105.8	106.1	105.5	105.0	105.9	106.0	105.7	105.9
A(3,1,4)	108.1	108.5	108.5	108.1	108.9	108.7	107.8	108.5	108.5
A(3,1,7)	111.6	111.2	111.2	112.1	111.3	111.4	112.1	111.3	111.3
A(4,1,7)	111.6	111.2	111.2	112.1	111.3	111.5	112.1	111.3	111.3
A(1,2,5)	111.5	111.3	111.4	111.2	110.9	110.9	111.7	111.4	111.6
A(1,2,6)	111.5	111.3	111.4	111.2	110.9	110.8	111.7	111.4	111.6
A(1,2,9)	110.0	110.8	110.5	109.7	110.6	110.0	109.8	110.7	110.3
A(5,2,6)	110.3	110.0	110.1	110.2	110.0	110.0	110.2	110.0	110.2
A(5,2,9)	106.6	106.6	106.6	107.2	107.2	107.5	106.6	106.6	106.4
A(6,2,9)	106.6	106.6	106.6	107.2	107.2	107.5	106.6	106.6	106.4
A(1,7,8)	110.1	110.9	110.4	107.8	108.8	107.7	108.1	109.3	109.0
D(3,1,2,5)	177.4	178.2	178.0	177.6	178.7	177.2	176.9	178.1	177.8
D(3,1,2,6)	-58.8	-58.6	-58.6	-59.2	-58.7	-60.2	-59.1	-58.6	-58.4
D(3,1,2,9)	59.3	59.8	59.7	59.2	60.0	58.5	58.9	59.7	59.7
D(4,1,2,5)	58.8	58.6	58.6	59.2	58.7	58.0	59.1	58.6	58.3
D(4,1,2,6)	-177.4	-178.2	-178.0	-177.6	-178.7	-179.5	-176.9	-178.1	-177.8
D(4,1,2,9)	-59.3	-59.8	-59.7	-59.2	-60.0	-60.8	-58.9	-59.7	-59.7
D(7,1,2,5)	-61.9	-61.6	-61.7	-61.6	-61.3	-62.4	-62.0	-61.6	-61.9
D(7,1,2,6)	61.9	61.6	61.7	61.6	61.3	60.1	62.0	61.6	61.9
D(7,1,2,9)	180.0	180.0	-180.0	180.0	180.0	178.8	-180.0	-180.0	-180.0
D(2,1,7,8)	180.0	180.0	180.0	180.0	180.0	172.2	-180.0	-180.0	-180.0
D(3,1,7,8)	-60.6	-60.5	-60.5	-60.9	-60.8	-68.5	-60.7	-60.6	-60.6
D(4,1,7,8)	60.6	60.5	60.5	60.9	60.8	53.0	60.7	60.6	60.6

1-C, 2-C, 3-H(1), 4-H(1), 7-O(1), 9-Br(2), 5-H(2), 6-H(2), 8-H(7)

Table IV.A.14. Optimized structures of 2-bromoethanol in its transition state for H$_2$O elimination at DFT, HF AND MP2 (FULL) levels of theory with 6-31G, 6-31+G** and 6-311++G** basis sets**

Coordinate (Å)	HF			MP2 (FULL)			B3LYP		
	6-31G**	6-31+G**	6-311++G**	6-31G**	6-31+G**	6-311++G**	6-31G**	6-31+G**	6-311++G**
R(1,2)	1.462	1.466	1.472	1.421	1.420	1.428	1.428	1.424	1.423
R(1,3)	1.077	1.078	1.078	1.084	1.083	1.088	1.087	1.087	1.084
R(1,4)	1.077	1.077	1.077	1.083	1.082	1.087	1.087	1.086	1.084
R(1,6)	1.621	1.605	1.586	1.760	1.783	1.737	1.792	1.834	1.825
R(1,9)	1.772	1.778	1.773	1.730	1.741	1.739	1.746	1.756	1.755
R(2,5)	1.075	1.075	1.075	1.078	1.079	1.083	1.084	1.084	1.082
R(2,7)	1.973	1.966	1.973	1.932	1.924	1.922	1.955	1.945	1.951
R(2,9)	1.628	1.631	1.634	1.518	1.489	1.531	1.494	1.452	1.458
R(6,8)	0.951	0.952	0.949	0.975	0.977	0.973	0.975	0.975	0.971
R(6,9)	1.074	1.078	1.077	1.165	1.188	1.165	1.191	1.220	1.222
A(2,1,3)	121.5	121.3	121.2	121.5	121.4	121.2	121.6	121.7	121.7
A(2,1,4)	116.0	115.6	115.1	118.0	118.3	117.4	118.5	119.0	118.7
A(2,1,6)	96.0	96.0	96.4	95.5	94.5	95.9	94.4	92.8	93.2
A(3,1,4)	113.1	113.0	112.7	114.4	115.1	114.6	114.6	115.4	115.2
A(3,1,6)	103.8	104.3	104.9	101.2	101.2	101.7	101.3	101.0	101.2
A(3,1,9)	123.7	124.0	125.0	121.3	120.2	121.7	120.2	118.8	119.5
A(4,1,6)	101.4	101.8	102.4	98.2	97.3	98.6	97.6	96.3	96.8
A(4,1,9)	113.1	113.5	113.4	112.8	113.2	112.9	113.6	113.8	113.8
A(1,2,5)	116.1	116.0	115.6	119.5	119.5	119.1	119.5	119.5	119.7
A(1,2,7)	111.8	112.5	112.1	115.8	117.1	116.5	116.2	117.5	117.3
A(5,2,7)	107.6	107.5	107.1	112.3	112.2	112.4	110.9	111.0	110.9
A(5,2,9)	133.3	133.1	134.4	120.6	118.2	120.1	120.5	117.7	118.1
A(7,2,9)	112.3	112.3	112.1	111.1	111.0	111.2	111.8	111.5	111.4
A(1,6,8)	113.8	115.1	114.5	108.2	114.0	111.3	110.5	117.0	116.3
A(8,6,9)	111.8	113.4	112.7	107.5	113.6	110.3	109.9	116.8	116.1
A(2,9,6)	114.6	113.4	112.8	123.2	123.6	121.6	124.0	125.3	124.7
D(3,1,2,5)	-117.4	-117.2	-114.5	-135.5	-139.5	-135.3	-137.0	-142.0	-140.6
D(3,1,2,7)	6.5	7.1	8.6	3.7	1.4	4.5	0.4	-2.6	-1.5
D(4,1,2,5)	26.7	25.8	26.9	15.5	13.7	14.3	15.9	14.5	14.6
D(4,1,2,7)	150.6	150.1	150.1	154.7	154.6	154.2	153.3	153.9	153.7
D(6,1,2,5)	132.4	132.1	133.8	117.8	114.5	117.2	116.9	113.3	114.1
D(6,1,2,7)	-103.6	-103.7	-103.1	-103.0	-104.6	-103.0	-105.7	-107.4	-106.8
D(2,1,6,8)	104.8	107.3	106.2	99.3	105.9	101.9	102.8	110.1	109.0
D(3,1,6,8)	-19.7	-17.2	-18.5	-24.3	-17.4	-21.8	-20.6	-12.9	-14.2
D(4,1,6,8)	-137.1	-134.9	-136.3	-141.3	-134.8	-139.3	-137.7	-130.4	-131.6
D(5,2,9,6)	-112.3	-111.9	-111.4	-118.2	-116.8	-117.6	-116.4	-115.0	-115.8
D(7,2,9,6)	100.9	102.1	101.0	107.4	111.5	108.2	110.6	115.2	114.1
D(8,6,9,2)	-107.1	-109.2	-108.2	-100.0	-106.3	-103.0	-103.6	-110.4	-109.4

1-C, 2-C, 3-H (1), 4-H(1), 6-O(1), 8-H(6), 7-Br(2), 5-H(2), 9-H(2)

Table IV.A.15. Optimized structures of 2-bromoethanol in its transition state for HBr elimination at DFT, HF AND MP2 (FULL) levels of theory with 6-31G**, 6-31+G** and 6-311++G** basis sets

Coordinate (Å)	HF			MP2 (FULL)			B3LYP		
	6-31G**	6-31+G**	6-311++G**	6-31G**	6-31+G**	6-311++G**	6-31G**	6-31+G**	6-311++G**
R(1,2)	1.380	1.383	1.384	1.395	1.396	1.399	1.402	1.404	1.399
R(1,3)	1.079	1.079	1.079	1.085	1.085	1.088	1.096	1.095	1.093
R(1,4)	1.221	1.207	1.207	1.246	1.235	1.251	1.253	1.238	1.239
R(1,8)	1.359	1.360	1.358	1.378	1.382	1.376	1.388	1.392	1.388
R(2,5)	1.071	1.072	1.072	1.076	1.077	1.081	1.082	1.083	1.081
R(2,6)	2.821	2.878	2.884	2.615	2.640	2.613	2.783	2.824	2.837
R(2,7)	1.072	1.073	1.073	1.077	1.078	1.082	1.084	1.085	1.083
R(4,6)	2.197	2.238	2.270	2.077	2.090	2.068	1.978	2.003	2.033
R(8,9)	0.945	0.945	0.943	0.965	0.967	0.962	0.967	0.967	0.963
A(2,1,3)	119.5	119.5	119.2	119.7	120.2	120.1	117.7	118.1	118.2
A(2,1,4)	71.1	72.7	72.7	67.9	69.3	68.7	81.5	82.9	82.0
A(2,1,8)	118.1	117.7	117.9	117.5	117.1	117.5	116.9	116.5	116.8
A(3,1,4)	105.6	105.6	105.3	106.0	106.3	105.8	104.9	105.1	104.7
A(3,1,8)	118.1	117.8	117.9	119.1	118.7	118.9	116.8	116.3	116.5
A(4,1,8)	112.8	112.8	112.9	112.9	112.5	112.4	112.2	111.8	112.0
A(1,2,5)	120.7	120.5	120.4	120.5	120.1	119.7	120.7	120.5	120.5
A(1,2,6)	100.1	98.7	99.7	103.4	102.3	102.8	90.2	89.0	90.1
A(1,2,7)	120.6	120.6	120.8	120.1	120.2	119.9	120.7	120.8	120.8
A(5,2,6)	81.9	82.4	82.2	86.9	88.1	89.8	87.4	88.3	87.3
A(5,2,7)	118.6	118.8	118.7	119.0	119.1	119.4	118.6	118.6	118.7
A(6,2,7)	84.6	85.6	84.8	85.9	86.6	87.3	90.5	91.5	91.0
A(1,4,6)	156.2	156.1	155.0	153.3	152.7	151.9	149.2	149.2	149.8
A(2,6,4)	32.3	32.1	32.1	34.4	34.6	35.0	38.3	38.0	37.4
A(1,8,9)	111.1	111.7	111.2	108.9	109.8	108.7	108.7	109.8	109.6
D(3,1,2,5)	-14.3	-15.6	-15.4	-7.2	-8.1	-6.0	-19.8	-20.9	-20.0
D(3,1,2,6)	-100.9	-101.9	-102.0	-101.6	-103.2	-103.2	-107.0	-108.4	-106.9
D(3,1,2,7)	169.5	168.1	168.3	165.3	163.7	162.5	162.3	160.5	161.8
D(4,1,2,5)	83.3	82.9	82.8	89.2	89.1	90.4	82.6	82.4	82.3
D(4,1,2,6)	-3.3	-3.3	-3.7	-5.2	-5.9	-6.8	-4.5	-5.0	-4.6
D(4,1,2,7)	-92.9	-93.4	-93.5	-98.3	-99.1	-101.1	-95.2	-96.1	-95.8
D(8,1,2,5)	-170.4	-170.0	-169.9	-165.6	-165.5	-164.5	-166.7	-166.7	-167.1
D(8,1,2,6)	103.1	103.8	103.5	100.1	99.5	98.2	106.1	105.9	106.0
D(8,1,2,7)	13.5	13.8	13.8	7.0	6.3	4.0	15.4	14.8	14.8
D(2,1,4,6)	10.3	10.5	11.1	14.3	16.2	18.0	12.6	13.9	12.7
D(3,1,4,6)	126.7	127.2	127.5	130.4	132.9	134.6	129.1	131.1	129.9
D(8,1,4,6)	-103.0	-102.9	-102.5	-97.5	-95.5	-94.0	-103.1	-101.9	-103.1
D(2,1,8,9)	-140.0	-141.3	-143.2	-141.9	-142.3	-142.2	-144.2	-144.5	-147.3
D(3,1,8,9)	63.6	63.9	61.9	59.6	60.0	59.0	68.6	69.1	65.2
D(4,1,8,9)	-60.1	-59.6	-61.4	-65.7	-64.9	-65.4	-52.5	-51.6	-55.2
D(1,2,6,4)	3.2	3.2	3.6	5.1	5.8	6.7	4.6	5.0	4.5
D(5,2,6,4)	-116.7	-116.6	-116.1	-115.6	-114.7	-113.8	-116.1	-115.6	-116.0
D(7,2,6,4)	123.4	123.6	123.9	125.1	126.0	126.7	125.3	125.8	125.4
D(1,4,6,2)	-8.9	-9.1	-9.6	-12.4	-14.0	-15.6	-10.1	-11.1	-10.2

1C, 2C, 3-H (1), 4-H(1), 8-O(1), 9-H(8), 5-H(2), 7-H(2), 6-Br(2)

Table IV.A.16. Optimized structures of 2-bromoethanol in its transition state for HOBr elimination at DFT and HF levels of theory with 6-31G**, 6-31+G** and 6-311++G** basis sets

Coordinate (Å)	HF			B3LYP		
	6-31G**	6-31+G**	6-31G**	6-31+G**	6-31G**	6-31+G**
R(1,2)	1.390	1.395	1.393	1.399	1.402	1.400
R(1,3)	1.074	1.074	1.075	1.087	1.087	1.086
R(1,4)	1.074	1.074	1.075	1.087	1.087	1.086
R(1,5)	1.802	1.788	1.792	1.772	1.773	1.741
R(1,6)	2.518	2.497	2.493	2.449	2.455	2.377
R(2,7)	1.072	1.072	1.073	1.083	1.083	1.082
R(2,8)	2.717	2.752	2.780	2.970	3.014	3.211
R(2,9)	1.072	1.072	1.073	1.083	1.083	1.082
R(3,5)	2.235	2.226	2.230	2.200	2.222	2.201
R(4,5)	2.235	2.226	2.230	2.242	2.223	2.200
R(5,6)	0.965	0.965	0.962	0.989	0.990	0.985
R(5,8)	2.119	2.115	2.127	2.151	2.164	2.201
A(2,1,3)	119.0	118.8	118.7	118.1	117.9	117.2
A(2,1,4)	119.0	118.7	118.7	117.9	117.9	117.2
A(2,1,5)	97.3	97.9	97.8	101.8	101.4	103.3
A(2,1,6)	114.7	115.7	115.8	121.2	121.2	124.7
A(3,1,4)	115.8	115.9	116.0	115.0	115.5	115.2
A(3,1,6)	89.7	89.6	89.6	91.3	88.7	88.3
A(4,1,6)	89.7	89.7	89.6	86.4	88.7	88.3
A(1,2,7)	120.6	120.6	120.6	121.1	121.0	121.1
A(1,2,8)	96.2	95.0	95.0	89.7	89.9	86.4
A(1,2,9)	120.6	120.6	120.6	121.1	121.0	121.1
A(7,2,8)	92.5	93.0	92.7	93.8	91.9	92.6

A(7,2,9)	117.5	117.6	117.7	117.7	117.8	117.8
A(8,2,9)	92.5	93.0	92.7	90.3	91.9	92.6
A(1,5,8)	108.3	109.5	110.0	112.9	114.8	120.0
A(3,5,4)	48.1	48.3	48.2	48.7	48.8	49.2
A(3,5,6)	110.9	110.0	109.6	109.8	105.4	101.5
A(3,5,8)	120.5	121.6	122.0	129.0	126.4	130.9
A(4,5,6)	110.9	110.1	109.6	101.0	105.4	101.5
A(4,5,8)	120.5	121.6	122.0	120.8	126.3	130.9
A(6,5,8)	123.2	122.9	123.0	120.9	122.4	121.3
A(2,8,5)	58.2	57.7	57.1	54.9	53.9	50.3
D(3,1,2,7)	7.7	8.4	8.7	17.3	14.8	17.4
D(3,1,2,8)	104.4	104.8	104.8	111.5	107.0	108.3
D(3,1,2,9)	-159.0	-158.7	-159.1	-158.3	-160.9	-160.8
D(4,1,2,7)	158.9	158.7	159.1	162.9	161.0	160.7
D(4,1,2,8)	-104.4	-104.8	-104.8	-102.9	-106.9	-108.4
D(4,1,2,9)	-7.7	-8.3	-8.7	-12.7	-14.8	-17.5
D(5,1,2,7)	-96.7	-96.5	-96.1	-88.3	-92.1	-90.9
D(5,1,2,8)	0.0	0.0	0.0	6.0	0.1	0.0
D(5,1,2,9)	96.7	96.5	96.1	96.2	92.2	90.9
D(6,1,2,7)	-96.7	-96.4	-96.1	-93.3	-92.1	-90.9
D(6,1,2,8)	0.0	0.0	0.0	0.9	0.1	0.0
D(6,1,2,9)	96.6	96.5	96.1	91.1	92.2	90.9
D(2,1,5,8)	0.0	0.0	0.0	-9.0	-0.1	0.1
D(1,2,8,5)	0.0	0.0	0.0	-5.9	-0.1	0.0
D(7,2,8,5)	121.2	121.0	121.1	115.3	121.0	121.0
D(9,2,8,5)	-121.2	-121.1	-121.1	-127.0	-121.1	-121.0
D(1,5,8,2)	0.0	0.0	0.0	5.0	0.0	0.0
D(3,5,8,2)	-28.2	-28.7	-28.8	-23.8	-30.8	-33.5
D(4,5,8,2)	28.2	28.7	28.8	35.8	30.9	33.4
D(6,5,8,2)	-180.1	180.1	180.0	163.8	180.0	-180.0

1C, 2C, 3-H(1), 4-H(1), 5-O(1), 6-H(5), 7-H(2), 9-H(2), 8-Br(2)

Table IV.A.17. Optimized structures of 2-bromoethanol in its transition state for HOBr elimination at MP2 (FULL) level of theory with 6-31G**, 6-31+G** and 6-311++G** basis sets

Coordinate (Å)	MP2 (FULL)		
	6-31G**	6-31+G**	6-311++G**
R(1,2)	1.392	1.395	1.428
R(1,3)	1.081	1.081	1.093
R(1,4)	1.081	1.081	1.090
R(1,5)	1.841	1.847	1.568
R(2,7)	1.078	1.079	1.085
R(2,9)	1.078	1.079	1.084
R(5,6)	0.995	0.997	0.982
R(5,8)	2.119	2.124	2.184
A(2,1,3)	118.8	118.7	114.5
A(2,1,4)	118.8	118.7	114.3
A(2,1,5)	97.7	98.0	107.7
A(3,1,4)	116.3	116.6	112.8
A(3,1,5)	98.6	98.4	100.1
A(4,1,5)	98.6	98.4	105.9
A(1,2,7)	121.0	120.9	120.2
A(1,2,9)	121.0	120.9	120.8
A(7,2,9)	117.9	118.1	119.0
A(1,5,6)	129.3	127.9	112.6
A(1,5,8)	111.4	113.3	112.5
A(6,5,8)	119.3	118.9	120.6
D(3,1,2,7)	11.7	11.7	36.0
D(3,1,2,9)	-163.2	-163.4	-142.0
D(4,1,2,7)	163.2	163.4	168.3
D(4,1,2,9)	-11.7	-11.7	-9.7
D(5,1,2,7)	-92.6	-92.5	-74.3
D(5,1,2,9)	92.6	92.5	107.6
D(2,1,5,6)	-180.0	180.0	-171.9
D(2,1,5,8)	0.0	0.0	-31.6
D(3,1,5,6)	59.2	59.3	68.2
D(3,1,5,8)	-120.8	-120.7	-151.5
D(4,1,5,6)	-59.2	-59.3	-49.2
D(4,1,5,8)	120.8	120.7	91.1

1C, 2C, 3-H(1), 4-H(1), 5-O(1), 6-H(5), 7-H(2), 9-H(2), 8-Br(2)

Table IV.A.18. Moments of inertia of 2-bromoethanol in its transition state for H_2O, HBr and HOBr elimination at various levels of theory (a.m.u. $Å^2$)

Theory/ Basis set	H_2O	HBr	HOBr
HF/6-31G*	35.64565 254.33893 267.26483	38.84902 345.67416 367.59119	50.88587 191.23950 235.40055
HF/6-31+G**	35.19240 254.82240 267.44162	39.67840 351.78585 374.37983	50.58910 193.58955 237.44442
HF/6-311++G**	35.19772 254.02061 266.68377	39.27300 356.42536 378.65187	50.47169 197.00584 240.73695
MP2/6-31G*	37.04520 256.47641 271.50774	37.80132 321.57797 341.99921	50.35728 211.60531 255.09895
MP2/6-31+G**	36.82726 260.04491 274.86122	38.85275 320.58250 341.85347	50.35733 211.60531 255.09895
MP2/6-311++G**	36.51575 256.95630 271.60696	38.84373 316.74882 338.09370	49.96412 210.75288 250.98036
B3LYP/6-31G*	37.06633 265.14193 279.66613	43.69059 310.23503 336.18426	50.83831 211.68951 255.32965
B3LYP/6-31+G**	37.20610 268.06864 282.84506	44.74714 312.07412 338.93492	50.31381 217.87056 261.31016
B3LYP/6-311++G**	37.21252 267.88107 282.67895	44.01578 318.51556 344.78508	48.36835 238.36949 279.89382

Table IV.A.19. Moments of inertia of 2-bromoethanol in $G_{g'}$, G_g, G_t, T_g and T_t conformers at various levels of theory (a.m.u. Å^2)

Theory/ Basis set	Gg'	Gg	Gt	Tg	Tt
HF/6-31G*	41.75037 215.93800 243.17413	41.231200 221.93296 247.32868	40.16642 222.98070 247.11101	17.82040 305.78071 315.97844	17.47504 303.13590 314.34130
HF/6-31+G**	41.26035 219.25820 245.97443	40.59814 225.73155 250.37730	39.49042 227.73543 251.11006	17.65273 306.97500 317.00910	17.30271 304.30591 315.33571
HF/ 6-311++G**	40.92400 221.99730 248.30936	40.36013 227.58672 251.89983	39.49092 227.71901 251.08510	17.71257 306.85943 316.97927	17.37208 304.24911 315.34554
MP2/6-31G*	42.79780 210.89010 239.05955	42.61533 216.40770 243.27363	41.33084 217.52359 242.68602	17.95013 306.26065 316.46717	17.63450 302.50808 313.80064
MP2/6-31+G**	42.58122 213.29950 241.32897	42.21282 219.86386 246.26209	40.87944 221.00610 245.40470	17.79713 307.92140 317.99647	17.46371 304.22164 315.31997
MP2/ 6-311++G**	42.06774 214.49720 241.88223	41.78102 220.43254 246.14095	40.87548 221.01770 245.41185	17.93100 305.34102 315.62323	17.61764 302.23129 313.41144
B3LYP/6-31G*	43.15138 215.64960 244.28727	42.62726 223.31669 250.21986	41.27194 225.29080 250.34506	18.10890 311.74686 322.07392	17.80635 307.74327 319.15117
B3LYP/ 6-31+G**	42.72941 219.35140 247.55160	41.83400 228.89271 254.74404	40.46464 231.66161 255.61893	17.95346 313.40366 323.56893	17.62287 309.52251 320.73102
B3LYP/ 6-311++G**	42.24730 222.85780 250.42196	41.50677 231.03572 256.44647	40.47757 231.64038 255.60730	17.97622 313.28904 323.53164	17.66390 309.41639 320.68421

Table IV.A.20. Energies of 2-bromoethanol in its transition state for H$_2$O, HBr and HOBr elimination at various levels of theory (in Hartree)

Theory	Basis set	H$_2$O	HBr	HOBr
HF	6-31G**	-2723.189143	-2723.223995	-2723.134334
	6-31+G**	-2723.211498	-2723.248024	-2723.157803
	6-311++G**	-2725.711346	-2725.751334	-2725.656873
MP2	6-31G**	-2723.836825	-2723.846968	-2723.812862
	6-31+G**	-2723.869556	-2723.878076	-2723.848195
	6-311++G**	-2725.974789	-2726.830935	-2726.798827
DFT	6-31G**	-2725.974789	-2725.995707	-2725.949598
	6-31+G**	-2726.003543	-2726.023475	-2725.978999
	6-311++G**	-2728.467372	-2728.490473	-2728.444695

Table IV.A.21. Energies of 2-bromoethanol in G$_t$, G$_{gp}$, G$_g$, T$_t$, T$_g$ conformers at various levels of theory (in Hartree)

Theory	Basis set	Gg'	Gg	Gt	Tg	Tt
HF	6-31G**	-2723.324231	-2723.319395	-2723.320246	-2723.321838	-2723.322188
	6-31+G**	-2723.343997	-2723.339763	-2725.841116	-2723.342292	-2723.343009
	6-311++G**	-2725.843835	-2725.839841	-2725.841112	-2725.842285	-2725.843067
MP2	6-31G**	-2723.950658	-2723.945619	-2723.946017	-2723.947488	-2723.94719
	6-31+G**	-2723.978829	-2723.974492	-2726.928287	-2723.976516	-2723.976874
	6-311++G**	-2726.931139	-2726.92723	-2726.928286	-2726.929063	-2726.929485
DFT	6-31G**	-2726.081027	-2726.076047	-2726.076099	-2726.077874	-2726.077059
	6-31+G**	-2726.106155	-2726.101946	-2728.566794	-2726.103935	-2726.103826
	6-311++G**	-2728.569909	-2728.565928	-2728.566804	-2728.567966	-2728.56789

Table IV.A.22. Optimized structures of ethylbromide at DFT, HF AND MP2 (FULL) levels of theory with 6-31G**, 6-31+G** and 6-311++G** basis sets

Coordinate (Å)	HF			MP2 (FULL)			B3LYP		
	6-31G**	6-31+G**	6-311++G**	6-31G**	6-31+G**	6-311++G**	6-31G**	6-31+G**	6-311++G**
R(1,2)	1.516	1.516	1.516	1.512	1.512	1.516	1.517	1.517	1.515
R(1,3)	1.087	1.087	1.088	1.090	1.091	1.095	1.097	1.098	1.096
R(1,4)	1.083	1.083	1.084	1.086	1.087	1.092	1.093	1.093	1.092
R(1,5)	1.083	1.083	1.084	1.086	1.087	1.092	1.093	1.093	1.092
R(2,6)	1.078	1.078	1.078	1.085	1.086	1.090	1.090	1.090	1.088
R(2,7)	1.078	1.078	1.078	1.085	1.086	1.090	1.090	1.090	1.088
R(2,8)	1.964	1.962	1.963	1.959	1.957	1.946	1.986	1.984	1.988
A(2,1,3)	109.2	108.9	108.9	109.5	109.0	109.3	109.4	109.0	109.1
A(2,1,4)	111.1	111.3	111.2	110.7	111.0	111.0	111.2	111.4	111.4
A(2,1,5)	111.1	111.3	111.2	110.7	111.0	111.0	111.2	111.4	111.4
A(3,1,4)	108.5	108.4	108.4	108.7	108.6	108.6	108.3	108.2	108.2
A(3,1,5)	108.5	108.4	108.4	108.7	108.6	108.6	108.3	108.2	108.2
A(4,1,5)	108.5	108.5	108.6	108.4	108.6	108.4	108.3	108.4	108.5
A(1,2,6)	112.5	112.3	112.3	112.4	112.1	111.8	112.8	112.5	112.7
A(1,2,7)	112.5	112.3	112.3	112.4	112.1	111.8	112.8	112.5	112.7
A(1,2,8)	111.2	111.8	111.8	111.0	111.7	111.4	111.2	111.9	111.8
A(6,2,7)	109.7	109.6	109.5	109.5	109.4	109.2	109.6	109.5	109.6
A(6,2,8)	105.2	105.2	105.2	105.6	105.6	106.1	104.9	104.9	104.8
A(7,2,8)	105.2	105.2	105.2	105.6	105.6	106.1	104.9	104.9	104.8
D(3,1,2,6)	-62.3	-62.0	-62.0	-62.0	-61.7	-61.4	-62.4	-62.2	-62.3
D(3,1,2,7)	62.3	62.0	62.0	62.0	61.7	61.4	62.4	62.2	62.3
D(3,1,2,8)	180.0	-180.0	-180.0	180.0	180.0	180.0	180.0	180.0	180.0
D(4,1,2,6)	57.4	57.4	57.4	57.8	57.9	58.3	57.2	57.2	57.1
D(4,1,2,7)	-178.1	-178.6	-178.6	-178.2	-178.7	-178.9	-177.9	-178.5	-178.3
D(4,1,2,8)	-60.4	-60.6	-60.6	-60.2	-60.4	-60.3	-60.4	-60.6	-60.6
D(5,1,2,6)	178.1	178.6	178.6	178.2	178.7	178.9	177.9	178.4	178.3
D(5,1,2,7)	-57.4	-57.4	-57.4	-57.8	-57.9	-58.3	-57.2	-57.2	-57.1
D(5,1,2,8)	60.4	60.6	60.6	60.2	60.4	60.3	60.4	60.6	60.6

1C, 2C, 3-H(1), 4-H(1), 5-H(1), 6-H(2), 7-H(2), 8-Br(2)

Table IV.A.23. Optimized structures of ethylbromide in its transition state for HBr elimination at DFT, HF AND MP2 (FULL) levels of theory with 6-31G**, 6-31+G** and 6-311++G** basis sets

Coordinate (Å)	HF			MP2 (FULL)			B3LYP		
	6-31G**	6-31+G**	6-311++G**	6-31G**	6-31+G**	6-311++G**	6-31G**	6-31+G**	6-311++G**
R(1,2)	1.376	1.378	1.379	1.389	1.391	1.396	1.399	1.402	1.398
R(1,3)	1.075	1.075	1.075	1.079	1.079	1.084	1.088	1.088	1.086
R(1,4)	1.246	1.228	1.228	1.267	1.251	1.267	1.267	1.249	1.246
R(1,5)	1.075	1.075	1.075	1.079	1.079	1.084	1.088	1.088	1.086
R(2,6)	2.862	2.926	2.940	2.665	2.695	2.664	2.819	2.857	2.876
R(2,7)	1.073	1.073	1.074	1.078	1.078	1.083	1.084	1.085	1.083
R(2,8)	1.073	1.073	1.074	1.078	1.078	1.083	1.084	1.085	1.083
R(4,6)	2.070	2.127	2.156	1.960	2.000	1.961	1.933	1.969	1.988
A(2,1,3)	119.6	119.5	119.5	119.5	119.3	119.1	118.3	118.2	118.2
A(2,1,4)	74.2	74.9	74.5	73.4	73.6	74.7	85.9	86.5	86.9
A(2,1,5)	119.6	119.5	119.5	119.5	119.3	119.1	118.3	118.2	118.2
A(3,1,4)	106.1	106.1	106.1	106.2	106.3	106.1	105.3	105.2	104.8
A(3,1,5)	117.9	117.9	118.1	118.4	118.4	118.7	116.3	116.3	116.5
A(4,1,5)	106.1	106.1	106.1	106.2	106.3	106.1	105.3	105.2	104.8
A(1,2,6)	94.1	93.4	94.1	96.7	96.6	96.1	86.8	86.3	86.3
A(1,2,7)	121.5	121.4	121.5	121.6	121.5	121.4	121.7	121.7	121.7
A(1,2,8)	121.5	121.4	121.5	121.6	121.5	121.4	121.7	121.7	121.7
A(6,2,7)	85.5	85.9	85.4	87.2	87.6	88.6	90.2	90.7	90.6
A(6,2,8)	85.5	85.9	85.4	87.2	87.6	88.6	90.2	90.7	90.6
A(7,2,8)	116.7	117.0	116.8	116.7	117.0	117.1	116.6	116.6	116.6
A(1,4,6)	158.9	159.8	159.7	153.6	154.1	151.9	147.5	148.1	148.0
A(2,6,4)	32.8	32.0	31.7	36.3	35.8	37.2	39.8	39.1	38.8
D(3,1,2,6)	-99.8	-100.2	-100.0	-99.5	-99.8	-100.3	-105.2	-105.4	-105.2
D(3,1,2,7)	-12.6	-12.9	-12.8	-8.6	-8.7	-8.1	-17.0	-16.8	-16.8
D(3,1,2,8)	173.0	172.6	172.9	169.6	169.0	167.6	166.6	166.1	166.4
D(4,1,2,6)	0.0	0.0	0.0	0.0	0.0	0.0	0.0	0.0	0.0
D(4,1,2,7)	87.2	87.2	87.1	90.9	91.2	92.1	88.2	88.6	88.4
D(4,1,2,8)	-87.2	-87.2	-87.1	-90.9	-91.2	-92.1	-88.2	-88.6	-88.4
D(5,1,2,6)	99.8	100.2	100.0	99.5	99.8	100.3	105.2	105.4	105.2
D(5,1,2,7)	-173.0	-172.6	-172.9	-169.6	-169.0	-167.6	-166.6	-166.1	-166.4
D(5,1,2,8)	12.6	12.9	12.8	8.6	8.7	8.1	17.0	16.8	16.8
D(2,1,4,6)	0.0	0.0	0.0	0.0	0.0	0.0	0.0	0.0	0.0
D(3,1,4,6)	116.9	116.9	116.8	116.6	116.5	116.4	118.3	118.3	118.4
D(5,1,4,6)	-116.9	-116.9	-116.8	-116.6	-116.5	-116.4	-118.3	-118.3	-118.4
D(1,2,6,4)	0.0	0.0	0.0	0.0	0.0	0.0	0.0	0.0	0.0
D(7,2,6,4)	-121.3	-121.3	-121.3	-121.5	-121.4	-121.4	-121.7	-121.7	-121.7
D(8,2,6,4)	121.3	121.3	121.3	121.5	121.4	121.4	121.7	121.7	121.7
D(1,4,6,2)	0.0	0.0	0.0	0.0	0.0	0.0	0.0	0.0	0.0

1C, 2C, 3-H(1), 4-H(1), 5-H(1), 6-Br(2), 7-H(2), 8-H(2)

Table IV.A.24. Normal mode vibrational frequencies of ethylbromide at DFT, HF AND MP2 (FULL) levels of theory with 6-31G**, 6-31+G** and 6-311++G** basis sets (cm^{-1})

HF			MP2 (FULL)			B3LYP		
6-31G**	6-31+G**	6-311++G**	6-31G**	6-31+G**	6-311++G**	6-31G**	6-31+G**	6-311++G**
275.6	276.3	277.3	281.1	277.5	278.4	318.8	261.5	258.5
307.9	311.4	307.2	296.3	298.9	296.8	484.5	287.6	283.0
599.5	597.5	599.4	599.2	596.2	609.1	646.7	551.1	546.4
829.3	837.6	830.8	790.6	798.7	787.1	886.2	779.9	774.8
1043.1	1044.8	1038.9	1012.8	1012.4	1001.3	1033.4	975.9	971.4
1128.5	1142.9	1130.5	1072.5	1079.4	1063.1	1112.5	1044.7	1033.4
1165.2	1165.6	1159.6	1121.7	1118.9	1105.9	1139.1	1080.6	1076.8
1376.5	1379.6	1369.9	1313.8	1308.7	1285.3	1326.7	1270.8	1263.4
1403.3	1413.5	1402.2	1331.8	1340.1	1322.8	1367.1	1290.3	1279.8
1548.1	1547.8	1537.1	1465.8	1462.7	1429.9	1474.7	1420.1	1413.1
1613.7	1609.0	1602.3	1545.2	1532.7	1499.0	1519.5	1490.1	1483.0
1620.0	1616.8	1610.1	1548.1	1534.0	1499.5	1529.0	1493.6	1485.5
1625.4	1619.6	1614.7	1561.0	1543.7	1513.2	1537.3	1504.0	1499.2
3187.9	3183.7	3165.9	3136.1	3124.2	3083.1	2856.3	3037.9	3024.2
3258.3	3252.4	3230.5	3191.0	3180.8	3138.2	2862.8	3102.6	3086.0
3278.1	3274.9	3255.1	3233.3	3220.0	3171.8	2898.8	3114.9	3100.2
3284.1	3278.5	3255.8	3249.5	3236.7	3185.6	2916.2	3132.5	3112.7
3345.6	3340.4	3317.5	3272.7	3261.1	3211.4	2929.2	3174.1	3158.3

Table IV.A.25. Normal mode vibrational frequencies of ethylbromide transition state for HBr elimination at DFT, HF AND MP2 (FULL) levels of theory with 6-31G**, 6-31+G** and 6-311++G** basis sets (cm^{-1})

HF			MP2 (FULL)			B3LYP		
6-31G**	6-31+G**	6-311++G**	6-31G**	6-31+G**	6-311++G**	6-31G**	6-31+G**	6-311++G**
-1112.3	-961.6	-901.0	-1566.0	-1440.4	-1589.5	-1427.6	-1331.9	-1335.5
232.6	212.9	214.2	221.5	218.6	218.8	253.8	238.8	225.0
297.3	278.8	280.7	335.6	313.0	323.1	307.5	308.3	299.0
309.4	314.1	287.3	368.9	350.1	332.8	308.1	328.7	313.2
891.9	892.0	886.5	828.3	825.9	797.4	673.1	676.2	660.5
915.0	912.3	906.6	868.2	857.8	846.8	828.8	831.7	830.7
1149.4	1191.4	1189.2	964.7	994.3	957.9	1003.2	1032.4	1035.3
1204.6	1229.3	1220.6	1073.3	1087.9	1052.0	1034.5	1062.1	1061.5
1345.4	1347.6	1337.1	1250.8	1255.0	1199.6	1218.1	1227.6	1215.0
1357.0	1369.0	1346.7	1275.0	1275.2	1252.7	1260.1	1265.6	1257.2
1442.9	1441.7	1434.7	1334.5	1335.2	1305.4	1288.7	1283.0	1269.9
1589.7	1592.8	1584.6	1432.3	1473.6	1417.2	1377.9	1419.6	1422.1
1622.4	1667.6	1665.4	1525.2	1526.3	1485.1	1477.7	1473.5	1468.7
1773.7	1846.0	1895.8	1664.3	1677.2	1626.3	1594.4	1596.1	1592.2
3315.0	3313.0	3288.2	3253.4	3246.8	3196.2	3137.0	3129.4	3109.8
3366.0	3361.4	3333.5	3284.5	3279.7	3226.9	3192.3	3185.8	3164.2
3414.9	3412.8	3388.5	3364.5	3358.5	3306.0	3228.0	3220.2	3199.1
3476.9	3474.9	3444.3	3400.3	3398.4	3340.8	3295.9	3290.2	3266.0

Table IV.A.26. Moment of inertia of ethylbromide in its ground state and transition state to eliminate HBr at various levels of theory (a.m.u. A^{02})

Theory/ Basis set	GS	TS
HF/6-31G**	16.69393 133.86107 144.30991	19.31981 192.81918 205.35434
HF/6-31+G**	16.54518 134.48301 144.78287	19.54251 199.56763 212.31204
HF/6-311++G**	16.55888 134.54710 144.85881	19.44179 202.48695 215.12908
MP2/6-31G**	16.74750 132.82567 143.27890	19.03253 174.43466 186.61069
MP2/6-31+G**	16.58197 133.68862 143.96706	19.12627 177.90152 190.15226
MP2/6-311++G**	16.71367 132.53064 142.90400	19.34232 173.82330 186.22630
B3LYP/6-31G**	16.90362 128.07474 138.37586	21.08555 177.28618 191.50111
B3LYP/6-31+G**	16.73489 136.80783 147.17693	21.24687 180.99608 195.36013
B3LYP/6-311++G**	16.72496 136.93683 147.31636	21.17857 183.18602 197.50397

Table IV.A.27. Energies of ethylbromide in its ground state and transition state to eliminate HBr at various levels of theory (In Hartree)

Theory/ Basis set	Ground State	Transition state
HF/6-31G**	-2648.477019	-2648.381208
HF/6-31+G**	-2648.492494	-2648.400812
HF/6-311++G**	-2650.972358	-2650.883157
MP2/6-31G**	-2648.924373	-2648.825678
MP2/6-31+G**	-2648.943317	-2648.847375
MP2/6-311++G**	-2651.842579	-2651.746168
B3LYP/6-31G**	-2650.872435	-2650.793560
B3LYP/6-31+G**	-2650.893787	-2650.813839
B3LYP/6-311++G**	-2653.336376	-2653.258854

Table IV.A.28. Normal mode vibrational frequencies of dibromoethane and for TS of HBr elimination from dibromoethane at HF, MP2 (FULL) and DFT levels of theory with 6-311++G** basis set (cm^{-1}).

Reactant			Transition State		
HF	MP2 (FULL)	B3LYP	HF	MP2 (FULL)	B3LYP
110.3	110.5	101.5	110.3	110.5	101.5
196.7	187.1	175.6	196.7	187.1	175.6
203.5	199	184.8	203.5	199	184.8
634.3	641.5	568.8	634.3	641.5	568.8
725.3	716.2	644.4	725.3	716.2	644.4
813.6	775.3	762.1	813.6	775.3	762.1
1039.6	979.1	944.6	1039.6	979.1	944.6
1127.8	1097	1061	1127.8	1097	1061
1211.7	1131.7	1101.9	1211.7	1131.7	1101.9
1335.6	1250.9	1217.6	1335.6	1250.9	1217.6
1398.3	1306.8	1285.5	1398.3	1306.8	1285.5
1426.5	1335	1285.6	1426.5	1335	1285.6
1605.6	1491.4	1483.6	1605.6	1491.4	1483.6
1615.3	1499	1488.6	1615.3	1499	1488.6
3269.8	3145.5	3109.6	3269.8	3145.5	3109.6
3275.2	3153.1	3118	3275.2	3153.1	3118
3331.2	3212.7	3169.9	3331.2	3212.7	3169.9
3353.3	3233.4	3192.7	3353.3	3233.4	3192.7

Table IV.A.29. Optimized structures of dibromoethane and for TS of HBr elimination from dibromoethane at HF, MP2 (FULL) and DFT levels of theory with 6-311++G** basis set (cm^{-1}).

	Reactant				Transition State		
Coordinates	**HF**	**MP2(full)**	**B3LYP**	**Coordinates**	**HF**	**MP2(full)**	**B3LYP**
R(1,2)	1.511	1.511	1.508	**R(1,2)**	1.38	1.397	1.398
R(1,3)	1.077	1.089	1.086	**R(1,3)**	1.233	1.286	1.252
R(1,4)	1.077	1.089	1.086	**R(1,4)**	1.074	1.084	1.086
R(1,8)	1.959	1.946	1.986	**R(1,8)**	1.896	1.891	1.93
R(2,5)	1.077	1.089	1.086	**R(2,6)**	1.074	1.083	1.083
R(2,6)	1.077	1.089	1.086	**R(2,7)**	1.074	1.084	1.083
R(2,7)	1.958	1.945	1.985	**R(3,5)**	2.09	1.904	1.951
A(2,1,3)	112.2	111.6	112.5	**A(2,1,3)**	76.1	75.2	87.6
A(2,1,4)	112.2	111.6	112.5	**A(2,1,4)**	119.9	120.2	119.2
A(2,1,8)	109.4	109.2	109	**A(2,1,8)**	121	120.4	119.7
A(3,1,4)	110.2	109.9	110.4	**A(3,1,4)**	106.2	106.9	105.8
A(3,1,8)	106.3	107.1	105.9	**A(3,1,8)**	109.3	108.4	107.1
A(4,1,8)	106.3	107.1	105.9	**A(4,1,8)**	114.5	115.2	112.3
A(1,2,5)	112.2	111.6	112.5	**A(1,2,6)**	121.9	121.7	122.2
A(1,2,6)	112.2	111.6	112.5	**A(1,2,7)**	120	119.7	120
A(1,2,7)	109.4	109.2	109	**A(6,2,7)**	117.8	118.1	117.8
A(5,2,6)	110.2	110	110.4	**A(1,3,5)**	158.3	150	146.8
A(5,2,7)	106.2	107.1	105.9	**D(3,1,2,6)**	89.4	96.5	91.3
A(6,2,7)	106.2	107.1	105.9	**D(3,1,2,7)**	-85.1	-91.5	-86.1
D(3,1,2,5)	55.3	56.5	54.4	**D(4,1,2,6)**	-169.7	-162.3	-162
D(3,1,2,6)	180	-180	-180	**D(4,1,2,7)**	15.8	9.7	20.6
D(3,1,2,7)	-62.3	-61.8	-62.8	**D(8,1,2,6)**	-15	-6.4	-17
D(4,1,2,5)	-180	180	180	**D(8,1,2,7)**	170.5	165.6	165.5
D(4,1,2,6)	-55.3	-56.5	-54.4	**D(2,1,3,5)**	2.6	-6.3	-0.4
D(4,1,2,7)	62.3	61.8	62.8	**D(4,1,3,5)**	-114.9	-123.9	-120.1
D(8,1,2,5)	-62.4	-61.8	-62.8	**D(8,1,3,5)**	121.1	111.3	119.9
D(8,1,2,6)	62.4	61.8	62.8				
D(8,1,2,7)	180	180	-180				

1-C, 2-C, 3-H(1), 4-H(1), 8-Br(1), 6- H(2), 7-Br(2), 5-H(2) (R)
1-C, 2-C, 3-H(1), 4-H(1), 8-Br(1), 6- H(2), 7-H(2), 5-Br(2) (TS)

Table IV.A.30. Optimized structures of chlorobromoethane and for TS of HBr elimination from chlorobromoethane at HF, MP2 (FULL) and DFT levels of theory with 6-311++G** basis set (cm^{-1}).

Reactant				Transition State			
Coordinates	**HF**	**MP2(full)**	**B3LYP**	**Coordinates**	**HF**	**MP2(full)**	**B3LYP**
R(1,2)	1.513	1.512	1.512	**R(1,2)**	1.389	1.397	1.399
R(1,3)	1.078	1.089	1.087	**R(1,3)**	1.282	1.283	1.256
R(1,4)	1.078	1.089	1.087	**R(1,4)**	1.083	1.084	1.086
R(1,8)	1.797	1.783	1.82	**R(1,8)**	1.633	1.733	1.769
R(2,5)	1.077	1.089	1.087	**R(2,6)**	1.081	1.083	1.083
R(2,6)	1.077	1.089	1.087	**R(2,7)**	1.083	1.083	1.082
R(2,7)	1.955	1.941	1.979	**R(3,5)**	1.914	1.927	1.953
A(2,1,3)	111.7	111.1	112	**A(2,1,3)**	72.5	73.6	86.6
A(2,1,4)	111.7	111.1	112	**A(2,1,4)**	120.3	120.4	119.3
A(2,1,8)	109.2	109	109	**A(2,1,8)**	120.4	120.4	119.5
A(3,1,4)	109.9	109.6	109.9	**A(3,1,4)**	105.3	106.4	105.2
A(3,1,8)	107	107.9	106.8	**A(3,1,8)**	108.3	109.4	108.1
A(4,1,8)	107	107.9	106.8	**A(4,1,8)**	115.4	115.4	112.6
A(1,2,5)	111.9	111.3	112.2	**A(1,2,6)**	120.4	121.4	122
A(1,2,6)	111.9	111.3	112.2	**A(1,2,7)**	119.6	119.6	119.9
A(1,2,7)	109.6	109.5	109.2	**A(6,2,7)**	118.5	118.5	118.1
A(5,2,6)	110.2	109.9	110.3	**A(1,3,5)**	150.7	150.7	147
A(5,2,7)	106.5	107.3	106.3	**D(3,1,2,6)**	98.3	98.3	93.9
A(6,2,7)	106.5	107.3	106.3	**D(3,1,2,7)**	-90.4	-90.4	-83.8
D(3,1,2,5)	56.1	57.3	55.5	**D(4,1,2,6)**	-162	-162	-160.6
D(3,1,2,6)	-179.7	-179.7	-179.6	**D(4,1,2,7)**	9.3	9.3	21.7
D(3,1,2,7)	-61.8	-61.2	-62	**D(8,1,2,6)**	-4	-5	-15.1
D(4,1,2,5)	179.7	179.7	179.6	**D(8,1,2,7)**	165.3	166.3	167.2
D(4,1,2,6)	-56.1	-57.3	-55.5	**D(2,1,3,5)**	-8.4	-9.4	-3.8
D(4,1,2,7)	61.8	61.2	62	**D(4,1,3,5)**	-126	-127	-123.2
D(8,1,2,5)	-62.1	-61.5	-62.4	**D(8,1,3,5)**	107.4	107.6	116.2
D(8,1,2,6)	62.1	61.5	62.4				
D(8,1,2,7)	180	180	180				

1-C, 2-C, 3-H(1), 4-H(1), 8-Cl(1), 6- H(2), 7-Br(2), 5-H(2) (R)
1-C, 2-C, 3-H(1), 4-H(1), 8-Cl(1), 6- H(2), 7-H(2), 5-Br(2) (TS)

Table IV.A.31. Normal mode vibrational frequencies of chlorobromoethane and for TS of HBr elimination from chlorobromoethane at HF, MP2 (FULL) and DFT levels of theory with 6-311++G** basis set (cm^{-1}).

Reactant			Transition State		
HF	**MP2 (FULL)**	**B3LYP**	**HF**	**MP2 (FULL)**	**B3LYP**
118.5	119	108.7	-1400.2	-1807.7	-1500.2
211.8	201	190.9	90.7	90	91.9
265.5	259.2	242.4	407.2	220.1	236
684.9	689	617.2	993.5	322.1	289.1
801.2	785.3	718.1	1296.8	386.7	371.9
822.2	803	771.1	1625.9	688.6	591.2
1069.4	1011.3	975.8	3351.1	759.1	691.9
1130.9	1100.8	1059.3	228.9	839.7	813.9
1236.3	1158.3	1129.8	702.9	980.8	989.8
1353.4	1272.8	1237.5	1135.5	1077.5	1041.1
1404	1314.5	1292.7	1400.2	1123.9	1162.8
1457.8	1372.4	1321.8	1826.2	1286.4	1256.9
1609.2	1493.9	1486.8	3448.5	1323.1	1320.6
1617	1499.7	1491.2	267	1434.5	1412.1
3264.7	3142.2	3100.7	782.5	1586.7	1543.2
3271.9	3151.3	3112.9	1190.1	3218.3	3153.2
3323.7	3207.5	3158.2	1491.7	3241.7	3167.7
3347.8	3229.6	3184.7	3331.4	3336.6	3276.2

Table IV.A.32. Normal mode vibrational frequencies of vinyl bromide and its TS for HBr elimination at HF, MP2 (FULL) and DFT levels of theory with 6-311++G basis set (cm^{-1}).**

Reactant			Transition State		
HF	MP2 (FULL)	B3LYP	HF	MP2 (FULL)	B3LYP
373.1	353	346.9	-1100.4	-1829.8	-1343.8
648	581.8	597.7	225.9	212	212.1
651.6	637.7	598.2	245.3	326.5	334.7
1074	827.4	934.4	575.1	570.1	560.2
1075.8	977.5	972.6	786.9	616.4	692.1
1106.8	1028.9	1018.3	936	715	771.7
1388.9	1298.8	1280.8	956	751.1	865.3
1514.9	1416.9	1402.7	1061.5	898.5	953.2
1794.7	1643.9	1652.1	1907.1	1466.6	1596.3
3295.4	3193.9	3139.6	2037.6	1862.7	1834.1
3377.5	3253.8	3210.3	3470	3381.8	3256.2
3393.2	3300.2	3233.8	3564.3	3460.1	3417.8

Table IV.A.33. Optimized structures of vinyl bromide and its TS for HBr elimination at HF, MP2 (FULL) and DFT levels of theory with 6-311++G basis set (cm^{-1}).**

Reactant				Transition State			
Coordinates	HF	MP2(full)	B3LYP	Coordinates	HF	MP2(full)	B3LYP
R(1,2)	1.312	1.335	1.323	R(1,2)	1.227	1.248	1.249
R(1,3)	1.076	1.085	1.085	R(1,3)	1.065	1.072	1.079
R(1,4)	1.074	1.084	1.083	R(1,4)	1.196	1.268	1.22
R(2,5)	1.072	1.083	1.081	R(2,5)	1.063	1.071	1.069
R(2,6)	1.896	1.884	1.909	R(4,6)	2.112	1.929	1.985
A(2,1,3)	119.4	119.1	119.3	A(2,1,3)	149.3	155.3	139.4
A(2,1,4)	122.6	122.3	122.8	A(2,1,4)	85.2	77.8	97.8
A(3,1,4)	118	118.6	117.9	A(3,1,4)	125.6	126.9	122.8
A(1,2,5)	124.1	123.5	124.6	A(1,2,5)	175	170.1	176.9
A(1,2,6)	123.2	123	123.4	A(1,4,6)	148.6	144.5	139
A(5,2,6)	112.6	113.5	112	D(3,1,2,5)	181	0	179.9
D(3,1,2,5)	0	0	0	D(4,1,2,5)	1	180	0
D(3,1,2,6)	180	180	180	D(2,1,4,6)	0	0.1	0
D(4,1,2,5)	180	180	180	D(3,1,4,6)	180	-179.9	-179.9
D(4,1,2,6)	0	0	0				

1-C, 2-C, 3-H (1), 4-H (1), 5-H (2), 6-Br (2) (For Both Reactant and Transition state)

Table IV.A.34. Energies of dibromoethane, chlorobromoethane and vinylbromide and their corresponding transition state for HBr elimination at HF, MP2 (FULL) and DFT levels of theory with 6-311++G** basis set (in Hartree).

Theory/Basis set	Reactant		
	Dibromoethane	Bromochloroethane	Vinyl bromide
HF/ (6-311++G**)	-5222.768995	-3109.906151	-2649.797666
MP2(full)/ (6-311++G**)	-5224.151322	-3110.956693	-2650.641928
DFT/ (6-311++G**)	-5226.888906	-3112.966054	-2652.118582
Theory/Basis set	TS for HBr elimination		
	Dibromoethane	Bromochloroethane	Vinyl bromide
HF/ (6-311++G**)	-5222.666815	-3109.803902	-2649.683229
MP2(full)/ (6-311++G**)	-5224.047565	-3110.85318	-2650.523376
DFT/ (6-311++G**)	-5226.803489	-3112.880989	-2652.017069

Table IV.A.35. Rotational constants of dibromoethane, chlorobromoethane and vinyl bromide in its ground state and transition state to eliminate HBr at HF, MP2 (FULL) and DFT levels of theory with 6-311++G** basis set (GHz).

Molecule	Theory/ 6-311++G**	Reactant			Transition state		
Dibromoethane	HF	28.73583	0.58784	0.58022	7.61206	0.6355	0.60036
	MP2(full)	28.51372	0.59568	0.58784	8.06359	0.70004	0.66128
	DFT	28.35867	0.57782	0.57038	7.2633	0.67933	0.6375
Chlorobromoethane	HF	29.07865	0.97769	0.95714	8.97402	0.99377	0.92592
	MP2(full)	28.89882	0.99097	0.96987	9.42182	1.10123	1.02477
	DFT	28.68674	0.96142	0.94133	8.45485	1.076	0.9918
Vinyl bromide	HF	55.97613	4.1455	3.85966	37.76208	2.81266	2.61768
	MP2(full)	54.56335	4.14976	3.85646	39.79826	3.26259	3.0154
	DFT	55.21806	4.0774	3.79702	34.25719	3.01635	2.77225

Table IV.A.36. Hindered rotor partition function in temperature range of 910-1102K calculated at 10K intervals at both ab initio and DFT (B3LYP) levels of theory with the 6-311++G* basis set for low frequency torsional modes of C-C and C-O bonds of 2-bromoethanol.

Temperature	Hindered rotor partition function					
	B3LYP		MP2 (FULL)		HF	
	C-C	C-O	C-C	C-O	C-C	C-O
910	13.319	5.622	13.479	5.980	13.569	5.660
920	13.575	5.773	13.734	6.025	13.896	5.732
940	14.034	5.922	14.192	6.168	14.324	5.864
960	14.495	6.067	14.651	6.308	14.755	5.994
980	14.959	6.211	15.113	6.446	15.186	6.122
1000	15.425	6.352	15.577	6.581	15.620	6.248
1020	15.894	6.490	16.042	6.713	16.054	6.373
1040	16.364	6.626	16.509	6.843	16.490	6.495
1060	16.836	6.760	16.978	6.971	16.927	6.616
1080	17.310	6.891	17.448	7.096	17.365	6.735
1102	17.947	7.920	18.000	7.320	17.903	6.893

Table IV.A.37. Free rotor partition function in temperature range of 910-1102K calculated at 10K intervals at both ab initio and DFT (B3LYP) levels of theory with the 6-311++G* basis set for low frequency torsional modes of C-C and C-O bonds of Gg' conformer of the 2-bromoethanol

Temperature	Hindered Rotor partition function					
	B3LYP		MP2(FULL)		HF	
	C-C	C-O	C-C	C-O	C-C	C-O
910	49.638	8.463	49.577	8.366	49.012	8.355
920	49.910	8.510	49.849	8.411	49.280	8.401
940	50.450	8.602	50.387	8.502	49.813	8.492
960	50.984	8.693	50.921	8.592	50.340	8.581
980	51.512	8.783	51.448	8.681	50.862	8.670
1000	52.035	8.872	51.971	8.770	51.378	8.758
1020	52.553	8.960	52.488	8.857	51.889	8.845
1040	53.065	9.048	53.000	8.943	52.396	8.932
1060	53.573	9.134	53.507	9.029	52.897	9.017
1080	54.076	9.220	54.010	9.114	53.394	9.102
1102	17.947	7.920	18.000	7.320	17.903	6.893

Table IV.A.38. Low frequency torsional modes of C-C and C-O rotors for the five different conformations of 2-bromoethanol at both ab initio and DFT (B3LYP) levels of theory with the 6-311++G* basis set.

Theory/ Basis Set	Rotors	$G_{g'}$	T_g	T_t	G_t	G_g
B3LYP/ 6-311++G**	C-C rotor	129.9	123.7	114.7	119.1	116.6
	C-O rotor	374.7	292.6	174.8	146.6	223.9
HF/6-311++G**	C-C rotor	144.4	136.8	135.1	133.5	129.2
	C-O rotor	386.4	284.2	233.2	193.8	319.2
MP2(FULL)/ 6-311++G**	C-C rotor	147.2	138.6	87.4	135.1	134.3
	C-O rotor	418.0	321.7	146.0	118.4	331.5

Table IV.A.39. Moment of inertia (Kg-m^2) calculated about the C-C and C-O bonds of the different conformers of the 2-bromoethanol at both ab initio and DFT (B3LYP) levels of theory with the 6-311++G* basis set

Conformers	C-C bond			C-O bond		
	B3LYP	HF	MP2 (FULL)	B3LYP	HF	MP2 (FULL)
$G_{g'}$	3.476E-46	3.389E-46	3.468E-46	1.011E-47	9.849E-48	9.874E-48
G_g	3.665E-46	3.551E-46	3.651E-46	1.022E-47	9.912E-48	9.973E-48
G_t	3.670E-46	3.551E-46	3.649E-46	1.017E-47	9.863E-48	9.965E-48
T_t	3.732E-46	3.605E-46	3.705E-46	1.014E-47	9.870E-48	9.933E-48
T_g	3.529E-46	3.437E-46	3.495E-46	1.019E-47	9.897E-48	9.958E-48

Table IV.A.40. The energies evaluated using the IRC calculations along the reaction coordinate for the 13 steps at DFT, HF AND MP2 (FULL) levels of theory with 6-311++G** basis set (in Hartree) for H_2O elimination reaction.

DFT		MP2(full)		HF	
Coordinate	Energy	Coordinate	Energy	Coordinate	Energy
0.099420	-2728.530400	0.099100	-2726.887485	0.098430	-2725.780928
0.199400	-2728.532438	0.199000	-2726.889099	0.198180	-2725.781578
0.299340	-2728.535309	0.298820	-2726.891279	0.297870	-2725.782399
0.399160	-2728.538522	0.398560	-2726.893704	0.397730	-2725.783328
0.498820	-2728.541679	0.498350	-2726.896226	0.497650	-2725.784347
0.598500	-2728.544659	0.598250	-2726.898805	0.597600	-2725.785458
-0.099540	-2728.530442	-0.099410	-2726.887639	-0.099560	-2725.781080
-0.199540	-2728.532765	-0.199410	-2726.889884	-0.199520	-2725.782657
-0.299540	-2728.536409	-0.299410	-2726.893526	-0.299500	-2725.785694
-0.399530	-2728.541096	-0.399410	-2726.898405	-0.399500	-2725.790358
-0.499530	-2728.546483	-0.499410	-2726.904266	-0.499490	-2725.796625
-0.599510	-2728.552202	-0.599400	-2726.910798	-0.599490	-2725.804297
0.000000	-2728.529597	0.000000	-2726.886827	0.000000	-2725.780625

Table IV.A.41. The energies evaluated using the IRC calculations along the reaction coordinate for the 13 steps at DFT, HF AND MP2 (FULL) levels of theory with 6-311++G** basis set (in Hartree) for HBr elimination reaction.

DFT		MP2(full)		HF	
Coordinate	Energy	Coordinate	Energy	Coordinate	Energy
0.099390	-2728.553712	0.099360	-2726.896773	0.099180	-2725.821461
0.199360	-2728.554897	0.199330	-2726.898042	0.199110	-2725.822076
0.299350	-2728.556859	0.299310	-2726.900087	0.299030	-2725.823043
0.399340	-2728.559539	0.399280	-2726.902835	0.399020	-2725.824332
0.499330	-2728.562868	0.499260	-2726.906195	0.498990	-2725.825907
0.599320	-2728.566724	0.599240	-2726.910057	0.598970	-2725.827737
-0.099150	-2728.553667	-0.099220	-2726.896755	-0.099080	-2725.821460
-0.199080	-2728.554564	-0.199210	-2726.897957	-0.198970	-2725.822076
-0.299010	-2728.555852	-0.299190	-2726.899833	-0.298920	-2725.823044
-0.398960	-2728.557413	-0.399170	-2726.902262	-0.398900	-2725.824325
-0.498920	-2728.559158	-0.499160	-2726.905113	-0.498890	-2725.825865
-0.598900	-2728.561014	-0.599140	-2726.908257	-0.598880	-2725.827608
0.000000	-2728.553311	0.000000	-2726.896320	0.000000	-2725.821222

Table IV.A.42. The energies evaluated using the IRC calculations along the reaction coordinate for the 13 steps at DFT, HF AND MP2 (FULL) levels of theory with 6-311++G basis set (in Hartree) for HOBr elimination reaction.**

DFT		MP2(full)		HF	
Coordinate	Energy	Coordinate	Energy	Coordinate	Energy
0.096820	-2728.509181	0.096590	-2726.860992	0.096730	-2725.727052
0.195970	-2728.509484	0.195600	-2726.861315	0.196730	-2725.727849
0.295700	-2728.509905	0.295290	-2726.861829	0.296730	-2725.729004
0.395520	-2728.510435	0.395180	-2726.862530	0.396670	-2725.730482
0.495480	-2728.511074	0.495150	-2726.863409	0.496650	-2725.732249
0.595460	-2728.511815	0.595140	-2726.864450	0.596650	-2725.734266
-0.096730	-2728.509182	-0.096700	-2726.861042	-0.096740	-2725.727061
-0.195800	-2728.509474	-0.195370	-2726.861323	-0.196730	-2725.727902
-0.295570	-2728.509871	-0.294800	-2726.861696	-0.296730	-2725.729151
-0.395440	-2728.510361	-0.394420	-2726.862124	-0.396700	-2725.730792
-0.495400	-2728.510938	-0.494300	-2726.862578	-0.496700	-2725.732800
-0.595380	-2728.511590	-0.594240	-2726.863029	-0.596700	-2725.735143
0.000000	-2728.508911	0.000000	-2726.860835	0.000000	-2725.726583

Table IV.A.43. This Table shows the potential energy as function of torsional angle evaluated at B3LYP/6-311++G** level of theory for 2-bromoethanol around C-C (T_t) and C-O (G_t and T_t) bonds. Angles are in degree and energy in kcal/mol.

Around C-C (T_t) bond		Around C-O bond (G_g)		Around C-O bond (T_g)	
Torsional Angle	Energy	Torsional Angle	Energy	Torsional Angle	Energy
0	8.20752	0	3.14742	0	2.71865
5	8.10471	5	3.28371	-5	2.68166
10	7.80335	10	3.35416	-10	2.57342
15	7.32451	15	3.36403	-15	2.4017
20	6.69821	20	3.32377	-20	2.1777
25	5.95916	25	3.24608	-25	1.91508
30	5.14841	30	3.14461	-30	1.62918
35	4.31052	35	3.03234	-35	1.33495
40	3.4891	40	2.92008	-40	1.04658
45	2.72446	45	2.82099	-45	0.77703
50	2.05426	50	2.74643	-50	0.53817
55	1.50887	55	2.70052	-55	0.33759
60	1.10484	60	2.68543	-60	0.18077
65	0.85104	65	2.70562	-65	0.07287
70	0.74895	70	2.76267	-70	0.01367
75	0.79188	75	2.85054	-75	0
80	0.97122	80	2.95998	-80	0.02602
85	1.27114	85	3.0846	-85	0.0817
90	1.65748	90	3.21611	-90	0.15761
95	2.08964	95	3.34348	-95	0.2452
100	2.52562	100	3.45593	-100	0.33539
105	2.92132	105	3.54847	-105	0.42218
110	3.24142	110	3.61658	-110	0.49739
115	3.45095	115	3.65483	-115	0.55739
120	3.52736	120	3.65839	-120	0.59937
125	3.47257	125	3.62704	-125	0.62063
130	3.2977	130	3.56298	-130	0.62144
135	2.99813	135	3.46974	-135	0.60188
140	2.61045	140	3.3533	-140	0.56603
145	2.16129	145	3.22077	-145	0.51746
150	1.68887	150	3.0801	-150	0.46211
155	1.23223	155	2.93838	-155	0.40666
160	0.8186	160	2.80228	-160	0.35479
165	0.47187	165	2.67688	-165	0.31182
170	0.21219	170	2.56694	-170	0.28115
175	0.05321	175	2.47478	-175	0.26205
180	0	-180	2.40088	180	0.25528
180	0	-175	2.3468	175	0.26203
-175	0.05319	-170	2.31218	170	0.28119
-170	0.21219	-165	2.29541	165	0.31183
-165	0.47187	-160	2.29389	160	0.35479
-160	0.8186	-155	2.30112	155	0.40666

-155	1.23225	-150	2.31144	150	0.46211
-150	1.68889	-145	2.31736	145	0.51746
-145	2.16126	-140	2.30811	140	0.56603
-140	2.61047	-135	2.27745	135	0.60187
-135	2.99811	-130	2.21996	130	0.62143
-130	3.29774	-125	2.13225	125	0.62062
-125	3.47263	-120	2.01629	120	0.59937
-120	3.52736	-115	1.87207	115	0.55739
-115	3.45095	-110	1.70001	110	0.49739
-110	3.24143	-105	1.50289	105	0.42218
-105	2.92133	-100	1.2837	100	0.33539
-100	2.52563	-95	1.0493	95	0.24519
-95	2.08964	-90	0.80989	90	0.15761
-90	1.6575	-85	0.57831	85	0.08169
-85	1.27116	-80	0.37096	80	0.02602
-80	0.97122	-75	0.20008	75	0
-75	0.79207	-70	0.0759	70	0.01367
-70	0.74897	-65	0.00738	65	0.07287
-65	0.85104	-60	0	60	0.18077
-60	1.10484	-55	0.05875	55	0.33759
-55	1.50887	-50	0.18571	50	0.53816
-50	2.05426	-45	0.37945	45	0.77702
-45	2.72446	-40	0.63602	40	1.04657
-40	3.4891	-35	0.94478	35	1.33494
-35	4.3105	-30	1.29024	30	1.62917
-30	5.14835	-25	1.65588	25	1.91506
-25	5.95917	-20	2.02288	20	2.17769
-20	6.69821	-15	2.37113	15	2.4017
-15	7.3245	-10	2.68265	10	2.57341
-10	7.80335	-5	2.94485	5	2.68166
-5	8.10472	0	3.14743	0	2.71864
0	8.20754	0	3.14742	0	2.71865

Table IV.A.44. The energies evaluated using the IRC calculations along the reaction coordinate at DFT levels of theory with 6-311++G** basis set (in Hartree) for HBr (61 steps), H₂O (61 steps) and HOBr (81 steps) elimination reaction.

HOBr		HBr		H₂O	
Coordinate	Energy	Coordinate	Energy	Coordinate	Energy
0.09682	-2728.509181	0.04969	-2728.55	0.04973	-2728.53
0.19597	-2728.509484	0.09968	-2728.55	0.09973	-2728.53
0.2957	-2728.509905	0.14968	-2728.55	0.14973	-2728.53
0.39552	-2728.510435	0.19968	-2728.55	0.19973	-2728.53
0.49548	-2728.511074	0.24967	-2728.56	0.24972	-2728.53
0.59546	-2728.511815	0.29967	-2728.56	0.29971	-2728.54
0.69546	-2728.512653	0.34967	-2728.56	0.3497	-2728.54
0.79546	-2728.513579	0.39967	-2728.56	0.39967	-2728.54
0.89545	-2728.514587	0.44967	-2728.56	0.44963	-2728.54
0.99545	-2728.51567	0.49967	-2728.56	0.49959	-2728.54
1.09544	-2728.516817	0.54967	-2728.56	0.54954	-2728.54
1.19543	-2728.518021	0.59966	-2728.57	0.59951	-2728.54
1.29542	-2728.519273	0.64966	-2728.57	0.64948	-2728.55
1.39542	-2728.520565	0.69966	-2728.57	0.69947	-2728.55
1.49541	-2728.521887	0.74966	-2728.57	0.74946	-2728.55
1.59541	-2728.52323	0.79966	-2728.58	0.79945	-2728.55
1.6954	-2728.524588	0.84966	-2728.58	0.84945	-2728.55
1.79539	-2728.525952	0.89966	-2728.58	0.89944	-2728.55
1.89539	-2728.527315	0.94966	-2728.58	0.94944	-2728.55
1.99539	-2728.528671	0.99965	-2728.58	0.99944	-2728.56
2.09538	-2728.530013	1.04964	-2728.59	1.04943	-2728.56
2.19538	-2728.531336	1.09962	-2728.59	1.09943	-2728.56
2.29538	-2728.532634	1.14958	-2728.59	1.14943	-2728.56
2.39537	-2728.533903	1.19951	-2728.59	1.19943	-2728.56
2.4953	-2728.535138	1.24938	-2728.59	1.24943	-2728.56
2.59529	-2728.536337	1.29922	-2728.59	1.29942	-2728.56
2.69528	-2728.537495	1.3491	-2728.59	1.34942	-2728.56
2.79526	-2728.538611	1.39904	-2728.59	1.39942	-2728.57
2.89525	-2728.53968	1.44901	-2728.59	1.44942	-2728.57
2.99525	-2728.5407	1.49899	-2728.59	1.49942	-2728.57
3.09523	-2728.54167	-0.04963	-2728.55	-0.04976	-2728.53
3.19522	-2728.542589	-0.09963	-2728.55	-0.09976	-2728.53
3.29521	-2728.543456	-0.14961	-2728.55	-0.14976	-2728.53
3.39517	-2728.544275	-0.1996	-2728.55	-0.19976	-2728.53
3.49515	-2728.545044	-0.24959	-2728.56	-0.24976	-2728.53
3.59513	-2728.545768	-0.29958	-2728.56	-0.29976	-2728.54
3.69511	-2728.546447	-0.34957	-2728.56	-0.34976	-2728.54
3.79509	-2728.547089	-0.39957	-2728.56	-0.39976	-2728.54
3.89486	-2728.547692	-0.44956	-2728.56	-0.44976	-2728.54

3.99469	-2728.548261	-0.49956	-2728.56	-0.49976	-2728.55
-0.09673	-2728.509182	-0.54955	-2728.56	-0.54976	-2728.55
-0.1958	-2728.509474	-0.59955	-2728.56	-0.59975	-2728.55
-0.29557	-2728.509871	-0.64955	-2728.56	-0.64975	-2728.55
-0.39544	-2728.510361	-0.69954	-2728.56	-0.69974	-2728.56
-0.4954	-2728.510938	-0.74954	-2728.56	-0.74974	-2728.56
-0.59538	-2728.51159	-0.79954	-2728.56	-0.79972	-2728.56
-0.69537	-2728.512308	-0.84953	-2728.57	-0.84971	-2728.57
-0.79536	-2728.51308	-0.89953	-2728.57	-0.8997	-2728.57
-0.89533	-2728.513896	-0.94952	-2728.57	-0.94969	-2728.57
-0.99532	-2728.514744	-0.99952	-2728.57	-0.99967	-2728.57
-1.0953	-2728.515613	-1.04952	-2728.57	-1.04966	-2728.58
-1.19524	-2728.516498	-1.09951	-2728.57	-1.09965	-2728.58
-1.29519	-2728.517388	-1.14951	-2728.57	-1.14965	-2728.58
-1.39516	-2728.518279	-1.1995	-2728.57	-1.19964	-2728.58
-1.49512	-2728.519167	-1.2495	-2728.57	-1.24963	-2728.58
-1.59509	-2728.520057	-1.29949	-2728.57	-1.29962	-2728.59
-1.69506	-2728.520944	-1.34949	-2728.57	-1.34962	-2728.59
-1.79502	-2728.521831	-1.39948	-2728.58	-1.39961	-2728.59
-1.895	-2728.522726	-1.44948	-2728.58	-1.44961	-2728.59
-1.99498	-2728.523625	-1.49947	-2728.58	-1.4996	-2728.59
-2.09495	-2728.524532	0	-2728.55	0	-2728.53
-2.19494	-2728.525453				
-2.29493	-2728.526385				
-2.39489	-2728.527332				
-2.49488	-2728.528293				
-2.59487	-2728.529269				
-2.69486	-2728.530261				
-2.79485	-2728.531269				
-2.89485	-2728.532293				
-2.99484	-2728.533334				
-3.09484	-2728.534392				
-3.19483	-2728.535465				
-3.29482	-2728.536554				
-3.39481	-2728.53766				
-3.49481	-2728.53878				
-3.59479	-2728.539916				
-3.69479	-2728.541066				
-3.79478	-2728.54223				
-3.89476	-2728.543408				
-3.99475	-2728.544598				
0	-2728.508911				

283

Chapter V

Computational Calculations of Enthalpy of Formation of Haloethanols

V.1. Abstract

The enthalpy of formation of haloethanols of the general formula XC_2H_4OH were calculated by the HF, MP2, B3LYP, G2, G3, G2MP2, G3B3, G3MP2B3, CBS-Q, CBS-QB3 and CCSD/cc-pVDZ level of theories applying isodesmic and atomization reactions. Benson's group additivity method was also used to estimate the enthalpy of formation of haloethanols at 298.15 K and at 1 atm in the gaseous state. The higher level calculated enthalpies of formations are in good agreement with the Benson's method. The mean enthalpies of formation (best value) of fluoroethanol, chloroethanol and bromoethanol at 298 K using isodesmic reactions are -96.78±0.03, -61.86±0.02 and -50.91±0.96 kcal/mol respectively. It has been found that thermodynamically fluoroethanol is the most stable compound. The calculated value of enthalpy of formation of fluoroethanol by atomization reaction at MP2/6-311++G** level of theory is 5 kcal/mol higher than the experimental value of enthalpy of formation of chlorofluoroethane. However, its enthalpy of formation is approximately 4 kcal/mol lower than 1, 2-Ethanediol at 298 K. These theoretical values of $\Delta H_f^0 (298K)$ would be helpful for experimentalists to evaluate the thermodynamic properties of haloethanols like Gibbs free energy of formation and entropy. It is inferred from our results that the combination of G3 method with isodesmic reaction provides accurate thermo chemical data for 2-chloroethanol. The combination of G3B3 method with isodesmic reaction gives better value of enthalpy of formation of 2-fluoroethanol because the enthalpy of

formation estimated using the average of G3, G3MP2B3, G3B3, CBS-Q and CBS-QB3 methods (best value) is very close to that evaluated by G3B3 method alone. These results have also been found to be in good agreement with the reported values.

V.2. Introduction

The major causes of the depletion of ozone layer are bromine and chlorine released from several resources in the environment. Hence, the Montreal Protocol and amendments (1987) led to the phase out of a series of chlorofluorocarbons, CFCs and halons in industrialized countries, not only because of their role in ozone depletion in the stratosphere, but also because of their high global warming potentials.[1-3] Therefore, hydrofluorocarbons (HFCs) have been suggested the replacement for chlorofluorocarbons (CFCs). They have been proved to be less responsible of the depletion of the ozone layer in the stratosphere.[4] Sellevag et al. have reported that the partially fluorinated alcohols are potential alternatives for CFCs and HCFCs in certain industrial applications.[5] There has been no literature report on the experimental calculation of enthalpy of formation of haloethanols. Also, there is no experimental data available on the thermodynamic properties of haloethanols to the best of our knowledge. Recently, computational methods have been well established to estimate accurately the enthalpies of formation of various molecules because the experimental measurements of thermodynamic properties are expensive and difficult to measure. Hence, the enthalpies of formation of haloethanols were calculated which gives information about its structure and reactivity. By definition ΔH_f^0 of any compound is the enthalpy change of the reaction by which it is formed from

its elements, reactants and products all being in the standard states. The goal of this work was to estimate accurate enthalpies of formation for haloethanols by higher level quantum chemistry methods using atomization and isodesmic reactions. This chapter also reports the comparison of results obtained by Benson's group additivity method and theoretical methods. Details of which are given in the next section. The ab initio, density functional theory, Gaussian 03 and complete basis set quantum chemical method of Peterson and co-workers were employed to evaluate the enthalpy of formation.[7-15] The experimental enthalpies of formation of chlorofluoroethane, dichloroethane and ethandiol are available.[16] The experimental values of these compounds were taken from NIST data base for comparison with theoretical values of haloethanols.[16] These values are given in the Table V.1.

In this chapter the molecular structural parameters, energies, vibrational frequencies and enthalpies of formation of XC_2H_4OH (X=F, Cl, Br) were determined using quantum chemical methods. The main aim of this study was to calculate the enthalpy of formation of haloethanols using congeneric (isodesmic) reactions and atomization reaction.[17] Thermodynamic coefficient of these haloethanols are not available in the literature to the best of our knowledge. Hence, these were evaluated using the thermodynamic properties of haloethanols and have been reported in the next section. In our laboratory, the experiments on the kinetic studies of the thermal decomposition of haloethanols have been performed at high temperature in shock tubes[18] for which these thermodynamic coefficients were needed for the purpose of modeling. These results on thermodynamic data are also useful for the determination of enthalpy of reaction of different gas phase unimolecular elimination reaction at high temperature in shock tube.

Also, our results on thermo chemical data would be useful information for the modeling of oxidation and combustion mechanism of haloethanols. These results would also be useful to understand the atmospheric chemistry of halogenated alcohols released into the troposphere.

However, after completion of this work, we found that there is one report available in literature on the experimental and theoretical calculation of enthalpy of formation of haloethanols.[6] In which, Bernardes et al. have reported the experimental standard molar enthalpies of formation of 2-chloro-, 2-bromo-, and 2-iodoethanol at 298.15K using rotating-bomb combustion calorimetry. However, enthalpies of formation of 2-fluoroethanol was not reported experimentally. They have investigated enthalpies of formation of 2-fluoroethanol at B3LYP/cc-pVTZ and CBS-QB3 level of theory using isodesmic and isogyric gas-phase reactions. Also, theoretical results on enthalpy of formation for 2-chloroethanol and 2-bromoethanol have not been reported. Details of these experimental and theoretical results are given in the next section.

Table V.1. Experimentally reported values of standard enthalpy of formation of different molecules at 0 K and 298 K.   (All values are given in kcal/mol)

S. No.	Name of the molecule	$\Delta_f H^0$ 0K (in kcal/mol)	$\Delta_f H^0$ 298 K (in kcal/mol)	Uncertainty	Reference
1	Methane (CH_4)	-15.92	-17.83	0.07	22
2	Ethane (C_2H_6)	-16.34	-20.08	0.10	22
3	Ethyl chloride (C_2H_5Cl)	-23.35	-26.84	0.18	21
4	Ethyl alcohol (C_2H_5OH)	-51.88	-56.12	0.12	22
5	Ethyl bromide (C_2H_5Br)	-	-15.20	0.50	23

6	Methyl fluoride (CH_3F)	-	-56.0	6.9	25
7	Ethyl fluoride (C_2H_5F)	-	-62.9	0.4	25
8	Methyl Bromide(CH_3Br	-5.02	-8.70	0.12	22
9	1,2-dichloro ethane ($Cl_2C_2H_4$)	-28.70	-31.55	0.84	24
10	1,2-difluoro ethane ($F_2C_2H_4$)	-	103.70	2.82	26
11	1,2-Ethanediol ($C_2H_6O_2$)	-87.93	-92.61	-	23
12	1-chloro-1-fluoro ethane (FC_2H_4Cl)	-71.80	-75.00	-	23
13	Methyl chloride (CH_3Cl)	-17.67	-19.57	0.14	24

V.3. Computational details

All calculations were performed using Gaussian-03 suites of programs for geometry optimization and for frequency calculation.[19] The computational methods HF, MP2, B3LYP, G2, G3, G2MP2, G3B3, G3MP2B3, CBS-Q, CBS-QB3 and CCSD/cc-pVDZ [see references (8-15) for details] were used to evaluate enthalpy of formation of haloethanols using atomization and isodesmic reactions.

Geometry optimization and frequency calculation were done at HF/6-311++G**, MP2 (full)/ 6-311++G** and B3LYP/6-311++G** level of theories for 2-fluoroethanol, 2-chloroethanol and 2-bromoethanol. The optimized parameters and normal mode vibrational frequencies are included in the Tables (see Tables V.A.1, V.A.3, V.A.13, V.A.17, V.A.18 and V.A.24). These tables are given at the end of this chapter.

The composite methods G2, G2MP2, G3 and G3B3 were used for single point energy calculation to evaluate enthalpy of formation. (The details of these calculations

are given in the references 10-13). The composite quantum chemistry method i.e. complete basis set developed by Peterson and co-workers were also used to determine the enthalpy of formation of haloethanols. In case of CBS-Q method geometry optimization and frequency calculations are performed at HF/6-31G (d'), MP2/6-31G (d') level of theories and single point energy calculations are performed at QCISD (T)/6-31+G (d'), MP4SDQ/CBSB4 and MP2/CBSB3 level of theories respectively. The CBS-QB3 method is identical to CBS-Q method but the HF and MP2 calculations are replaced by B3LYP/CBSB7 method. For details see reference 15. Optimized structural parameters, normal mode vibrational frequencies, total energies and enthalpies of all the molecules involved in the calculation of enthalpy of formation by isodesmic and atomization reactions at all level of theories are included in Tables V.A.1-V.A.37 at the end of this chapter.

V.4. Atomization energies and heat of formation

Atomization energies were evaluated using the calculated values of energies (sum of electronic and zero point energy) with the methods described in the computational details above. The expression for computing the atomization energy of the molecule is shown below.

$$\sum D_0(XC_2H_4OH) = E_0(X) + 2E_0(C) + 5E_0(H) + E_0(O) - E_0(XC_2H_4OH)$$

$$(1)$$

Curtiss *et al.* have reported the experimental value of standard enthalpy of formation of elements C, H, O, F, Cl & Br and these were used to evaluate the enthalpy of formation at 0 K of the haloethanols[7]. These values have been reported in the Table V.2.

Table V.2. Experimental enthalpies of formation, $\Delta_f H^0$ (0K), of elements and H^0 (298K) – H^0 (0K) is taken for elements in their standard states. Both the values are given in kcal/mol.

Element	$\Delta_f H^0$ (0K)	H^0 (298K)-H^0 (0K)
H	51.63±001	1.01
C	169.98±0.1	0.25
O	58.99±0.02	1.04
F	18.47±0.07	1.05
Cl	28.59±0.001	1.1
*Br	28.19±0.03	1.4

*Data for Br is taken from NIST chemistry web book.

The enthalpy of formation at 0 K is calculated using the following expression:

$$\Delta H_f^0(XC_2H_4OH,0K) = \Delta H_f^0(X,0K) + 2\Delta H_f^0(C,0K) + \Delta H_f^0(O,0K) + 5\Delta H_f^0(H,0K) - \sum D_0(XC_2H_4OH) \qquad (2)$$

The enthalpy of formation at 298 K is calculated using the following expression:

$$\Delta H_f^0(XC_2H_4OH,298K) = \Delta H_f^0(XC_2H_4OH,0K) +$$
$$(H_{XC_2H_4OH}^O(298K) - H_{XC_2H_4OH}^0(0K)) -$$
$$\left[\begin{array}{l} \{H_X^0(298K) - H_X^0(0K)\} + 5\{H_H^0(298K) - H_H^0(0K)\} + \\ 2\{H_C^0(298K) - H_C^0(0K)\} + \{H_O^0(298K) - H_O^0(0K)\} \end{array} \right] \qquad (3)$$

Here $H^O_{XC_2H_4OH}(298K) - H^0_{XC_2H_4OH}(0K)$ is defined as $H_{corr} - E_{zpe}$. Where $H_{corr} = E_{tot}$ + k_BT and $E_{tot} = E_t + E_r + E_v + E_e$.

The calculated enthalpies of formation (at 0 K and 298 K) via atomization reactions for haloethanols at HF/6-311++G**, MP2/6-311++G**, B3LYP/6-311++G**, G2, G3, G2MP2, G3B3, G3MP2B3, CBS-Q, CBS-QB3 and CCSD/cc-pVDZ level of theories are shown in the Table V.3. This Table also includes the atomization energy of the molecules at different levels of theories.

Table V.3. Enthalpies of formation (kcal/mol) for FC$_2$H$_4$OH, ClC$_2$H$_4$OH and BrC$_2$H$_4$OH calculated from atomization total energies.

Level of theory	FC$_2$H$_4$OH			ClC$_2$H$_4$OH			BrC$_2$H$_4$OH		
	^{a}AE	$\Delta H^0_f(()K)$	$\Delta H^0_f(298K)$	AE	$\Delta H^0_f(0K)$	$\Delta H^0_f(298K)$	AE	$\Delta H^0_f(0K)$	$\Delta H^0_f(298K)$
HF/ 6-311++G**	531.23	144.34	140.30	515.00	170.69	166.72	505.00	180.29	174.59
MP2/ 6-311++G**	742.33	-66.76	-70.59	704.12	-18.43	-22.15	693.27	-7.98	-13.49
B3LYP/ 6-311++G**	758.89	-83.32	-87.19	729.77	-44.08	-47.87	719.41	-34.12	-39.64
G2	773.00	-97.43	-101.35	745.05	-59.36	-63.18	733.88	-48.59	-54.13
G2MP2	773.79	-98.22	-102.14	746.24	-60.55	-64.37	-	-	-
G3	771.08	-95.51	-99.43	743.49	-57.80	-61.62	-	-	-
G3MP2B3	770.69	-95.12	-99.02	743.59	-57.90	-61.66	-	-	-
G3B3	771.08	-95.51	-99.41	743.38	-57.69	-61.45	-	-	-
CBS-Q	771.62	-96.05	-100.02	745.06	-59.37	-63.24	740.10	-54.81	-60.42
CBS-QB3	772.35	-96.78	-100.70	745.52	-59.83	-63.64	736.34	-51.05	-56.66

^{a}AE (Atomization Energy)

V.5. Isodesmic reactions for calculation of heat of formation of haloethanols

Isodesmic reactions where number of each type of bond in the reactants is similar to that in the products were used to calculate the enthalpy of formation of haloethanols. These isodesmic reactions preserve both bonding environment as well as the type of bond in both reactants and products. It is expected that due to the cancellation of errors this method would give more reliable results.[17] The following isodesmic reactions were used to evaluate the enthalpy of formation of fluoroethanol, chloroethanol and bromoethanol.

1. $FC_2H_4OH + C_2H_6 \rightarrow C_2H_5F + C_2H_5OH$

2. $ClC_2H_4OH + C_2H_6 \rightarrow C_2H_5Cl + C_2H_5OH$

3. $BrC_2H_4OH + C_2H_6 \rightarrow C_2H_5Br + C_2H_5OH$

Expression for enthalpy of formation by isodesmic reactions is shown below:

$$\Delta H_{f,XC_2H_4OH} = \Delta H_{f,C_2H_5OH}^{Expt} + \Delta H_{f,C_2H_5X}^{Expt} - \Delta H_{f,C_2H_6}^{Expt} - \Delta H_{Rxn}^{Calc} \quad \textbf{(4)}$$

Where the enthalpy of reaction has been defined as follow:

$$\Delta H_{Rxn}^{Calc} = \Delta H_{f,C_2H_5OH}^{Calc} + \Delta H_{f,C_2H_5X}^{Calc} - \Delta H_{f,C_2H_6}^{Calc} - \Delta H_{f,XC_2H_4OH}^{Calc} \quad \textbf{(5)}$$

The experimental values of enthalpy of formation for ethanol, ethyl halide and ethane used in reactions 1, 2 and 3 are given in the Table V.1 and were taken from the NIST chemistry web book.[16] The values of enthalpies (sum of electronic and thermal enthalpy) calculated at different level of theories of the reactants and products considered in the isodesmic reaction were used to evaluate the enthalpy of reaction. In general it has been found that the calculated value of enthalpy of formation by isodesmic reactions gives more accurate and improved results as compared to the atomization reactions. However the results obtained for $\Delta H_f^0(298K)$ at higher level of calculations with composite methods like G3, G3B3 and G3MP2B3 using isodesmic work reactions are in

good agreement with the atomization reaction method. The calculated values of enthalpy of formation are given in the Table V.4 along with the HF, MP2, B3LYP, G2, G3, G2MP2, G3B3, G3MP2B3, CBS-Q, CBS-QB3 and CCSD/cc-pVDZ methods. The values of calculated enthalpy of formation of haloethanols at 298K via isodesmic reactions at HF/6-311++G**, MP2/6-311++G**, B3LYP/6-311++G**, G2, G3, G2MP2, G3B3, G3MP2B3, CBS-Q, CBS-QB3 and CCSD/cc-pVDZ level of theories are given in the Table V.4. The enthalpy of isodesmic reactions considered for evaluating the heat of formation of haloethanols is also given in the Table V.4.

Table V.4. Enthalpies of formation (kcal/mol) for FC_2H_4OH, ClC_2H_4OH and BrC_2H_4OH calculated from isodesmic reactions total energies.

Level of theory	FC_2H_4OH		ClC_2H_4OH		BrC_2H_4OH	
	ΔH_r	$\Delta H_f^0(298K)$	ΔH_r	$\Delta H_f^0(298K)$	ΔH_r	$\Delta H_f^0(298K)$
HF (6-311++G**)	-1.54	-97.40	-0.94	-61.94	-0.91	-50.33
MP2 (6-11++G**)	-2.39	-96.55	-0.91	-61.97	-0.81	-50.43
DFT (6-311++G**)	-2.39	-96.55	-1.51	-61.37	-1.39	-49.85
G2	-2.17	-96.77	-1.06	-61.82	-0.86	-50.38
G2MP2	-2.17	-96.77	-1.09	-61.79	-	-
G3	-2.14	-96.80	-1.02	-61.86	-	-
G3MP2B3	-2.17	-96.77	-1.05	-61.83	-	-
G3B3	-2.15	-96.79	-0.98	-61.90	-	-
CBS-Q	-2.11	-96.83	-0.99	-61.89	1.24	-52.48
CBS-QB3	-2.21	-96.73	-1.03	-61.85	-1.35	-49.89
CCSD/cc-pVDz	-1.34	-97.60	-0.67	-62.21	-0.53	-50.71
GROUP ADITIVITY		-97.50		-62.50		-51.40
BOND ADITIVITY		-104.09		58.99		49.39

In Benson's group additivity method a group is defined as a polyvalent atom in a molecule along with all its ligands.[20] Group additivity method involves summation of different group properties in order to estimate the thermodynamic properties of the molecule. There are three such groups for haloethanols which includes $C-(X)(H)_2(C)$, $C-(H)_2(O)(C)$ and $O-(H)(C)$ where X=F, Cl and Br. Benson has reported the values of standard enthalpy of formation of these groups.[20] The enthalpies of the three groups $C-(Cl)(H)_2(C)$, $C-(H)_2(O)(C)$ and $O-(H)(C)$ as reported by Benson for chloroethanol in kcal/mol are -16.50, -8.10 and -37.90 respectively.[20] The enthalpies of formation evaluated using group additivity method are in good agreement with the values calculated by higher level quantum chemistry methods as shown in the Table V.3. This probably provides evidence that the calculated values of enthalpy of formation using isodesmic reactions are reasonable. The bond additivity scheme involves the summation of the standard enthalpy of formation of different bonds present in the molecule.[20] The enthalpies of formation of different groups and bonds at 298 K are given in the Tables V.5 and V.6.

Table V.5. Literature value of $\Delta H_f^0(298)kcal/mol$ **for use in group additivity calculation**

Groups	$\Delta H_f^0(298)kcal/mol$
$C-(Cl)(H)_2(C)$	-16.50
$C-(H)_2(O)(C)$	-8.10
$O-(H)(C)$	-37.90
$C-(F)(H)_2(C)$	-51.50
$C-(Br)(H)_2(C)$	-5.40

Table V.6. Literature value of $\Delta H_f^0(298)kcal/mol$ **for use in bond additivity calculation**

TYPE OF BONDS	$\Delta H_f^0 (298) kcal / mol$
C-H	-3.83
C-C	2.73
C-F	-52.50
C-Cl	-7.40
C-Br	2.20
O-H	-27.00
C-O	-12.00

V.6. Results and discussion

The standard enthalpy of formation increases from fluoroethanol to bromoethanol. The enthalpy of reaction estimated via isodesmic reactions for the reaction 1, 2 and 3 are -2.21, -1.03 and -1.35 kcal/mol respectively at CBS-QB3 level of theory. The enthalpy change of reaction of reaction 1 is highest. This higher uncertainty associated with enthalpy change of reaction 1 is attributed to the difficulty in treating fluorine quantum mechanically because of its small size. Hence the calculated enthalpy of formation of fluoroethanol calculated via isodesmic reaction 1 is the least accurate among the three at 298 K.   The standard enthalpy of formation of fluoroethanol, chloroethanol and bromoethanol at CBS-QB3 level of theory are -96.73, -61.84 and -49.89 kcal/mol respectively. This suggests that fluoroethanol is the most stable compound among the haloethanols. Bromoethanol is less stable and more reactive. It has been found that at higher level of calculations the enthalpy of formation of haloethanols calculated via the atomization reaction is very close to that calculated via the isodesmic reaction. The atomization energy of fluoroethanol, chloroethanol and bromoethanol calculated at CBS-QB3 level of theory are 772.35, 745.52 and 736.33 kcal/mol respectively. It is well known fact that the value evaluated of enthalpy of formation of the haloethanols depends upon the choice of the isodesmic reaction.

$$4.\ FC_2H_4OH + CH_4 \rightarrow CH_3F + C_2H_5OH$$
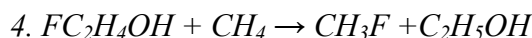
The enthalpy of reaction of reaction 1 and 4 are -2.51 and 4.35kcal/mol respectively at G3B3 level of theory. However reaction 4 also preserves the same kind of bond environment on both sides of the equation. But the calculated value of enthalpy of formation via reaction 1 is close to that calculated by group additivity method as compared to reaction 4. This suggests that the reaction 1 has the better cancellation of the errors as compared to the reaction 4. Hence in our study reaction 1, 2 and 3 were the best choice for estimating the enthalpy of reaction for calculating the enthalpy of formation of haloethanols. The experimental enthalpies of formation of reference molecules considered in isodesmic reaction 1, 2 and 3 have less uncertainty. Hence one can expect less uncertainty in the enthalpy of reaction 1, 2 and 3 as compared to reaction 4.

There is a large difference in the enthalpy of formation calculated by atomization method between the lower level of theories like HF/6-311++G**, MP2/6-311++G** and B3LYP/6-311++G** and group additivity method. The enthalpy of formation estimated using atomization reaction for the fluoroethanol, chloroethanol and bromoethanol at B3LYP/6-311++G** level of theory are 10.31, 14.63 and 11.76 kcal/mol higher than that evaluated using group additivity method respectively. However, the enthalpy of formation estimated using atomization reaction for the fluoroethanol, chloroethanol and bromoethanol at MP2/6-311++G** level of theory are 26.91, 40.35 and 37.91 kcal/mol higher than that evaluated using group additivity method respectively. Therefore, DFT predicts better values of enthalpy of formation as compared to MP2 theory. The values of enthalpy of formation predicted by the G2, G2MP2, G3, G3B3, G3MP2B3, CBS-Q, CBS-QB3 and CCSD/cc-pVDZ level of theories differ from each other by approximately

1 kcal/mol using atomization reactions and are very close to the values predicted by Benson's group contributing method.[20] However the predicted values of enthalpy of formation of haloethanols via isodesmic reactions at all level of theories differ from each other by 0.3 to 0.5 kcal/mol. These values are in good agreement with the values calculated by both group and bond additivity methods as shown in the table V.3. Frenkel et al. have reported the experimental enthalpy of formation of ethandiol which differs from the calculated value of enthalpy of formation of fluoroethanol by approximately 4 kcal/mol.[21] The enthalpy of formation value of fluoroethanol and chloroethanol differ by approximately 35kcal/mol at CBS-QB3 level of theory via isodesmic reaction. These data indicate that fluoroethanol is more stable than chloroethanol.

The experimental enthalpy of formation for chlorofluoroethane and ethandiol at 0 K and 298 K are included in the Table V.7 together with the calculated group additivity values.[21] These values were compared with the calculated best values of haloethanols at 0 K (atomization reaction) and 298 K (congeneric reaction).

Table V.7. Best values of enthalpies of formation at 0 k and 298 K in kcal/mol

Molecular formula	ΔH_f^0 (0K)	ΔH_f^0 (298K)	Group additivity
FC_2H_4OH	-95.79	-96.78	-97.50
ClC_2H_4OH	-58.51	-61.86	-62.50
BrC_2H_4OH	-51.48	-50.91	-51.40
FC_2H_4Cl	-71.80	-75.00	-68.00
HOC_2H_4OH	-87.93	-92.61	-92.00

It is found that the enthalpy of formation of fluoroethanol is approximately 4kcal/mol lower than the ethandiol. However the calculated value of chloroethanol at 298 K is approximately 13kcal/mol higher than the experimental value of enthalpy of formation of chlorofluoroethane.[21] This is attributed to the fact that the C-O bond is

weaker than the C-F bond.[20] The difference between calculated value of fluoroethanol and experimental value of chlorofluoroethane at 298 K is approximately 20 kcal/mol.[21] This is attributed to the fact that the C-Cl bond is weaker than C-O bond.[20] The best values ΔH_f^0(298K) for fluoroethanol and chloroethanol were estimated by taking the average of G3, G3B3, G3MP2B3, CBS-Q and CBS-QB3 methods using isodesmic enthalpies. In case of bromoethanol, it was obtained by taking the average of three G2, CBS-Q and CBS-QB3 methods. Similar procedure was followed to evaluate the best value of ΔH_f^0 at 0 K for haloethanols using atomization enthalpies. The mean enthalpies of formation (best value) of fluoroethanol, chloroethanol and bromoethanol at 298K using isodesmic reactions are -96.78±0.03, -61.86±0.02 and -50.91±0.96 kcal/mol respectively. The mean enthalpies of formation (best value) of fluoroethanol, chloroethanol and bromoethanol at 0 K with atomization reactions are -95.79, -58.51 and -51.48 kcal/mol respectively. The mean absolute deviation for G3, G3B3, G3MP2B3, CBS-Q and CBS-QB3 level of theories from the best value of fluoroethanol and chloroethanol are 0.02 and 0.02 respectively. The standard deviation for enthalpy of formation at 298 K using isodesmic reaction of fluoroethanol and chloroethanol are 0.03 and 0.02 respectively. The mean absolute deviation and standard deviation of enthalpy of formation for bromoethanol was evaluated using B3LYP, G2, CBS-Q, CBS-QB3 and CCSD/cc-pVDZ theories are 0.75 and 0.96 respectively. The deviation from the mean value of the enthalpy of formation of haloethanols for different higher level quantum chemistry methods is shown in the Figure V.1.
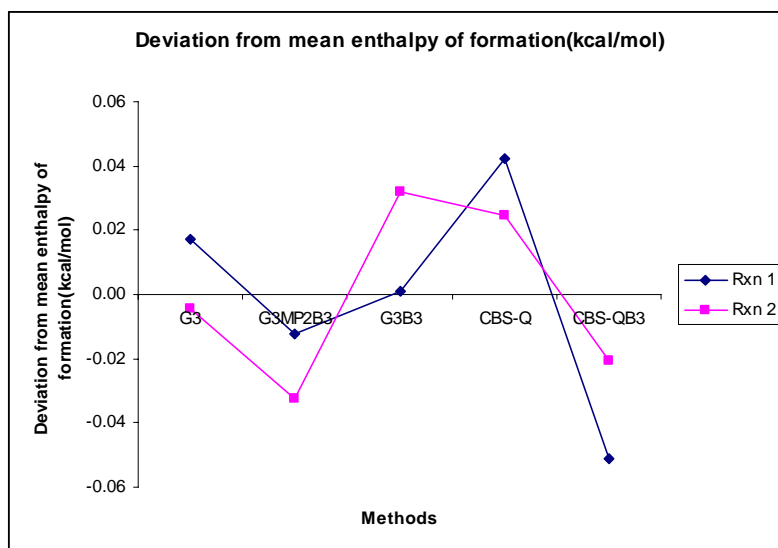
Figure V.1. Deviation from mean enthalpy of formation (kcal/mol) for the methods used for calculating the mean value.

The values calculated by HF, MP2, B3LYP were not considered in the average. The higher level of theories like G_n and CBS methods show a faster convergence and come closer to the Benson's group additivity method. The equilibrium ground state structures of fluoroethanol, chloroethanol, bromoethanol, ethyl fluoride, ethyl chloride, ethyl bromide, ethanol and ethane have been shown in the Figure V.2.

A.   B.

C.   D.   E.

F.   G.   H.
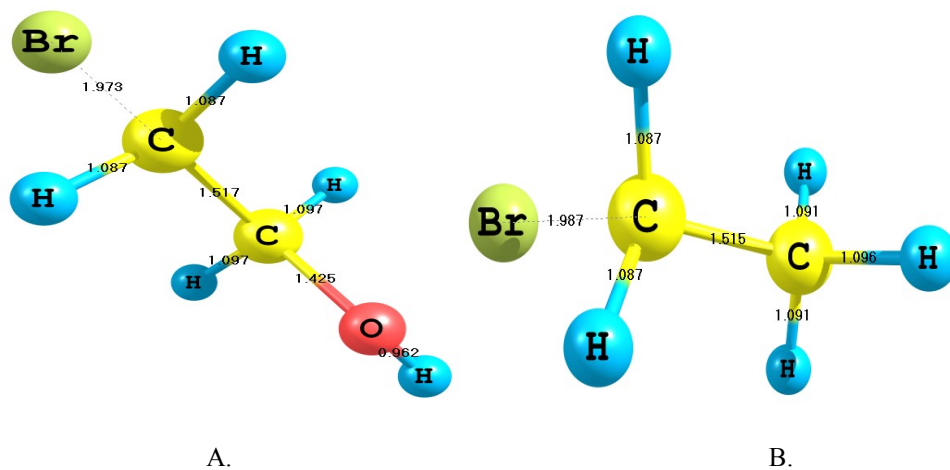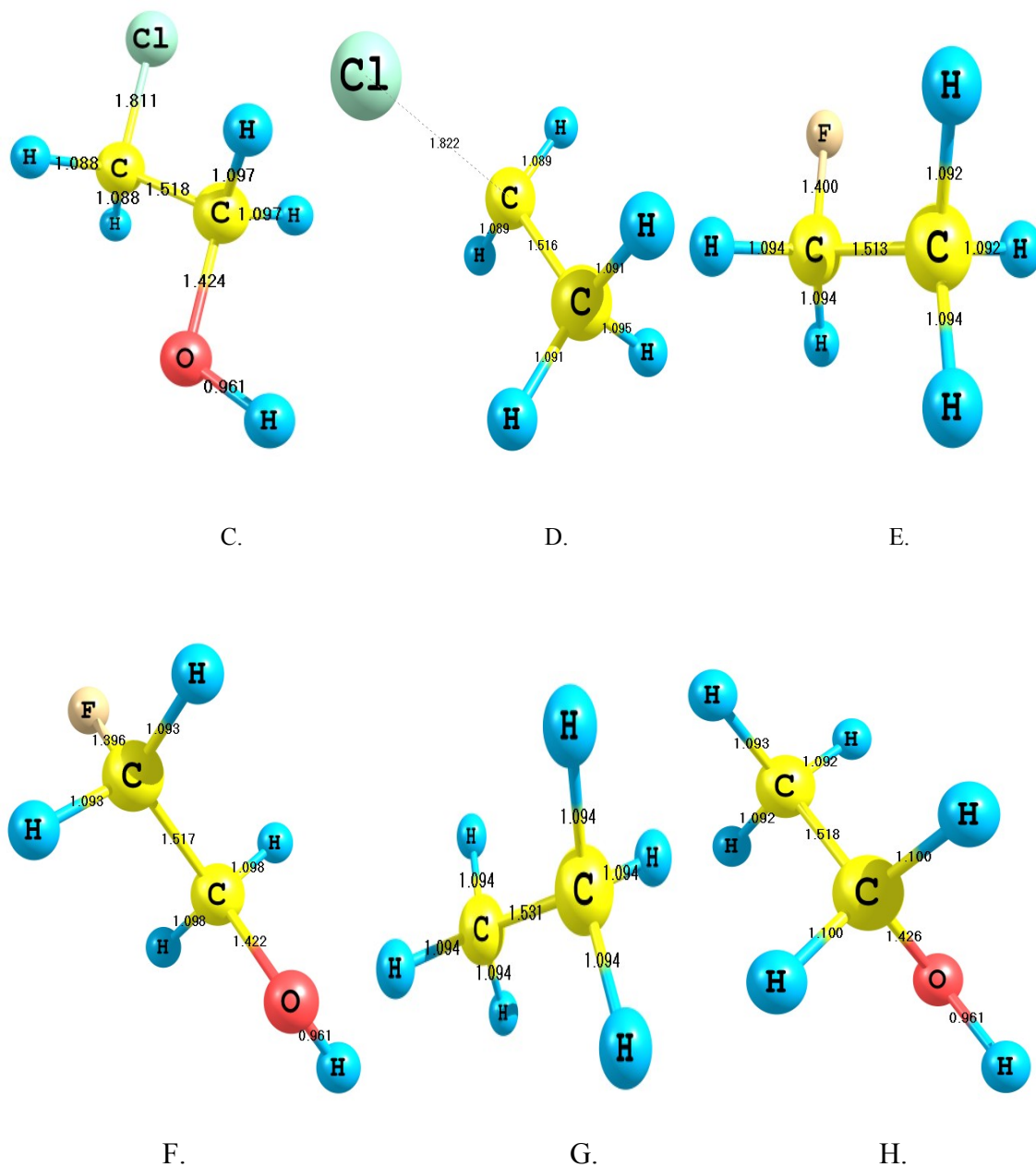
Figure V.2. Optimized geometries of (A) 2-Bromoethanol (T_t) (B) Ethylbromide (C) 2-Chloroethanol (T_t) (D) Ethylchloride (E) Ethylfluoride (F) 2-Fluoroethanol (T_t) (G) Ethane (H) Ethanol at B3LYP/CBSB7 level of theory in CBS-QB3 calculations.

V.7. Calculation of thermodynamic coefficient using computational approach

In fact, the thermodynamic property which was needed to simulate the reaction mechanism of thermal decomposition of haloethanols (2-fluoroethanol, 2-chloroethanol and 2-bromoethanol) at high temperature was found to be absent in database. Hence, these values were estimated following a computational approach. First, optimization for the global minima ($G_{g'}$) of 2-fluoroethanol, 2-chloroethanol and 2-bromoethanol were performed at B3LYP/6-311++G** level of theory. Second, the results obtained from these calculations were used for the estimation of the standard thermodynamic parameters such as standard enthalpy, heat capacity, and entropy of three haloethanols using statistical thermodynamics. Third, these thermodynamic properties were determined at the interval of 100K in the temperature range of 200-4000K. These data are given in the Tables from V.A.38 to V.A.40 at the end of this chapter.

Fourth, the data of $C_p°/R$, $H°/RT$, and $S°/R$ as functions of temperature were fitted to polynomial as given in following expressions in the two temperature ranges to obtain fourteen thermodynamic coefficients. These expressions were taken from chemkin software manual.[27]

$$\frac{C_p^0}{R} = a_1 + a_2 T + a_3 T^2 + a_4 T^3 + a_5 T^4 \tag{6}$$

$$\frac{H^0}{RT} = a_1 + \frac{a_2}{2} T + \frac{a_3}{3} T^2 + \frac{a_4}{4} T^3 + \frac{a_5}{5} T^4 + \frac{a_6}{T} \tag{7}$$

$$\frac{S^0}{R} = a_1 \ln T + a_2 T + \frac{a_3}{2} T^2 + \frac{a_4}{3} T^3 + \frac{a_5}{4} T^4 + a_7 \tag{8}$$

These fourteen thermodynamic coefficients in the two temperature ranges (200-1500K and 1500-4000K) obtained for haloethanols by the polynomial fitting for the plot of C_p^0/R, S^0/R and H^0/RT as functions of temperature is presented in the Table V.8. These coefficients which were needed for modeling of haloethanols have been given for the three species in the chemkin format as well in the Table V.A.41.

The purpose of performing all these calculation was to evaluate the thermodynamic parameters which are needed for estimating the reverse rate coefficients for the given reaction in the chemkin interpreter. As we are aware that the reverse rate coefficients can easily be evaluated by using the following expression reaction:

$$k_R = \frac{k_F}{K} \tag{9}$$

And the equilibrium constant can also be obtained without any difficulty using the relation for thermodynamic property (tempearature dependent Gibbs free change of the reaction) as shown below.

$$\Delta_r G^0 = -RT \ln K \tag{10}$$

This, in turn, can be used for evaluating the reverse rate coefficient.

Table V.8: Fourteen thermodynamic polynomial coefficients in the two temperature ranges obtained for haloethanols by the polynomial fitting for the plot of C_p^0/R, S^0/R and H^0/RT as functions of temperature.

Temperature Range(K)	Thermodynamic Coefficient	2-Fluoroethanol	2-Chloroethanol	2-Bromoethanol
200-1500	a_1	1.00435221×10^1	9.78995309	9.81528220
	a_2	$1.23183625 \times 10^{-2}$	$1.29870370 \times 10^{-2}$	$1.30482056 \times 10^{-2}$
	a_3	$-4.24388361 \times 10^{-6}$	$-4.71039402 \times 10^{-6}$	$-4.77513494 \times 10^{-6}$
	a_4	$6.75289970 \times 10^{-10}$	$8.03054375 \times 10^{-10}$	$8.23308347 \times 10^{-10}$
	a_5	$-4.04313161 \times 10^{-14}$	$-5.26610986 \times 10^{-14}$	$-5.47193158 \times 10^{-14}$
	a_6	4.56644387×10^4	2.84364086×10^4	2.30408663×10^4
	a_7	-2.79636175×10^1	-2.50838130×10^1	-2.36753095×10^1
1500-4000	a_1	2.34302225	2.42097860	2.67638420
	a_2	$2.48741744 \times 10^{-2}$	$2.70120214 \times 10^{-2}$	$2.70280049 \times 10^{-2}$
	a_3	$-8.82084111 \times 10^{-6}$	$-1.31097643 \times 10^{-5}$	$-1.36976723 \times 10^{-5}$
	a_4	$-8.36664176 \times 10^{-10}$	$2.03583485 \times 10^{-9}$	$2.54120850 \times 10^{-9}$
	a_5	$8.02587288 \times 10^{-13}$	$1.58587651 \times 10^{-13}$	$3.35759923 \times 10^{-14}$
	a_6	4.88722097×10^4	3.12799826×10^4	2.57514777×10^4
	a_7	1.53011971×10^1	1.55646965×10^1	1.55567939×10^1
[a]$\Delta_f H^0$	[b]Experimental	[c]101.20 ± 1.20	63.83 ± 0.19	52.96 ± 0.17
	Calculated	96.78 ± 0.03	61.86 ± 0.02	50.91 ± 0.96

[a] These values of $\Delta_f H^0$ for haloethanols is given at 298 K in gas phase in terms of kcal/mol., [b] Reference [6], [c] This is calculated value obtained using the combination of B3LYP/cc-PVTZ and CBS-QB3 levels.

Comparisons of calculated value of enthalpy at 298 K with experimental literature value of H_{298} have also been shown in Table V.8. This indicates that the reported value of experimental standard molar enthalpies of formation of 2-chloro-, 2-bromoethanol at 298.15K are approximately 2kcal/mol higher as compared to our predicted theoretical results. Moreover, Bernandes et al. have not been able to determine the experimental

value of enthalpy of formation of 2-fluoroethanol due to the lack of a sample with the high purity which was required for the calorimetric measurements. Hence, the theoretical enthalpy of formation of 2-fluoroethanol was derived by B3LYP/cc-pVTZ and CBS-QB3 calculations using isodesmic and isogyric gas phase reactions which is 101.2±1.2kcal/mol. However, this value was found to be overestimated by 4.42kcal/mol as compared to our reported best value.

V.8. Conclusion

Ab initio, DFT and higher level quantum chemistry calculation have been performed to estimate the enthalpy of formation of haloethanols for which the experimental data are not available. These results were compared with the enthalpy of formation of chlorofluoroethane and ethandiol and difluoroethane. Enthalpy of formation calculated with High level G_n and CBS-Q methods are in good agreement with the Benson's group additivity method which provides evidence that these values of enthalpies of formation of haloethanols calculated via isodesmic reactions are reasonable. The calculated mean enthalpies of formation (G3, G3B3, G3MP2B3, CBS-Q and CBS-QB3) of fluoroethanol, chloroethanol and bromoethanol at 298 K via isodesmic reactions which minimizes systematic calculation error are -96.78±0.03, -61.86±0.02 and -50.91±0.96 kcal/mol respectively. These results on 2-chloro and 2-bromoethanol have been found to be in good agreement with the reported experimental values. However, only accurate experimental results on 2-fluoroethanol can validate our data. The atomization method predicts higher molecular stability for all haloethanols in our study as compared to the isodesmic method at higher level of calculation at 298 K. It

has been found that the enthalpy of formation calculated via isodesmic reaction (best value) of fluoroethanol at 298 K is approximately 7kcal/mol higher than the experimental enthalpy of formation of difluoroethane. In conclusion, based upon heat of formation calculation, a higher level quantum chemistry method predicts that the fluoroethanol is the most stable and less reactive molecule among the haloethanols. It is hoped that the enthalpy of formation reported here would be helpful for the modeling of gas phase reaction mechanism of combustion, pyrolysis and oxidation of haloethanols.

V.9.References

1. Zurer, P.S.; Chemical and Engineering News, **1993**, 71, 8.

2. Climate Change 2001: The Scientific Basis. Cambridge University Press, Cambridge, UK, 2001.

3. Rajakumar B.; Burkholder J. B.; Portmanna R. W.; Ravishankara A. R. Phys. Chem. Chem. Phys., **2005**, 7, 2498.

4. Mogelberg, T.E.; Bilde M. *J. Phys. Chem*. **1996**,100, 8882.

5. Sellevag S. R.; Nielsen C. J.; Søvde O. A.; Myhre G.; Sundet J. K.; Stordal F.; Isaksen I. S. A.; Atmos. Environ., **2004**, 38, 6725.

6. Bernardes, C. E. S.; Minas, M. E.; Amaral, M. P. F.; Ferreira, A. I. M. C. L.; Ribeiro, M. A. V.; Cabral, B.; J. Phys. Chem. A; **2007**, 111, 1713.

7. Curtiss L.A.; Raghavachari K.; Redfern P.C.; Pople J.A.; J. Chem. Phys. **1997**,106, 1063.

8. (a) Becke, A. D. *J*. Chem. Phys. **1993**, *98*, 5648. (b) Perdew, J. P. Phys. *Re*V. **1986**, *B33*, 8822.

9. (a) Becke, A. D. *J.* Chem. Phys. **1993**, *98*, 5648. (b) Lee, C.; Yang, W.; Parr, R. G. *Phys. Re*V. **1989**, *B37*, 785.

10. Curtiss, L. A.; Raghavachari, K.; Trucks, G. W.; Pople, J. A. J. Chem. Phys. **1991**, *94*, 7221.

11. Curtiss, L. A.; Raghavachari, K.; Redfern, P. C.; Rassolov V.; Pople, J. A. J. Chem. Phys. **1998**, 109, 764.

12. Curtiss, L. A.; Raghavachari, K.; Pople, J. A. J. Chem. Phys. **1993**, *98*, 1293.

13. Baboul, A. G.; Curtiss, L. A.; Redfern, P. C.;   Raghavachari, K. J. Chem. Phys. **1999**, *110*, 7650.

14. Petersson, G. A.; Bennett, A.; Tensfeldt, T. G.; Al-Laham, M. A.; Shirley, W. A.; Mantzaris, J. *J.* Chem. Phys. **1988**, *89*, 2193.

15. Gordon, M. H.; Pople, J. A.; Frisch, M. J. Chem. Phys. Lett. **1988**, *153*, 503.

16. Stein, S. E.; Rukkers, J. M.; Brown, R. L *NIST-Standard Reference Data Base 25*; National Institute of Standards and Technology: Washington, DC.

17. Hehre, W.J.; Random, L.; Schleyer, P. R.; Pople, J. A. ab –initio Molecular orbital theory; chapter 6; John wiley & sons ; New York, **1986.**

18. Rajakumar B.; Reddy K. P. J.; Arunan E.; *J. Phys. Chem. A* **2003,** *107, 9782.*

19. Frisch, M. J.; Trucks, G. W.; Schlegel, H. B.; Scuseria, G. E.; Robb, M. A.; Montgomery, J. R. C. J. A.; Vreven, T.; Kudin, K. N.; Burant, J. C.; Millam, J. M.; Iyengar, S. S.; Tomasi, J.; Barone, V.; Mennucci, B.; Cossi, M.; Scalmani, G.; Rega, N.; Petersson, G. A.; Nakatsuji, H.; Ehara, M. H. M.; Toyota, K.; Fukuda, R.; Hasegawa, J.; Ishida, M.; Nakajima, T.; Honda, Y.; Kitao, O.; Nakai, H.; Klene, M.; Li, X.; Knox, J. E.; Hratchian, H. P.; Cross, J. B.; Adamo, C.; Jaramillo, J.; Gomperts, R.; Stratmann, R. E.; Yazyev, O.; Austin, A. J.; Cammi, R.; Pomelli, C.; Ochterski, J. W.; Ayala, P. Y.; Morokuma, K.; Voth, G. A.; Salvador, P.; Dannenberg, J. J.; Zakrzewski, V. G.; Dapprich, S.; Daniels, A. D.; Strain, M. C.; Farkas, O.; Malick, D. K.; Rabuck, A. D.; Raghavachari, K.; Foresman, J. B.; Ortiz, J. V.; Cui, Q.; Baboul, A. G.; Clifford, S.; Cioslowski, J.; Stefanov, B. B.; Liu, G.; Liashenko, A.; Piskorz, P.; Komaromi, I.; Martin, R. L.; Fox, D. J.; Keith, T.; Al-Laham, M. A.; Peng, C. Y.; Nanayakkara, A.;

Challacombe, M.; Gill, P. M. W.; Johnson, B.; Chen, W.; Wong, M. W.; Gonzalez, C.; Pople, J. A. *Gaussian 03*, Revision A.1; Gaussian, Inc.: Pittsburgh, PA, 2003.

20. Benson S. W.; Thermo chemical kinetics, 2nd ed.; John Wiley & Sons, New York, **1976.**

21. Frenkel, M; Marsh, K.N.; Wilhoit, R.C.; Kabo, G.J.; Roganov, G.N., Thermodynamics of Organic Compounds in the Gas State, Thermodynamics Research Center, College Station, TX, **1994.**

22. Gurvich, L.V.; Veyts, I. V.; Alcock, C. B., Thermodynamic Properties of Individual Substances, 4th Ed, Hemisphere Pub. Co., New York, **1989.**

23. Kudchadker, S.A.; Kudchadker, A.P. J. Phys. Chem. Ref. Data, **1979,** 8, 519.

24. Manion, J.A. J. Phys. Chem. Ref. Data, **2002,** 31, 123.

25. Bakowies, D. *J. Phys. Chem. A.* **2009,** 113, 11517.

26. Berry R.J.; Ehlersa C.J.; Burgess D.R.; Zachariahb M.R.; Nydenc M.R.; Schwartza3d M.; J. Mol. Struct. (Theochem) **1998**, 422, 89.

27. CHEMKIN 10101, Reaction Design: San Diego, 2010.

Table V.A.1. Optimized structures of 2-Bromoethanol (T$_t$) at different level of theories. HF, MP2 (FULL) and DFT levels of theory calculations were done with 6-311++G** basis sets.

Structural parameter	HF	MP2	B3LYP	CBS-Q	G2	CBS-QB3	CCSD
R(1,2)	1.515	1.514	1.517	1.52	1.512	1.517	1.524
R(1,3)	1.078	1.089	1.087	1.093	1.089	1.087	1.1
R(1,4)	1.078	1.089	1.087	1.093	1.089	1.087	1.1
R(1,7)	1.954	1.939	1.974	1.933	1.953	1.973	1.954
R(2,5)	1.086	1.096	1.096	1.102	1.098	1.097	1.108
R(2,6)	1.086	1.096	1.096	1.102	1.098	1.097	1.108
R(2,8)	1.402	1.423	1.428	1.42	1.425	1.425	1.421
R(8,9)	0.94	0.96	0.962	0.965	0.972	0.962	0.965
A(2,1,3)	111.5	110.7	111.6	110.8	111.2	111.5	111
A(2,1,4)	111.5	110.9	111.7	110.8	111.2	111.5	111
A(2,1,7)	110.5	110	110.3	109.9	109.6	110.5	110.4
A(3,1,4)	110.1	110.1	110.2	109.6	110.2	110.2	109.6
A(3,1,7)	106.5	107.5	106.4	107.8	107.2	106.5	107.3
A(4,1,7)	106.5	107.5	106.4	107.8	107.2	106.5	107.3
A(1,2,5)	109.9	109.6	109.9	109.6	109.7	109.7	109.4
A(1,2,6)	109.9	109.8	109.9	109.6	109.7	109.7	109.4
A(1,2,8)	106.1	105.8	105.9	105.5	105.2	105.6	105.7
A(5,2,6)	108.5	108.7	108.5	108	108.2	108.4	108
A(5,2,8)	111.2	111.5	111.3	112	112	111.7	112.1
A(6,2,8)	111.2	111.4	111.3	112	112	111.7	112.1
A(2,8,9)	110.4	107.7	109	108.2	107.8	108.2	107
D(3,1,2,5)	-177.9	-179.5	-177.8	-178.3	-177.8	-177.6	-178
D(3,1,2,6)	-58.6	-60.2	-58.4	-59.9	-59	-58.8	-59.9
D(3,1,2,8)	61.7	60.1	61.9	60.9	61.6	61.8	61.1
D(4,1,2,5)	58.6	58	58.3	59.9	59	58.8	59.9
D(4,1,2,6)	178	177.3	177.7	178.3	177.8	177.6	178
D(4,1,2,8)	-61.7	-62.4	-62	-60.9	-61.6	-61.8	-61.1
D(7,1,2,5)	-59.7	-60.8	-59.7	-59.2	-59.4	-59.4	-59
D(7,1,2,6)	59.7	58.5	59.7	59.2	59.4	59.4	59.1
D(7,1,2,8)	180	178.8	180	180	180	-180	180
D(1,2,8,9)	180.1	171.8	-179.9	180	180	-180	180.1
D(5,2,8,9)	60.6	52.6	60.7	60.8	60.8	60.8	60.9
D(6,2,8,9)	-60.4	-69	-60.5	-60.8	-60.9	-60.8	-60.8

1-C, 2-C, 3-H(1), 4-H(1), 7-Br(1), 5-H(2), 6-H(2), 8-O(2), 9-H(8)

Table V.A.2. Optimized structures of ethylbromide at different level of theories. HF, MP2 (FULL) and DFT levels of theory calculations with 6-311++G** basis sets.

Structural parameter	HF	MP2	B3LYP	CBS-Q	G2	CBS-QB3	CCSD
R(1,2)	1.515	1.516	1.515	1.522	1.513	1.515	1.524
R(1,3)	1.078	1.09	1.088	1.094	1.089	1.088	1.101
R(1,4)	1.078	1.09	1.088	1.094	1.089	1.088	1.101
R(1,7)	1.963	1.945	1.987	1.942	1.962	1.987	1.963
R(2,5)	1.084	1.092	1.092	1.095	1.091	1.091	1.103
R(2,6)	1.084	1.092	1.092	1.095	1.091	1.091	1.103
R(2,8)	1.088	1.095	1.096	1.098	1.095	1.096	1.106
A(2,1,3)	112.3	111.8	112.6	112	112.5	112.7	112.1
A(2,1,4)	112.3	111.8	112.6	112	112.5	112.7	112.1
A(2,1,7)	111.8	111.4	111.8	111	110.9	111.8	111.4
A(3,1,4)	109.5	109.2	109.5	108.9	109.4	109.6	109.1
A(3,1,7)	105.2	106.1	104.8	106.3	105.6	104.7	105.9
A(4,1,7)	105.2	106.1	104.8	106.3	105.6	104.7	105.9
A(1,2,5)	111.2	111	111.4	110.9	110.8	111.4	111
A(1,2,6)	111.2	111	111.4	110.9	110.8	111.4	111
A(1,2,8)	108.9	109.4	109.1	109.6	109.5	109.1	109.4
A(5,2,6)	108.6	108.4	108.4	108.3	108.4	108.4	108.4
A(5,2,8)	108.4	108.5	108.2	108.5	108.6	108.2	108.5
A(6,2,8)	108.4	108.5	108.2	108.5	108.6	108.2	108.5
D(3,1,2,5)	-178.6	-178.9	-178.4	-178.8	-178.2	-178.3	-178.8
D(3,1,2,6)	-57.5	-58.3	-57.1	-58.5	-57.7	-57.1	-58.2
D(3,1,2,8)	62	61.4	62.3	61.4	62.1	62.3	61.5
D(4,1,2,5)	57.5	58.3	57.1	58.5	57.7	57.1	58.2
D(4,1,2,6)	178.6	178.9	178.4	178.8	178.2	178.3	178.8
D(4,1,2,8)	-62	-61.4	-62.2	-61.4	-62.1	-62.3	-61.5
D(7,1,2,5)	-60.6	-60.3	-60.6	-60.2	-60.2	-60.6	-60.3
D(7,1,2,6)	60.6	60.3	60.6	60.2	60.2	60.6	60.3
D(7,1,2,8)	180	180	-180	180	-180	180	-180

1-C, 2-C, 3-H(1), 4-H(1), 7-Br(1), 5-H(2), 6-H(2), 8-H(2)

Table V.A.3.Optimized structures of 2-chloroethanol (T$_t$) at different level of theories.

Structural parameter	G2	CBS-QB3	G2MP2	G3MP2B3	G3	CCSD
R(1,2)	1.513	1.518	1.513	1.522	1.513	1.524
R(1,3)	1.09	1.088	1.09	1.091	1.09	1.101
R(1,4)	1.09	1.088	1.09	1.091	1.09	1.101
R(1,7)	1.782	1.811	1.782	1.811	1.782	1.798
R(2,5)	1.098	1.097	1.098	1.1	1.098	1.109
R(2,6)	1.098	1.097	1.098	1.1	1.098	1.109
R(2,8)	1.424	1.424	1.424	1.422	1.424	1.419
R(8,9)	0.971	0.961	0.971	0.969	0.971	0.965
A(2,1,3)	110.3	111	110.3	110.9	110.3	110.6
A(2,1,4)	110.3	111	110.3	110.9	110.3	110.6
A(2,1,7)	110.4	110.5	110.4	110.4	110.4	110.3
A(3,1,4)	109.3	109.8	109.3	109.4	109.3	109.2
A(3,1,7)	108.3	107.2	108.3	107.5	108.3	108
A(4,1,7)	108.3	107.2	108.3	107.5	108.3	108
A(1,2,5)	109.7	109.5	109.7	109.5	109.7	109.3
A(1,2,6)	109.7	109.5	109.7	109.5	109.7	109.3
A(1,2,8)	105.2	105.7	105.2	105.8	105.2	105.8
A(5,2,6)	108.2	108.4	108.2	108	108.2	107.9
A(5,2,8)	111.9	111.9	111.9	112	111.9	112.3
A(6,2,8)	111.9	111.9	111.9	112	111.9	112.2
A(2,8,9)	107.9	108.3	107.9	108	107.9	107.2
D(3,1,2,5)	-179	-178.1	-179	-178.2	-179	-178.3
D(3,1,2,6)	-60.2	-59.4	-60.2	-60	-60.2	-60.5
D(3,1,2,8)	60.4	61.2	60.4	60.9	60.4	60.6
D(4,1,2,5)	60.2	59.4	60.2	60	60.2	60.5
D(4,1,2,6)	179	178.1	179	178.2	179	178.4
D(4,1,2,8)	-60.4	-61.2	-60.4	-60.9	-60.4	-60.6
D(7,1,2,5)	-59.4	-59.4	59.4	-59.1	-59.4	-58.9
D(7,1,2,6)	59.4	59.3	59.4	59.1	59.4	58.9
D(7,1,2,8)	180	180	-180	180	180	-180
D(1,2,8,9)	180	180	-180	-179.9	180	-180
D(5,2,8,9)	60.8	60.9	60.9	60.8	60.8	60.9
D(6,2,8,9)	-60.9	-60.9	-60.9	-60.6	-60.9	-60.9

1-C, 2-C, 3-H(1), 4-H(1), 7-Cl(1), 5-H(2), 6-H(2), 8-O(2), 9-H(8)

Table V.A.4. Optimized structures of 2-chloroethanol (T_t) at different level of theories. HF, MP2 (FULL) and DFT levels of theory calculations were done with 6-311++G** basis sets.

Structural parameter	HF	MP2	B3LYP	G3B3	CBS-Q
R(1,2)	1.515	1.514	1.518	1.522	1.52
R(1,3)	1.078	1.089	1.088	1.091	1.094
R(1,4)	1.078	1.089	1.088	1.091	1.094
R(1,7)	1.796	1.779	1.813	1.811	1.785
R(2,5)	1.086	1.096	1.096	1.1	1.102
R(2,6)	1.086	1.096	1.096	1.1	1.102
R(2,8)	1.401	1.422	1.427	1.422	1.419
R(8,9)	0.94	0.96	0.962	0.969	0.965
A(2,1,3)	111.1	110.4	111.2	110.9	110.4
A(2,1,4)	111.1	110.4	111.3	110.9	110.4
A(2,1,7)	110.2	109.7	110.1	110.4	110.3
A(3,1,4)	109.8	109.7	109.8	109.4	109.2
A(3,1,7)	107.2	108.3	107.1	107.5	108.2
A(4,1,7)	107.2	108.3	107.1	107.5	108.2
A(1,2,5)	109.8	109.5	109.7	109.5	109.6
A(1,2,6)	109.8	109.5	109.8	109.5	109.6
A(1,2,8)	106.2	106.1	106	105.8	105.4
A(5,2,6)	108.4	108.5	108.5	108	108.1
A(5,2,8)	111.3	111.6	111.4	112	112.1
A(6,2,8)	111.3	111.6	111.4	112	112.1
A(2,8,9)	110.4	107.7	109.1	108	108.2
D(3,1,2,5)	-178.3	59.8	-178.8	-178.2	-178.8
D(3,1,2,6)	-59.2	178.7	-59.6	-60	-60.3
D(3,1,2,8)	61.3	-60.7	60.8	60.9	60.4
D(4,1,2,5)	59.2	-178.7	58.5	60	60.3
D(4,1,2,6)	178.3	-59.8	177.6	178.2	178.8
D(4,1,2,8)	-61.2	60.7	-62	-60.9	-60.4
D(7,1,2,5)	-59.6	-59.5	-60.2	-59.1	-59.2
D(7,1,2,6)	59.6	59.5	59	59.1	59.2
D(7,1,2,8)	-180	180	179.4	180	180
D(1,2,8,9)	-180	180	175.4	-179.9	180
D(5,2,8,9)	60.6	60.8	56	60.8	60.8
D(6,2,8,9)	-60.5	-60.8	-65.3	-60.6	-60.9

1-C, 2-C, 3-H(1), 4-H(1), 7-Cl(1), 5-H(2), 6-H(2), 8-O(2), 9-H(8)

Table V.A.5. Optimized structures of ethylchloride at different level of theories.

Structural parameter	G2	CBS-QB3	G2MP2	G3MP2B3	G3
R(1,2)	1.514	1.516	1.514	1.519	1.514
R(1,3)	1.09	1.089	1.09	1.092	1.09
R(1,4)	1.09	1.089	1.09	1.092	1.09
R(1,7)	1.789	1.822	1.789	1.823	1.789
R(2,5)	1.091	1.091	1.091	1.094	1.091
R(2,6)	1.091	1.091	1.091	1.094	1.091
R(2,8)	1.094	1.095	1.094	1.097	1.094
A(2,1,3)	111.5	112.2	111.5	112	111.5
A(2,1,4)	111.5	112.2	111.5	112	111.5
A(2,1,7)	111.4	111.6	111.4	111.6	111.4
A(3,1,4)	108.6	109.2	108.6	108.9	108.6
A(3,1,7)	106.8	105.6	106.8	106	106.8
A(4,1,7)	106.8	105.6	106.8	106	106.8
A(1,2,5)	110.9	111.2	110.9	111.2	110.9
A(1,2,6)	110.9	111.2	110.9	111.2	110.9
A(1,2,8)	109.5	109.3	109.5	109.3	109.5
A(5,2,6)	108.5	108.5	108.5	108.4	108.5
A(5,2,8)	108.5	108.3	108.5	108.4	108.5
A(6,2,8)	108.5	108.3	108.5	108.4	108.5
D(3,1,2,5)	-179.5	-178.8	-179.5	-179.1	-179.5
D(3,1,2,6)	-58.9	-57.8	-58.9	-58.2	-58.9
D(3,1,2,8)	60.8	61.7	60.8	61.4	60.8
D(4,1,2,5)	58.9	57.8	58.9	58.2	58.9
D(4,1,2,6)	179.5	178.8	179.5	179.1	179.5
D(4,1,2,8)	-60.8	-61.7	-60.8	-61.4	-60.8
D(7,1,2,5)	-60.3	-60.5	-60.3	-60.5	-60.3
D(7,1,2,6)	60.3	60.5	60.3	60.5	60.3
D(7,1,2,8)	180	180	180	180	180

1-C, 2-C, 3-H(1), 4-H(1), 7-Cl(1), 5-H(2), 6-H(2), 8-H(2)

Table V.A.6. Optimized structures of ethylchloride at different level of theories. HF, MP2 (FULL) and DFT levels of theory calculations were done with 6-311++G basis sets.**

Structural parameter	HF	MP2	B3LYP	G3B3	CBS-Q
R(1,2)	1.515	1.515	1.516	1.519	1.521
R(1,3)	1.079	1.09	1.089	1.092	1.094
R(1,4)	1.079	1.09	1.089	1.092	1.094
R(1,7)	1.803	1.785	1.824	1.823	1.792
R(2,5)	1.084	1.092	1.092	1.094	1.095
R(2,6)	1.084	1.092	1.092	1.094	1.095
R(2,8)	1.087	1.094	1.095	1.097	1.098
A(2,1,3)	111.9	111.4	112.2	112	111.6
A(2,1,4)	111.9	111.4	112.2	112	111.6
A(2,1,7)	111.5	111	111.5	111.6	111.3
A(3,1,4)	109.2	108.9	109.1	108.9	108.6
A(3,1,7)	106	107	105.7	106	106.7
A(4,1,7)	106	107	105.7	106	106.7
A(1,2,5)	111	110.8	111.2	111.2	110.9
A(1,2,6)	111	110.8	111.2	111.2	110.9
A(1,2,8)	109.1	109.7	109.3	109.3	109.5
A(5,2,6)	108.6	108.4	108.5	108.4	108.5
A(5,2,8)	108.5	108.6	108.3	108.4	108.5
A(6,2,8)	108.5	108.6	108.3	108.4	108.5
D(3,1,2,5)	-179	-179.3	-178.9	-179.1	-179.4
D(3,1,2,6)	-58.1	-59	-57.8	-58.2	-58.8
D(3,1,2,8)	61.5	60.9	61.7	61.4	60.9
D(4,1,2,5)	58.1	59	57.8	58.2	58.8
D(4,1,2,6)	179	179.3	178.9	179.1	179.4
D(4,1,2,8)	-61.5	-60.9	-61.7	-61.4	-60.9
D(7,1,2,5)	-60.5	-60.1	-60.5	-60.5	-60.3
D(7,1,2,6)	60.5	60.1	60.5	60.5	60.3
D(7,1,2,8)	180	180	-180	-180	180

1-C, 2-C, 3-H(1), 4-H(1), 7-Cl(1), 5-H(2), 6-H(2), 8-H(2)

Table V.A.7. Optimized structures of ethylfluoride at different level of theories

Structural parameter	G2	CBS-QB3	G2MP2	G3MP2B3	G3
R(1,2)	1.509	1.513	1.509	1.516	1.509
R(1,3)	1.094	1.094	1.094	1.098	1.094
R(1,4)	1.094	1.094	1.094	1.098	1.094
R(1,7)	1.399	1.4	1.399	1.394	1.399
R(2,5)	1.092	1.092	1.092	1.095	1.092
R(2,6)	1.092	1.092	1.092	1.095	1.092
R(2,8)	1.093	1.094	1.093	1.096	1.093
A(2,1,3)	111.7	111.6	111.7	111.3	111.7
A(2,1,4)	111.7	111.6	111.7	111.3	111.7
A(2,1,7)	109.2	109.7	109.2	109.7	109.2
A(3,1,4)	108.7	109	108.7	108.3	108.7
A(3,1,7)	107.7	107.4	107.7	108	107.7
A(4,1,7)	107.7	107.4	107.7	108	107.7
A(1,2,5)	110.2	110.6	110.2	110.5	110.2
A(1,2,6)	110.2	110.6	110.2	110.5	110.2
A(1,2,8)	110.5	110.3	110.5	110.5	110.5
A(5,2,6)	108.6	108.5	108.6	108.4	108.6
A(5,2,8)	108.7	108.4	108.7	108.4	108.7
A(6,2,8)	108.7	108.4	108.7	108.4	108.7
D(3,1,2,5)	-178.9	-179	-178.9	-179.5	-178.9
D(3,1,2,6)	-59.1	-58.8	-59.1	-59.5	-59.1
D(3,1,2,8)	61	61.1	61	60.5	61
D(4,1,2,5)	59.1	58.8	59.1	59.5	59.1
D(4,1,2,6)	178.9	179	178.9	179.5	178.9
D(4,1,2,8)	-61	-61.1	-61	-60.5	-61
D(7,1,2,5)	-59.9	-60.1	-59.9	-60	-59.9
D(7,1,2,6)	59.9	60.1	59.9	60	59.9
D(7,1,2,8)	-180	180	180	-180	180

1-C, 2-C, 3-H(1), 4-H(1), 7-F(1), 5-H(2), 6-H(2), 8-H(2)

Table V.A.8. Optimized structures of ethylfluoride at different level of theories. HF, MP2 (FULL) and DFT levels of theory calculations were done with 6-311++G basis sets.**

Structural parameter	HF	MP2	B3LYP	G3B3	CBS-Q
R(1,2)	1.511	1.51	1.513	1.516	1.517
R(1,3)	1.083	1.093	1.093	1.098	1.098
R(1,4)	1.083	1.093	1.093	1.098	1.098
R(1,7)	1.374	1.397	1.407	1.394	1.391
R(2,5)	1.085	1.092	1.092	1.095	1.096
R(2,6)	1.085	1.092	1.092	1.095	1.096
R(2,8)	1.086	1.094	1.094	1.096	1.097
A(2,1,3)	111.7	111.7	112	111.3	111.5
A(2,1,4)	111.7	111.7	112	111.3	111.5
A(2,1,7)	109.8	109.6	109.9	109.7	109.5
A(3,1,4)	109	109.2	109.1	108.3	108.6
A(3,1,7)	107.2	107.2	106.8	108	107.8
A(4,1,7)	107.2	107.2	106.8	108	107.8
A(1,2,5)	110.7	110.5	110.8	110.5	110.3
A(1,2,6)	110.7	110.5	110.8	110.5	110.3
A(1,2,8)	109.8	109.8	109.7	110.5	110.5
A(5,2,6)	108.6	108.8	108.7	108.4	108.5
A(5,2,8)	108.5	108.6	108.3	108.4	108.6
A(6,2,8)	108.5	108.6	108.3	108.4	108.6
D(3,1,2,5)	-179.1	-178.9	-179	-179.5	-179.2
D(3,1,2,6)	-58.6	-58.5	-58.2	-59.5	-59.3
D(3,1,2,8)	61.2	61.3	61.4	60.5	60.8
D(4,1,2,5)	58.6	58.5	58.2	59.5	59.3
D(4,1,2,6)	179.1	178.9	179	179.5	179.2
D(4,1,2,8)	-61.2	-61.3	-61.4	-60.5	-60.8
D(7,1,2,5)	-60.2	-60.2	-60.4	-60	-59.9
D(7,1,2,6)	60.2	60.2	60.4	60	59.9
D(7,1,2,8)	180	180	-180	180	180

1-C, 2-C, 3-H(1), 4-H(1), 7-F(1), 5-H(2), 6-H(2), 8-H(2)

Table V.A.9. Optimized structures of ethane at different level of theories.

Structural parameter	G2	CBS-QB3	G2MP2	G3MP2B3	G3	CCSD
R(1,2)	1.524	1.531	1.524	1.531	1.524	1.534
R(1,3)	1.093	1.094	1.093	1.096	1.093	1.106
R(1,4)	1.093	1.094	1.093	1.096	1.093	1.106
R(1,7)	1.093	1.094	1.093	1.096	1.093	1.106
R(2,5)	1.093	1.094	1.093	1.096	1.093	1.106
R(2,6)	1.093	1.094	1.093	1.096	1.093	1.106
R(2,8)	1.093	1.094	1.093	1.096	1.093	1.106
A(2,1,3)	111.2	111.4	111.2	111.3	111.2	111.2
A(2,1,4)	111.2	111.4	111.2	111.3	111.2	111.2
A(2,1,7)	111.2	111.4	111.2	111.3	111.2	111.2
A(3,1,4)	107.7	107.5	107.7	107.5	107.7	107.7
A(3,1,7)	107.7	107.5	107.7	107.5	107.7	107.7
A(4,1,7)	107.7	107.5	107.7	107.5	107.7	107.7
A(1,2,5)	111.2	111.4	111.2	111.3	111.2	111.2
A(1,2,6)	111.2	111.4	111.2	111.3	111.2	111.2
A(1,2,8)	111.2	111.4	111.2	111.3	111.2	111.2
A(5,2,6)	107.7	107.5	107.7	107.5	107.7	107.7
A(5,2,8)	107.7	107.5	107.7	107.5	107.7	107.7
A(6,2,8)	107.7	107.5	107.7	107.5	107.7	107.7
D(3,1,2,5)	-180	-180	-180	180	-180	180
D(3,1,2,6)	-60	-60	-60	-60	-60	-60
D(3,1,2,8)	60	60	60	60	60	60
D(4,1,2,5)	60	60	60	60	60	60
D(4,1,2,6)	-180	180	180	180	-180	180
D(4,1,2,8)	-60	-60	-60	-60	-60	-60
D(7,1,2,5)	-60	-60	-60	-60	-60	-60
D(7,1,2,6)	60	60	60	60	60	60
D(7,1,2,8)	-180	180	180	180	-180	180

1-C, 2-C, 3-H(1), 4-H(1), 7-H(1), 5-H(2), 6-H(2), 8-H(2)

Table V.A.10.Optimized structures of ethane at different level of theories. HF, MP2 (FULL) and DFT levels of theory calculations were done with 6-311++G** basis sets.

Structural parameter	HF	MP2	B3LYP	G3B3	CBS-Q
R(1,2)	1.527	1.527	1.53	1.531	1.531
R(1,3)	1.086	1.093	1.094	1.096	1.096
R(1,4)	1.086	1.093	1.094	1.096	1.096
R(1,7)	1.086	1.093	1.094	1.096	1.096
R(2,5)	1.086	1.093	1.094	1.096	1.096
R(2,6)	1.086	1.093	1.094	1.096	1.096
R(2,8)	1.086	1.092	1.094	1.096	1.096
A(2,1,3)	111.2	111.2	111.4	111.3	111.2
A(2,1,4)	111.2	111.2	111.4	111.3	111.2
A(2,1,7)	111.2	111.1	111.4	111.3	111.2
A(3,1,4)	107.7	107.7	107.5	107.5	107.6
A(3,1,7)	107.7	107.7	107.5	107.5	107.6
A(4,1,7)	107.7	107.7	107.5	107.5	107.6
A(1,2,5)	111.2	111.2	111.4	111.3	111.2
A(1,2,6)	111.2	111.2	111.4	111.3	111.2
A(1,2,8)	111.2	111.2	111.4	111.3	111.2
A(5,2,6)	107.7	107.7	107.5	107.5	107.6
A(5,2,8)	107.7	107.7	107.5	107.5	107.6
A(6,2,8)	107.7	107.7	107.5	107.5	107.6
D(3,1,2,5)	180	180	-180	180	-180
D(3,1,2,6)	-60	-60	-60	-60	-60
D(3,1,2,8)	60	60	60	60	60
D(4,1,2,5)	60	60	60	60	60
D(4,1,2,6)	180	-180	180	180	-180
D(4,1,2,8)	-60	-60	-60	-60	-60
D(7,1,2,5)	-60	-60	-60	-60	-60
D(7,1,2,6)	60	60	60	60	60
D(7,1,2,8)	180	180	180	180	-180

1-C, 2-C, 3-H(1), 4-H(1), 7-H(1), 5-H(2), 6-H(2), 8-H(2)

Table V.A.11. Optimized structures of ethanol at different level of theories

Structural parameter	G2	CBS-QB3	G2MP2	G3MP2B3	G3	CCSD
R(1,2)	1.512	1.518	1.512	1.52	1.512	1.523
R(1,3)	1.092	1.092	1.092	1.095	1.092	1.104
R(1,4)	1.092	1.092	1.092	1.095	1.092	1.104
R(1,7)	1.093	1.093	1.093	1.096	1.093	1.105
R(2,5)	1.099	1.1	1.099	1.103	1.099	1.111
R(2,6)	1.099	1.1	1.099	1.103	1.099	1.111
R(2,8)	1.428	1.426	1.428	1.425	1.428	1.423
R(8,9)	0.971	0.961	0.971	0.969	0.971	0.965
A(2,1,3)	110	110.3	110	110.4	110	110.1
A(2,1,4)	110	110.3	110	110.4	110	110.1
A(2,1,7)	110.7	110.8	110.7	110.6	110.7	110.8
A(3,1,4)	108.4	108.2	108.4	108.2	108.4	108.3
A(3,1,7)	108.8	108.6	108.8	108.6	108.8	108.8
A(4,1,7)	108.8	108.6	108.8	108.6	108.8	108.8
A(1,2,5)	110.2	109.9	110.2	109.9	110.2	109.8
A(1,2,6)	110.2	109.9	110.2	109.9	110.2	109.8
A(1,2,8)	107	107.7	107	107.8	107	107.5
A(5,2,6)	107.6	107.6	107.6	107.2	107.6	107.3
A(5,2,8)	110.9	110.9	110.9	111	110.9	111.2
A(6,2,8)	110.9	110.9	110.9	111	110.9	111.2
A(2,8,9)	107.7	108.2	107.7	107.9	107.7	107
D(3,1,2,5)	-179.6	-179.4	-179.6	-179.1	-179.6	-179.2
D(3,1,2,6)	-61	-61.2	-61	-61.4	-61	-61.5
D(3,1,2,8)	59.7	59.7	59.7	59.7	59.7	59.6
D(4,1,2,5)	61	61.2	61	61.3	61	61.5
D(4,1,2,6)	179.6	179.4	179.6	179.1	179.6	179.2
D(4,1,2,8)	-59.7	-59.7	-59.7	-59.8	-59.7	-59.7
D(7,1,2,5)	-59.3	-59.1	-59.3	-58.9	-59.3	-58.9
D(7,1,2,6)	59.3	59.1	59.3	58.9	59.3	58.8
D(7,1,2,8)	-180	-180	180	180	-180	-180
D(1,2,8,9)	-180	180	-180	-180	180	-180
D(5,2,8,9)	59.7	59.7	59.7	59.6	59.7	59.8
D(6,2,8,9)	-59.7	-59.7	-59.7	-59.6	-59.7	-59.8

1-C, 2-C, 3-H(1), 4-H(1), 7-H(1), 5-H(2), 6-H(2), 8-O(2), 9-H(8)

Table V.A.12. Optimized structures of ethanol at different level of theories. HF, MP2 (FULL) and DFT levels of theory calculations were done with 6-311++G basis sets.**

Structural parameter	HF	MP2	B3LYP	G3B3	CBS-Q
R(1,2)	1.514	1.513	1.517	1.52	1.519
R(1,3)	1.085	1.092	1.093	1.095	1.096
R(1,4)	1.085	1.092	1.093	1.095	1.096
R(1,7)	1.086	1.093	1.094	1.096	1.097
R(2,5)	1.089	1.097	1.099	1.103	1.104
R(2,6)	1.089	1.097	1.099	1.103	1.104
R(2,8)	1.405	1.426	1.431	1.425	1.423
R(8,9)	0.94	0.96	0.962	0.969	0.965
A(2,1,3)	110.5	110.2	110.5	110.4	110
A(2,1,4)	110.5	110.2	110.5	110.4	110
A(2,1,7)	110.4	110.4	110.4	110.6	110.8
A(3,1,4)	108.3	108.6	108.3	108.2	108.3
A(3,1,7)	108.6	108.7	108.5	108.6	108.8
A(4,1,7)	108.6	108.7	108.5	108.6	108.8
A(1,2,5)	110	110.1	110.1	109.9	110.1
A(1,2,6)	110	110.1	110.1	109.9	110.1
A(1,2,8)	108.4	107.6	108	107.8	107.2
A(5,2,6)	107.7	108.1	107.8	107.2	107.4
A(5,2,8)	110.3	110.5	110.4	111	111.1
A(6,2,8)	110.3	110.5	110.4	111	111.1
A(2,8,9)	110.2	107.7	109	107.9	108
D(3,1,2,5)	-179.4	-179.7	-179.6	-179.1	-179.5
D(3,1,2,6)	-60.8	-60.7	-60.8	-61.4	-61.2
D(3,1,2,8)	59.9	59.8	59.8	59.7	59.6
D(4,1,2,5)	60.8	60.5	60.5	61.3	61.3
D(4,1,2,6)	179.4	179.5	179.3	179.1	179.5
D(4,1,2,8)	-59.9	-60	-60.1	-59.8	-59.6
D(7,1,2,5)	-59.3	-59.6	-59.6	-58.9	-59.1
D(7,1,2,6)	59.3	59.4	59.2	58.9	59.1
D(7,1,2,8)	-180	179.9	179.8	180	-180
D(1,2,8,9)	180	-179.9	180	-180	-180
D(5,2,8,9)	59.4	59.9	59.5	59.6	59.7
D(6,2,8,9)	-59.5	-59.7	-59.6	-59.6	-59.7

1-C, 2-C, 3-H(1), 4-H(1), 7-H(1), 5-H(2), 6-H(2), 8-O(2), 9-H(8)

Table V.A.13.Optimized structures of 2-fluoroethanol(T_t) at different level of theories.

Structural parameter	G2	CBS-QB3	G2MP2	G3MP2B3	G3	CCSD
R(1,2)	1.511	1.517	1.511	1.52	1.511	1.521
R(1,3)	1.093	1.093	1.093	1.096	1.093	1.104
R(1,4)	1.093	1.093	1.093	1.096	1.093	1.104
R(1,7)	1.397	1.396	1.397	1.39	1.397	1.388
R(2,5)	1.098	1.098	1.098	1.101	1.098	1.11
R(2,6)	1.098	1.098	1.098	1.101	1.098	1.11
R(2,8)	1.424	1.422	1.424	1.421	1.424	1.419
R(8,9)	0.97	0.961	0.97	0.969	0.97	0.964
A(2,1,3)	110.7	110.6	110.7	110.6	110.7	110.3
A(2,1,4)	110.7	110.6	110.7	110.6	110.7	110.3
A(2,1,7)	108.2	108.8	108.2	108.6	108.2	109
A(3,1,4)	109.4	109.6	109.4	108.9	109.4	109
A(3,1,7)	108.9	108.6	108.9	109.1	108.9	109.1
A(4,1,7)	108.9	108.6	108.9	109.1	108.9	109.1
A(1,2,5)	109.2	109	109.2	109	109.2	108.9
A(1,2,6)	109.2	109	109.2	109	109.2	108.9
A(1,2,8)	105.8	106.3	105.8	106.7	105.8	106.2
A(5,2,6)	108.2	108.3	108.2	107.8	108.2	107.9
A(5,2,8)	112.2	112	112.2	112.2	112.2	112.4
A(6,2,8)	112.2	112	112.2	112.2	112.2	112.4
A(2,8,9)	107.9	108.4	107.9	108	107.9	107.2
D(3,1,2,5)	-178.3	-178.2	-178.3	-178.4	-178.3	-178.5
D(3,1,2,6)	-60.2	-60.2	-60.2	-61	-60.2	-61.1
D(3,1,2,8)	60.7	60.8	60.7	60.3	60.7	60.2
D(4,1,2,5)	60.2	60.2	60.2	60.9	60.2	61
D(4,1,2,6)	178.3	178.2	178.3	178.3	178.3	178.4
D(4,1,2,8)	-60.7	-60.8	-60.7	-60.4	-60.7	-60.3
D(7,1,2,5)	-59.1	-59	-59.1	-58.7	-59.1	-58.8
D(7,1,2,6)	59.1	59	59.1	58.7	59.1	58.7
D(7,1,2,8)	-180	-180	180	180	-180	-180
D(1,2,8,9)	-180	-180	180	179.9	-180	179.9
D(5,2,8,9)	61.1	61	61	60.7	61.1	60.9
D(6,2,8,9)	-61	-60.9	-61	-60.8	-61	-61

1-C, 2-C, 3-H(1), 4-H(1), 7-F(1), 5-H(2), 6-H(2), 8-O(2), 9-H(8)

Table V.A.14. Optimized structures of 2-fluoroethanol (T_t) at different level of theories. HF, MP2 (FULL) and DFT levels of theory calculations were done with 6-311++G basis sets.**

Structural parameter	HF	MP2	B3LYP	G3B3	CBS-Q
R(1,2)	1.512	1.514	1.518	1.52	1.518
R(1,3)	1.082	1.092	1.092	1.096	1.097
R(1,4)	1.082	1.091	1.092	1.096	1.097
R(1,7)	1.371	1.393	1.401	1.39	1.389
R(2,5)	1.087	1.096	1.097	1.101	1.102
R(2,6)	1.087	1.096	1.097	1.101	1.102
R(2,8)	1.401	1.422	1.426	1.421	1.419
R(8,9)	0.94	0.959	0.961	0.969	0.964
A(2,1,3)	111	110.6	111.1	110.6	110.5
A(2,1,4)	111	110.9	111.1	110.6	110.5
A(2,1,7)	108.7	108.7	108.8	108.6	108.7
A(3,1,4)	109.6	109.9	109.7	108.9	109.2
A(3,1,7)	108.3	108.4	108	109.1	109
A(4,1,7)	108.3	108.3	108	109.1	109
A(1,2,5)	109.4	109.3	109.4	109	109.1
A(1,2,6)	109.4	109.3	109.4	109	109.1
A(1,2,8)	106.6	105.9	106.2	106.7	105.9
A(5,2,6)	108.4	108.8	108.5	107.8	108
A(5,2,8)	111.5	111.8	111.6	112.2	112.3
A(6,2,8)	111.5	111.7	111.6	112.2	112.3
A(2,8,9)	110.5	107.8	109.1	108	108.3
D(3,1,2,5)	-178.3	180	-178.4	-178.4	-178.4
D(3,1,2,6)	-59.7	-61.1	-59.6	-61	-60.6
D(3,1,2,8)	61	59.4	61	60.3	60.5
D(4,1,2,5)	59.6	57.8	59.2	60.9	60.6
D(4,1,2,6)	178.3	176.7	178	178.3	178.4
D(4,1,2,8)	-61.1	-62.8	-61.4	-60.4	-60.5
D(7,1,2,5)	-59.4	-61.1	-59.6	-58.7	-58.9
D(7,1,2,6)	59.3	57.8	59.2	58.7	58.9
D(7,1,2,8)	180	178.3	179.8	180	-180
D(1,2,8,9)	179.9	172.4	179.9	179.9	-180
D(5,2,8,9)	60.6	53.5	60.7	60.7	61
D(6,2,8,9)	-60.7	-68.7	-60.9	-60.8	-61

1-C, 2-C, 3-H(1), 4-H(1), 7-F(1), 5-H(2), 6-H(2), 8-O(2), 9-H(8)

Table V.A.15. Optimized structures of methylfluoride at different level of theories. HF, MP2 (FULL) and DFT levels of theory calculations were done with 6-311++G basis sets.**

Structural parameter	HF	MP2	B3LYP	G3B3	CBS-Q	G2	CBS-QB3	G2MP2	G3MP2B3
R(1,2)	1.082	1.091	1.092	1.097	1.096	1.092	1.093	1.092	1.097
R(1,3)	1.082	1.091	1.092	1.097	1.096	1.092	1.093	1.092	1.097
R(1,4)	1.082	1.091	1.092	1.097	1.096	1.092	1.093	1.092	1.097
R(1,5)	1.366	1.388	1.395	1.383	1.383	1.39	1.389	1.39	1.383
A(2,1,3)	110.2	110.2	110.3	109.3	109.7	109.8	109.8	109.8	109.3
A(2,1,4)	110.2	110.2	110.3	109.3	109.7	109.8	109.8	109.8	109.3
A(2,1,5)	108.8	108.8	108.6	109.6	109.3	109.1	109.2	109.1	109.6
A(3,1,4)	110.2	110.2	110.3	109.3	109.7	109.8	109.8	109.8	109.3
A(3,1,5)	108.8	108.8	108.6	109.6	109.3	109.1	109.2	109.1	109.6
A(4,1,5)	108.8	108.8	108.6	109.6	109.3	109.1	109.2	109.1	109.6

1-C, 2-H(1), 3-H(1), 4-H(1), 5-F(1)

Table V.A.16. Optimized structures of methane at different level of theories. HF, MP2 (FULL) and DFT levels of theory calculations were done with 6-311++G** basis sets.

Structural parameter	HF	MP2	B3LYP	G3B3	CBS-Q	G2	CBS-QB3	G2MP2	G3MP2B3
R(1,2)	1.084	1.09	1.091	1.093	1.093	1.089	1.091	1.089	1.093
R(1,3)	1.084	1.09	1.091	1.093	1.093	1.089	1.091	1.089	1.093
R(1,4)	1.084	1.09	1.091	1.093	1.093	1.089	1.091	1.089	1.093
R(1,5)	1.084	1.09	1.091	1.093	1.093	1.089	1.091	1.089	1.093
A(2,1,3)	109.5	109.5	109.5	109.5	109.5	109.5	109.5	109.5	109.5
A(2,1,4)	109.5	109.5	109.5	109.5	109.5	109.5	109.5	109.5	109.5
A(2,1,5)	109.5	109.5	109.5	109.5	109.5	109.5	109.5	109.5	109.5
A(3,1,4)	109.5	109.5	109.5	109.5	109.5	109.5	109.5	109.5	109.5
A(3,1,5)	109.5	109.5	109.5	109.5	109.5	109.5	109.5	109.5	109.5
A(4,1,5)	109.5	109.5	109.5	109.5	109.5	109.5	109.5	109.5	109.5

1-C, 2-H(1), 3-H(1), 4-H(1), 5-H(1)

Table V.A.17. Normal mode vibrational frequencies of 2-bromoethanol (T_t) at different level of theories (cm^{-1}).

HF	MP2	B3LYP	CBS-Q	G2	CBS-QB3	CCSD
135.5	91.6	115.1	138.3	137.7	117.8	128.6
230.1	147.2	175	241	240.6	201.6	224.4
239.4	227	218	272.8	250.3	217.8	234.8
359.1	347.6	329.3	362.4	359	328.4	341.3
726.9	723.6	668.4	739.2	725.5	666.3	708.5
844.6	806	788.9	842.1	846.7	796.3	793
1085.6	1039.6	1011.8	1091.2	1095.6	1011	1024.5
1109.5	1052.3	1013.7	1111.6	1112.8	1018.2	1048
1174.6	1086.4	1039.1	1186.8	1190	1051.4	1108.6
1312.9	1218.3	1199.3	1320.1	1324.3	1201.9	1214.5
1315.1	1249.2	1215.3	1326.9	1331.4	1220.4	1231.5
1387.7	1302.3	1268.1	1402.1	1403.6	1276.6	1299.4
1419.7	1325.1	1302.2	1424	1430.2	1303.6	1307.9
1574.5	1462.8	1437.9	1591.2	1598.6	1451.9	1468.5
1618.2	1507.2	1487.8	1631.4	1642.8	1491.1	1499.4
1652.5	1539.1	1522.7	1668.5	1682.4	1527.7	1531.8
3176.9	3071.4	3008	3193.6	3212.2	2996.6	3039
3216	3126.4	3046.8	3236.3	3251.9	3034	3084.2
3266.1	3147.2	3105.8	3291.3	3312.2	3106.8	3131.3
3335.3	3222.4	3172.5	3364.6	3385.1	3173.3	3202.6
4185.3	3902.6	3844.7	4121.9	4114.4	3842.3	3867.4

Table V.A.18. Normal mode vibrational frequencies of 2-chloroethanol (T$_t$) at different level of theories (cm^{-1}) .

HF	MP2	B3LYP	G3B3	CBS-Q	G2	CBS-QB3	G2MP2	G3MP2B3	G3	CCSD
141.3	48.3	119.2	124.5	142.1	142.2	122.1	142.2	124.5	143	133
240.9	151.8	182.1	203.7	270.1	259.4	207.5	258.6	203.7	256.7	232.1
270.1	253.9	247.6	248.8	275.2	271.9	247.2	271.9	248.8	272	251.6
417	403	384.3	386.3	416.6	418.4	383.7	418.5	386.3	418.3	395.3
818	822.1	752.5	761.9	822.3	825.9	750.6	826.4	761.9	824.8	798.8
859.6	826.7	803.3	810.8	858.6	866.1	808.9	866.4	810.8	866.4	808.4
1090.7	1055.5	1016.5	1024.1	1095.9	1100.1	1020	1100	1024.1	1100	1053.7
1158	1094.4	1048.1	1076.8	1163	1173.8	1057.8	1174.2	1076.8	1173.9	1069.8
1181.8	1096	1060.7	1080.4	1190.8	1196	1059.2	1195.8	1080.4	1195.2	1116.9
1319	1225.9	1203.2	1218.4	1325.1	1331.6	1206.1	1331.7	1218.4	1331.4	1219.1
1325.4	1255.3	1229.4	1245.6	1339.6	1345.5	1236.8	1345.2	1245.6	1345.2	1250.3
1419.6	1326.3	1302.8	1315	1423.4	1431	1303.6	1431	1315	1431	1309.3
1422.4	1342.5	1304	1322.5	1431.1	1442.7	1304.8	1442.9	1322.5	1442.5	1319.2
1581.9	1472.1	1443.4	1474.7	1598.4	1607.2	1456.5	1607.1	1474.7	1607	1477.3
1622.2	1511.7	1491.9	1521.3	1634.9	1645	1493.8	1645	1521.3	1645	1504.2
1653.4	1538.8	1523.5	1557.6	1669.8	1683.7	1528.6	1683.6	1557.6	1683.6	1534.6
3173.6	3071.2	3005.9	3013.7	3192.1	3209	2995.5	3208.7	3013.7	3208.7	3032.6
3211.7	3125	3044.4	3049.5	3234.6	3247.9	3032.7	3247.7	3049.5	3247.8	3076.7
3259.1	3144.4	3096.7	3118.4	3286.1	3301.6	3097.2	3300.7	3118.4	3301.1	3124.4
3324.1	3216.4	3159.1	3181.1	3356	3367.9	3159.3	3367	3181.1	3367.6	3192.3
4187.3	3903.2	3848.3	3763.3	4123.8	4115.6	3847.4	4115.8	3763.3	4116.7	3874.1

Table V.A.19. Normal mode vibrational frequencies of ethylbromide at different level of theories (cm^{-1}).

HF	MP2	B3LYP	CBS-Q	G2	CBS-QB3	CCSD
276.4	277.6	258.2	276.4	277.9	255.7	272.7
307.3	296.8	283.2	310.7	309.8	282.4	292.2
599.9	609.9	547	616.3	600	541.4	590.2
830.6	786.9	774.7	828.9	834.2	774.3	774.8
1039.4	1001.3	971.6	1042.9	1047.8	971.5	993.8
1130.4	1063.2	1033.4	1132	1133.5	1031.8	1044.9
1160	1106	1076.9	1163.8	1171.9	1077.1	1096.9
1370	1285.4	1263.3	1377.9	1385.8	1263.3	1271.4
1402.3	1323.1	1280.1	1409.8	1414.3	1274.5	1294.6
1537.2	1430.2	1413.4	1549.8	1564.8	1413.4	1417.1
1602.3	1499	1483.1	1622.4	1631.5	1483.9	1485.7
1610.3	1499.6	1485.7	1624.5	1637.3	1487	1489.4
1614.7	1513.1	1499.3	1632.6	1642	1501	1498.3
3166.7	3083.2	3024.4	3194.3	3208.8	3025.7	3064.6
3231.1	3138.5	3085.9	3264.2	3276.4	3088.5	3121.5
3255.4	3171.5	3100.2	3280.7	3302	3102.9	3149.4
3256.3	3186	3112.3	3289	3302.1	3115.7	3163.8
3317.8	3211.5	3158	3345.9	3367.7	3161.2	3191.4

Table V.A.20. Normal mode vibrational frequencies of ethylchloride at different level of theories (cm^{-1}).

HF	MP2	B3LYP	G3B3	CBS-Q	G2	CBS-QB3	G2MP2	G3MP2B3	G3	CCSD
279.4	279.8	262.1	266.3	277.8	278.4	258.1	278.3	266.3	278.9	274.6
355.4	340.8	330.3	331.5	355.2	357.8	329.1	357.7	331.5	357.8	336.9
711.6	727.1	649.8	657.3	717.8	719.2	647.9	718.8	657.3	718.5	697.5
845.9	803	791.4	797.6	845.5	853.5	791.5	853.3	797.6	853.7	790.3
1048.1	1016.6	979.1	989.8	1051.1	1057.6	978.3	1057.8	989.8	1057.6	1005.4
1170	1112.5	1079.4	1092.8	1173.7	1182.1	1076.3	1182.2	1092.8	1182.2	1085.8
1176.1	1115.1	1087.3	1099	1180.3	1190.3	1087.1	1190.2	1099	1190.3	1103.8
1380.6	1298.6	1274.5	1290.3	1387	1397.2	1274.3	1397.2	1290.3	1397.2	1280.3
1443	1369.1	1323	1341.1	1448.6	1462.8	1318	1462.7	1341.1	1462.7	1330
1538.6	1433.1	1415.5	1441	1550.8	1565.9	1416.8	1565.9	1441	1566	1419
1601.3	1496.6	1483.7	1514.4	1620.9	1630.3	1485	1630.3	1514.4	1630.3	1485.4
1612.8	1502.2	1490.3	1519.5	1628.7	1639.4	1491	1639.3	1519.5	1639.4	1495.2
1617.8	1513.3	1500.5	1531	1634.7	1644.9	1502.8	1644.9	1531	1645	1500.5
3169.2	3087.3	3029	3054.9	3197.5	3213.3	3031.6	3213.3	3054.9	3212.9	3067.7
3231	3132.6	3082.4	3104.6	3264	3276.4	3083.8	3276.6	3104.6	3276	3112.7
3248.7	3176.6	3097.5	3125.9	3276.9	3290.9	3100.4	3291.2	3125.9	3290.7	3153
3251.8	3182.5	3109.4	3139.6	3287.7	3298.2	3112.7	3298.6	3139.6	3297.9	3160.1
3304.8	3204.8	3145	3168.2	3336	3348.1	3146.9	3348.5	3168.2	3348	3182

Table V.A.21. Normal mode vibrational frequencies of ethylfluoride at different level of theories (cm^{-1}).

HF	MP2	B3LYP	G3B3	CBS-Q	G2	CBS-QB3	G2MP2	G3MP2B3	G3	CCSD
271.5	268.8	252.5	267.1	270.9	273.3	260.1	273.6	267.1	274	265.1
442.8	417.6	409.5	406.3	437.3	439.8	408.7	439.8	406.3	439.8	409.6
869.9	824.7	813.8	820.6	868	877.6	816.7	877.7	820.6	877.8	812.3
954.8	904.6	877.5	904.5	962.6	971.1	887.5	971	904.5	970.8	907
1152.2	1097.4	1044.8	1080.3	1160.9	1168.5	1056.9	1168.3	1080.3	1167.9	1110.3
1217.2	1143.6	1117.8	1145.6	1229.3	1240.3	1125.9	1239.8	1145.6	1239.3	1141.7
1290.7	1208	1181	1205.9	1301.2	1309.4	1188.5	1309.3	1205.9	1309.2	1200.2
1408.3	1323.6	1294.4	1311	1418.2	1421.7	1300.6	1421.7	1311	1421.6	1309.3
1516.6	1415.9	1397.3	1428	1531.9	1547	1404.1	1546.9	1428	1547	1402.4
1558.6	1453.2	1420.3	1456.1	1576.4	1587.6	1430.4	1587.5	1456.1	1587.5	1448.4
1596.5	1500.3	1480.6	1513.2	1617.1	1626.8	1479	1626.9	1513.2	1626.9	1480.7
1616.2	1518.8	1497.4	1529.2	1635.2	1645.2	1499.3	1645.2	1529.2	1645.2	1501.7
1644.4	1541.5	1515.7	1557.3	1668.1	1683.2	1521.8	1683.1	1557.3	1683.1	1527.3
3169.7	3091.6	3033	3043.3	3196.9	3212.9	3032.3	3212.7	3043.3	3212.5	3067.2
3206.3	3110.3	3041.9	3058.4	3227.1	3243.1	3035.4	3243.4	3058.4	3243.2	3074.2
3234.1	3166.2	3081.7	3081.7	3263.7	3274.9	3073.2	3275.3	3081.7	3275.2	3119.3
3236	3182.8	3098.6	3128.1	3270.7	3280.6	3100.9	3280.4	3128.1	3280.1	3157.7
3262.5	3199	3116.5	3138.6	3290.2	3301	3114.5	3301.4	3138.6	3301.3	3166.6

Table V.A.22. Normal mode vibrational frequencies of ethane at different level of theories (cm^{-1})

HF	MP2	B3LYP	G3B3	CBS-Q	G2	CBS-QB3	G2MP2	G3MP2B3	G3	CCSD
328.4	329	308.3	314.2	326.3	325.2	306.3	326	314.2	325.4	333.9
880.6	833	826.4	831.6	880.7	889.2	827.1	889.5	831.6	889.3	825.2
880.6	833.5	827.5	832.8	880.7	889.3	827.1	889.5	832.8	889.3	825.2
1051.7	1037.2	997	1009.7	1057.2	1061.5	996.3	1062.3	1009.7	1061.6	1032.2
1319.6	1238.2	1217	1234.9	1327.2	1337.4	1218.7	1337.7	1234.9	1337.5	1226.9
1319.6	1238.3	1217.8	1235.7	1327.2	1337.4	1218.7	1337.7	1235.7	1337.5	1226.9
1517	1419.5	1407.7	1432.2	1531.6	1547.8	1408.8	1547.8	1432.2	1547.8	1406
1549.8	1446	1423.3	1453.7	1566.9	1579.9	1424.7	1580	1453.7	1579.9	1438.6
1615.1	1520.1	1503.2	1531.8	1635	1644.2	1504.9	1644.2	1531.8	1644.2	1501.3
1615.1	1520.6	1503.5	1532.2	1635	1644.2	1504.9	1644.2	1532.2	1644.2	1501.3
1618.5	1520.9	1505.3	1537.5	1640.5	1650.2	1507.5	1650.2	1537.5	1650.2	1504.3
1618.5	1521.2	1505.8	1537.8	1640.5	1650.2	1507.5	1650.2	1537.8	1650.2	1504.3
3155	3083.3	3023.7	3047.5	3183.6	3199.9	3026.2	3199.7	3047.5	3199.7	3052.3
3162.5	3085.2	3023.9	3048.3	3190.2	3206	3026.8	3205.8	3048.3	3205.9	3058.1
3201.7	3157	3069.1	3098.9	3238.8	3249.4	3072.5	3249.2	3098.9	3249.3	3123.2
3201.7	3159.8	3069.2	3099	3238.8	3249.4	3072.5	3249.2	3099	3249.3	3123.3
3228.1	3178.6	3094	3123.3	3264.2	3274.5	3097.8	3274.4	3123.3	3274.4	3144.7
3228.1	3181.8	3094.1	3123.4	3264.2	3274.5	3097.8	3274.4	3123.4	3274.4	3144.8

Table V.A.23. Normal mode vibrational frequencies of ethanol at different level of theories (cm^{-1})

HF	MP2	B3LYP	G3B3	CBS-Q	G2	CBS-QB3	G2MP2	G3MP2B3	G3	CCSD
261.3	154.6	230.8	251.8	268.7	269.9	247.9	270.6	251.8	270.9	256.1
295.2	272.3	270.9	306.3	327.4	315.1	284.3	317.2	306.3	317	302.5
447	422.4	416.2	417.1	444.7	447.7	416.9	447.7	417.1	447.8	416.5
877.5	829.5	820.6	830.2	878.7	886.9	826.1	886.9	830.2	887.1	823
967	921.3	895.7	911.3	973	978	902.4	978	911.3	978	921.6
1122.8	1066.5	1031.3	1042.7	1129.3	1132.7	1034.6	1132.9	1042.7	1132.8	1064.1
1198.5	1126.7	1094.3	1123.8	1209.1	1217.2	1108	1217.2	1123.8	1217	1142.7
1282.5	1198.4	1175.4	1194.6	1291.2	1298.7	1180.1	1298.7	1194.6	1298.8	1192.2
1369.8	1284.2	1261.4	1292.1	1393.2	1395.2	1277.7	1395.5	1292.1	1395.5	1301.8
1412.7	1321.7	1298.3	1310.2	1418.5	1423.7	1301.5	1423.9	1310.2	1423.8	1307.1
1521	1415.4	1402.9	1427.7	1534.2	1549.5	1405.6	1549.6	1427.7	1549.6	1404.7
1585	1474.8	1445.6	1481.5	1606.5	1613.2	1460.3	1613.3	1481.5	1613.3	1481.4
1597.4	1495.7	1480.8	1513.7	1618.9	1628.8	1480.4	1628.8	1513.7	1628.8	1485.9
1616.6	1520.2	1499.5	1531.8	1636.3	1645.8	1503.3	1645.8	1531.8	1645.9	1503.8
1652.9	1547.8	1525.3	1561.2	1672.5	1685.9	1531.4	1685.8	1561.2	1685.9	1535.5
3139.7	3052.5	2978.9	2983.3	3158.2	3175.3	2965.9	3175.4	2983.3	3175	3008.3
3164	3089.7	3004.8	3006.8	3186.7	3200.2	2989.7	3200.5	3006.8	3200.1	3041.9
3168.3	3097	3033.4	3058.2	3196.9	3212.1	3035.9	3211.9	3058.2	3211.7	3068.1
3230.5	3181.4	3099.4	3129	3267.4	3276.7	3103.9	3276.3	3129	3276.2	3155.4
3242.3	3189.5	3106.4	3134.2	3279	3288.5	3107.1	3288.6	3134.2	3288.3	3159.6
4188.3	3902.3	3843.8	3750.1	4123	4115.7	3842.3	4114.3	3750.1	4114.6	3864.9

Table V.A.24. Normal mode vibrational frequencies of 2-fluoroethanol (T$_t$) at different level of theories (cm^{-1})

HF	MP2	B3LYP	G3B3	CBS-Q	G2	CBS-QB3	G2MP2	G3MP2	G3	CCSD
140.7	77.3	108.8	133.5	149.2	150.1	124.2	150.6	133.5	151.3	131.5
231.8	160.1	191.4	240.5	281	258.2	224	262.2	240.5	262.8	249.9
317.1	294.1	289.6	286.1	311.9	313.4	287	313.6	286.1	313.9	285.1
505	476.7	464.3	470.6	505.3	507.2	467.6	507.4	470.6	507.1	475.7
884.8	840.9	826.5	834	881.9	890.8	837.2	891.1	834	891.1	831.6
1094.1	1046.8	1009.3	1029.8	1101.8	1108.3	1021.6	1108.7	1029.8	1108.7	1050.9
1163	1094.7	1047	1090.8	1176.2	1187.7	1062.1	1187.3	1090.8	1186.4	1116.5
1190.9	1104.1	1062	1094.7	1200.8	1205.1	1074	1205.1	1094.7	1204.3	1126.7
1267.7	1186.2	1160	1184.3	1278.1	1285.4	1169.2	1285.5	1184.3	1285.3	1182.2
1334.9	1251.6	1226.5	1240.8	1352.8	1355.3	1230.1	1355.3	1240.8	1355.1	1240.4
1345.3	1267.5	1235.6	1260.6	1354.1	1355.9	1249.7	1356.3	1260.6	1356.2	1267.4
1413.4	1326.4	1300.6	1313.9	1418.7	1425	1302.4	1425	1313.9	1425	1305.8
1502.5	1404.5	1379.1	1410.5	1519.2	1528.1	1392.8	1528.2	1410.5	1528.1	1400.9
1607.9	1495.9	1462.1	1498.4	1627.2	1634.7	1478.3	1634.8	1498.5	1634.7	1504.2
1645.1	1540.3	1512	1551.5	1664.3	1679.8	1518.4	1679.8	1551.5	1679.8	1526
1656.5	1549.2	1527.4	1564.6	1674.6	1688.8	1533.2	1688.8	1564.6	1688.7	1539.4
3165.9	3074	3000.3	3003.7	3182.5	3199.9	2987.4	3199.7	3003.7	3199.7	3028.6
3200.6	3125.7	3036.8	3036.1	3220.5	3234.5	3021.2	3234.4	3036.1	3234.4	3070.3
3227.5	3127.9	3059	3063.1	3249.2	3264.8	3050.4	3264.5	3063.1	3264.5	3087.7
3283.7	3196.5	3115.3	3115	3309.5	3320.5	3105.7	3320.3	3115	3320.3	3148.3
4197.7	3916.4	3856	3766	4133.5	4127.1	3855.7	4125.7	3766	4125.2	3879.1

Table V.A.25. Normal mode vibrational frequencies of methylfluoride at different level of theories (cm^{-1})

HF	MP2	B3LYP	G3B3	CBS-Q	G2	CBS-QB3	G2MP2	G3MP2B3	CCSD
1156.8	1078.3	1033.6	1092.5	1176.3	1187.3	1059.1	1186.4	1092.5	1105.6
1295.6	1216.5	1184.2	1205.5	1309.7	1312.4	1190.3	1312.1	1205.5	1206
1295.6	1216.5	1184.2	1205.5	1309.7	1312.4	1190.3	1312.1	1205.5	1206
1611.1	1517.2	1480	1523.6	1638.8	1652	1484.7	1651.8	1523.6	1498.1
1614.1	1520.2	1488.5	1523.6	1638.8	1653.3	1484.7	1653.3	1523.6	1498.1
1614.1	1520.2	1488.5	1532.1	1640.1	1653.3	1498.5	1653.3	1532.1	1505.7
3193	3097.9	3029	3037	3211.6	3232.1	3022.7	3232.4	3037	3062.1
3276.4	3201.9	3113	3110.5	3299.9	3312.3	3100.6	3312.6	3110.5	3152.4
3276.4	3201.9	3113	3110.6	3299.9	3312.3	3100.6	3312.6	3110.6	3152.4

Table V.A.26. Normal mode vibrational frequencies of methane at different level of theories (cm^{-1})

HF	MP2	B3LYP	G3B3	CBS-Q	G2	CBS-QB3	G2MP2	G3MP2B3
1451.9	1362.5	1339.7	1373.7	1471.8	1487.9	1341.7	1486.8	1373.7
1451.9	1362.5	1339.7	1373.7	1471.8	1487.9	1341.7	1486.8	1373.7
1451.9	1362.5	1339.7	1373.7	1471.8	1487.9	1341.7	1486.8	1373.7
1666.4	1570.6	1558.3	1594	1694.5	1702.6	1561.2	1702.2	1594
1666.4	1570.6	1558.3	1594	1694.5	1702.6	1561.2	1702.2	1594
3153.7	3076.5	3026.4	3052.9	3180.7	3197.2	3026.4	3202.2	3052.9
3256.3	3214.1	3132.2	3163.2	3294	3301.7	3132.6	3307.2	3163.2
3256.3	3214.1	3132.2	3163.2	3294	3301.7	3132.6	3307.2	3163.2
3256.3	3214.1	3132.2	3163.2	3294	3301.7	3132.6	3307.2	3163.2

Table V.A.27. Molecular energies and enthalpies of different molecules at HF level of theory with 6-311++G** basis set (All values are in Hartree).

Molecule	Sum of electronic and zero-point Energies	Sum of electronic and thermal Enthalpies
FC_2H_4OH	-252.93209	-252.92635
ClC_2H_4OH	-612.980558	-612.974628
BrC_2H_4OH	-2725.843071	-2725.836974
C_2H_5OH	-154.04517	-154.040046
C_2H_5Cl	-538.109937	-538.105089
C_2H_5Br	-2650.97235	-2650.967379
C_2H_5F	-178.062445	-178.057765
C_2H_6	-79.173357	-79.169007
CH_3F	-139.041452	-139.037623
CH_4	-40.162194	-40.158394
C	-37.68957	-37.687209
O	-74.807396	-74.805036
H	-0.499818	-0.497457
Cl	-459.474232	-459.471871
Br	-2572.352675	-2572.350315
F	-99.399893	-99.397532

Table V.A.28. Molecular energies and enthalpies of different molecules at MP2 level of theory with 6-311++G** basis set (All values are in Hartree).

Molecule	Sum of electronic and zero-point Energies	Sum of electronic and thermal Enthalpies
FC_2H_4OH	-253.720476	-253.714402
ClC_2H_4OH	-613.735372	-613.729043
BrC_2H_4OH	-2726.929474	-2726.923081
C_2H_5OH	-154.621442	-154.61605
C_2H_5Cl	-538.648583	-538.643686
C_2H_5Br	-2651.842576	-2651.837557
C_2H_5F	-178.636144	-178.63139
C_2H_6	-79.533628	-79.529236
CH_3F	-139.445159	-139.44131
CH_4	-40.353066	-40.349256
C	-37.76328	-37.76092
O	-74.940067	-74.937707
H	-0.502257	-0.499897
Cl	-459.635377	-459.633017
Br	-2572.846764	-2572.844403
F	-99.559588	-99.557228

Table V.A.29. Molecular energies and enthalpies of different molecules at B3LYP level of theory with 6-311++G** basis set (All values are in Hartree)

Molecule	Sum of electronic and zero-point Energies	Sum of electronic and thermal Enthalpies
FC_2H_4OH	-254.285645	-254.279641
ClC_2H_4OH	-614.645547	-614.639333
BrC_2H_4OH	-2728.567889	-2728.561505
C_2H_5OH	-155.015606	-155.010307
C_2H_5Cl	-539.414259	-539.409276
C_2H_5Br	-2653.336374	-2653.331255
C_2H_5F	-179.05578	-179.050974
C_2H_6	-79.782267	-79.777836
CH_3F	-139.752384	-139.748524
CH_4	-40.489405	-40.485591
C	-37.857267	-37.854907
O	-75.089879	-75.087519
H	-0.502257	-0.499897
Cl	-460.166883	-460.164522
Br	-2574.105735	-2574.103374
F	-99.760581	-99.75822

Table V.A.30. Molecular energies and enthalpies of different molecules at G2 level of theory (All values are in Hartree)

Molecule(G2)	Sum of electronic and zero-point Energies G2(0 K)	Sum of electronic and thermal Enthalpies (G2 Enthalpy)
FC_2H_4OH	-253.915297	-253.909363
ClC_2H_4OH	-613.914564	-613.908399
BrC_2H_4OH	-2726.750719	-2726.74438
C_2H_5OH	-154.764468	-154.759159
C_2H_5Cl	-538.78237	-538.777326
C_2H_5Br	-2651.618165	-2651.612988
C_2H_5F	-178.784911	-178.78006
C_2H_6	-79.630883	-79.626397
CH_3F	-139.554216	-139.550357
CH_4	-40.410891	-40.407075
C	-37.784301	-37.78194
O	-74.98203	-74.979669
H	-0.5	-0.497639
Cl	-459.676627	-459.674267
Br	-2572.530577	-2572.528216
F	-99.632814	-99.630453

Table V.A.31. Molecular energies and enthalpies of different molecules at G2MP2 level of theory (All values are in Hartree)

Molecule	Sum of electronic and zero-point Energies G2MP2(0 K)	Sum of electronic and thermal Enthalpies (G2MP2 Enthalpy)
FC_2H_4OH	-253.908508	-253.90258
ClC_2H_4OH	-613.902379	-613.896214
BrC_2H_4OH	-	-
C_2H_5OH	-154.760512	-154.755207
C_2H_5Cl	-538.772225	-538.767181
C_2H_5Br	-	-
C_2H_5F	-178.780131	-178.77528
C_2H_6	-79.628927	-79.624442
CH_3F	-139.550264	-139.546404
CH_4	-40.409629	-40.405813
C	-37.783887	-37.781527
O	-74.978678	-74.976317
H	-0.5	-0.497639
Cl	-459.666717	-459.664356
Br	-	-
F	-99.628941	-99.62658

Table V.A.32. Molecular energies and enthalpies of different molecules at G3 level of theory (All values are in Hartree)

Molecule(G3)	Sum of electronic and zero-point Energies G3(0 K)	Sum of electronic and thermal Enthalpies (G3 Enthalpy)
FC_2H_4OH	-254.10444	-254.09851
ClC_2H_4OH	-614.36722	-614.36105
BrC_2H_4OH	-	-
C_2H_5OH	-154.90475	-154.89944
C_2H_5Cl	-539.18719	-539.18214
C_2H_5Br	-	-
C_2H_5F	-178.92623	-178.92138
C_2H_6	-79.723397	-79.718911
CH_3F	-	-
CH_4	-	-
C	-37.827717	-37.825356
O	-75.030991	-75.02863
H	-0.501003	-0.498642
Cl	-459.99096	-459.9886
Br	-	-
F	-99.684205	-99.681844

Table V.A.33. Molecular energies and enthalpies of different molecules at G3B3 level of theory (All values are in Hartree)

Molecule(G3B3)	Sum of electronic and zero-point Energies G3B3(0 K)	Sum of electronic and thermal Enthalpies (G3B3 Enthalpy)
FC_2H_4OH	-254.10942	-254.10346
ClC_2H_4OH	-614.37202	-614.36577
BrC_2H_4OH	-	-
C_2H_5OH	-154.90808	-154.90278
C_2H_5Cl	-539.18999	-539.18495
C_2H_5Br	-	-
C_2H_5F	-178.92934	-178.9245
C_2H_6	-79.724862	-79.720395
CH_3F	-139.65207	-139.6482
CH_4	-40.458272	-40.454456
C	-37.828452	-37.826091
O	-75.032293	-75.029932
H	-0.501087	-0.498726
Cl	-459.99274	-459.99038
Br	-	-
F	-99.68599	-99.683629

Table V.A.34. Molecular energies and enthalpies of different molecules at G3MP2B3 level of theory (All values are in Hartree)

Molecule	Sum of electronic and zero-point Energies G3MP2(0 K)	Sum of electronic and thermal Enthalpies (G3MP2 Enthalpy)
FC_2H_4OH	-253.956285	-253.950326
ClC_2H_4OH	-613.959393	-613.953141
BrC_2H_4OH	-	-
C_2H_5OH	-154.798241	-154.792947
C_2H_5Cl	-538.817927	-538.812885
C_2H_5Br	-	-
C_2H_5F	-178.816693	-178.811854
C_2H_6	-79.65549	-79.651023
CH_3F	-139.575057	-139.571193
CH_4	-40.424357	-40.42054
C	-37.790785	-37.788425
O	-74.992064	-74.989704
H	-0.502141	-0.49978
Cl	-459.690073	-459.687713
Br	-	-
F	-99.64377	-99.64141

Table V.A.35. Molecular energies and enthalpies of different molecules at CBS-Q level of theory (All values are in Hartree)

Molecule	Sum of electronic and zero-point Energies CBS-Q (0 K)	Sum of electronic and thermal Enthalpies (CBS-Q Enthalpy)
FC_2H_4OH	-253.92829	-253.92245
ClC_2H_4OH	-613.92663	-613.92055
BrC_2H_4OH	-2727.057	-2727.0508
C_2H_5OH	-154.7682	-154.76296
C_2H_5Cl	-538.78946	-538.78446
C_2H_5Br	-2651.9163	-2651.9111
C_2H_5F	-178.79296	-178.78815
C_2H_6	-79.629747	-79.625292
CH_3F	-139.56194	-139.55809
CH_4	-40.409558	-40.405746
C	-37.785144	-37.782784
O	-74.987059	-74.984699
H	-0.499818	-0.497457
Cl	-459.68286	-459.6805
Br	-2572.8212	-2572.8188
F	-99.642202	-99.639842

Table V.A.36. Molecular energies and enthalpies of different molecules at CBS-QB3 level of theory (All values are in Hartree)

Molecule	Sum of electronic and zero-point Energies CBS-QB3 (0 K)($E_0 + E_{ZPE}$)	Sum of electronic and thermal Enthalpies (CBS-QB3 Enthalpy) ($E_0 + H_{CORR}$)
FC_2H_4OH	-253.93137	-253.925433
ClC_2H_4OH	-613.92914	-613.922952
BrC_2H_4OH	-2727.0549	-2727.048504
C_2H_5OH	-154.77016	-154.764885
C_2H_5Cl	-538.79086	-538.785844
C_2H_5Br	-2651.917	-2651.911897
C_2H_5F	-178.795	-178.79019
C_2H_6	-79.630573	-79.626128
CH_3F	-139.56384	-139.55998
CH_4	-40.409999	-40.406184
C	-37.785377	-37.783017
O	-74.987629	-74.985269
H	-0.499818	-0.497457
Cl	-459.68361	-459.681244
Br	-2572.824	-2572.821601
F	-99.643075	-99.640715

Table V.A.37. Molecular energies and enthalpies of different molecules at CCSD level of theory (All values are in Hartree)

Molecule (CCSD/cc-pVDZ)	Sum of electronic and zero-point Energies	Sum of electronic and thermal Enthalpies
FC_2H_4OH	-253.56125	-253.55541
ClC_2H_4OH	-613.59303	-613.58697
BrC_2H_4OH	-2726.4666	-2726.4604
C_2H_5OH	-154.53051	-154.52531
C_2H_5Cl	-538.56289	-538.55796
C_2H_5Br	-2651.4362	-2651.4311
C_2H_5F	-178.53224	-178.52747
C_2H_6	-79.499632	-79.495237
CH_3F	-139.36138	-139.35754
CH_4	-	-
C	-	-
O	-	-
H	-	-
Cl	-	-
Br	-	-
F	-	-

Table V.A.38. Data for heat capacity, entropy and heat content of 2-fluoroethanol evaluated at the interval of 100K in the temperature range of 200-4000K.

	2-Fluoroethanol		
T(K)	Cp(cal/mol/K)	S(cal/mol/K)	ddH(kcal/mol)
100.00	11.336	55.805	0.930
200.00	14.276	64.618	2.218
298.15	17.474	70.882	3.767
300.00	17.543	70.989	3.800
400.00	21.374	76.558	5.746
500.00	24.990	81.726	8.066
600.00	28.090	86.563	10.724
700.00	30.698	91.097	13.669
800.00	32.902	95.342	16.852
900.00	34.785	99.328	20.239
1000.00	36.405	103.081	23.800
1100.00	37.811	106.618	27.512
1200.00	39.030	109.962	31.355
1300.00	40.093	113.129	35.313
1400.00	41.023	116.133	39.369
1500.00	41.838	118.994	43.513
1600.00	42.553	121.716	47.734
1700.00	43.181	124.314	52.022
1800.00	43.738	126.800	56.367
1900.00	44.230	129.178	60.767
2000.00	44.668	131.458	65.213
2100.00	45.057	133.647	69.699
2200.00	45.406	135.750	74.223
2300.00	45.719	137.777	78.779
2400.00	46.001	139.728	83.365
2500.00	46.255	141.611	87.978
2600.00	46.484	143.430	92.615
2700.00	46.692	145.189	97.275
2800.00	46.881	146.891	101.953
2900.00	47.053	148.537	106.649
3000.00	47.208	150.136	111.362
3100.00	47.352	151.687	116.090
3200.00	47.486	153.191	120.834
3300.00	47.605	154.656	125.588
3400.00	47.717	156.078	130.354
3500.00	47.820	157.462	135.131
3600.00	47.916	158.812	139.919
3700.00	48.004	160.124	144.713
3800.00	48.088	161.405	149.520
3900.00	48.164	162.655	154.331
4000.00	48.234	163.877	159.152

Table V.A.39. Data for heat capacity, entropy and heat content of 2-chloroethanol evaluated at the interval of 100K in the temperature range of 200-4000K.

2-Chloroethanol			
T(K)	Cp(cal/mol/K)	S(cal/mol/K)	ddH(kcal/mol)
100.00	11.678	57.505	0.935
200.00	14.919	66.659	2.275
298.15	18.317	73.224	3.898
300.00	18.387	73.337	3.934
400.00	22.244	79.156	5.966
500.00	25.777	84.508	8.370
600.00	28.762	89.479	11.102
700.00	31.257	94.106	14.106
800.00	33.363	98.423	17.340
900.00	35.165	102.457	20.770
1000.00	36.721	106.245	24.364
1100.00	38.074	109.811	28.107
1200.00	39.252	113.174	31.974
1300.00	40.282	116.358	35.951
1400.00	41.185	119.379	40.026
1500.00	41.977	122.247	44.185
1600.00	42.674	124.978	48.418
1700.00	43.289	127.584	52.717
1800.00	43.834	130.074	57.075
1900.00	44.314	132.457	61.482
2000.00	44.744	134.742	65.935
2100.00	45.127	136.934	70.430
2200.00	45.468	139.042	74.959
2300.00	45.774	141.071	79.522
2400.00	46.052	143.023	84.113
2500.00	46.300	144.909	88.731
2600.00	46.527	146.730	93.372
2700.00	46.730	148.489	98.035
2800.00	46.917	150.191	102.717
2900.00	47.087	151.840	107.419
3000.00	47.239	153.439	112.134
3100.00	47.383	154.993	116.867
3200.00	47.512	156.499	121.611
3300.00	47.631	157.961	126.370
3400.00	47.741	159.386	131.138
3500.00	47.844	160.772	135.918
3600.00	47.937	162.120	140.705
3700.00	48.026	163.435	145.504
3800.00	48.107	164.716	150.311
3900.00	48.181	165.968	155.124
4000.00	48.250	167.187	159.947

Table V.A.40. Data for heat capacity, entropy and heat content of 2-bromoethanol evaluated at the interval of 100K in the temperature range of 200-4000K.

2-Bromoethanol			
T(K)	Cp(cal/mol/K)	S(cal/mol/K)	ddH(kcal/mol)
100.00	12.082	59.859	0.954
200.00	15.375	69.319	2.335
298.15	18.767	76.066	4.006
300.00	18.836	76.181	4.042
400.00	22.646	82.122	6.116
500.00	26.119	87.560	8.559
600.00	29.044	92.588	11.319
700.00	31.487	97.254	14.350
800.00	33.552	101.597	17.605
900.00	35.320	105.655	21.052
1000.00	36.850	109.455	24.661
1100.00	38.181	113.033	28.415
1200.00	39.345	116.405	32.292
1300.00	40.361	119.596	36.279
1400.00	41.252	122.620	40.361
1500.00	42.036	125.495	44.524
1600.00	42.727	128.229	48.764
1700.00	43.334	130.839	53.069
1800.00	43.874	133.332	57.428
1900.00	44.350	135.715	61.840
2000.00	44.775	138.002	66.298
2100.00	45.155	140.196	70.793
2200.00	45.495	142.304	75.327
2300.00	45.801	144.333	79.892
2400.00	46.073	146.288	84.486
2500.00	46.322	148.174	89.106
2600.00	46.544	149.995	93.750
2700.00	46.747	151.757	98.415
2800.00	46.934	153.458	103.098
2900.00	47.101	155.110	107.801
3000.00	47.254	156.709	112.519
3100.00	47.395	158.260	117.251
3200.00	47.524	159.768	121.996
3300.00	47.643	161.231	126.754
3400.00	47.753	162.655	131.525
3500.00	47.854	164.042	136.305
3600.00	47.947	165.392	141.095
3700.00	48.035	166.707	145.894
3800.00	48.114	167.988	150.703
3900.00	48.191	169.238	155.519
4000.00	48.260	170.459	160.339

Table V.A.41. Fourteen thermodynamic coefficients of haloethanols in the chemkin format evaluated in the temperature range of 200-4000K linked by the common temperature of 1500K.

```
FC2H4OH                        O  1H  5C  2F  1G  200.000 4000.000 1500.00       1
 1.00435221E+01   1.23183625E-02  -4.24388361E-06   6.75289970E-10   -4.04313161E-14     2
 4.56644387E+04  -2.79636175E+01   2.34302225E+00   2.48741744E-02   -8.82084111E-06     3
-8.36664176E-10   8.02587288E-13   4.88722097E+04   1.53011971E+01                       4


ClC2H4OH                       O  1H  5C  2Cl 1G  200.000 4000.000 1500.00       1
 9.78995309E+00   1.29870370E-02  -4.71039402E-06   8.03054375E-10  -5.26610986E-14    2
 2.84364086E+04  -2.50838130E+01   2.42097860E+00   2.70120214E-02  -1.31097643E-05    3
 2.03583485E-09   1.58587651E-13   3.12799826E+04   1.55646965E+01                     4


BrC2H4OH                       O  1H  5C  2Br 1G  200.000 4000.000 1500.00       1
 9.81528220E+00   1.30482056E-02  -4.77513494E-06   8.23308347E-10   -5.47193158E-14     2
 2.30408663E+04  -2.36753095E+01   2.67638420E+00   2.70280049E-02   -1.36976723E-05     3
 2.54120850E-09   3.35759923E-14   2.57514777E+04   1.55567939E+01                       4
```

352

Chapter VI

Shock Tube Ignition Delay Studies of JP-10 &

JP-10+Triethyl Amine

VI.1. Abstract

The ignition measurement of Jet Propellent-10 (JP-10) was performed behind reflected shock waves in the temperature range of 1300-1675 K and the pressure range of 15-20 atm. However, the ignition of JP-10 with Triethyl amine (TEA) was investigated in the temperature range of 1275-1650 K and the pressure range of 15-20 atm. The ignition delay time was measured from the increase of pressure and CH emission in the JP-10-O_2-Ar system. Present investigation has shown that the 10% addition of TEA to JP-10 brings about significant reduction in the ignition delay times attributed to the reduction in the activation energy by almost 6 kcal/mol. The C-C bond breaking energy in JP-10 and barriers for H abstraction from JP-10 by H have also been estimated to explain the experimental results.

VI.2. Introduction

JP-10, also known as exo-tetrahydrodicyclopentadiene ($C_{10}H_{16}$), has been of great interest in the area of combustion chemistry. Due to its strained structure, JP-10 has high volumetric energy density compared to other petroleum based fuels that makes it suitable for being used as a propellant in missiles, supersonic-combustion ramjets, etc. The other advantage that JP-10 has is its being a single component fuel, thus, making detailed combustion and pyrolysis study simpler. Many studies have been performed in the past to investigate the combustion behavior of JP-10[1-7] but the detailed mechanism followed during the reaction is still not well established. These studies include shock tube

experiments[1-7] flow reactors with gas chromatography[8-10] and micro-flow tube with mass spectroscopy[11].

Shock tube experiments on JP-10 ignition are reported here. These studies were done using online measurement of the CH emission near the end of the shock tube. Ignition delay studies on such fuels are suitable for developing chemical kinetic models that gives better insight in to the decomposition mechanisms. Accurate ignition time measurements are also needed to validate computation fluid dynamics codes used for designing and modeling supersonics. Recently, focus has been on measurements of individual species concentration time histories[1-14] that improve the understanding of the details of reaction mechanisms. Shock tubes used in combination with radiative emission or laser absorption methods are an excellent way to generate these.

The major disadvantage of JP-10 and similar fuels is their slow combustion kinetics, i.e., the ignition delay of JP-10 combustion is large. To reduce the ignition delay times of JP-10, combustion should take place at a very high temperature or the initial concentration of JP-10 in JP-10 – oxygen mixture should be high. The ignition may also be reduced through additives having relatively lower first step barrier than JP-10. The knowledge of first step leading to decomposition of JP-10 may help in deciding good additives. The use of additives in fuels is not new. Jee et al.[15] have shown that addition of CH_3Br promotes the ignition of CH_4 significantly. Shin et al. [16] found that CH_3Cl reduces the ignition delay of CH_4 but not significantly as CH_3Br. Mikolaitis et al.[5] have studied JP-10 ignition delay without and with additives like methylated PCU alkene dimer, nitronorbornane, dinitronorbornane and ethylhexyl nitrate. They found that none of the

additives lowered ignition delays of JP-10 to any appreciable degree in the temperature and pressure range studied.

Along with shock tube ignition experiments on pure JP-10, experiments on JP-10 with an additive, Triethylamie (TEA) is reported here. TEA has been earlier used as an initiator for cracking of heptane[17]. No reports are available on ignition experiments of JP-10 with TEA as an additive to the best of our knowledge.

VI.3. Experimental method

Thermal decomposition studies using single pulse shock tube for molecules of interest to atmospheric chemistry have been studied previously[18, 19] and toxic molecules are currently under study. The schematic diagram and details of shock tube facility used for the present combustion experiments on JP-10 is given in the chapter II. Details of the experimental set up and its calibration technique is available elsewhere[20] also. A typical experimental signal is shown in Figure VI.1. The figure shows the CH emission signal as well as pressure signal obtained from one pressure transducers.
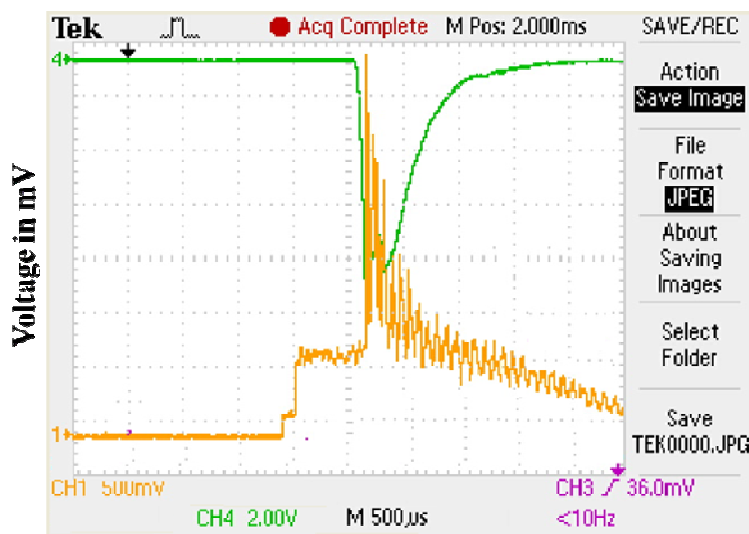
Figure VI.1. A typical signal obtained in the digital oscilloscope showing CH emission (upper trace) and pressure rise (bottom two traces) for JP-10 ignition. y-axis is in *mV* and x-axis is in *μs*.

For every experiment, the shock tube was pumped down to a pressure close to 10^{-5} torr. The ball valve near the end flange is kept closed initially. A mixture of ppm level concentration of JP-10 and oxygen (equivalent ratio $\phi = 1$) diluted in argon was prepared barometrically and has been used for all experiments. The test sample was pre-mixed uniformly in a separate stainless steel chamber for a period of one hour using a circulation diaphragm (oil-less) pump and was loaded in the driven section. The segment from ball valve to the end of driven section (where the sample is loaded) is maintained at a pressure of about 5 torr less than the other segment to avoid back mixing of the sample. In all experiments, the driven section pressure was varied between 300 to 450 Torr. The ball valve is opened just before rupturing the diaphragm and is closed immediately after the experiment. Experiments with TEA mixed with JP-10 were also carried out following similar procedure. 10 % by volume of TEA was mixed with JP-10 and the equivalence

ratio of 1 was maintained in all experiments. Experiments on pure TEA were also done maintaining equivalence ratio of 1.

VI.4. Results and discussion

VI.4.A. Pure JP-10

Experiments with pure JP-10 – Oxygen mixture were carried out to compare with previous reports and also for comparison with JP-10 ignition delay with TEA as an additive. The ignition delay time referred here is the measure of time lag between pressure rise from the arrival of reflected shock to the onset of ignition (that instigates further rise in the pressure signal). Ignition delay is also measured from CH emission signal. The difference of the arrival of reflected shock and CH emission is taken as the ignition delay at that point. This correlates well with the pressure ignition delay data. Experimental data on ignition delay studies of pure JP-10 is given in Table VI.1.

Table VI.1. Experimental data for the ignition of pure JP-10.

Run no.	T_5 (K)	Ignition delay (τ) (μs)
1	1323	610
2	1337	560
3	1382	404
4	1397	340
5	1367	448
6	1397	328
7	1381	360
8	1308	668
9	1513	144
10	1321	950
11	1707	52
12	1428	560

13	1460	548
14	1350	670
15	1443	540
16	1336	780
17	1566	144
18	1461	356
19	1294	1010
20	1686	80
21	1513	200
22	1413	356
23	1686	44
24	1708	28
25	1567	156
26	1586	80
27	1343	600
28	1390	468
29	1530	136
30	1350	592
31	1605	52
32	1567	84
33	1427	324
34	1460	220

During the experiments, it was observed that the ignition delay depends on temperature behind reflected shock, pressure behind reflected shock and the concentration of the sample loaded. It is observed that an increase in value of any of these parameters leads to a decrease in ignition delay of JP-10. Pure JP-10 experiments were done in the temperature (T_5) range 1300 to 1675 K. The corresponding pressure (P_5) range was approximately 15 - 20 atm. An ignition delay (τ) in the range of 50 - 900 μs was present for these experiments. The ln (τ) against 1000/T is plotted in Figure VI.2. The effective Arrhenius parameters for the overall ignition experiment are obtained by a linear fit to the experimental data (see reference 20 for details).
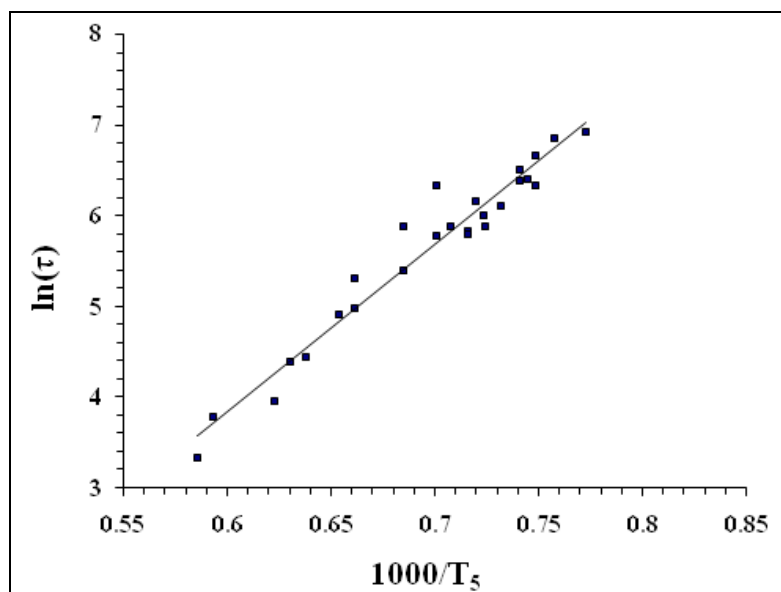
Figure VI.2. Arrhenius plot of a set of experimental results for ignition delay of JP-10. τ is in μs and T_5 is in K.

From the current data, the Arrhenius expression takes the form $\tau=10^{-16.61\pm0.32}$ exp (36.92±1.8/RT). The activation energy is given in kcal/mol. This correlation is obtained from Figure VI.2. Activation energy from Davidson et al.[1] data comes to be 54.00 kcal/mol. These experiments were performed covering a temperature range of 1200 to 1700 K and pressure range of 1 to 9 atm. Colket and Spadaccini[3] have performed JP-10 ignition experiments in a temperature range of 1100 to 1500 K and pressure of 3 to 8 atm. The activation energy comes to be 46.83 kcal/mol. Olchansky and Burcat[4] have done similar experiments and the activation comes to be 34.80 kcal/mol. The temperatures for the experiments were between 1150 and 1700 K while the pressure was maintained between 1.75 and 9.28 atm. The variation in activation energy in all the above reports may be due to the varying experimental conditions. These experiments were done at more or less similar temperatures but at significantly different pressures.

VI.4.B. JP-10 with TEA

Ignition delay plays a crucial role in propulsion applications. Several experiments have been reported till date on ignition delays of endothermic fuels. One of such experiment[3] reveals that the relative ignition delay times for different fuels vary as methane > JP-10 ≈ heptane > reformed endothermic fuel > ethylene > hydrogen. Varying the temperature, pressure, initial concentrations, etc. may reduce ignition delay times. Mixing additives with the main fuel may also reduce ignition delay. TEA has been used as an initiator for cracking of heptane[17]. TEA was found to be an effective promoter for cracking of heptane at the temperature of 550–650 °C. The mechanism study shows that the accelerating effect is mainly due to the release of radical CH_3CH_2 from TEA by the scission of C–N bond. Taking cue from this study, ignition experiments were performed on JP-10 – TEA mixture. A 1% mixture in Argon was prepared with TEA constituting 10% of the fuel (JP-10). Equivalence ratio of 1 was maintained throughout the experiments. Experimental data on ignition delay studies of JP-10 – TEA mixture is given in Table VI.2. The ignition delay times observed for the JP-10 – TEA ignition was about 70 - 690 μs. Figure VI.3 shows the ln (τ) vs. $1000/T_5$ plot for these experiments. Experimental results of pure JP-10 are also plotted for comparison.

Table VI.2. Experimental data for the ignition of JP-10 and TEA mixture

Run No.	T_5 (K)	Ignition delay (τ) (μs)
1	1494	84
2	1503	40
3	1460	84
4	1478	100
5	1512	84
6	1548	32
7	1606	28
8	1586	40
9	1568	52
10	1496	52
11	1445	60
12	1461	84
13	1531	52
14	1496	80
15	1567	72
16	1337	460
17	1444	90
18	1412	220
19	1444	44
20	1461	60
21	1280	464
22	1478	60
23	1337	324
24	1268	468
25	1281	460
26	1413	100
27	1242	580
28	1382	232
29	1323	352
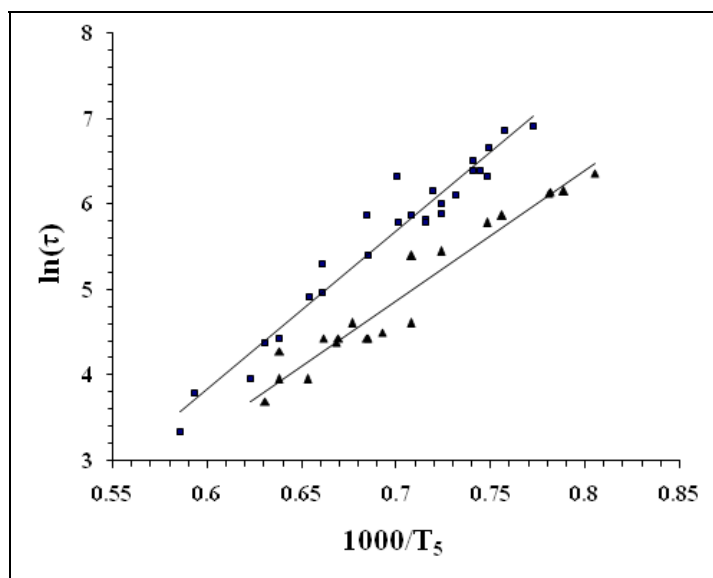
Figure VI.3. Arrhenius plot of a set of experimental results for ignition delay of JP-10 –

TEA mixture. Triangles are experimental points for the ignition delay of JP-10 – TEA

mixture (bottom fit) while square represent ignition delay for pure JP-10 (top fit as in

Figure VI.3). τ is in μs and T_5 is in K.

Table VI.3. Arrhenius parameters for ignition delay data of JP-10 with and without

TEA compared with reported results.

Reference	T_5 (K)	P_5 (atm.)	E_a (kcal/mol)	A (s)
[1]	1200 – 1700.	1 – 9	54.00	$10^{-15.54}$
[3]	1100 – 1500	3 – 8	46.83	$10^{-16.88}$
[4]	1150 – 1700	1.75 – 9.28	34.80	$10^{-12.42}$
JP-10 (present work)	1300 – 1675	15 – 20	36.92 ± 1.8	$10^{-16.61 \pm 0.32}$
JP-10 + TEA (present work)	1275 – 1650	15 – 20	30.57 ± 1.7	$10^{-13.43 \pm 0.29}$

Significant reduction in ignition delay times is present when TEA is added to JP-10. The Arrhenius expression for these experiments comes to be $\tau = 10^{-13.43\pm0.29}\exp(30.57\pm1.7/RT)$; the activation energy being in kcal/mol. Table VI.3 compares activation energies obtained from previous reported results with the current work.

The activation energy for JP-10 – TEA mixture is reduced by more than 6kcal/mol and is even lower than all the reported results on the activation energies from ignition of pure JP-10. Another important point to note from Figure VI.3 is that the experimental points for JP-10 – TEA mixture always remain below that of pure JP-10 and the separation between the two increases at lower temperatures. This proves the effectiveness of TEA in promoting ignition at lower temperatures. At higher temperatures, sufficient energy is present and a self-initiating process may help JP-10 in reducing ignition delay. The advantage of an additive can be appreciated only at lower temperatures, where the ignition delay times are really large. It will be interesting to perform experiments at temperatures lower than needed for the decomposition of JP-10 (below 1000 K). Experiments on pure TEA ignition are also reported. CH emission was present in these experiments as well. Experimental data on ignition of TEA is given in Table VI.4. The experimental data is plotted in Figure VI.4.

Table VI.4. Experimental data for the ignition of TEA

Run No.	T_5 (K)	Ignition delay (τ) (μs)
1	1496	84
2	1307	476
3	1377	216
4	1544	84
5	1351	344
6	1429	100

7	1500	92
8	1436	80
9	1490	52
10	1252	470
11	1289	364
12	1398	80
13	1492	88
14	1273	464
15	1443	76
16	1153	1680
17	1240	572
18	1565	84
19	1456	40
20	1477	32
21	1411	44
22	1411	44
23	1336	96
24	1262	72
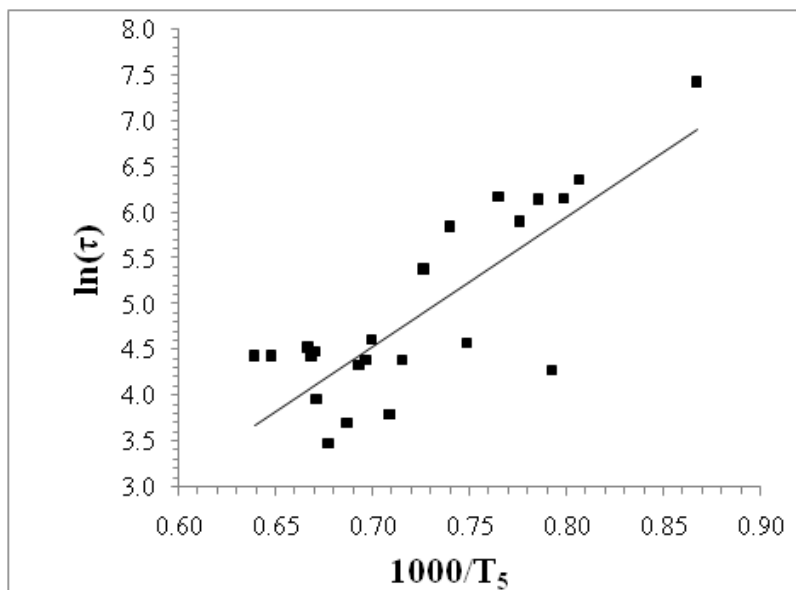
Figure VI.4. Arrhenius plot of a set of experimental results for ignition delay of TEA. τ

is in μs and T_5 is in K.

Arrhenius equation for TEA comes to be $\tau = 10^{-12.36 \pm 3.81} \exp (28.12 \pm 4.53/RT)$; activation energy in cal/mol. The activation energy is close to that obtained for JP-10 – TEA mixture using a similar procedure. This confirms that TEA is indeed causing the reduction in ignition delay.

VI.4.C. TEA as an ignition enhancer

The combustion of hydrocarbons follows a complex set of chemical reactions before forming the equilibrium products. It is the first step that rules any combustion mechanism and decides how fast the reaction proceeds, i.e., the exact nature of ignition delay. It is well known that pyrolysis and combustion follow the initiation[21] and the equilibrium products formed remain the same. We make use of previous reports on pyrolysis of JP-10 to get insight into the first step of decomposition of pure JP-10.

The most detailed reaction mechanism for decomposition of JP-10 has been proposed by Herbinet et al.[9]. Ring opening in such kind of molecules is a well-known process that leads to the formation of bi-radical. Tsang[12] has shown that the experimentally obtained global rate parameters are consistent with a bi-radical mechanism for ring opening. A detailed theoretical kinetic study on cycloalkanes ratifies this[22]. Herbinet et al.[9] have come up with a similar mechanism for the decomposition of JP-10 that accounts for the major products. During pyrolysis of JP-10, C3–C9 bond (Figure VI.5) has the smallest barrier but C3–C14 bond breaks first owing to the stability of the products formed (see reference 9). Activation energy needed to break C3–C14

bond is about 77 kcal/mol. Generally, the barrier for C–C bond breaking is about 87

kcal/mol for cycloalkanes but it is lowered in case of JP-10 due to its strained structure[9].

Figure VI.5. JP-10 ($C_{10}H_{16}$) structure showing carbon and hydrogen labels.

In the presence of TEA, clearly the C-N bond breaking followed by $C_2H_5 \rightarrow C_2H_4$

+ H will generate the important H atom. Theoretical quantum chemical calculations have

been done to calculate C–H bond energies for JP-10. Gaussian 03 package[23] is used with

6-311++G** basis expansion in conjunction with density functional theory approach for

all the calculations reported. C–H bond energies for unique C–H bonds are presented in

Table VI.5.

Table VI.5. C–H bond energies for the entire unique C–H bonds in JP-10.

C – H bond*	Bond Energy (kcal/mol)
C1 – H5	102.9
C2 – H16	110.7
C9 – H10	107.7
C12 – H13	102.9
C18 – H19	101.5
C24 – H25	102.2

* The bonds are labeled according to Figure VI.5.

The calculated C–H bond energies are in agreement with earlier reports on small ring hydrocarbons (24 and references therein). Owing to the large difference in the C–C and C–H bond energies, C–C bond dissociation, as suggested by Herbinet et al.[9] is the first step for the pyrolysis of JP-10. This should apply in case of combustion of JP-10 as well since pyrolysis and combustion mechanism follow similar path[21]. Since, product analysis has not been done for the experiments reported here, no reaction mechanism is proposed and stress is only on the first step of the combustion reaction leading to final products.

When TEA is added to JP-10, the combustion mechanism is totally different. The C–N bond energy in TEA is less than C–C and C–H bond energies in JP-10 and in TEA as well. The bond energy for C–N bond dissociation in TEA has been calculated theoretically (using the above mentioned approach). The barrier for breaking the C–N bond comes to be 66 kcal/mol. Further, C_2H_5 radical liberated from this reaction dissociates immediately to C_2H_4 and H. The barrier for this has been calculated to be 42.2 kcal/mol. This is in agreement with previously reported bond energy for C–H bond dissociation from C_2H_5 radical[25]. In presence of a third body, the barrier for this reaction is reduced and the rate of reaction is enhanced.

$(C_2H_5)_3N \rightarrow {}^*C_2H_5 + (C_2H_5)_2N^*$ Activation energy = 66.0 kcal/mol

$C_2H_5 \rightarrow C_2H_4 + H^*$ Activation energy = 42.2 kcal/mol

Several possibilities arise when TEA is added to JP-10. It is apparent that C–N bond breaking in TEA supersedes C–C bond scission in JP-10. The intermediates or products formed from the dissociation of TEA may react with JP-10 or with O_2 and lead to

intermediates / stable products. We discuss a few possible reactions that may be a consequence of TEA dissociation in the TEA – JP-10 reaction system:

1. $H + C_{10}H_{16} \rightarrow \ ^*C_{10}H_{15} + H_2$ (Activation energy – Table VI.6)
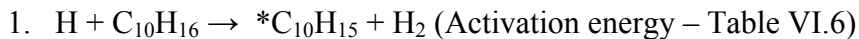
   H atom liberated from C_2H_5 easily abstracts H from JP-10 to form H_2 and $C_{10}H_{15}$ radical. The barrier for H abstraction from JP-10 has been calculated for the entire unique C–H bonds and is tabulated (Table VI.6). Optimized geometry of JP-10 for the transition state of hydrogen abstraction reaction at B3LYP/6-311++g** level of theory have also been given in the figure VI.6. It is strange to find that the H abstraction barrier is least for H13 while the weakest C–H bond was found to be C18–H19. The difference between the bond energies of C12–H13 and C18–H19 bonds is 1.4 kcal/mol. Such differences may be assigned to uncertainties in the bond energy at this level of calculation (24 and references therein).

2. $H + O_2 \rightarrow \ ^*HO_2$ (No barrier)

   $HO_2 + C_{10}H_{16} \rightarrow \ ^*C_{10}H_{15} + H_2O_2$
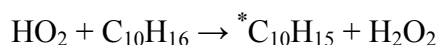
   The reaction of H atom with O_2 forms HO_2 and is barrier less. HO_2 is also an efficient abstractor of H and leads to similar products as in case 1.

3. $H + O_2 \rightarrow O^* + \ ^*OH$

   $^\cdot OH + C_{10}H_{16} \rightarrow \ ^*C_{10}H_{15} + H_2O$
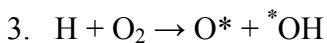
   H atom can react with O_2 to form OH that again abstracts H atom from JP-10. Relative rate constants for the gas-phase reactions of OH radicals with a series of bi- and tri-cyclic alkanes have been determined at room temperature[26]. Using a rate constant for the reaction of OH radicals with cyclohexane of 7.57 x 10^{-12} cm^3/molec-s, the rate constants for the reaction with JP-10 was 11.4cm^3/molec-s.

4. $^{*}C_2H_5 + C_{10}H_{16} \rightarrow$ $^{*}C_{10}H_{15} + C_2H_6$
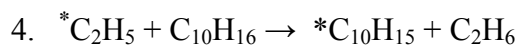
Another possibility is that the ethyl radical reacts with JP-10 to give ethane and

$C_{10}H_{15}$ radical.
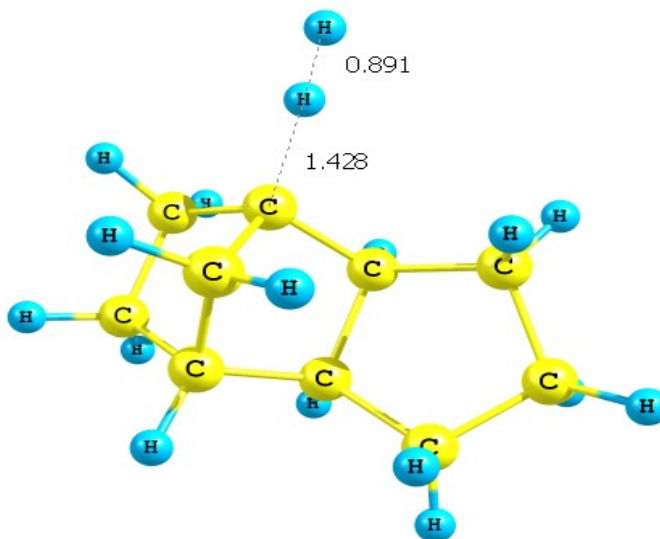
Figure VI.6. Optimized geometry of JP-10 for the transition state of hydrogen

abstraction reaction at B3LYP/6-311++g** level of theory.

Table VI.6. Activation energies for H abstraction for the entire unique H atoms of

JP-10

H atom*	Activation energy (kcal/mol)
H5	5.49
H10	8.26
H13	3.24
H16	7.39
H19	6.27
H25	5.44

* The bonds are labeled according to Figure VI.5

From the above discussion, it is evident that the first step in the decomposition / combustion of JP-10 in presence of TEA is H abstraction. Comparing H abstraction rates by OH, H and C_2H_5 from Benzene (C_6H_6), we find that OH radical abstracts the H atom most efficiently and the rate is the highest for this[27-29]. The H abstraction barrier follows the sequence OH > H> C_2H_5 for Benzene[27-29]. A similar situation should exist for the case of JP-10. Attempts were made to calculate the activation energy for H abstraction by OH but have to be abandoned because of the large computational time involved. H abstraction subsequently leads to the formation of stable products via intermediates as proposed by Herbinet et al.[9]. We have concentrated on the first step as it plays a definitive role in deciding the rate of ignition. More details on the dissociation mechanism of TEA may be found elsewhere[17].

VI.5. Conclusions

Ignition delay measurements on JP-10 and JP-10 – TEA mixture have been done. Ignition delay is appreciably reduced on the addition of 10 % TEA. The first step for the mechanism behind this reduction is discussed. C–C bond dissociation has been proposed earlier as the first step for the combustion / pyrolysis of pure JP-10. C–H bond energies for JP-10 have been estimated using quantum chemical calculations. The barriers for these come to be over 100 kcal/mol and are significantly higher than the proposed barrier for C–C bond scission. In presence of TEA, the reaction scenario is entirely different. C–N bond energy has been calculated theoretically for TEA. The activation energy needed to break this bond is around 66 kcal/mol. The formation of C_2H_5 radical and eventually C_2H_4 and H plays an important role in the ignition of JP-10. The barriers for H abstraction from JP-10 by H are also presented. These calculations suggest that in presence of TEA, the first step is H abstraction from JP-10. Thus, TEA acts as an ignition enhancer and this enhancement is due to the prompt release of C_2H_5 from TEA by the scission of the C–N bond.

VI.6.References

1. Davidson, D.F.; Horning, D.C.; Herbon, J.T.; Hanson, R.K.; Proc. Combust. Inst., **2000**, 28, 1687.

2. Davidson, D.F.; Horning, D.C.; Hanson, R.K.; AIAA, **1999**, 99, 2216.

3. Colket, M.B.; Spaddaccini, L.J.; J. Propulsion and Power, **2001,** 17, 315.

4. Olchansky, E.; Burcat, A.; 21st International Symposium on Shock Waves, **2001**, 5962,

5. Mikolaitis, D.W.; Segal, C.; Chandy, A.; J. Propulsion and Power, **2003**, 19, 601.

6. Li, S.C.; Varatharajan, B.; Williams, F.A.; AIAA, **2001**, 39, 2351.

7. Wang, S.; Gou, H.; Fan, B.; He, Y.; Zhang, S.; J. Ping: Chinese Journal of Chemical Physics, **2007**, 20, 48.

8. Striebich, R.C.; Lawrence, J.; J. Anal. Appl. Pyrolysis, **2003**, 70, 339.

9. Herbinet, O.; Sirjean, B.; Bounaceur, R.; Fournet, R.; Leclerc, F. B; Scacchi, G.; Marquaire, P. M.; J. Phys., Chem. A, **2006**, 110, 11298.

10. Rao, P.N.; Kunzru, D.; J. Anal. Appl. Pyrolysis, **2006**, 76, 154.

11. Nakra, S.; Green, R.J.; Anderson, S.L.; Combust. Flame, **2006**, 144, 662.

12. Tsang, W.; Int. J. Chem. Kin., **1978**, 10, 599.

13. Tsang, W.; Int. J. Chem. Kin., **1978**, 10, 1119.

14. Davidson, D.F.; Horning, D.C.; Oehlschlaeger, M.A.; Hanson, R.K.; AIAA**, 1999**, 01, 3707.

15. Jee, S.B.; Kim, K.; Shin, K.S.; Bull. Korean, Chem, Soc., **2000**, 21, 1015.

16. Shin, K.S.; Park, K.; Kim, K.; Bull. Korean Chem. Soc., **2001**, 22, 330.

17. Wang, Z.; Lin, R.; Fang, W.; Li, G.; Guo, Y.; Qiu, Z.; Energy, **2006**, 31, 2773.

18. Rajkumar B.; Reddy, K.P.J.; Arunan, E.; J. Phys. Chem A, **2002**, 106, 8366.

19. Rajkumar, B.; Reddy, K.P.J.; Arunan, E.; J. Phys. Chem A, **2003**, 107, 9782.

20. Nagaboopathy M., Vijayanand C., Hegde G., Reddy K.P.J., Arunan E., Curr. Sci. **2008**, 95, 78.

21. Frenklach, M.; Phys. Chem. Chem. Phys., **2002**, 4, 2028.

22. Sirjean, B.; Galude, P.A.; Rulz-Lopez, M.F.; Fournet, R.; J. Phys. Chem. A, **2006,** 110, 12693.

23. Frisch, M. J.; Trucks, G. W.; Schlegel, H. B.; Scuseria, G. E.; Robb, M. A.; Montgomery, J. R. C. J. A.; Vreven, T.; Kudin, K. N.; Burant, J. C.; Millam, J. M.; Iyengar, S. S.; Tomasi, J.; Barone, V.; Mennucci, B.; Cossi, M.; Scalmani, G.; Rega, N.; Petersson, G. A.; Nakatsuji, H.; Ehara, M. H. M.; Toyota, K.; Fukuda, R.; Hasegawa, J.; Ishida, M.; Nakajima, T.; Honda, Y.; Kitao, O.; Nakai, H.; Klene, M.; Li, X.; Knox, J. E.; Hratchian, H. P.; Cross, J. B.; Adamo, C.; Jaramillo, J.; Gomperts, R.; Stratmann, R. E.; Yazyev, O.; Austin, A. J.; Cammi, R.; Pomelli, C.; Ochterski, J. W.; Ayala, P. Y.; Morokuma, K.; Voth, G. A.; Salvador, P.; Dannenberg, J. J.; Zakrzewski, V. G.; Dapprich, S.; Daniels, A. D.; Strain, M. C.; Farkas, O.; Malick, D. K.; Rabuck, A. D.; Raghavachari, K.; Foresman, J. B.; Ortiz, J. V.; Cui, Q.; Baboul, A. G.; Clifford, S.; Cioslowski, J.; Stefanov, B. B.; Liu, G.; Liashenko, A.; Piskorz, P.; Komaromi, I.; Martin, R. L.; Fox, D. J.; Keith, T.; Al-Laham, M. A.; Peng, C. Y.; Nanayakkara, A.; Challacombe, M.; Gill, P. M. W.; Johnson, B.; Chen, W.; Wong, M. W.;

Gonzalez, C.; Pople, J. A. *Gaussian 03*, Revision A.1; Gaussian, Inc.: Pittsburgh, PA, **2003**.

24. Bach, R.D.; Dmitrenko, O.; J. American. Chem. Soc., **2004**, 126, 4444.

25. Hase, W.L.; Schlegel, H.B.; Balbyshev, V.; Page, M.; J. Phys. Chem., **1996**, 100, 5354.

26. Atkinson, R.; ASschmann, S.M.; Carter, W.P.L.; Int. Journ. Chem. Kin., **1983**, 15, 37.

27. Seta, T.; Akajima, M.; Miyoshi, A.; J. Phys. Chem. A, **2006**, 110, 5081.

28. Barckholtz, C.; Barchholtz, T.A.; Hadad, C.M.; J. Phys. Chem. A, **2001**, 105, 140.

29. Zhang ,H.X.; Ahonkhai, S.I.; Back, M.H.; Canadian Journ. Chem., **1989**, 67, 1541.

Chapter VII

Conclusions and Future Directions

VII.I. Conclusions

A single pulse shock tube facility has been used to study the thermal decomposition of any molecule of interest. The facility is similar to others that are used for chemical kinetic studies all over the globe. Two important modifications have been successfully implemented. Firstly, single pulse operation is achieved by adjusting the length of the driver and driven section in such a way that the reflected shock meets the expansion fan before the contact surface. A dump tank has also been added to the shock tube to quench the multiple reflections. A ball valve is used to ensure that all the reactant molecules experience T_5. Secondly, shock tube is calibrated externally by using chemical thermometer to get T_5. The validity of external standard method to determine the reflected shock temperature was confirmed by using the well-established internal standard method.

In order to verify and validate our experimental results with theory, ab initio and DFT methods have been used on all the experimentally investigated molecules. The major objective of the theoretical calculations is to find the transition sate for the unimolecular elimination channels. TST calculations have been performed in the same temperature range in which the experiments were carried out, to get the Arrhenius parameters for the experimentally determined elimination channels and compared with the experimental results.

The thermal decomposition of 2-chloroethanol has been investigated in the temperature range of 930-1100 K using shock tube apparatus. The rate coefficients for unimolecular HCl and H_2O elimination from CEOH studied behind single pulse reflected

shock wave have been reported both experimentally and theoretically. The first order

overall decomposition rate constant is given by $10^{14.61\pm0.34}$ exp [-(58.70±1.55)/(RT)] s^{-1}.

Experimentally determined gas phase first order rate coefficients for major HCl and H_2O

elimination channels are $10^{14.37\pm0.35}$ exp [-(57.50±1.64)/(RT)] s^{-1} and $10^{14.95\pm0.33}$ exp [-

(67.95±1.50)/(RT)] s^{-1} respectively. Experimental results predicts that the reaction rates

for HCl and H_2O elimination reactions are faster than those of the 2-fluoroethanol. The

production of ethylene was explained through HOCl elimination reaction. More

experimental and spectroscopic investigations would be needed to verify the occurrence

of HOCl elimination process. A kinetic model comprising of 45 elementary steps and 28

species both stable and unstable was constructed. This scheme was validated by the

comparison to experimental results. The model predictions are satisfactory for the

concentrations of all products in the temperature range of investigation. Sensitivity

analyses reveals that only 21 steps and 23 species are needed to account for the pyrolysis

mechanism. The rate coefficient for HOCl elimination reaction derived from fitting to

complex mechanism is $10^{17.73\pm1.60}$ exp [-(81.50±3.50)/ (RT)] s^{-1}. The mechanism

proposed here is similar to that of the fluoroethanol.

Arrhenius parameters for the three unimolecular elimination channels have been

evaluated using the TST calculations employing both ab initio and DFT methods to

support our experimental results. The calculated values of activation energies at level HF,

and MP2 (FULL) with 6-311++G** basis set for H_2O elimination was overestimated by

18.80 and 3.37 kcal mol^{-1}, respectively. Higher level G3B3 and CBS-QB3 calculations

also overestimate the barrier for both HCl and H_2O elimination reaction. However, DFT

underestimates by 0.82 kcal mol^{-1}. The calculated values of activation energies at level

HF, and MP2 (FULL) with 6-311++G** basis set for HCl elimination was overestimated by 5.92 and 10.05 kcal mol^{-1}, respectively. However, DFT underestimates by 3.96 kcal mol^{-1}. The predicted rate coefficient at DFT (HR) level gives good agreement with experimental k value for the HCl elimination. However experimental k for H_2O elimination is approximately 5 times faster than that calculated using DFT harmonic oscillator results. Experimental A of HCl elimination is higher by an order of magnitude than that of the ethyl chloride and chlorofluoroethane. Transition states structures have been verified by performing the IRC calculations. Present study has revealed both experimentally and theoretically that the fluorine substitution leads to an increase in E_a, however, Cl and OH substitution do not.

The thermal decomposition of 2-bromoethaonl has been investigated in the temperature range of 910-1102 K using shock tube apparatus. The Arrhenius parameters for all of the unimolecular elimination channels have been evaluated using the TST calculations employing both ab initio and DFT methods to support our experimental results. The experimental first order overall thermal decomposition rate coefficient derived by using the Arrhenius expression is $10^{14.08\pm0.23}$ exp $[-(55.66\pm1.07)/(RT)]$ s^{-1}. The experimental rate coefficient for HBr elimination is $10^{13.48\pm0.30}$ exp $[(-53.42\pm1.39)/(RT)]$ s^{-1}and that for the H_2O elimination is $10^{14.47\pm0.46}$ exp $[-(66.47\pm2.15)/(RT)]$ s^{-1}. These experimental results have been found to be in very good agreement with the earlier reported data within the uncertainty limit for HBr and H_2O elimination reactions. The reaction scheme proposed for the thermal decomposition of 2-Bromoethanol containing the 47 elementary reactions and 28 species can successfully account for the yields of products as a function of temperature. The reduced kinetic model proposed here using

sensitivity analysis contains 32 reactions and 27 species. This mechanism was ultimately validated by the comparison to experimental results. The mechanism proposed here is similar to that of the fluoroethanol and chloroethanol. The reported experimental rate coefficients for the unimolecular elimination reactions of HBr and H_2O can adequately be described by the TST fitted results. More specifically, the estimated activation energies for H_2O elimination at MP2 (FULL) and DFT level of theory with 6-311++G** basis set were overestimated by +3.16 and underestimated by -0.39 kcal mol^{-1} respectively. The calculated activation energies for HBr elimination at HF and DFT level with 6-311++G** basis set were overestimated by +6.00 and underestimated by -2.04 kcal mol^{-1} respectively. The pre-exponential factor evaluated using the hindered rotor approximation for low frequency torsional mode resulted in the good agreement between theoretical and experimental values for the HBr elimination. The formation of ethene was explained by considering the possibility of HOBr elimination. The expression for the rate coefficient derived from fitting to complex mechanism for HOBr elimination reaction is $10^{15.91\pm0.63}$ exp [(-67.70±3.20)/(RT)] s^{-1}. Additionally, the TST fitted Arrhenius parameters for HOBr elimination reaction has also been estimated using both ab initio and DFT methods. This study also provides the IRC results performed for the verification of the three transition states. Present study has revealed both experimentally and theoretically for HBr elimination that the bromine, chlorine and fluorine substitution leads to an increase in E_a, however, OH do not. For H_2O elimination the Br substitution does not bring about significant variation but F does increase the E_a.

Ab initio, DFT and higher level quantum chemistry calculation have been performed to estimate the enthalpy of formation of haloethanols for which the

experimental data are not available. These results were compared with the enthalpy of formation of chlorofluoroethane and ethandiol and difluoroethane. Enthalpy of formation calculated with high level G_n and CBS-Q methods are in good agreement with the Benson's group additivity method which provides evidence that these values of enthalpies of formation of haloethanols calculated via isodesmic reactions are reasonable. The calculated mean enthalpies of formation (G3, G3B3, G3MP2B3, CBS-Q and CBS-QB3) of fluoroethanol, chloroethanol and bromoethanol at 298 K via isodesmic reactions which minimizes systematic calculation error are -96.78±0.03, -61.86±0.02 and -50.91±0.96 kcal/mol respectively. However, only accurate experimental results can validate our data. The atomization method predicts higher molecular stability for all haloethanols in our study as compared to the isodesmic method at higher level of calculation at 298 K. It has been found that the enthalpy of formation calculated via isodesmic reaction (best value) of fluoroethanol at 298 K is approximately 7kcal/mol higher than the experimental enthalpy of formation of difluoroethane. In conclusion, based upon heat of formation calculation, a higher level quantum chemistry method predicts that the fluoroethanol is the most stable and less reactive molecule among the haloethanols. It is hoped that the enthalpy of formation reported here would be helpful for the modeling of gas phase reaction mechanism of combustion, pyrolysis and oxidation of haloethanols.

Ignition delay measurements on JP-10 and JP-10 – TEA mixture have been done. Ignition delay is appreciably reduced on the addition of 10 % TEA. The first step for the mechanism behind this reduction is discussed. C–C bond dissociation has been proposed earlier as the first step for the combustion / pyrolysis of pure JP-10. C–H bond energies

for JP-10 have been estimated using quantum chemical calculations. The barriers for these come to be over 100kcal/mol and are significantly higher than the proposed barrier for C–C bond scission. In the presence of TEA, the reaction scenario is entirely different. C–N bond energy has been calculated theoretically for TEA. The activation energy needed to break this bond is around 66kcal/mol. The formation of C_2H_5 radical and eventually C_2H_4 and H plays an important role in the ignition of JP-10. The barriers for H abstraction from JP-10 by H are also presented. These calculations suggest that in presence of TEA, the first step is H abstraction from JP-10. Thus, TEA acts as an ignition enhancer and this enhancement is due to the prompt release of C_2H_5 from TEA by the scission of the C–N bond.

VII.2. Future directions

The future direction of this research could be many-fold. Firstly, pulsed laser-induced fluorescence imaging technique can be coupled with shock tube for carrying out the investigation on the measurements of gas-phase chemical reactions which are involved in combustion and pyrolysis at high-temperature and pressure. This will certainly generate useful information on a concentration-time profile of radical species quantitatively using a single laser pulse. These results in turn can successfully be used for the determination of important kinetic parameters of such reactions.

Atomic resonance absorption technique (ARAS) which is one of the widely used techniques in shock tube studies can also be incorporated so that the variation in the hydrogen atom concentration could be followed as a function of time. Direct on-line real

time measurement of hydrogen concentration would yield the rate coefficient of the reactions of interest directly. The reaction of naphthalene with hydrogen atom can be studied using this technique for the determination of the thermal rate constant of this reaction at high temperature. This will yield valuable information of the kinetics of this reaction at high temperature and pressure that has never been reported before.

There is no theoretical and experimental report available so far on gas phase HCl elimination kinetics from 2-chloroethylbenzen at high temperature and pressure. As mentioned, the experimental data on this molecule are not available. Hence, a systematic study has to be performed in order to understand the effect of neighbouring group participation or anchimeric assistance of phenyl nucleus on activation barrier of HCl elimination in the gas phase at high temperature. These kinetic data would also give better insight into the β-substitution effect when compared to C_2H_5Cl and $C_2H_4Cl_2$. Theoretical calculation can also be performed to evaluate the kinetics of 1, 2-HCl, C_6H_6, H_2 & 1, 1-HCl elimination reactions at different level of theory using harmonic oscillator, hindered rotor and free rotor models for low frequency torsional modes for both reactant and transition state to verify the experimental results. Already, a systematic study on this has started in our laboratory. Preliminary experimental data for HCl elimination from 2-chloroethylbenzen has shown the good agreement with the theoretical results. Generating more experimental data would certainly lead to accurate determination of kinetics of this reaction.

Similar investigations on 2-hydroxyethylbenzene can also be performed both experimentally and theoretically to determine the kinetics of H_2O elimination reaction at high temperature and pressure using shock tube.

Also, there has been no report available on the thermal activation experiments on the bromochloroethane and bromofluoroethane for the determination of the kinetics of HBr, HCl and HF elimination reactions in gas-phase at high temperature using shock tube. Hence, a systematic experimental study on these molecules has to be carried out in our laboratory to obtain the kinetics of these reactions. Also, there are not much theoretical investigations available in literature on kinetics of these reactions. Hence, extensive higher level quantum chemistry calculations should also be performed for retrieving the theoretical rate coefficients using transition state theory calculation employing different models. This would be useful for the verification of experimental data. These information's would also be useful for the comparison with kinetic parameters of these reactions reported employing other techniques.

List of publications

1. *"Thermal Decomposition of 2-Chloroethanol: Single Pulse Shock Tube Experiments, Modeling, Quantum Chemistry and TST Calculations", Chakravarty H. K., K.P.J. Reddy, E. Arunan.* **Manuscript under correction.**

2. *"Thermal Decomposition of 2-Bromoethanol: Single Pulse Shock Tube Experiments, Modeling, Quantum Chemistry and TST Calculations", Chakravarty H. K., K.P.J. Reddy, E. Arunan.* **Manuscript under correction.**

3. *"Computational Calculations of Enthalpy of Formation of Haloethanols", Chakravarty H. K., E. Arunan.* **Manuscript under correction.**

4. *"Shock tube Ignition delay studies of JP-10 and JP-10+Triethyl amine", Chakravarty H. K., K.P.J. Reddy, E. Arunan.* **Manuscript under correction.**